

https://dspace.org/

The evolution of marginal-marine systems of the Amibberg formation, Karasburg Basin, Southern Namibia: implications for Early-Middle Permian palaeogeography in South Western Gondwana

Berti, Michael

2015-05-07
http://hdl.handle.net/10539/17657

Downloaded from a DSpace repository. https://dspace.org/

THE EVOLUTION OF MARGINAL-MARINE SYSTEMS OF THE AMIBBERG FORMATION, KARASBURG BASIN, SOUTHERN NAMIBIA: IMPLICATIONS FOR EARLY-MIDDLE PERMIAN PALAEOGEOGRAPHY IN SOUTH WESTERN GONDWANA

Michael Berti

A Dissertation submitted to the Faculty of Science, University of the Witwatersrand, Johannesburg, in fulfilment of requirements for the degree of Master of Science

Johannesburg, 2014

Declaration

I declare that this Dissertation is my own, unaided work. It is being submitted for the Degree of Master of Science at the University of the Witwatersrand, Johannesburg. It has not been submitted before for any degree or examination at any other University.

_____
(M.Berti)

_____day of _____20_____

Abstract

The Karasburg Basin is situated in southern Namibia and preserves a heterogeneous succession of Karoo Supergroup strata up to 1000m thick. The uppermost preserved succession in this basin is the Amibberg Formation which is 250m thick and consists of intervals of sandstone, siltstone and mudstone. This study uses facies analysis, sequence stratigraphy and petrography to determine the palaeogeography and provenance for the Amibberg Formation. This is then used to establish environmental variability across the Karasburg – Aranos – Main Karoo basins and to define an equivalent of the Amibberg Formation in the Main Karoo Basin.

Detailed stratigraphic logging of five outcrop localities has led to the identification of seven distinct lithofacies and two dominant ichnofacies (*Cruziana* and *Skolithos*). These lithofacies include: 1) Massive, laminated and bioturbated mudstones interpreted as offshore deposits (OS); 2) Bioturbated siltstones and sandstones which are representative of offshore-transitional environments (OST); 3) Interbedded sandstones and siltstones also interpreted as offshore-transitional deposits (OST) and generated by river-fed hyperpycnal plumes; 4) Sharp based, massive sandstones interpreted as being deposited on the distal lower shoreface (dLSF); 5) Non-amalgamated hummocky cross-stratified (HCS) and wave rippled sandstones interpreted as distal lower shoreface deposits (dLSF); 6) Amalgamated HCS and wave rippled sandstones interpreted as proximal lower shoreface deposits (pLSF); and 7) Soft-sediment deformed (SSD) sandstones and siltstones occurring in close juxtaposition with dLSF and pLSF deposits. The vertical arrangement of these lithofacies shows a general coarsening and shallowing upward trend. Overall the rocks of the Amibberg Formation consist of wave-dominated shoreface deposits with significant influence by tidal processes.

Petrographically, the sandstone samples fall into the class of quartz and feldspathic wackes and are sourced from craton interior provenances. Geochemical analysis of mudstones and nodules indicate high levels of microbial activity under predominantly oxic conditions during the deposition of the Amibberg Formation.

Five poorly defined 4^{th} order T-R cycles are observable within the strata of the Amibberg Formation. Large regressive intervals are capped by thin transgressive tracts and these cycles are interpreted to have formed due to eustatic processes. Overall, the Amibberg Formation represents a regressive shoreline.

Based on the mean palaeocurrent vectors a NNE-SSW palaeoshoreline orientation is deduced and the shoreface must have occupied a palaeohigh on the northern side of the western Cargonian Highlands. This emergent highland acted as an extensive headland and assisted in the connectivity of the Karasburg and Aranos basins, with partial connectivity with the Main Karoo Basin during the Early Permian. Based on this study, the Amibberg Formation is considered an equivalent of the Waterford Formation in the Main Karoo Basin based on similar: stratigraphic position; thickness; sedimentary structures; trace fossil assemblages and stacking patterns.

Key words: Karasburg Basin, Amibberg Formation, Karoo Supergroup, lithofacies, provenance, T-R cycles, palaeoshoreline, Cargonian Highlands, Waterford Formation.

Acknowledgements

I would like to thank my supervisor Dr. Zubair Jinnah for all his help in all aspects of this project. Without his tireless work and backing I would never have been able to complete this MSc. To all others at the School of Geosciences, especially Cameron Penn-Clarke, goes a great thanks for all types of academic assistance. MJ Masetlane and Kofi Acheampong are thanked for nodule and mudstone sample collection and preparation. With regards to funding, I would like to express my sincere gratitude to the NRF and University Research Office at The University of the Witwatersrand for financial assistance. Thanks go to those at Aussenkjer Farm (Eben Naude and Milo Vasiljevic) and the Namibian geological survey (Helke Mocke). Special thanks go to Wendy Young for patiently corrected any spelling and grammatical errors. To my mother for her everlasting support, encouragement and countless cups of coffee; and my father for always giving of his time, accompanying me in the field, and always showing interest in my work; I cannot thank you both enough. To Sandy, for putting up with me and pretending to understand my geological monologues, goes a great deal of love and gratitude. Lastly I would like to thank the rest of my family and friends for their support during this project: without them none of this would have been possible.

CONTENTS **PAGE**

DECLARATION……..……..i

ABSTRACT…….……..ii

ACKNOWLEDGEMENTS…….....……iv

LIST OF FIGURES……...ix

LIST OF TABLES……..xiii

CHAPTER 1 – INTRODUCTION…….1

1.1 Introduction……1

1.2 Previous Work…….....2

1.3 Project Outline……...……4

1.4 Geological Setting……...……6

1.4.1 Tectonic Framework of Karoo aged Basins……...……6

1.4.2 Structural Framework and Palaeogeography of the Karasburg Basin……..…..…..9

1.4.3 Stratigraphy and Structural Setting of the Karoo Supergroup……..…….12

1.4.4 Stratigraphic Correlation……...…….……..…….23

1.5 Hypotheses……...……..26

CHAPTER 2 – LITHOFACIES AND PALAEOENVIRONMENTAL RECONSTRUCTION……27

2.1 Introduction……...……27

2.2 Aims……..……27

2.3 Previous Work……..……27

2.4 Methods……...……..28

2.5 Lithofacies Descriptions and Interpretations…….……35

2.5.1 Lithofacies 1 - Massive to Plane-bedded Mudstone……..….35

2.5.2 Lithofacies 2 - Bioturbated Siltstone and Sandstone……..…….41

2.5.3 Lithofacies 3 - Interbedded Sandstone and Siltstone……..…43

2.5.4 Lithofacies 4 - Sharp Based, Massive Sandstone……..……..…….47

2.5.5 Lithofacies 5 - Discrete Hummocky Cross-stratified and Wave Rippled Sandstone……..…….....48

2.5.6 Lithofacies 6 - Amalgamated Hummocky Cross-stratified and Wave Rippled Sandstone....……..…….....50

2.5.7 Lithofacies 7 - Soft-sediment Deformed Sandstone and Siltstone……..…..57

2.6 Lithofacies Stacking Patterns ……...59

2.7 Photographic Interpretations……64

2.8 Ripple Descriptions……...……..……..71

2.9 Discussion……71

2.9.1 Palaeocurrent Interpretation…….…..71

2.9.2 Ichnology……78

2.9.3 Lithostratigraphic Correlation…….…….…..91

CHAPTER 3 –PETROGRAPHY AND PROVENANCE……..93

3.1 Introduction……..…….93

3.2 Methodology……...……...…….....……93

3.3 Petrography of Sandstones……..……..……94

3.4 Detrital Framework Grains…….……..98

3.4.1 Quartz……...98

3.4.2 Plagioclase……...…….98

3.4.3 Orthoclase…….……....98

3.4.4 Micas……..…..98

3.4.5 Clay Minerals…….….100

3.4.6 Heavy Minerals……..…….....100

3.5 Detrital Modes and Sandstone Classification……..……100

3.6 Lithofacies Based Petrographic Descriptions…….……107

3.6.1 Lithofacies 1……...…….107
3.6.2 Lithofacies 2……...…….109
3.6.3 Lithofacies 3……109
3.6.4 Lithofacies 4……...….109
3.6.5 Lithofacies 5……112
3.6.6 Lithofacies 6……..……..113
3.6.7 Lithofacies 7……115
3.7 Sandstone Provenance and Tectonic Setting……...…118
3.8 Carbon Isotope Data for Nodules……..……..122
3.9 Geochemistry of Mudstones……..……..123

CHAPTER 4 – SEQUENCE STRATIGRAPHY……..131
4.1 Introduction……131
4.2 Hierarchy……...…..133
4.3 Base Level Curves……...…134
4.4 Sequence Stratigraphic Interpretation……...…..138

CHAPTER 5 – DISCUSSION AND CONCLUSIONS…….……141
5.1 Palaeogeographic Reconstruction and Provenance Discussion……..141
5.2 Basin Connectivity Discussion……..……..146
5.3 Stratigraphic Correlation Discussion……..150
5.3.1 Amibberg Formation……..…….152
5.3.2 Ripon Formation…….…….152
5.3.3 Fort Brown Formation……...……..153
5.3.4 Kookfontein Formation……..…….153
5.3.5 Koedoesberg/Waterford Formation……...……..154
5.3.6 Waterford Formation (Southern Sub-basin)……154
5.3.7 Carnarvon/Waterford Formation…….……155
5.4 Conclusions…….……156

5.4.1 Hypothesis 1……157
5.4.2 Hypothesis 2……158
5.4.3 Hypothesis 3……..…….159
5.5 Concluding Remarks……...……159
5.6 Recommendations……..…….161

CHAPTER 6 – REFERENCES……..162

CHAPTER 7 – APPENDICES……187

List of Figures

Figure 1.1: Location of the Main Karoo Basin and various subsidiary basins in southern Africa……..……...3

Figure 1.2: Map showing the location of the study area for this work within the context of southern Africa…..5

Figure 1.3: Detailed geological map showing Karoo Supergroup lithologies and outcrop localities……....7

Figure 1.4: Generalised tectonic setting of the Main Karoo Basin during the Late Triassic……..……..9

Figure 1.5: Formation and evolution of the Pan-Gondwanan foreland system……..10

Figure 1.6: Map showing present day Karoo deposits in relation to palaeohighlands…….13

Figure 1.7: Idealised stratigraphic sections through various basins…….16

Figure 1.8: Correlation panel showing lithological and stratigraphic data from various Karoo basins……...25

Figure 2.1: Dickneus stratigraphic column…….…..…30

Figure 2.2: Northern Amibberg stratigraphic column…….....…31

Figure 2.3: Norotshama stratigraphic column…….….32

Figure 2.4: Tafelberg stratigraphic column……..33

Figure 2.5: Platberg stratigraphic column…….……...34

Figure 2.6: Lithofacies 1 - Mudstone…….……..36

Figure 2.7: Lithofacies 1 - Nodules associated with the mudstone lithofacies……37

Figure 2.8: Lithofacies 1 - Distinctive nodules associated with the mudstone lithofacies……..……39

Figure 2.9: Lithofacies 1 - Distinctive nodules associated with the mudstone lithofacies……..40

Figure 2.10: Lithofacies 2 - Bioturbated siltstone and sandstone……..……..44

Figure 2.11: Lithofacies 3 - Interbedded sandstone and siltstone…….…..……..45

Figure 2.12: Lithofacies 3 - Interbedded sandstone and siltstone……...…….……46

Figure 2.13: Lithofacies 4 - Sharp based massive sandstone…….…..…….49

Figure 2.14: Lithofacies 5 - Discrete HCS and wave rippled sandstone…….……51

Figure 2.15: Lithofacies 6 - Amalgamated HCS and wave rippled sandstone……..……..54

Figure 2.16: Lithofacies 6 - Amalgamated HCS and wave rippled sandstone……..……..56

Figure 2.17: Lithofacies 6 - Quartz-rich HCS and wave rippled sandstone……..…….…….57

Figure 2.18: Lithofacies 7 - SSD sandstones and siltstones (*in-situ*)……..…….60

Figure 2.19: Lithofacies 7 - SSD sandstones and siltstones (detached)…….……..61

Figure 2.20: Other Important Photos……...…….62

Figure 2.21: Interpreted photograph of an amalgamated HCS and wave rippled unit…….……64

Figure 2.22: Interpreted photograph of an amalgamated HCS and wave rippled unit…….……65

Figure 2.23: Interpreted photograph of the uppermost amalgamated HCS and wave rippled unit…….…...66

Figure 2.24: Interpreted photograph of an arrangement of discrete HCS and wave rippled intervals……..…..67

Figure 2.25: Interpreted photomosaic of the Northern Amibberg locality……..68

Figure 2.26: Interpreted photomosaic of the Tafelberg locality…….……..69

Figure 2.27: Interpreted photomosaic of a section of the Amibberg Massif……..……...70

Figure 2.28: Symmetrical wave ripple palaeocurrents…...…….……72

Figure 2.29: Asymmetrical wave ripple palaeocurrents……...……73

Figure 2.30: Geophysical map of southern Africa……...74

Figure 2.31: Wave ripples……..……..75

Figure 2.32: Distribution of trace fossils occurring in HCS tempestite deposits……....……79

Figure 2.33: *Skolithos* ichnofacies……...……80

Figure 2.34: *Cruziana* ichnofacies 1……82

Figure 2.35: *Cruziana* ichnofacies 2……...……83

Figure 2.36: *Asterosoma*……..……86

Figure 2.37: *Palaeophycus*……...……88

Figure 2.38: *Planolites*……...……..89

Figure 2.39: Mixed ichnofacies…….……...…90

Figure 2.40: Lithostratigraphic correlation…….……92

Figure 3.1: Photo micrographs……...……..95

Figure 3.2: Photo micrographs...……..97

Figure 3.3: Photo micrographs……...……...…….99

Figure 3.4: Photo micrographs...……...……..101

Figure 3.5: Photo micrographs…...……...…….102

Figure 3.6: Photo micrographs…...……103

Figure 3.7: Photo micrographs……...……104

Figure 3.8: QFL Diagram……...106

Figure 3.9: QFL diagram of the wacke field……...108

Figure 3.10: Photo micrographs……...……..110

Figure 3.11: Photo micrographs……...……111

Figure 3.12: Photo micrograph……..……...……112

Figure 3.13: Photo micrographs……...……..…114

Figure 3.14: Photo micrographs...……..……116

Figure 3.15: Photo micrographs……...……...…117

Figure 3.16: Photo micrographs……...……...…118

Figure 3.17: Photo micrographs……...……...……119

Figure 3.18: QFL ternary diagrams……...121

Figure 3.19: TiO_2 vs Ni bivariate plot for mudstone samples……..……..……125

Figure 3.20: Th/U trend with increasing height in the Aussenkjer and Amibberg formations……..125

Figure 3.21: Relationship of stratigraphic height and certain palaeoredox proxies……..…….126

Figure 3.22: Crossplots of various trace element ratios used as palaeoredox proxies……..….127

Figure 3.23: Crossplots of various trace element ratios used as palaeoredox proxies……..…….128

Figure 4.1: Empirical approach……..……132

Figure 4.2: Sequence stratigraphic correlation……..……..135

Figure 4.3: Idealised shoreline profile……...…….136

Figure 4.4: Sequence stratigraphic interpretation of outcrop…….137

Figure 4.5: Idealised stratigraphic section with interpreted base level curve……...….140

Figure 5.1: Relative mineral percentage graphs……..……147

Figure 5.2: Palaeogeographic reconstruction of southern Gondwana during the Late Palaeozoic……...150

Figure 5.3: Final lithostratigraphic correlation…….…….160

List of Tables

Table 2.1: Thickness and locations of the 5 measured stratigraphic columns in the study area……..28

Table 2.2: Legend for corresponding stratigraphic columns……29

Table 2.3: Characteristics of lithofacies recognised in the Amibberg Formation……..…….76

Table 3.1: Characteristics of each sample as well as their classification and appropriate lithofacies…..……...96

Table 3.2: Point count data from sandstone samples……...……..……105

Table 3.3: Point count data from carbonate nodule samples……..……106

Table 3.4: δ13C data for nodules of the Amibberg Formation……...…….…..122

Table 3.5: Geochemical proxies for mudstones of the Aussenkjer and Amibberg formations……..…….124

Chapter 1: Introduction

1.1 Introduction

Karoo basins of Carboniferous to Jurassic age are widely distributed not only on the African continent but also further afield in Antarctica, South America and Australia all of which were formed during the assemblage of Gondwana. The Main Karoo Basin of South Africa is the largest of all the basins associated with the Karoo Supergroup and contains the most complete stratigraphic record. Other basins to the north of the Main Karoo Basin include the Karasburg, Huab, Aranos and Kalahari basins (Fig. 1.1). At their maximum extent, Karoo aged basins covered over 4.5 million km^2, of which 300 000 km^2 are still preserved in southern Africa (Smith et al., 1993). Although these successions are referred to as discrete basins, and are geographically distinct from the Main Karoo Basin today, the original basin geometry is not preserved (Stollhofen et al., 2008), and the original continuity of sedimentary fill across basins remains unknown. Furthermore, other Karoo-aged basins in Namibia, Botswana and Zimbabwe, and several other southern African countries have been studied in little detail and these may prove to be interconnected with the Main Karoo Basin (Smith et al., 1993). These can be classified as compressional, extensional, strike-slip or sag sedimentary basins which formed in response to the same regional stress - collision between South America, Antarctica and Africa during the Palaeozoic. One of these understudied areas is the Karasburg Basin in southern Namibia which encompasses the area of study for this project. It has been previously referred to as the Warmbad Basin (Haughton and Frommurze, 1936), the Nabas Basin (De Villiers and Söhnge, 1959) and the Orange River Basin (Frakes and Crowell, 1970) but will herein be referred to as the Karasburg Basin of Schreuder and Genis (1975). The reason that some of these subsidiary basins have been neglected is as a result of the absence of coal-bearing strata. For this reason little is known about the stratigraphy, structural setting and fill of these basins and hence less has been written about the palaeoenvironmental and palaeoclimatic conditions which prevailed during deposition of the Ecca Group in these basins.

The focus of this work is on the Ecca Group which was deposited during the Permian and consists predominantly of marine sediments. More specifically the focus of this work is on the Amibberg Formation of the Ecca Group and its equivalents in the Aranos and Main Karoo basins.

The Amibberg Formation represents the uppermost preserved stratigraphic interval in the Karasburg Basin of southern Namibia. The Karasburg Basin has been the focus of numerous works; however, the focus has been on the glaciogenic Dwyka Group rocks and the lowermost Ecca Group strata. Apart from the work conducted by Werner (2006), no detailed work has been conducted on the upper Ecca Group rocks in the Karasburg Basin. For this reason the Amibberg Formation is poorly understood and no detailed facies analysis, provenance studies or regional palaeoenvironmental/palaeogeographical reconstructions have been carried out. Furthermore, present day Karoo basins in Namibia are widely distributed and often inaccessibly covered and obscured by Cenozoic Kalahari Group deposits. The Karasburg Basin, however, provides good exposure of Karoo Supergroup successions and has an uncertain relationship with both the Aranos Basin in the north and the Main Karoo Basin in the south. It is important to determine a stratigraphic relationship between basins and their formation in terms of time and space (i.e. environmental variability across the Aranos – Karasburg – Main Karoo basins) to aid in the understanding of southern African geology and to gain knowledge of sea level fluctuations during this period in Earth's history. The Amibberg Formation is therefore the frontier for Karoo sedimentology, not only in Namibia but in the whole of southern Africa.

1.2 Previous Work

Ever since du Toit (1927) recognized the importance of Karoo stratigraphy and palaeontology in Gondwanan tectonics, the Karoo Supergroup has been the subject of a great deal of research. Furthermore, the fact that all of southern Africa's coal occurs within the Karoo Supergroup has led to many tectonic and sedimentological studies. A variety of papers focusing on the stress fields and overall tectonic processes

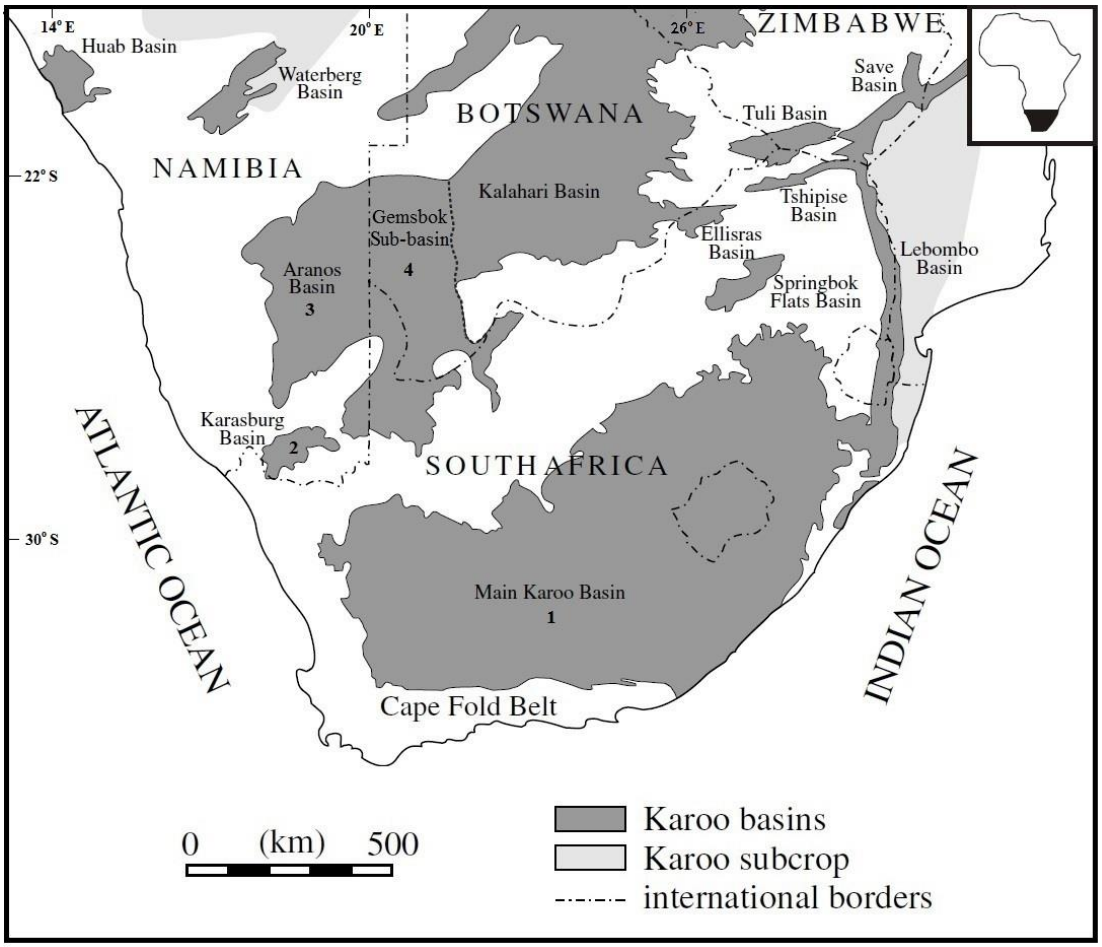


Figure 1.1. Location of the Main Karoo Basin and various subsidiary basins in southern Africa (modified after Catuneanu et al., 2005). The numbers provided indicate areas of interest for this project. 1 - Main Karoo Basin; 2 - Karasburg Basin; 3 - Aranos Basin; 4 - Gemsbok Sub-basin.

associated with the Karoo Supergroup has been conducted (eg. Catuneanu et al., 1998; Pysklywek and Mitrovica, 1999; Johnson et al., 2006; Bumby and Guiraud, 2005). Research on the north-east portion of the Main Karoo Basin has been undertaken by a number of authors due to the coal-bearing strata in this area **(**e.g. Roberts, 1986; Cairncross and Cadle, 1988; Tavener-Smith et al., 1988**)** and many recent studies have focused on the sub-basins found in the Main Karoo Basin of South Africa, namely the Tanqua and Laingsburg sub-basins (e.g. Bouma and Wickens, 1991; Wickens 1994; Johnson et al., 2001; Van der Werff and Johnson, 2003). Other work conducted on subsidiary basins of southern Africa include Johnson et al., (1996) and Catuneanu et al., (2005) who gave an overview and compiled the stratigraphies of all of the southern African basins. Other more focused work on the Kalahari Basin of Botswana has been carried out (e.g. Segwabe, 2008; Nxumalo 2011). The abundance of work done here is due to the identified coal resources or as a result of coaliferous potential of these basins. However, basins that have been found to lack coal-bearing

strata, such as the Karasburg Basin, have been neglected due to the lack of economic interest. Nevertheless, there have been studies conducted in the Karasburg Basin. Initial studies of Karoo Supergroup rocks in the Karasburg Basin were given by Range (1912), Versfeld (1914), Wagner (1915) and du Toit (1921). Subsequent detailed studies and mapping were conducted by Haughton and Frommurze (1927 and 1936) on the Dwyka, Ecca and volcanic rocks in this basin. The Dwyka and Ecca group strata were also briefly mapped and described by Schreuder and Genis (1975). Frakes and Crowell (1970) and Martin (1981b) gave a brief summary of the Dwyka geology of this area, but since then this Karoo outcrop region remained sufficiently understudied except for minor work by Anderson (1975) and Visser (1982 and 1983a) on the lower parts of the Dwyka Group. The discovery of tuff layers in the Dwyka Group rocks on the southern margin of the Karasburg Basin resulted in a detailed study of this area by Geiger (1999 and 2000). Werner (2006) conducted detailed stratigraphic and sedimentological work in this basin, identifying the Amibberg Formation as being approximately 250m thick and consisting of mudstone dominated intervals with discrete sandstone beds and thick amalgamated sandstone packages. This work furthermore states that hummocky cross-stratification and other wave influenced structures predominate in the study area. This, coupled with the nature and architecture of the rocks that comprise this formation, is indicative of a marine wave-dominated shoreface environment. However, the work of Werner (2006) focused predominantly on the pyroclastic tuff layers present in the Dwyka Group as well as the lowermost Ecca Group in the Karasburg and Aranos basins, as did Stollhofen et al., (2008).

1.3 Project Outline

In this project, new data on facies architecture, thickness trends, sandstone composition and mudstone geochemistry is provided for the Amibberg Formation. This data is then used to put the Amibberg Formation into a sequence stratigraphic context, as well as to reconstruct the Amibberg depositional system and determine the provenance of these rocks. This information is then used to provide a correlation with the Amibberg Formation and the corresponding formation in the Main Karoo Basin that exhibits similar age constraint and physical characteristics. Furthermore, this will aid in identifying and characterising the palaeogeographic relationship between the

Karasburg Basin, the Aranos Basin to the north and the Main Karoo Basin to the southeast.

This study will focus on strata of the Karasburg Basin (Fig. 1.2 and Fig. 1.3) which is situated in southern Namibia, on the border with South Africa, and covers approximately 9000 km² (Schreuder and Genis, 1975). The Karasburg Basin contains Karoo Supergroup rocks which, in total, can be up to 1000m thick in certain localities in the outcrop area from Aussenkjer to Noordoewer. This basin forms a WSW-ENE oriented area approximately 160 km long and 60km wide (Stollhofen et al., 2008). The NE portion of the Karasburg Basin contains only Dwyka Group rocks due to the erosion of the Ecca Group, whereas the SW basin contains both Dwyka and Ecca Group rocks. The Dwyka and lower Ecca are well exposed throughout the study area whereas the upper Ecca Group rocks only outcrop at certain localities such as Tafelberg, Norotshama and Amibberg. Associated Jurassic volcanics also form a considerable part of the Karasburg Basin. However, a detailed study of these rocks is outside the scope of this work.

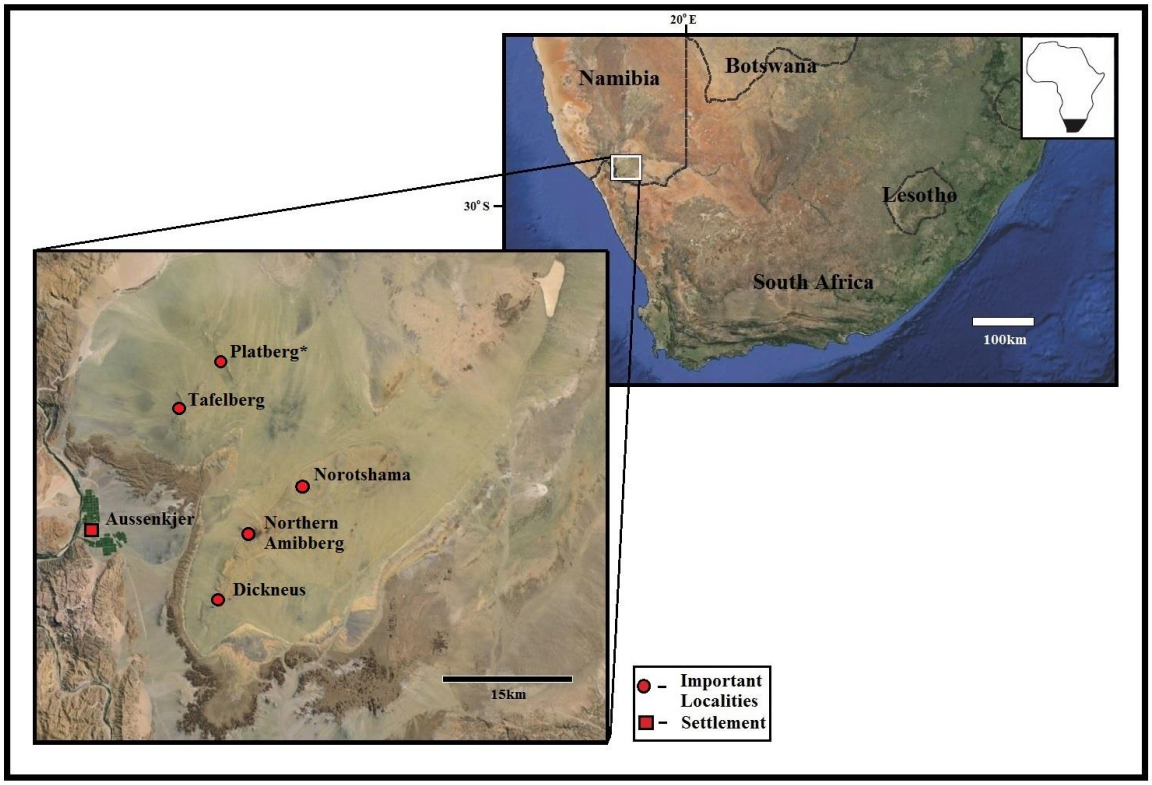


Figure 1.2. Map showing the location of the study area for this work within the context of southern Africa. The locations of measured stratigraphic sections are also displayed [(*- denotes informal locality names) (Satellite images obtained from Google Earth)].

Detailed maps produced by Schreuder and Genis (1975) and the Geological Survey of Namibia (1999) give an overview of the lithologies present in the study area. These, as well as field observations by the author, formed the basis on which field work was planned in the Karasburg Basin.

This dissertation consists of five chapters: Chapter 1 offers an introduction to the Karoo Supergroup rocks and the tectonic and structural frameworks of selected Karoo basins. Chapter 2 contains the results of a lithofacies study and paleoenvironmental reconstruction. Chapter 3 consists of the petrophysical study of sandstones and a geochemical study of the mudrocks from the Amibberg Formation. Chapter 4 deals with sequence stratigraphy in the upper Ecca Group rocks in the study area. Chapter 5 deals with a discussion on palaeogeography and provenance; a stratigraphic correlation between the Karasburg Basin, the Aranos Basin and the Main Karoo Basin and concludes with the important implications of this work.

1.4 Geological Setting

1.4.1 Tectonic Framework of Karoo Aged Basins

As mentioned previously, Karoo basins can be classified as either compressional, extensional, strike-slip or intracratonic thermal sag basins which were formed during the assemblage of the super continent Gondwana during the Late Proterozoic. This lasted until the end of the Palaeozoic, when it came to form part of Pangaea (de Wit and Ransome, 1992). These Karoo-aged basins were formed during a first order cycle of supercontinent assembly and subsequent breakup when Pangaea was under the influence of convergent and divergent tectonic regimes, from the southern and northern margins of Gondwana respectively (Rust, 1975; Bumby and Guiraud, 2005; Catuneanu et al., 2005). The basin-forming processes were also induced by two major forces: 1) Initial glacial erosion and isostatic depression which continued in intracratonic rift systems such as the Karasburg and Aranos basins or, by the formation of an early retro-arc foreland basin in the Main Karoo Basin (Fig. 1.4**)** (Catuneanu et al., 1998) and 2) A period of erosion in the interior of southern Gondwana which lasted until the Late Palaeozoic, with some exceptions at the southern margin.

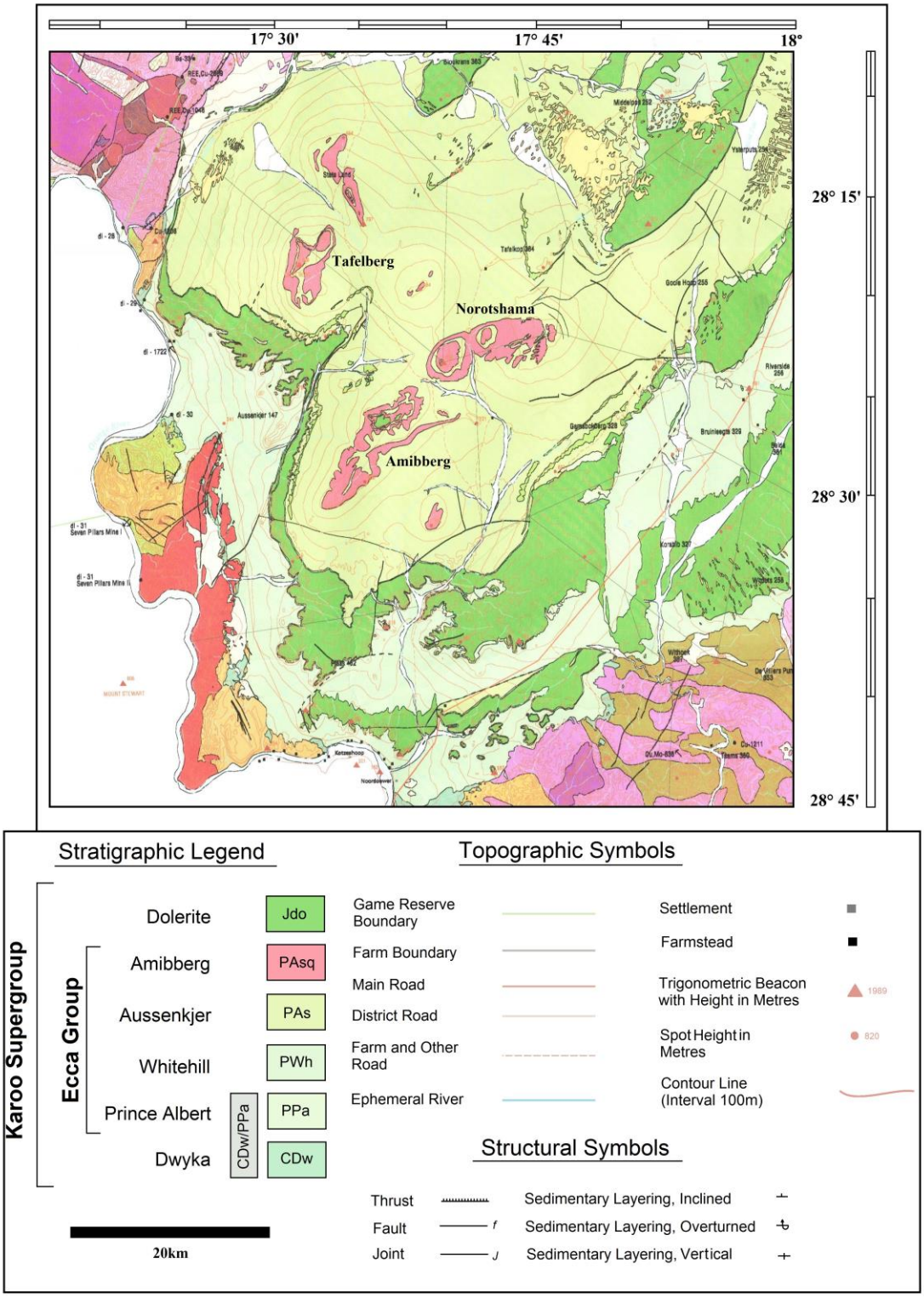


Figure 1.3. Detailed geological map showing Karoo Supergroup lithologies and outcrop localities. This map corresponds to the close-up satellite image of the study area from Fig. 1.2. (adapted from the Geological Survey of Namibia, 1999).

Sedimentation resumed in the Early Carboniferous in numerous basins depositing strata at various time scales (Visser, 1987). A brief summary of the tectonic stresses

at work during basin formation will be given below as a more detailed section is outside of the scope of this work.

Oceanic crust was subducted under the southern margin of the Gondwanan supercontinent at the Samfrau subduction zone (Fig. 1.4). This occurred during the Late Palaeozoic and the Jurassic. During this process a magmatic arc formed to the south of Gondwana and numerous mountainous highlands developed (Werner, 2006). At the southern margin of Gondwana a retroarc foreland system developed due to convergence and associated orogenic processes, and other peripheral basins formed further to the north (Catuneanu et al, 2005). Orogenic loading led to subsidence in the retroarc foreland basin and partitioned the Karoo foreland system into a foredeep, forebulge and backbulge (Catuneanu et al, 2005). Later, accommodation space was created due to dynamic subsidence whereby the subducting plate was influenced by the drag force of viscous mantle corner flow (Pysklywec & Mitrovica, 1999).

Extensional and transtensional tectonic stresses led to the formation of several African Karoo rift basins north of the Main Karoo Basin (e.g. Ruhuhu and Luangwa Basins) as well as the sag basins to the west (e.g. Karoo basins of Angola and the Paraná Basin)(Werner, 2006). The eastern basin region developed a complex set of rift systems and similar lithofacies successions in these rift basins indicate that they evolved due to comparable tectonic forces (Catuneanu et al., 2005). These linear, east African type basins are interpreted to have developed by fracturing over mainly Proterozoic fold belts (Wopfner, 1993; Wopfner, 1994), similar to the formative processes of extensional basins in Namibia. The western region basins are interpreted as sag basins that developed in depressions formed due to rifting during the pre-opening history of the Atlantic Ocean (Fig. 1.5) (Catuneanu et al., 2005). The origin of these western Karoo sag basins may be related to the release of heat subsequent to the formation of the Karoo rift basins of eastern Africa (Veevers et al., 1994a; Veeves et al., 1994b and Veevers et al., 1994c) and these basins represent much quieter tectonic environments compared to the eastern rift basins, and exhibited slower subsidence rates (Catuneanu et al., 2005). These Karoo sag basins were mainly formed over Archaean basements.

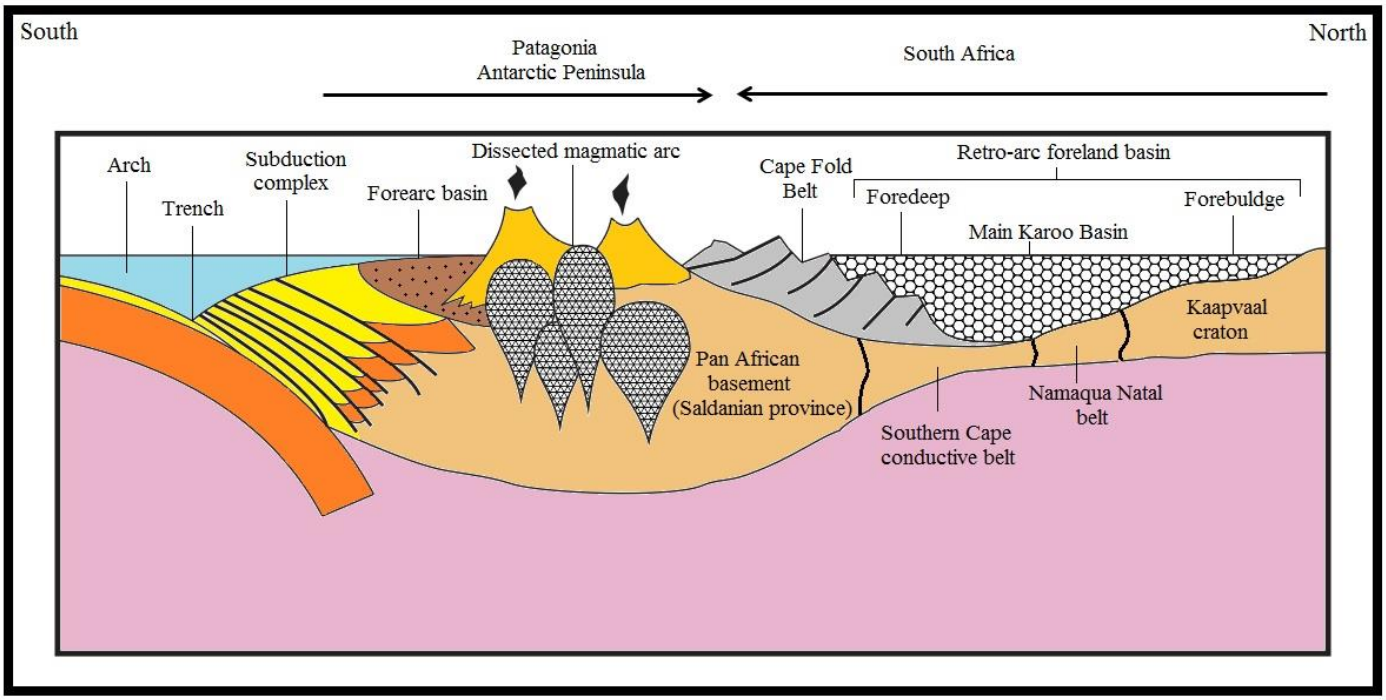


Figure 1.4. Generalised tectonic setting of the Main Karoo Basin during the Late Triassic showing the relationship and proximity of the inferred magmatic arc and subduction zone to the south as well as the Cape Fold Belt (modified after Johnson et al., 1996; Johnson et al., 1997 and Turner, 1999).

1.4.2 Structural Framework and Palaeogeography of the Karasburg Basin

During the Late Carboniferous the Karasburg Basin was surrounded by mountainous, highland regions both to the south and north of the basin. Visser (1983a) shows that ice flow for the Dwyka tillite facies were from the north and east whereas the deltaic units were deposited from the northwest. This indicates that the basin was bounded on at least three sides by mountains (Visser, 1987). The largely E-W striking palaeohigh known as the Cargonian Highland attained an elevation of 2000-2500m to the north and 1500m where it formed a palaeoescarpment to the south (Fig. 1.6) (Visser, 1983a). This extensive continental highland was dissected by numerous river systems which provided sediment input to the west. This input was probably caught by the shallow Ecca interior sea way which acted as a sediment trap and formed due to an aborted rift on the western edge of the craton (Visser and Praekelt, 1996). This sea way represented a body of open water that extended northwards into southwestern Gondwana (Visser, 1983a). Frakes and Crowell (1972) also indicated that open water was needed to provide sufficient moisture for the growth of the ice sheets during the Late Carboniferous and Early Permian. Evidence for this sea way is the presence of

marine fossils in both the Aranos and Karasburg basins (Martin and Wilczewsky, 1970; McLachlan and Anderson, 1973; Pickford, 1995), and the presence of the same fossils in both Namibia and Argentina (Santos et al., 1996). Supporting evidence is also present in corresponding glacial striations from southern Africa and South America.

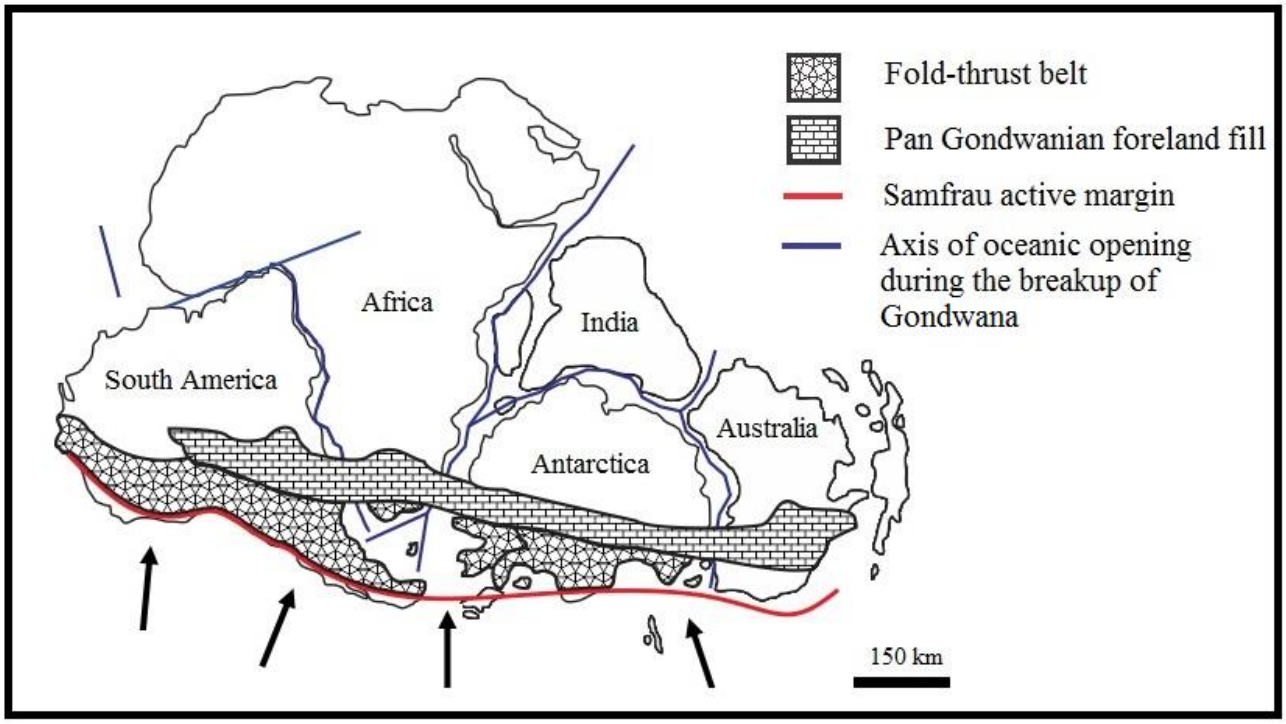


Figure 1.5. Formation and evolution of the Pan-Gondwanan foreland system and associated arc volcanism due to the subduction of the palaeo-Pacific plate at the Samfrau active margin. The distribution of fold and thrust belts and foreland fill are also shown (modified after Stollhofen, 1999 and Catuneanu and Elango, 2001).

The southern Cargonian Highland formed a steep palaeoescarpment with walls standing 500m above mean sea level (Frakes and Crowell, 1972). During the Carboniferous a 3000m thick ice mass expanded westward into the continental interior (Visser, 1987). Subsequent glacial erosion of the Cargonian Highlands may have overdeepened the Karasburg Basin in excess of 1000 m (Frakes and Crowell, 1972). During the deposition of the marine Ecca Group the western part of the Cargonian Highland was probably largely transgressed by the Ecca interior sea way (Werner, 2006). A regressive phase during the deposition of the Ecca Group delivered abundant plant material in tempestitic sediments to the upper Ecca strata in the Karasburg Basin. This required a vegetated land area in the proximity of the basin, probably in the area of the Cargonian Highlands (Werner, 2006). The Ecca interior

sea way facilitated the connectivity of Namibian basins with the Paraná and Sauce Grande basins of South America, with the Uruguay Shield present as a large island (Visser and Praekelt, 1998). During the break-up of Gondwana the Karoo deposits in southwestern Namibia were largely eroded.

The Karoo deposits of the Karasburg and Aranos basins and the Gemsbok Sub-basin were separated from the northerly Namibian Karoo outcrop areas (Huab, Waterberg, Kaokoveld and Owambo basins) by the Windhoek Highland (Fig. 1.6) (Visser, 1983a; Visser, 1983b; Visser 1987; Oelofsen, 1981; Oelofsen and Araújo, 1983). However, during periods of transgression some southerly Ecca Group sediments may have been able to negotiate this highland to connect to more northerly basins (Werner, 2006). The Windhoek Highland consisted of a massive inland plateau which may have extended westwards into South America attaining altitudes of around 3000m above sea level (Visser, 1987). Basement ridges such as the Cargonian and Windhoek highlands would have acted as high points in inter-rift areas and been on the periphery of marine systems that occupied rift basins (Stollhofen et al., 2008).

The WSW-ENE trending Karasburg-Orange fault zone (Stollhofen, 1999; Dingle and Scrutton, 1974) forms a ridge also known as the present day Karas Mountains. It is speculated that a transpressive ridge (Karasburg Ridge) of this type could have separated former contiguous sedimentary environments, for instance the Karasburg Basin from the Aranos Basin (Fig. 1.6). However, the fault patterns from southern Namibian Karoo basins indicated by Visser (1983a) are more closely associated with the Gariep Mobile Belt (Daly et al., 1989; Gresse and Germs, 1993).

During the Late Carboniferous and Early Permian climatic warming resulted in the melting of extensive glaciers and only small ice caps remained along the Cargonian Highlands (Visser, 1983a). This resulted in isostatic rebound in the Windhoek Highland and Karasburg Ridge which facilitated the erosion and reworking of the glacial sediments (Visser, 1983a). Following a prolonged period of climatic warming and the complete melting of ice-sheets regional subsidence cancelled out the effects of isostatic rebound along the western parts of the Cargonian and Windhoek highlands causing the large-scale transgression of these areas (Visser, 1983a). Shorelines of the Ecca interior sea way transgressed up to the palaeo-escarpment along the west coast

of Namibia. This coast-line was very irregular and resulted in linear fjords extending for hundreds of kilometres into the Cargonian Highlands (Martin, 1975; Visser and Kingsley, 1982). The Ecca interior sea way breached these mountainous highlands creating large, partially emergent islands to the north of the Karasburg Basin (Visser, 1983a). This resulted in the progradation of wave-dominated deltas from the west and northwest into the Karasburg Basin. The Ecca interior sea way was shallow with various portions of the basins being deeper at times due to regional transgressions (Oelofsen and Araujo, 1983).

1.4.3 Stratigraphy and Structural Setting of the Karoo Supergroup

It is beyond the scope of this thesis to review extensively the stratigraphy of all areas comprising Karoo Supergroup rocks. However, it is important to have a stratigraphic overview of the Karoo basins that form the backbone of this work.

1.4.3.1 Main Karoo Basin

The Main Karoo Basin covers approximately two thirds of the current land area of South Africa, but was much more extensive during the Permian (Johnson et al., 2006), and represents the most complete stratigraphic profile of Karoo Supergroup rocks in the world. For the purpose of this study the Dwyka and Ecca groups (Fig. 1.7) will be outlined in detail whereas the Beaufort Group, "Stormberg Series" and the Drakensberg Group fall outside of the scope of this work.

The Karoo Supergroup in southern Africa comprises rocks which were deposited successively in glacial, deep marine, shallow marine, deltaic, fluvial, lacustrine and aeolian environments (Johnson et al., 1996). In southern Africa, the Karoo Supergroup comprises five groups: the Late Carboniferous to Early Permian glacial deposits of the basal Dwyka Group followed by the Permian Ecca Group and Middle Permian – Middle Triassic Beaufort Group, followed by the Late Triassic Molteno, Elliot and Clarens formations and finally the Jurassic volcanics of the Drakensberg Group.

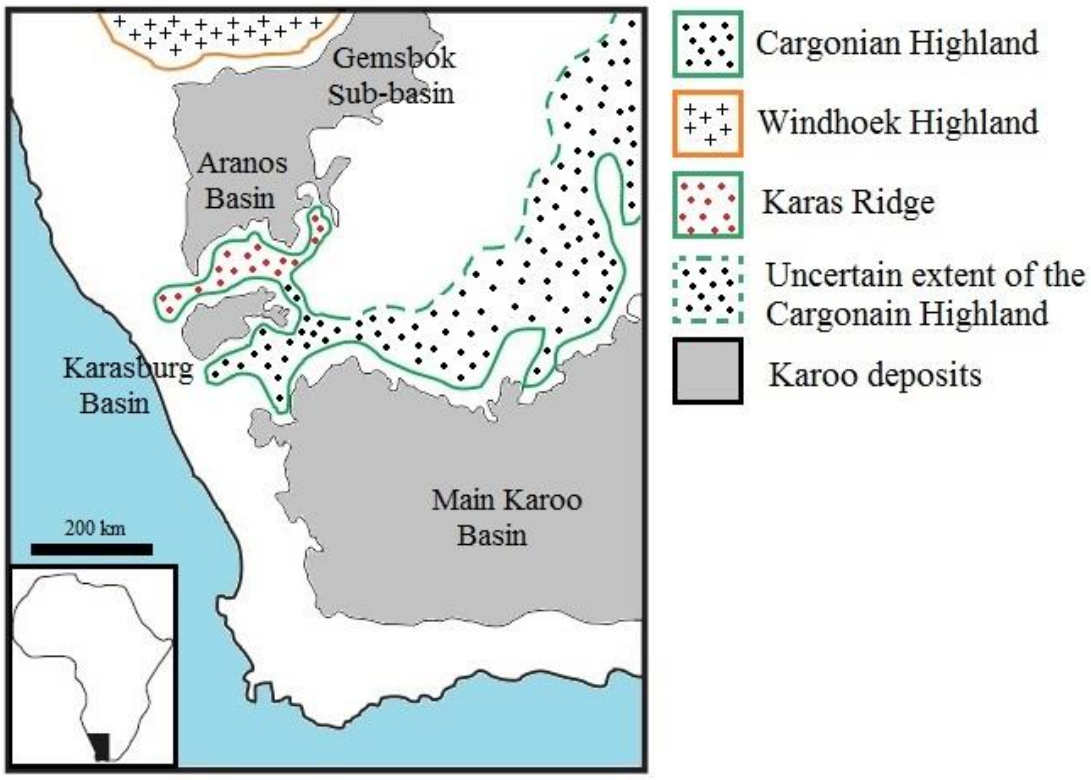


Figure 1.6. Map showing present day Karoo deposits in relation to the inferred position of the Windhoek Highland, Cargonian Highland and Karas/Karasburg Ridge (modified after Visser, 1983a).

1.4.3.1.1 Dwyka Group

The Dwyka Group represents glacially influenced deposits (Fig. 1.7) that accumulated over 10 Ma during the 300–290 Ma interval (Wopfner, 2002; Catuneanu, 2004a) though deposition may have started earlier at about 305 Ma (Visser, 1997; Bangert et al., 1999). Along the northern margin of the Main Karoo Basin these rocks rest on Precambrian bedrock; in the south they unconformably overlie the Cape Supergroup and in the east they unconfomably overlie the Natal Group and Msikaba Formation. These rocks are not wholly homogeneous and a variety of lithofacies types have been identified. The feature that unifies the Dwyka Group is the presence of glacial rafted clasts that have fallen out of suspension and been incorporated into the sediments. Visser (1987) recognized two distinct facies based on lithological differences. The northern facies is the Mbizane Formation that varies in thickness and has a high mudrock content and a low percentage of massive diamictite (~20%). These rocks are interpreted as representing predominantly valley-fill accumulations as a result of increased warming and glacial retreat (Visser, 1983). The southern facies is the Elandsvlei Formation which has uniform thickness as well as low mudrock content and a high percentage of massive diamictite (~70%).

1.4.3.1.2 Ecca Group

Rubidge (1858) was the first to propose the term ‘‘Ecca’’ for the sedimentary rocks exposed near Grahamstown, South Africa. The Ecca Group attains a maximum thickness (3000m) in the southern part of the Main Karoo Basin, whereas elsewhere in southern Africa it is considerably thinner (Catuneanu et al., 2005). The lithostratigraphic subdivisions of the Ecca Group in southern Africa are depicted in Fig. 1.7.

After de-glaciation of the Dwyka Group there was a subsequent sea-level rise due to the melting of ice sheets (Visser, 1991). This formed a large and extensive shallow marine environment, represented by basal Ecca Group marine shales of the Prince Albert and Whitehill formations (Visser, 1992) which are the only fairly extensive formations in the Ecca Group and are preserved throughout most of the Main Karoo Basin. The overlying formations are best grouped according to their location in the Main Karoo Basin. For this reason, in terms of the Ecca Group, the Main Karoo Basin is divided into three distinct lithological areas (Fig. 1.7). These are the Tanqua and Laingsburg sub-basins and a Karoo outcrop area in the north and north-eastern part of the basin.

In terms of the Tanqua Sub-basin, the formations present are the Prince Albert and Whitehill formations mentioned above, as well as the: (1) Collingham Formation composed of interlaminated tuffaceous siltstones and mudstones interpreted as being deposited out of suspension in relatively deep water (Johnson et al., 2006); (2) Tierberg Formation dominated by mudstones and interpreted as fluvially-dominated prodelta to distal delta-front deposited during regression in a relatively shallow water environment (Johnson et al., 2006); (3) Skoorsteenberg Formation containing sand-rich turbidites interbedded with mudstones deposited by a submarine fan complex (Wickens, 1994; Wickens, 1996); (4) Kookfontein Formation comprising pro-delta and delta-front mudstones and sandstones (Wickens, 1996); (5) Waterford Formation which consists of alternating layers of sandstone and mudrock with abundant soft-sediment deformation features. This is interpreted as being deposited in relatively shallow water at a steeply inclined delta-front (Johnson et al., 2006).

The formations present in the Laingsburg Sub-basin are the Prince Albert, Whitehill and Collingham formations mentioned previously as well as the: (1) Vischkuil Formation consisting of dark shales alternating with subordinate sandstones, siltstones and tuff layers. The nature of the sediments points towards deposition by gravity driven mechanisms with suspension of mud in a basin-plain to outer basin-floor fan environment during a time of seismic activity (Johnson et al., 2006); (2) Laingsburg Formation comprising four sandstone-rich intervals separated by shale units and interpreted as being deposited by submarine fans (Wickens, 1994; Wickens, 1996); (3) Fort Brown Formation which consists of upward coarsening rhythmite and mudrock with minor sandstone. This formation resembles modern day prodelta and distal delta-front deposits (Johnson, 1976); (4) Waterford Formation which comprises alternating very fine-grained lithofeldspathic sandstones, mudrocks and clastic rhythmite units deposited in relatively shallow water conditions (Johnson et al., 2006).

The coal rich north and northeastern part of the Main Karoo Basin contains the following formations: the (1) Pietermaritzburg Formation which comprises coarsening upward dark silty mudrock which records a major postglacial transgression in relatively shallow water on an unstable shelf (Johnson et al., 2006); the (2) Vryheid Formation which is composed of upward coarsening cycles of sandstones and siltstones deposited in a deltaic setting. This formation hosts most of South Africa's coal deposits which were formed in a swamp environment on alluvial plains and coal deposits which were formed in a swamp environment on alluvial plains and backswamps (Johnson et al., 2006); the (3) Volksrust Formation which is made up of black-grey silty shale with bioturbated sandstone or siltstone lenses. It is interpreted as being deposited in a lacustrine to possibly lagoonal and shallow coastal embayment environment (Tavener-Smith et al., 1988).

Assigning age constraints to the Ecca Group is difficult and most age determinations and correlations rely on fossil wood biostratigraphy (Bamford, 2000) and palynology. Radiometric dates have been determined from tuff beds from both the Dwyka Group

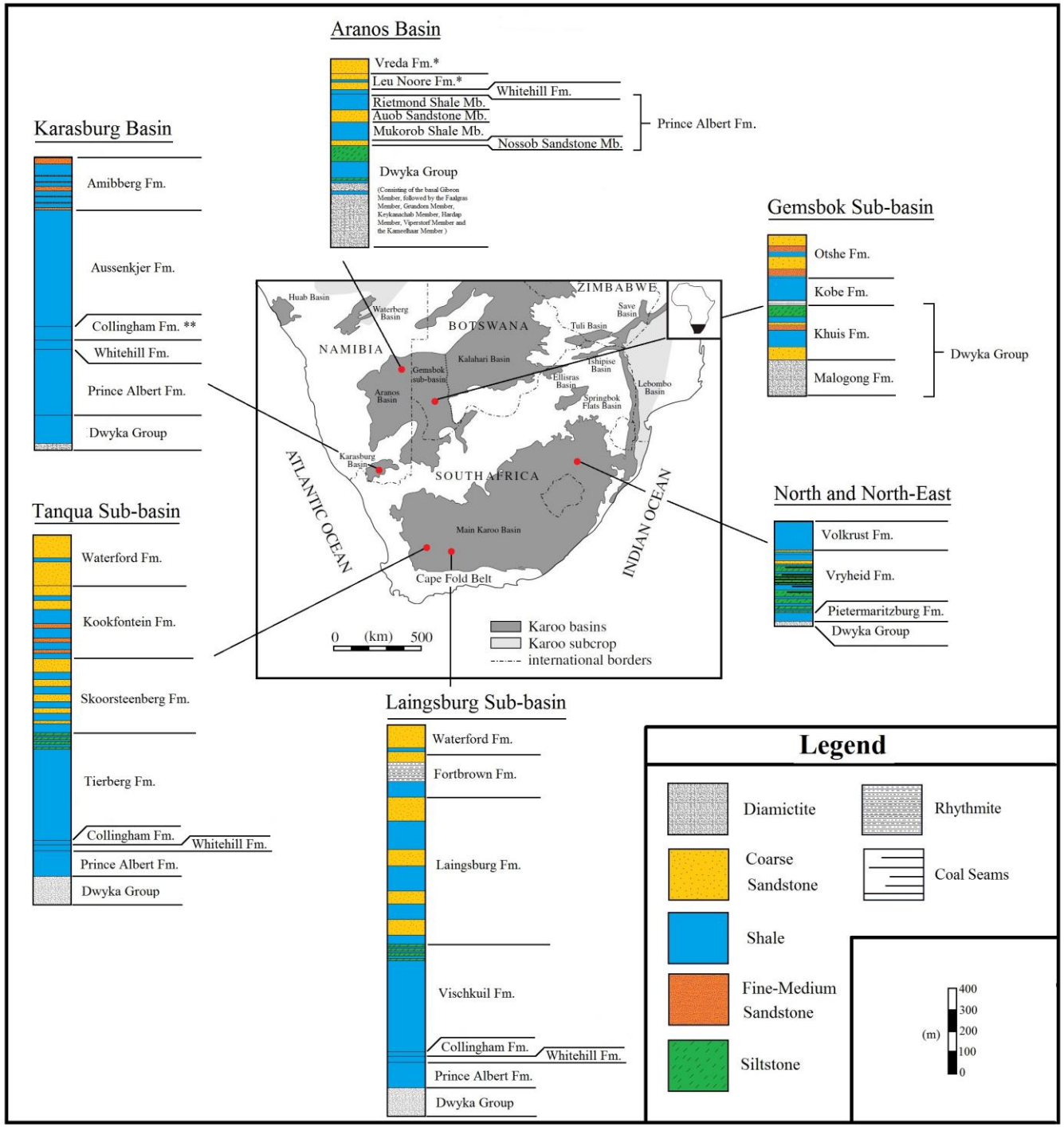


Figure 1.7. Idealised stratigraphic sections through each basin/sub-basin of interest showing both the Dwyka and Ecca stratigraphies (modified after Johnson et al., 1996; Nxumalo, 2011; and Werner, 2006). The location of each section is displayed on a map of southern Africa. * - denotes a formation with an unknown thickness. **- denotes a formation which may not actually be present in the basin. Note that thickness of formations may vary within a given basin.

and the lower Ecca Group strata. These ages determined for the Namibian Dwyka, and for the Prince Albert Formation by Bangert et al. (1999) are similar to the 290 Ma age inferred from palynomorphs (Loock and Visser, 1985; MacRae, 1988; Visser, 1990).

1.4.3.1.3 Beaufort Group

The term Beaufort ‘‘Beds’’ was first introduced in the late 1800's (quoted in North, 1878) for sedimentary rocks near Beaufort West, South Africa, and now includes a wide range of fluvially deposited Permo-Triassic strata. The Beaufort Group is divided into the Adelaide and Tarkastad Subgroups. Sandstones in these subgroups are often interpreted as being channelised deposits whereas mudstones represent overbank deposits that settled out of suspension (Johnson et al., 2006). This whole group is classified as being deposited in fluvio-lacustrine setting.

1.4.3.1.4 "Stormberg Series"

Rocks of the Beaufort Group are in turn overlain by the informally named "Stormberg Series" which consists of the Late Triassic Molteno Formation which was deposited under seasonally warm to humid climatic conditions, in a broad, perennial braided system associated with braidplain areas of limited extent (Hancox, 2000; Bordy et al., 2005; Bumby and Guiraud, 2005). In contrast, the overlying argillaceous Elliot Formation was deposited by high and low sinuosity fluvial systems under semi-arid climatic conditions (Hancox, 2000; Bordy et al., 2005). Progressive aridification led to the deposition of aeolian dune complexes of the Clarens Formation (Smith et al., 1993; Johnson et al., 2006).

1.4.3.1.5 Drakensberg Group

The 1370m thick Drakensberg Group reflects volcanism and fissure-type eruptions of basaltic lava during and preceding continental breakup. This group is associated with numerous dolerite dykes and sills, as well as diatremes and vents present in southern Africa (du Toit, 1954; Bristow and Saggerson, 1983; Van Rooy, 1991). Recent age determinations (Marsh et al., 1997; Duncan et al., 1997; Marsh, 2002) indicate that

the entire Drakensberg Group was formed in a very short time interval at 193 Ma. This outpouring of these rocks terminated the sedimentary deposition in the Main Karoo Basins.

1.4.3.2 Karasburg Basin

The basement of the Karasburg Basin consists of Late Precambrian and Cambrian sediments of the Nama Group (Martin, 1981a) as well as rocks of the Orange River Group and older granite gneisses. Glacial erosion produced a hiatus from the Late Proterozoic to the Late Carboniferous. Grooves and scars give a fluctuation of directions but have a dominant north-south trend and indicate the direction of palaeoice flow (Frakes and Crowell, 1970). During the Late Carboniferous to Late Permian the basin was filled, in sequence, with glacial deposits of the Dwyka Group (Fig. 1.7) followed by the Prince Albert, Whitehill, Aussenkjer and Amibberg formations of the Ecca Group (Fig. 1.7). A brief summary of lithostratigraphic and chronostratigraphic details will be given below for each of the groups/formations present within the Karasburg Basin.

Above the older basement rocks the glacial to glacio-marine deposits of the Dwyka Group are present and include two distinct facies, the Dwyka tillite and the Dwyka shale. The Dwyka-Ecca boundary between the glaciogenic Dwyka Group and the post-glacial Prince Albert Formation is not sharp or distinct, but variable because the vertical extent of the Dwyka is based on the presence of dropstones throughout the stratigraphy. For this reason it is difficult to assign a thickness to the entire Dwyka Group in the Karasburg Basin.

The post-glacial Prince Albert Formation consists predominantly of basinal shales with minor intercalation of pyroclastic tuff layers. No sandstone occurs in this formation but it does get progressively coarser in uppermost parts of the formation. Above this is the marine Whitehill Formation consisting almost entirely of white weathering, black carbonaceous shales with abundant fossils present. The thickness of the Whitehill Formation varies and is in the region of 40-45m (Werner, 2006). A major dolerite sill, continuous throughout the Karasburg Basin has intruded the uppermost part of the Whitehill Formation (Werner, 2006). The Whitehill in this

outcrop area shows a remarkable correlation with the Main Karoo Basin based on the presence of *Mesosaurus* fossils and can be considered the only synchronous unit in the Karoo Supergroup (Oelofsen, 1981). Conformably overlying the Whitehill Formation is the Aussenkjer Formation (SACS, 1980; Miller, 1992). Earlier researchers (Schreuder and Genis, 1975) failed to recognize the pyroclastic tuff layers and numerous chert-like horizons in the basal 75m of post-Whitehill shales, which were found by Werner (2006), who regarded them as strong evidence for the correlation with the Collingham Formation. The stratigraphic position of the Aussenkjer and Amibberg Formations is not yet sufficiently understood and has only been poorly investigated previously (Werner, 2006). The Aussenkjer Formation conformably overlies the Collingham Formation and has a rather poorly defined thickness of between 400m and 620m. This formation consists predominantly of marine shales with rare sandstone bodies present. The uppermost formation present in the Karasburg Basin is the Amibberg Formation which consists of three major sandstone "packages" separated by shale-dominated intervals which have been interpreted as being representative of a wave-dominated shoreline (Werner, 2006).

1.4.3.3 Aranos Basin

The Aranos Basin forms part of the larger Kalahari Basin and Gemsbok Sub-basin and extends from southeastern Namibia eastward into southwest Botswana. It is filled by Karoo Supergroup rocks that cover an area of approximately 80,000 km^2. Most of the Karoo rocks are covered by Cenozoic Kalahari Group sediments that can be up to 250m thick, but some Karoo Supergroup rocks outcrop along the northern, western and southern margins of the basin (Miller, 2008). Much of what is known about the Aranos Basin comes from field observations at outcrop scale in an area between Keetmanshoop and Mariental, and from boreholes drilled for coal exploration during the early 1980's (Kingsley, 1985; Hegenberger, 1992) in areas where outcrop in heavily overlain by the Cenozoic Kalahari Group.

The basement of the Aranos Basin consists of shales and quartzites of the Cambrian Nama Group which is unconformably overlain by the Dwyka Group. The glaciogenic Dwyka Group (Fig. 1.7) consists of a basal diamictite overlain by a succession of glacio-marine mudstones that contain dropstones and a variety of fossil remains such

as starfish, bivalves, crinoid remains and gastropods (Hegenberger, 1992; Cairncross, 2001) and attains a thickness of up to 460m (Nxumalo, 2011). Glacial striations in the Aranos Basin give an indication of two main directions of ice flow. One direction indicates flow towards S-SSW, the other towards WSW-SW (Wagner, 1915; du Toit, 1921; Frakes and Crowell, 1970; Martin and Wilczweski, 1970; Heath, 1972; Stratten, 1977; Schalk and Germs, 1980; Visser, 1983a; Genis and Schalk, 1984). These different directions were interpreted to originate from two different ice centres. The Dwyka Group can be further subdivided into the basal Gibeon Member, followed by the Faalgras Member, Grundorn Member, Keykanachab Member, Hardap Member, Viperstorf Member and the Kameelhaar Member as per Johnson et al., (1996).

The Ecca Group (Fig. 1.7) consists of the Nossob, Mukorob, Auob, and Rietmond members as well as the uppermost Neu Loore and Vreda formations (Miller, 2005; Miller, 2008). These collectively attain a maximum thickness of 1200m (Kingsley, 1985). The shallow-water Prince Albert Formation incorporates the arenaceous lower Nossob Member (between 6m and 15 m in thickness and consisting of two upward coarsening sandstone units with an intercalated shale zone), the overlying shaley Mukorob Member (consisting of 75m to 160m dark greenish-grey shale) and the uppermost sandstone-rich Auob Member(between 100m and 150m thick, comprising coal seams and upward-coarsening deltaic sequences of medium-coarse grained, micaceous, sandstone with local intercalations of sandy shale) (Miller, 2005; Miller, 2008). The Auob Member is overlain by the Rietmond Member (Miller, 2008) and is dominated by laminated dark grey shale with minor thin sandstone bands. The Rietmond Member is interpreted to have been deposited during a major transgression over the entire Aranos Basin (Miller, 2008) and although the Rietmond shales were assigned in the past to the Prince Albert Formation, newer observations by Werner et al., (2002) indicate that these shales actually represent lateral equivalents of the lower part of the Whitehill Formation. The Whitehill Formation which is well developed in the southwestern part of the basin consists mainly of dark carbonaceous shale and mudstone (Cairncross, 2001; Miller, 2008). Fossils such as *Mesosaurus tenuidens*, a small crustacean *Notocaris tapscotti*, *Eurydesma mytloides*, *Glossopteris* leaves and petrified wood have been found in the Whitehill Formation (Miller, 2008).

A major unconformity separates the Rietmond Formation from the Neu Loore Formation, the latter of which comprises alternating coarse- to fine-grained, orange-red to orange-brown micaceous sandstones and shales (Miller, 2005). This is overlain by sandstones and minor shales assigned to the Vreda Formation. The Karoo Supergroup in the Aranos Basin is capped by basalts of the Kalkrand Formation and associated dolerite sills have extensively intruded the sequence, particularly the upper part of the Auob Member (Hegenberger, 1992; Miller, 1992; Cairncross, 2001; Miller, 2008). The Beaufort Group equivalent sedimentary rocks have not been recognised in the Aranos Basin although sedimentary units interbedded with the Kalkrand basalts contain large amounts of well-rounded Aeolian quartz grains (Miller, 2008).

1.4.3.4 Gemsbok Sub-basin

Smith (1984) spatially sub-divided the Karoo Supergroup in Botswana, along with the Tuli Basin (Zimbabwe and South Africa), into seven sub-divisions based on geological setting and facies changes. These are: (1) western, (2) southeast, (3) southern and (4) northern belts of the Central Kalahari Sub-basin together with (5) southwest Botswana; (6) northeast Botswana and (7) northwest Botswana. Subtle lithostratigraphic differences were documented in each of these sub-divisions. For the purpose of this study, only the south-western portion of the Kalahari Karoo Basin will be outlined in detail as this is important due to its proximity and apparent connectivity to the Aranos Basin in southeast Namibia. This sub-basin is commonly referred to as the Gemsbok Sub-basin and extends south and west into South Africa and Namibia respectively (Smith, 1984).

Much of the Gemsbok Sub-basin is covered by Cenozoic Kalahari Group sediments and therefore the knowledge we have of the basins stratigraphy has been obtained by aeromagnetic surveys, seismic data and stratigraphic boreholes (Reeves, 1978; Smith, 1984; Exploration Consultants Limited, 1998).

The Karoo Supergroup in the Gemsbok Sub-basin is subdivided into the basal Dwyka Group, followed by the Ecca and Beaufort group equivalents as well as the upper Stormberg Group (Smith, 1984; Key et al., 1998; Modie, 2007).

The glaciogenic Dwyka Group (Fig. 1.7) consists of basal massive tillite units of the Malogong Formation which is 183m thick. Overlying the Malogong Formation is the Khuis Formation, a 202m thick sequence consisting of pebbly mudstones, black to grey shales, calcareous sandstone, banded calcareous siltstone, varves, and siltstone (Smith, 1984; Carney et al., 1994; Exploration Consultants Limited, 1998).

The shallow marine deposits of the Ecca Group consists of the lower Kobe Formation characterised by massive, argillaceous, dark grey siltstones up to 75m thick. The Kobe Formation also contains thin lenses of sandstones, silty mudstones, and a few bands of bright coal. *Eurydesma* (a shallow marine bivalve) is present in the siltstones of this unit (Smith, 1984; Exploration Consultants Limited, 1998). Conformably overlying these sediments is the 218m thick Otshe Formation (Smith, 1984; Exploration Consultants Limited, 1998). It is dominated by micaceous, fine-grained sandstones interbedded with dark grey siltstones, coal, sub-arkosic sandstones with dark grey siltstones and mudstones in an upward-fining sequence.

The Kule Formation has only been recognised in boreholes drilled in an area of southwest Botswana and is considered the equivalent of the Beaufort Group in the Main Karoo Basin (Smith, 1984; Exploration Consultants Limited, 1998; Key et al., 1998). This formation consists of a basal fine-grained sandstone of approximately 15m in thickness, grading into dark grey mudstone, up to 25m thick, with subordinate sideritic and limonitic banded siltstones. A diachronous unconformity separates the Lebung Group from the underlying Kule or Otshe formations (Smith, 1984). The Lebung Group is divided into two formations. The 9m thick Dondong Formation which consists of conglomeratic sandstone grading into an upper, 4m thick red-brown mudstone, is considered to have been formed in a fluvial environment (Smith, 1984; Bordy et al., 2010). This is overlain by the arenaceous Nkalatlou Sandstone Formation which is an equivalent of the Clarens Formation in the Main Karoo Basin of South Africa (Smith, 1984; Bordy et al., 2010). Overall, the Lebung Group consists mainly of red clastics that were deposited under oxidizing continental conditions (Smith, 1984).

The overlying Stormberg Lava Group is correlated with the Drakensberg Group of the Main Karoo Basin in South Africa. It represents the youngest unit of the Karoo

sequence in southwest Botswana and consists of volcanic rocks such as finely crystalline dark grey, black, brown or purple amygdaloidal or massive basalts (Carney et al., 1994).

1.4.4 Stratigraphic Correlation

The generalised stratigraphic columns of sedimentary successions of the Karoo basins in south-central Africa and their large-scale correlations are illustrated in Fig. 1.8. Individual formation thickness and gross lithology are also depicted in Fig. 1.8. Fig. 1.8 consists of a generally north-south trending section through the Laingsburg and Tanqua sub-basins of the Main Karoo Basin and ending in the Aranos Basin in northern Namibia as well as a southwest-northeast section extending from the Aranos Basin to the Gemsbok Sub-basin in southwest Botswana. Only the Main Karoo, Aranos and Karasburg basins, as well as the Gemsbok Sub-basin, have been used for this correlation as the other basins outlined previously have little value to a stratigraphic correlation with the other basins and sub-basins.

The Dwyka Group is up to 800m thick in the Main Karoo Basin and consists of the northern Mbizane Formation and a southern Elandsvlei Formation (Visser, 1990). This group consists of various rock types displaying features reflecting a glacial or glacio-marine related origin. In the Aranos Basin, the Dwyka Formation has been subdivided into seven members (SACS, 1980) and can be correlated with the Malogong and Khuis formations in southwest Botswana (Smith, 1984; Key et al., 1998). Dwyka Group deposition occurred from the Late Carboniferous to the Early Permian in all basins and sub-basins.

The entire Ecca Group was deposited from the Early Permian to the Late Permian. In the Main Karoo Basin, the Prince Albert Formation, which overlies the Dwyka Group, consists essentially of mudrock. However, in the Aranos Basin of Namibia, two prominent sandstone members occur in this interval. The Whitehill Formation consists of black (white weathering) carbonaceous shale, which is significantly different in character from the underlying and overlying shale units in the most Karoo aged basins. The age of the Whitehill Formation has been variously dated as Late

Sakmarian (Oelofsen and Araujo, 1987), late Kungurian to early Ufimian (Visser, 1990; Visser, 1992) or late Kazanian (MacRae, 1992).

For the uppermost formations in the Karasburg Basin a variety of different correlations have been put forward: for example, the Aussenkjer Formation is believed to have a more appropriate correlation with the Tierberg Formation of the Main Karoo Basin (Johnson et al., 1997). The uppermost formation present in the Karasburg Basin is the Amibberg Formation which has is considered to correlate to the Waterford Formation (Johnson et al., 1996).

The Nossob Member at the base of the Ecca Group in the Aranos Basin has been interpreted to be equivalent to the Ncojane Sandstone Member at the base of the Kobe Formation in southwest Botswana (Smith, 1984). The Kobe Formation and Mukorob Member were correlated based on character similarities they share that represent deposition by similar sedimentary processes (Smith, 1984). Overlying these are the Otshe Formation and the Auob Member, respectively. Faulting makes the correlation of the Otshe Formation in southwest Botswana difficult (Miller, 2008). However, the uppermost part of the Otshe Formation may correlate with much of the Auob Member.

Due to the relative absence of macrofossil palaeontological records in the Dwyka and Ecca groups, assigning an age and correlation to the Karoo formations in the subsidiary basins to the north of the Main Karoo Basin is in most cases based on correlations with corresponding units in the main basin. The chronostratigraphic interpretation of formations from various basins is not unequivocal, however, and a regional synthesis of the available data needs to be undertaken (Johnson et al., 1996).

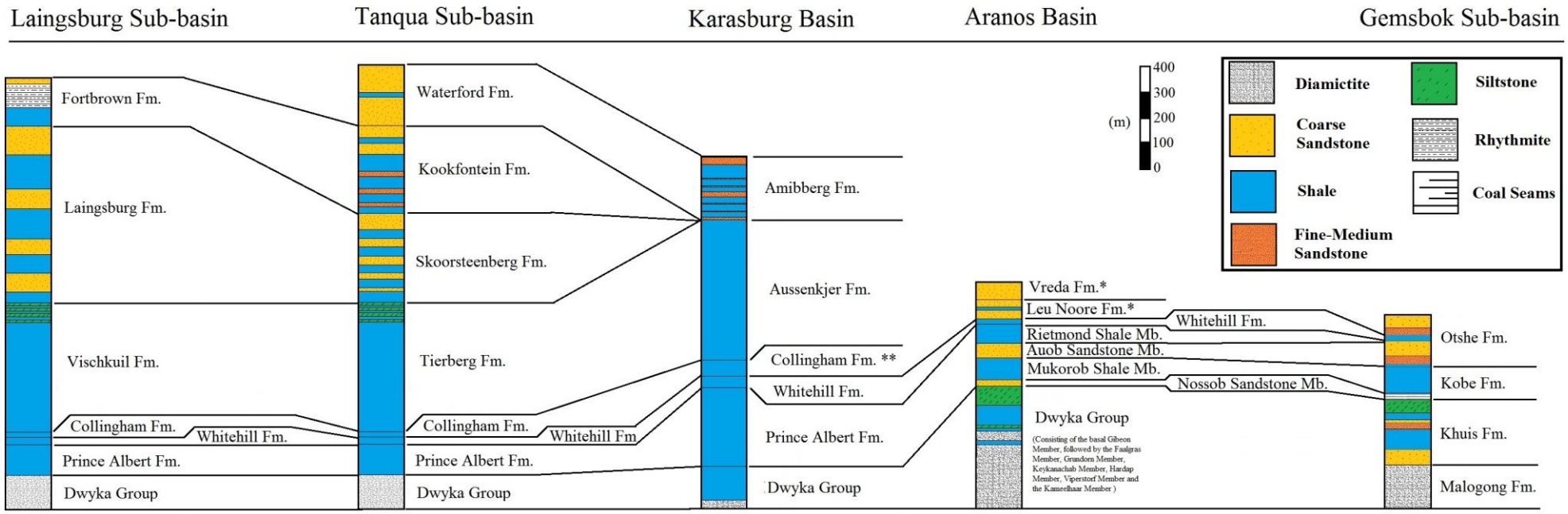


Figure 1.8. Correlation panel showing lithological and stratigraphic data from the Main Karoo Basin (western foredeep), Karasburg, Aranos and Gemsbok basins (modified after Johnson et al. 1996).

1.5. Hypotheses

1. **The Karasburg Basin and Aranos Basin were connected at the time of deposition, and the Karasburg Basin contains a more distal set of palaeoenvironments than the Aranos Basin.**

   Palaeotransport indicators and Karoo Supergroup lithologies do not indicate an obvious structural separation between the Aranos and Karasburg basins. Fossil remains also indicate that the Main Karoo Basin and Karasburg Basin were at least partially connected during the Permian. The environmental variability across the Aranos - Karasburg - Main Karoo basins will be investigated using data from facies analysis, sequence stratigraphy and provenance studies.

2. **The Amibberg Formation correlates to the Waterford Formation in the Main Karoo Basin.**

   The Amibberg Formation in the Karasburg Basin has been equated with various formations in the Main Karoo Basin. Lithostratigraphy and sequence stratigraphy will be used to provide a concrete stratigraphic correlation between the Amibberg Formation and its equivalents in the Main Karoo Basin.

3. **The western Cargonian Highland was subaerial during deposition of the Amibberg Formation, and acted as a major sediment source in the Karasburg Basin.**

   Lithofacies analysis, provenance, and shoreline orientation will be used investigate the nature of the Cargonian Highland and the role it played in the separation of the Karasburg Basin from the Main Karoo Basin.

Chapter 2: Facies and Palaeoenvironmental Reconstruction

2.1 Introduction

This chapter presents detailed lithological and sedimentological descriptions of the Amibberg Formation. No previous studies of the Permian Amibberg Formation have dealt with the problems of interpreting depositional environments by using an integrated high-resolution facies analysis and stratigraphic approach. The excellent exposure provides a perfect location for detailed stratigraphic logging, and tracing major and minor lithologies along strike. This provides an ideal starting point to reconstruct the depositional environment for the Amibberg Formation.

2.2 Aims

The aim of this chapter is to present detailed sedimentological work which is then used to reconstruct the palaeoenvironmental conditions in which the Amibberg Formation was deposited. This detailed understanding of the depositional environment provides the framework for petrographic, palaeogeographic and sequence stratigraphic work in the following chapters.

2.3 Previous work

As mentioned previously (in Chapter 1) recent, detailed studies conducted on the Amibberg Formation are limited to the work done by Werner (2006). This study focused on geochronological dating of tuff horizons found in the lower Ecca Group strata in the Karasburg Basin. However, this work did present sedimentological and stratigraphic data as well as brief interpretations of depositional environment for the Amibberg Formation. Yet, it lacked a detailed systematic facies-based approach which is provided here.

2.4 Methods

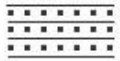
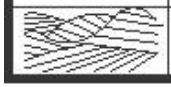
Field work involved the measuring of detailed stratigraphic columns through the Amibberg Formation using a Brunton transit compass and a Jacob Staff.
Field measurements include descriptions of rock type, grain size, shape and sorting, sedimentary structures, trace fossils and palaeocurrent data. A total of 5 measured stratigraphic (Fig. 2.1-2.5) columns totalling 582.5m (Table 2.1) coupled with detailed photo mosaics were used to map changes in the lithology, structure and geometry within the formation. Photomosaics were taken to assist physical correlations across large distances, thus permitting three-dimensional reconstructions.

Seven lithofacies were then identified and characterised on the basis of lithology, physical sedimentary structures, bed contacts and ichnological data. Facies interpretations are constrained by lateral and vertical facies relationships, which are continuously exposed over tens of kilometres along strike.

Table 2.1. Thickness and locations of the 5 measured stratigraphic columns in the study area (* denotes unofficial names of locality).

Column Name	Column Thickness (m)	Column GPS Co-ordinates (decimal degrees)	
		Latitude:	Longitude:
Dickneus (Fig. 2.1)	86m	-28.494036	17.554648
Northern Amibberg (Fig. 2.2)	126m	-28. 419178	17. 590207
Tafelberg (Fig. 2.3)	126.5m	-28.299315	17.527697
Norotshama (Fig. 2.4)	132.5m	-28.385883	17.66795
Platberg* (Fig. 2.5)	111.5m	-28.281094	17.560361

Lithology and Structures

	**Mudstone**
	**Sandstone**
	**Interbedded**
	**Siltstone**
	Nodule Horizon
	**Bioturbation**
	**SSD**
	**Wave Ripple**
	**Planar Lamination**
	**Interbedded**
	**HCS**

Abbreviations

WR	Wave Ripples
LB	Lenticular Bedding
FB	Flaser Bedding
DW	Dewatering Structures
CV	Convoluted Bedding
Pll	Planar Laminations
AWR	Asymmetrical Wave Ripples
CR	Climbing Ripples
FS	Fish Scales
ThB	Thinly Bedded
TB	Thickly Bedded

Trace Fossil Abbreviations

Py	*Pycodes*	*Mo*	*Monocraterion*
Coch	*Cochlictnus*	*Ar*	*Arencolites*
Ast	*Asterecites*	*As*	*Asterosoma*
Pl	*Planolites*		
Sk	*Skolithos*		
Pph	*Palaeophycus*		
Pd	*Paleodictyon*		
Cr	*Crosopodia*		
Sc	*Schaublichtnus*		
Hl	*Helminotropsis*		
Th	*Thalassinoides*		

Table 2.2. Legend for corresponding stratigraphic columns on pages 30-34.

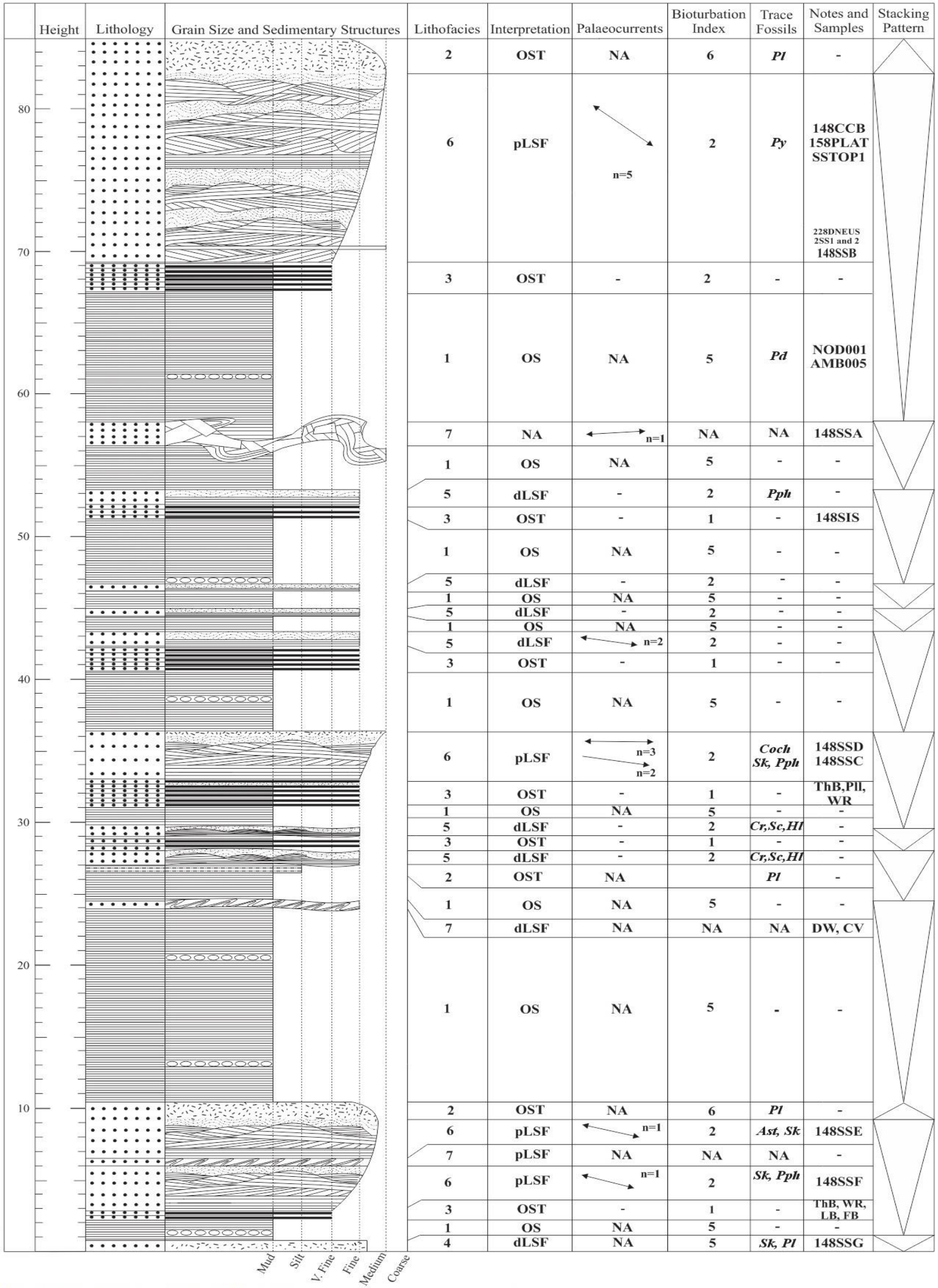


Figure 2.1. Dickneus stratigraphic column.

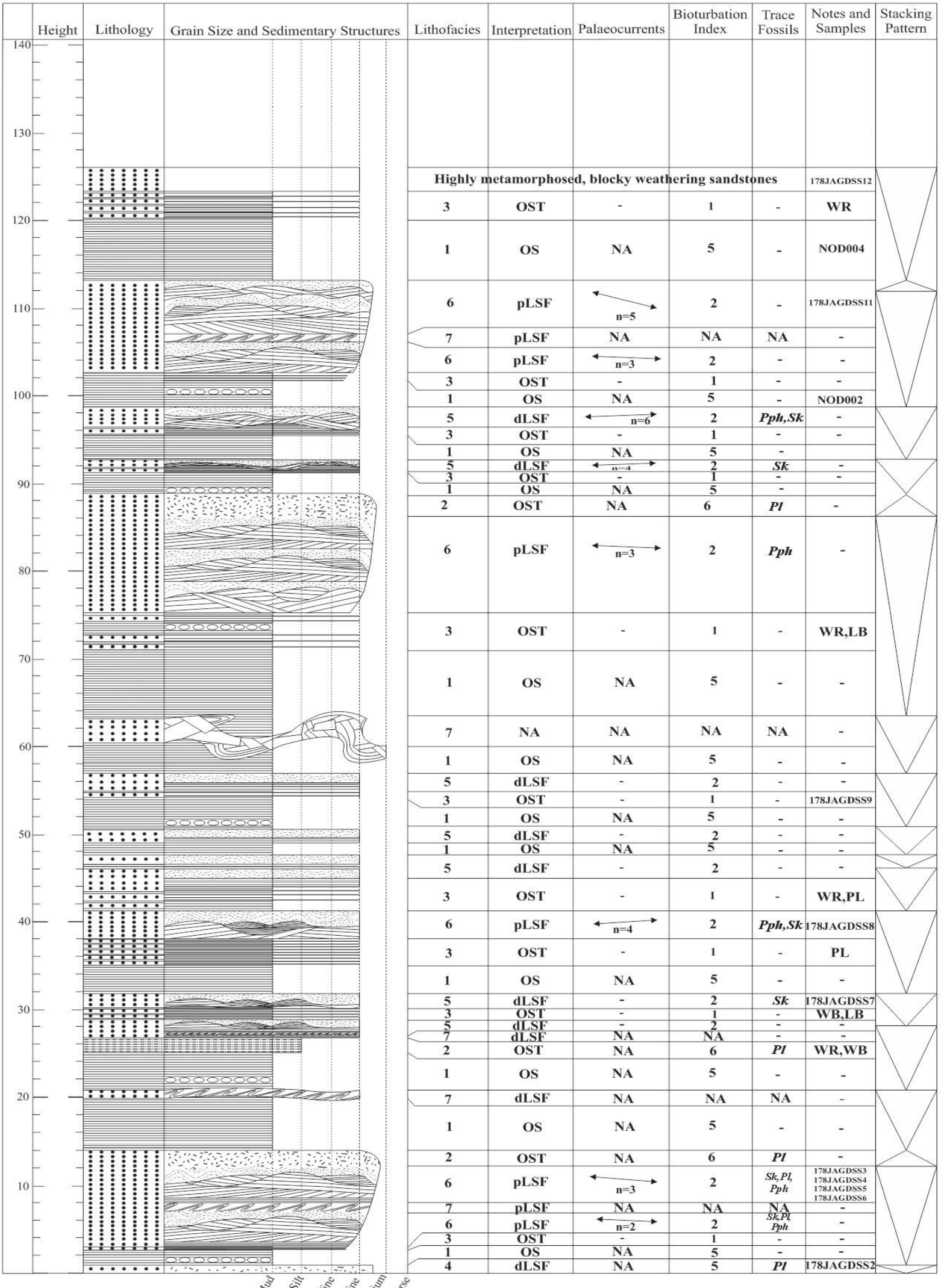


Figure 2.2. Northern Amibberg stratigraphic column.

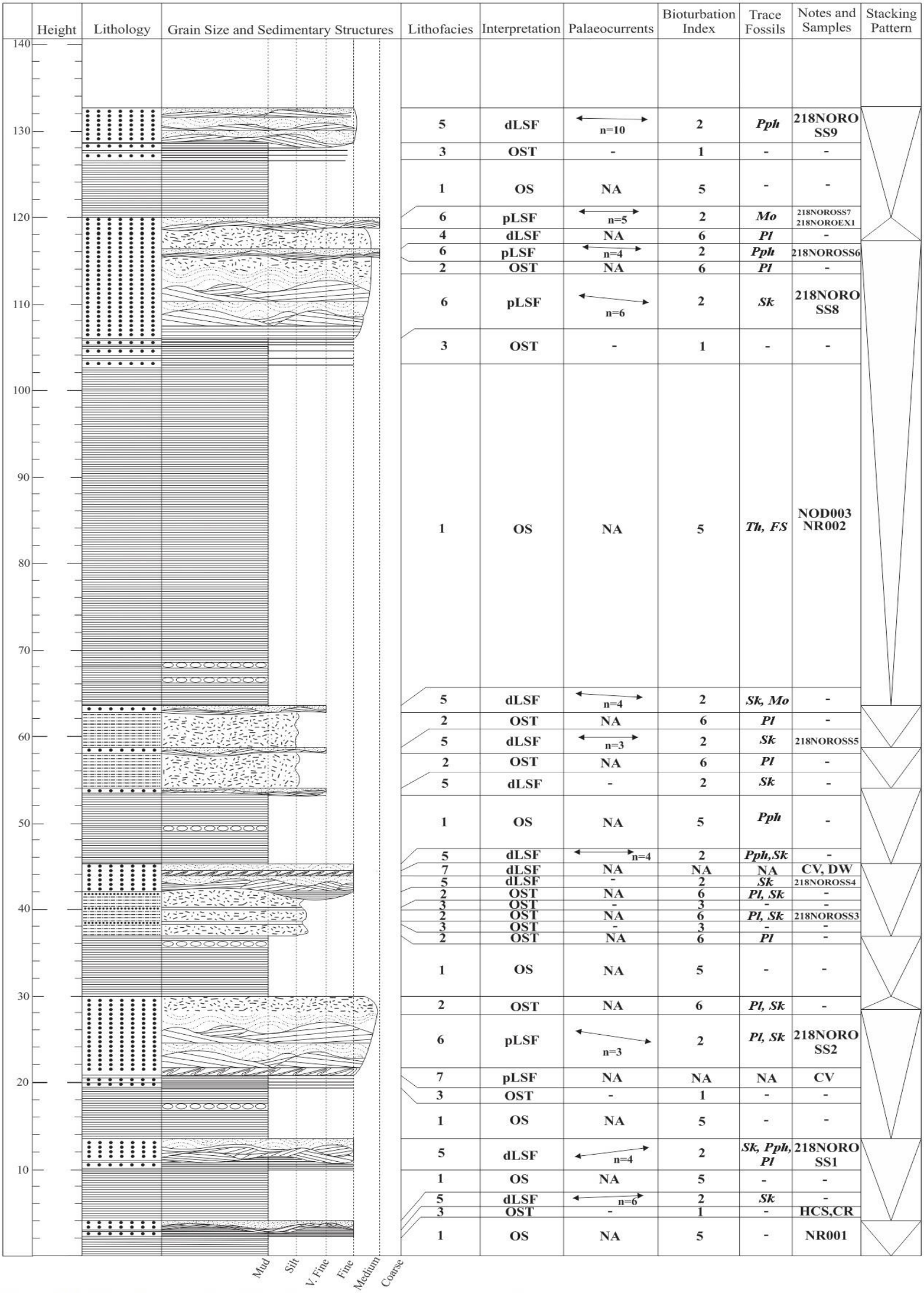


Figure 2.3. Norotshama stratigraphic column.

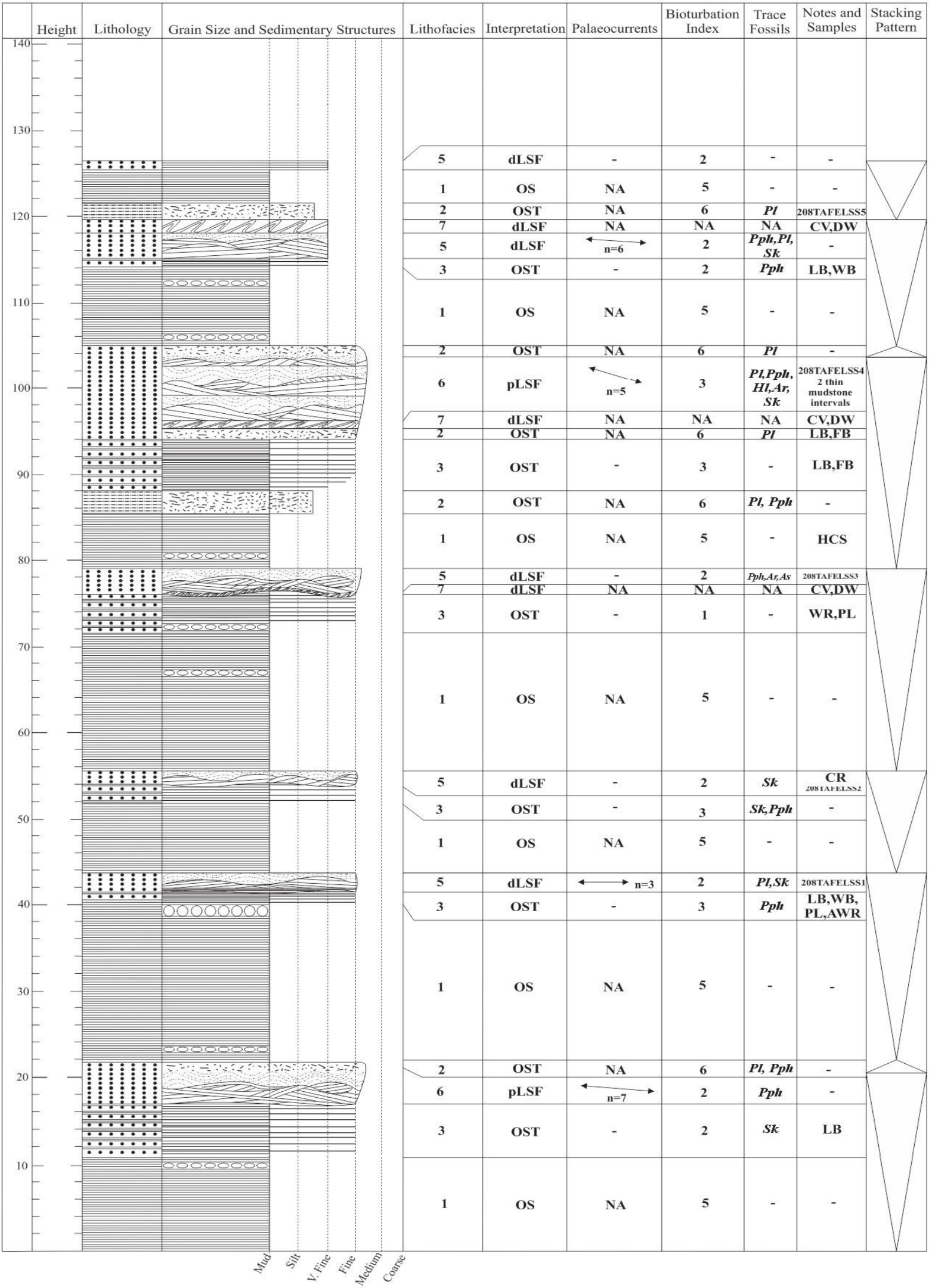


Figure 2.4. Tafelberg stratigraphic column.

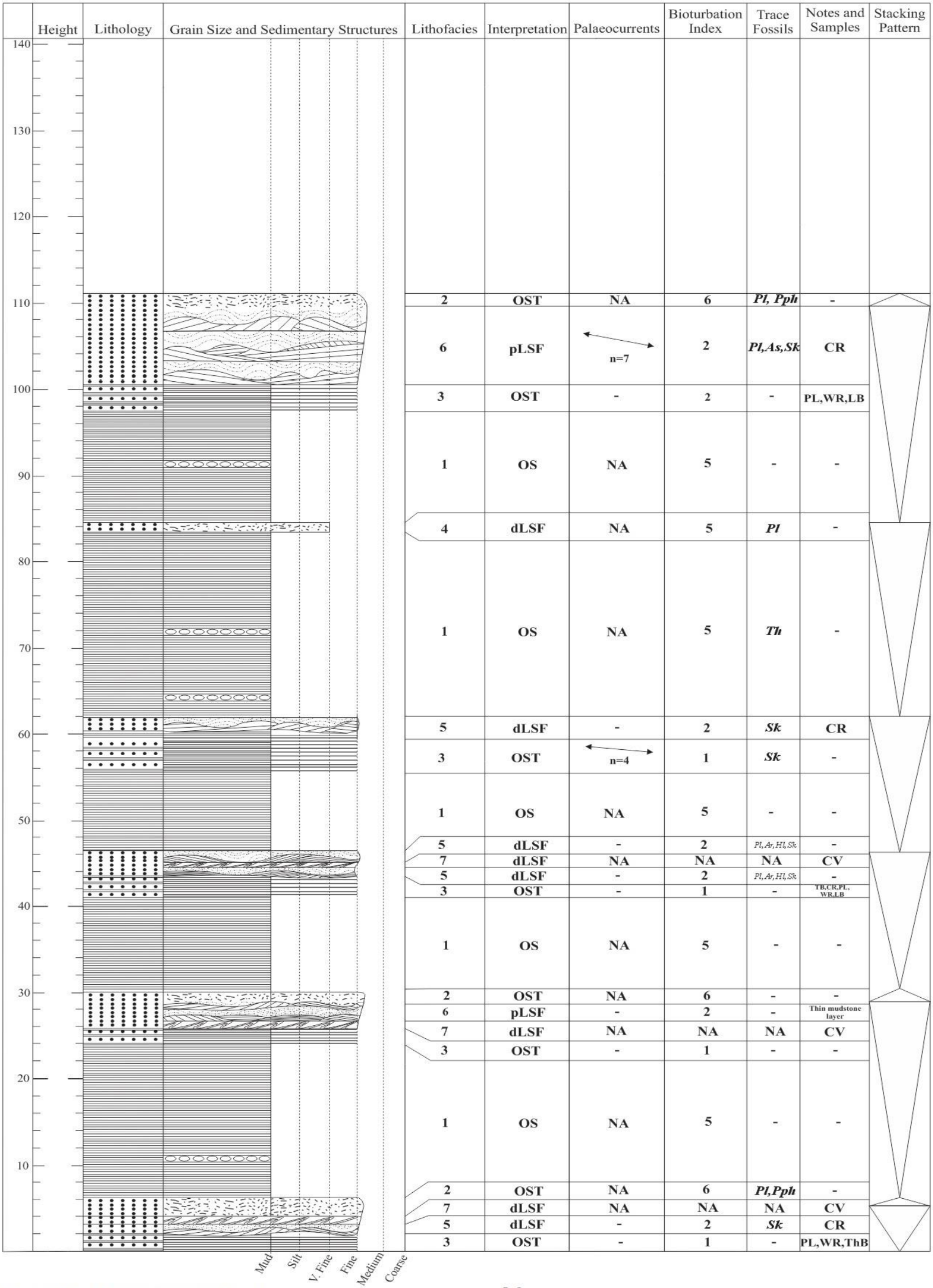


Figure 2.5. Platberg stratigraphic column

2.5 Lithofacies Descriptions and Interpretations

2.5.1 Lithofacies 1 – Massive to Plane-bedded Mudstone

Description:

The mudstones lithofacies consist of fine mud-sized particles that are dark grey to olive green in colour and are generally structureless with no bedding although rare, thin planar laminations of siltstone are present. The thicker mudstone units that make up this facies seem to be laterally extensive and tabular, whereas other units of this facies may be lenticular and thicken and thin along strike. The thickness of this facies ranges between 1.2m and 39m (Fig. 2.6B and C). This facies shows an upward-coarsening profile and typically has a gradational contact with overlying lithologies (Fig. 2.6A). A sharp base is typically evident with the underlying strata. This facies has a gradational upper contact when it underlies interbedded sandstone and siltstones of lithofacies 3 and a sharp contact with other sandstone facies.

Nodules are present throughout the Amibberg Formation and are almost wholly contained within mudstone beds of lithofacies 1. These nodule horizons are genetically linked to certain stratigraphic levels and align along sedimentary bedding in a stratiform manner (Fig. 2.7F). In most cases, nodules occur as isolated bodies and are laterally segmented but continuous over large horizontal distances. The surrounding stratum is deformed around the nodules in many instances (Fig. 2.7E). The nodules occur as lenticular bodies and are often ellipsoidal, oblate and spherical in shape and vary in size from 0.2 to 3m diameter. These nodules have an orange-brown weathering colour due to the presence of the iron-rich mineral limonite (Fig. 2.7A) and internally they are dark grey-black in colour with miniscule red haematite nodules present. Generally, sedimentary structures are rare, but in some instances traces are observable on the nodule surfaces as well as relict sedimentary structures (Fig. 2.6.D) which are well preserved on the outer limonite crust of these nodules (Fig. 2.7B). Bioturbation is also evident on the top of some of the nodules and is generally intense (BI = 5-6) when observable in outcrop. However, identifying the ichnological signatures in this facies is difficult due to the nature of the sediment. Traces observed on nodule surfaces include: *Rosellia*, *Palaeophycus*, *Paleodictyon*

and *Thalassinoides* with *Pseudo-Plagiogmus* present on bedding surfaces of mudstones.

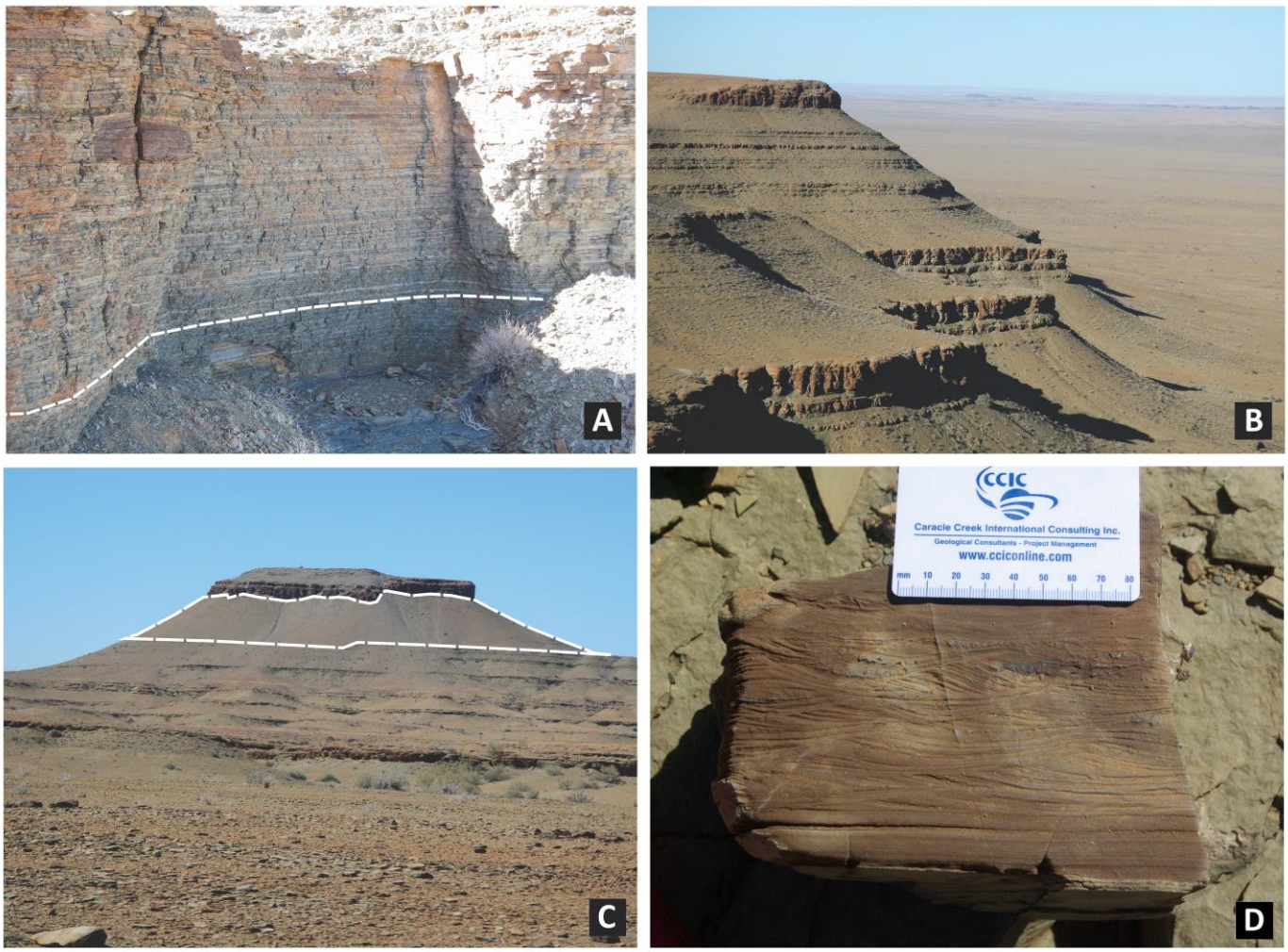


Figure 2.6. Lithofacies 1 - Mudstone. A) Photo showing the gradational contact (hyphenated line) between mudstones of lithofacies 1 and interbedded sandstones and siltstones of lithofacies 3. The contact between the two lithofacies is placed at the first interbedded sandstone layer (outcrop is approximately 3.4m in height). B) Outcrop photo showing the relationship between resistant sandstone layers and less resistant, thick mudstone intervals of lithofacies 1 (Photo of the Amibberg looking to the SW). C) Photo of Norotshama peak showing the uppermost preserved sandstone in the study area underlain by the thickest unit associated with lithofacies 1 (outlined). Mudstone unit below sandstone is approximately 40m thick. D) Climbing ripple cross-lamination preserved in a nodule horizon interbedded in mudstones (scale is 8cm wide).

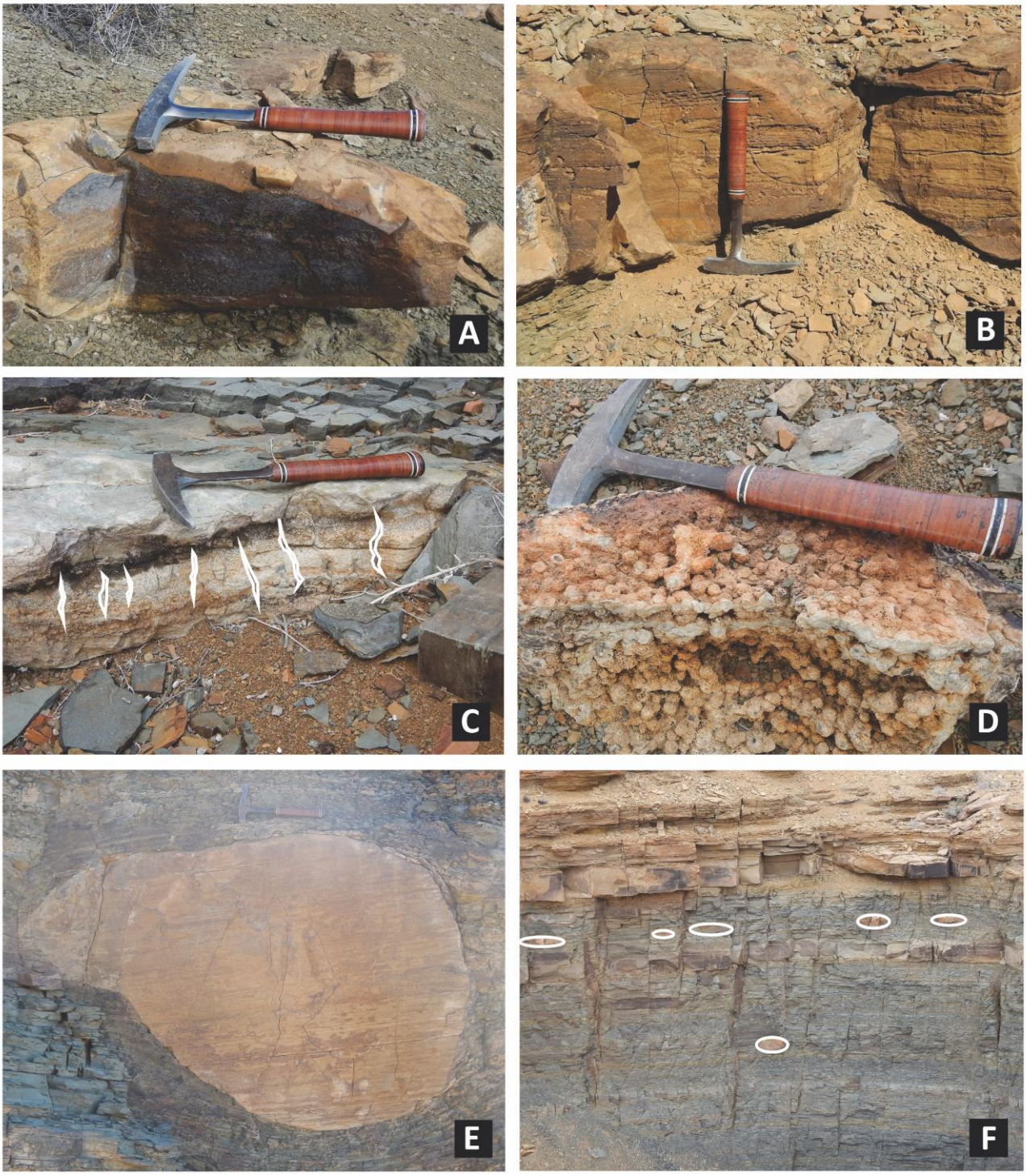


Figure 2.7. Lithofacies 1 - Nodules associated with the mudstone lithofacies. A) Close up of nodule with distinctive brown surface colour (limonite) that is internally dark-grey and homogenous (hammer is 32cm). B) Nodule showing relict sedimentary structures on the outer weathering surface (hammer is 32cm). C) Metamorphosed nodule showing vertically orientated calcite veins (outlined). This nodule horizon in a metamorphosed equivalent of the nodules in figure 2.8 A-E (hammer is 32cm). D) Recrystallized spheres on the surface of a carbonate nodule due to contact metamorphism (hammer is 32cm). E) Large nodule with distinctive non-spherical shape. Note the bending of the strata around the nodule growth (hammer is 32cm). F) Preservation of nodules (outlined) within mudstone unit, showing preference to certain stratigraphic intervals (lowermost nodule is approximately 20cm in diameter).

One important nodule horizon can be used as a marker horizon for correlation of the various measured columns. It is only present in a single stratigraphic horizon and appears as isolated bodies throughout the study area (Fig. 2.8A). This important carbonate nodule horizon is hard, resistant; 10 – 15 cm thick and dark grey-black internally with fine mud-sized particles, becoming olive-brown near the surfaces and a yellowish-brown weathering colour. It has a sharp to wavy contact (Fig. 2.8E) with both the underlying and overlying mudstones. The most distinguishing characteristic of this marker layer is the presence of calcite veins which are sigmoidal in shape and are orientated perpendicular to bedding (Fig. 2.8B). The veins can range between 0.2 and 3cm in thickness and 3 to 8cm in length. Other observable defining features include trace fossils on the bed surfaces. These traces are approximately 0.75cm thick with positive relief, convex burrows, sharp boundaries and smooth burrow surfaces, often a honeycomb/hexagonal shape is evident, though these are often incomplete or truncated (Fig. 2.8C). These traces appear to have a thicker main burrow with thinner branching burrows. This is interpreted to represent *Paleodictyon*. Internally chevron shaped crenulations of biogenic origin are also present in this nodule horizon (Fig. 2.8D). At the base of the thickest mudstone unit in the study area (39m at Norotshama) nodules with a pervasive crenulated texture as well as nodules that preserve distinctive trace fossil are present (see trace fossil section below). The nodules are a dark red-brown colour (Fig. 2.8F) and are bedded within lithofacies 1. These nodules also display distinctive funnel-like impressions (Fig. 2.9B) and are closely associated in the same stratigraphic interval with nodules that preserve white-weathering fish scales (Fig. 2.9A) as identified by Werner (2006).

In one measured stratigraphic column (Northern Amibberg) nodule horizons were found that have a pale white to brown weathering colour but are pale green internally. These nodules have a botryoidal surface texture and variable internal structure with white-grey upright calcite veins (Fig. 2.7C and D). The surface composition of the nodules consists of amalgamated/fused spherical grains which have been recrystallized due to contact metamorphism whereby a sill has intruded very close to the locality. These nodules provide little detail lithologically and are hence of little value.



Figure 2.8. Lithofacies 1 – Distinctive nodules associated with the mudstone lithofacies. A) Shows the outcrop locality of the distinctive nodule horizon used for study area correlation from the Amibberg Massif (Book for scale is 19cm long). B) Preferred orientation of black, sigmoidal calcite veins (pencil is 15cm long). C) Conspicuous traces on the bed surface of these nodules interpreted to represent *Paleodictyon* (Pencil is 15cm long). D) Algal crenulations found internally within these nodules (hammer is 32cm long). E) Photo showing the conspicuous nodule marker horizon interbedded with mudstones. Note the undulatory nature of the lower bounding surface and less so the upper bounding surface (note book is 19cm in length). F) Nodule horizon found in the lower part of the 40m thick mudstone horizon (Norotshama). This horizon has a pervasive algal texture throughout and especially on the bed surface of these nodules. They are also closely associated with the white-weathering fish scales (scale evident in bottom right-hand corner).

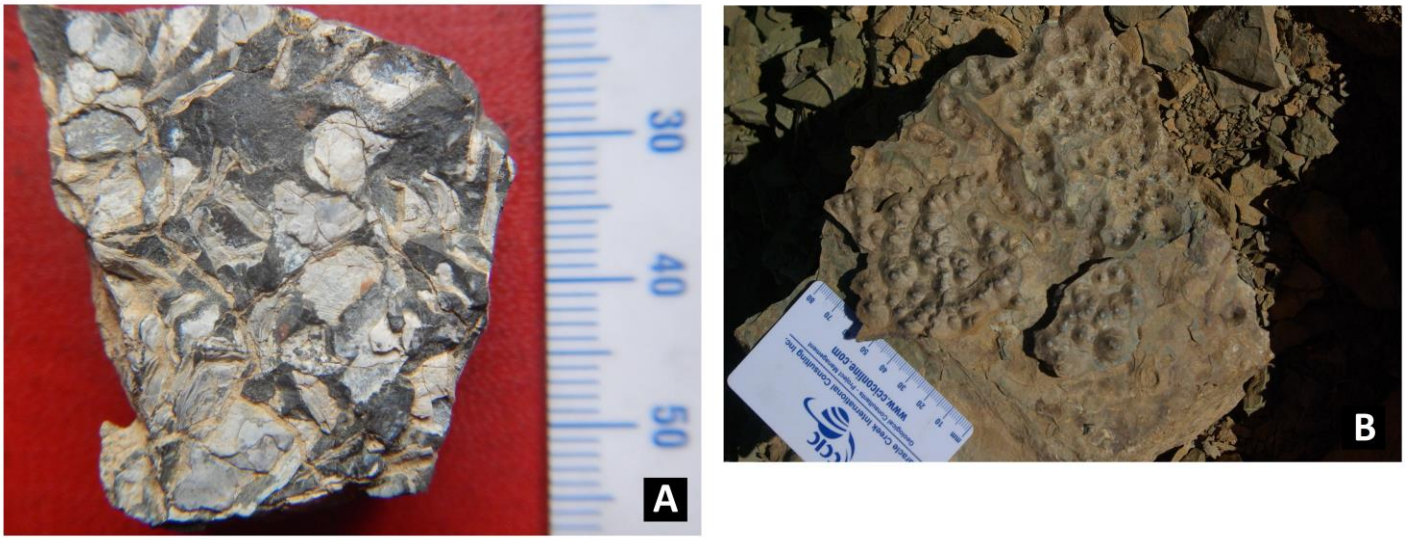


Figure 2.9. Lithofacies 1 – Distinctive nodules associated with the mudstone lithofacies. A) White-weathering fish scales found in the lower part of the 40m thick mudstone horizon (Norotshama). This sample found *ex-situ* but closely related to the nodule horizon in figure 2.3 F (scale in mm on the right). B) Sample found in the lower part of the 40m thick mudstone horizon (Norotshama) which has internally preserved algal features with distinctive funnel-like impressions. Feature unknown (scale bottom left).

Interpretation:

These mudstones are interpreted as forming in an outer shelf to offshore environment where mud-sized particles fall out of suspension in low energy settings. The rarity of sedimentary structures suggests deposition below mean storm wave base (e.g. Van Wagoner et al., 1990; Hampson et al., 2008); however, relict sedimentary structures do indicate minor wave influence during sedimentation. Thin siltstone laminations are interpreted as recording episodic influxes of silt as river-fed hyperpycnal flows (Stevens, 2004; Pattison, 2005a; Pattison, 2005b; Chaiwongsaen, 2007; Pattison et al., 2007a). The intense levels of bioturbation further reinforce the low energy environmental conditions of deposition and although the trace fossils found in this lithofacies are not indicative of an offshore environment, they do provide some support to the stable environment - offshore interpretation for these mudstones. The thickening and thinning of various mudstone units along strike as well as the scoured or sharp contact with some overlying sandstones indicate that these units were deposited as mudstone belts (Vakarelov et al., 2012).

The carbonate nodules are interpreted to have formed due to a reduction in siliciclastic input with an increase in carbonate production. The presence of *Paleodictyon* (a deep sea farming trace), which belongs to the *Nereites* ichnofacies, further suggests deposition in the abyssal zone i.e. offshore. Due to the nature and shape of these burrows not having perfect hexagonal appearance it is further classified as *Paleodictyon (Glenodictyum) imperfectum*. The name *Paleodictyon (Glenodictyum) imperfectum* refers to the angularity of individual hexagonal features as well as the fact that the hexagons are less regular than other ichnospecies such as *Paleodictyon (Glenodictyum) strozzii* (Seilacher, 2007). Due to the fact that many of the nodules preserve ichnofossils and sedimentary structures it is possible to deduce that they precipitated pre-burial even though not all nodule-bearing stratigraphic horizons preserve ichnofossils, and ichnofossil diversity varies through the stratigraphy. Other supporting features include the lack of internal layering in nodules and the bending of strata around the nodules. These all imply that nodular growth took place before compaction and are therefore synsedimentary features. Furthermore, it is possible to conclude that nodule growth is related to microbial activity whereby microbial communities stimulate carbonate precipitation. These microbes may have also acted as important food sources in subglacial and postglacial seas, and attracted and supported a diverse invertebrate community. Nodules are cemented differentially from the surrounding strata by authigenic minerals and hence differ from the host rock in terms of lithology and morphology (Dong et al. 2008).

Generally, this lithofacies is interpreted to have been deposited in distal parts of the basin in an offshore setting whereby microbial activity was abundant leading to the formation of carbonate nodules.

2.5.2 Lithofacies 2 - Bioturbated Siltstone and Sandstone

Description:

This lithofacies consists of intensely bioturbated siltstones and sandstones with no evident bedding. This lithofacies contains fine-grained sand to silt sized particles that have mixed horizons with a bioturbation index of 4-6 and therefore few sedimentary

structures are preserved. However, weakly defined planar laminations as well as wave rippled bed surfaces have been observed in outcrop. The associated ripple cross laminae are absent. Minor sand lenses are observed in bioturbated siltstone beds and the trace fossils evident in this lithofacies include *Palaeophycus* and *Planolites*. The rocks that comprise this lithofacies typically have sharp upper and lower contacts (Fig. 2.10C and F). However, this contact can be wavy in places especially when in close juxtaposition with HCS sandstones (Fig. 2.10D). This lithofacies is generally the least laterally continuous as it does thin and thicken along strike to various degrees but can also be lenticular in terms of geometry. Therefore precisely determining the thickness of these rocks is difficult; however, they generally range between a few meters to tens of centimetres in thickness. The colour of these rocks varies considerably from yellowish-orange sandstones (Fig. 2.10B) to olive green and dark grey siltstones (Fig. 2.10A). Rocks of this lithofacies occur in close juxtaposition with amalgamated HCS sandstones (Fig. 2.10C and D), mudstone and interbedded sandstones and siltstones. Often bioturbated sandy-siltstones occur below HCS sandstones and bioturbated sandstones occur above HCS sandstones in amalgamated units (Fig. 2.10E).

Interpretation:

Rocks of this lithofacies are considered to represent offshore-transitional deposits due to the high levels of fair-weather bioturbation and their position in the measured stratigraphic columns. Bioturbation coupled with the identified trace fossils *Palaeophycus* and *Planolites* found in siltstones and sandstones indicate prolonged periods of relative calm and low-energy environments during episodes of reduced sedimentation (i.e. fair-weather conditions) whereby the sediment was deposited by suspension settling. This settling involved a net slow, continuous accumulation. This accumulated sediment was then colonized by stable environment trace makers of the *Cruziana* ichnofacies. These organisms burrowed and moved within the sediment destroying internal bedding and structure. Charvin et al., (2010) also associated the *Cruziana* ichnofacies with the offshore-transitional zone as well as moderate to intense levels of reworking. Following these prolonged periods of stable conditions intermittent high energy periods due to storm wave interaction with the shoreface occurred, which is supported by wave rippled bed surfaces. This seems to be the case

where this facies is present above large amalgamated layers of wave influenced sandstones deposited on the proximal lower shoreface.

2.5.3 Lithofacies 3 - Interbedded Sandstone and Siltstone

Description:

This facies consists of interbedded very fine- to fine-grained sandstone and siltstones. This strongly heterolithic facies shows clearly discernible sandstone and siltstone beds (Fig. 2.11A and B). These two lithologies occur in various proportions relative to one another [sand/silt ratio from 1:1 to 1:10] with siltstone being dominant and the sandstone interbeds rarely exceeding 10cm in thickness. These sandstone beds range from being thinly bedded (3-30cm) to thickly laminated (0.3-1cm). The thickness of this facies is highly variable ranging from 0.35m to 7.0m. In most cases a clear distinction can be made between well-sorted sandstones and mud-rich siltstone (Fig. 2.12A). The siltstones are olive-green and the sandstones are a light yellow colour. The sandstones in this facies display wave rippled bed tops/lamination, hummocky cross-stratification as well as planar and ripple cross-laminations. Flaser, wavy and lenticular bedding (Fig. 2.12B, C and D) are also relatively common as are intraformational mudstone rip-up clasts. The sandstones of this facies typically have a sharp or wavy base as well as gradational contacts with the underlying and overlying lithologies (Fig. 2.11A) but in some cases a scoured and erosive contact is evident where HCS is present. Usually the underlying lithologies are mudstones of lithofacies 1 and the overlying lithologies consist of sandstone facies. This facies consists of units that are laterally extensive and those that are more localized (lenticular) that "pinch out" over tens to hundreds of meters. Bioturbation associated with this lithofacies is usually weak to moderate (BI = 1-3) and this facies generally shows a coarsening and thickening upward trend, at outcrop scale, with regard to sandstones as well as an increase in sandstone/shale ratio. Normal grading is observed in individual sandstone beds. Traces found in this lithofacies include: *Palaeophycus, Skolithos* and *Arencolites*.

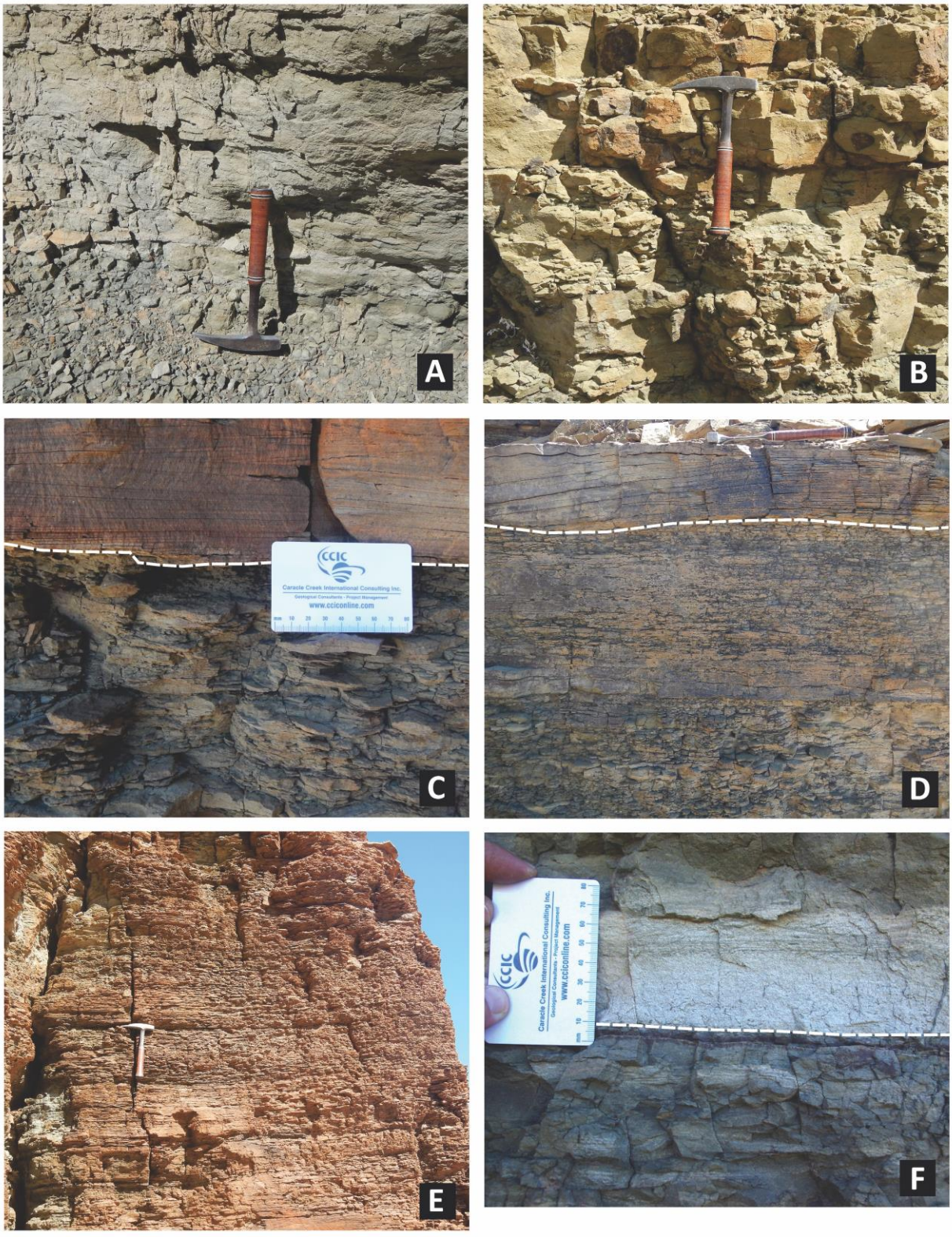


Figure 2.10. Lithofacies 2 – Bioturbated siltstone and sandstone. A) Appearance of bioturbated siltstone in outcrop. Structures are absent and an olive green-grey colour is evident (hammer is 32cm long). B) Appearance of bioturbated sandstone in outcrop. Distinct layering and structures are absent and a yellow-brown colour is evident (hammer is 32cm long). C) Contact between underlying bioturbated siltstone and overlying discrete HCS sandstone of lithofacies 5 indicated by hyphenated line. Note the relatively sharp contact in this photo (scale in middle-right of photo). D) Contact between underlying bioturbated siltstone and overlying discrete HCS sandstone of lithofacies 5 indicated by the hyphenated line. Note the undulatory contact in this instance whereby the overlying HCS bed forms hummocks and swales (hammer is 32cm long). E) Bioturbated sandstone with yellow-orange weathering colour occurring above an amalgamated HCS succession of lithofacies 6 (hammer is

32cm long). F) Bioturbated siltstone with relict laminated sand lenses (lenticular bedding) occurring below a 4cm thick, structurally deficient, bioturbated sandstone with *Skolithos* and *Arencolites* trace fossils. Overlying this is a thin planar laminated sandstone. Note the sharp contact between the bioturbated siltstone and the bioturbated sandstone (hyphenated line) as well as the gradual contact between the bioturbated sandstone and laminated sandstone above (scale left of photo).

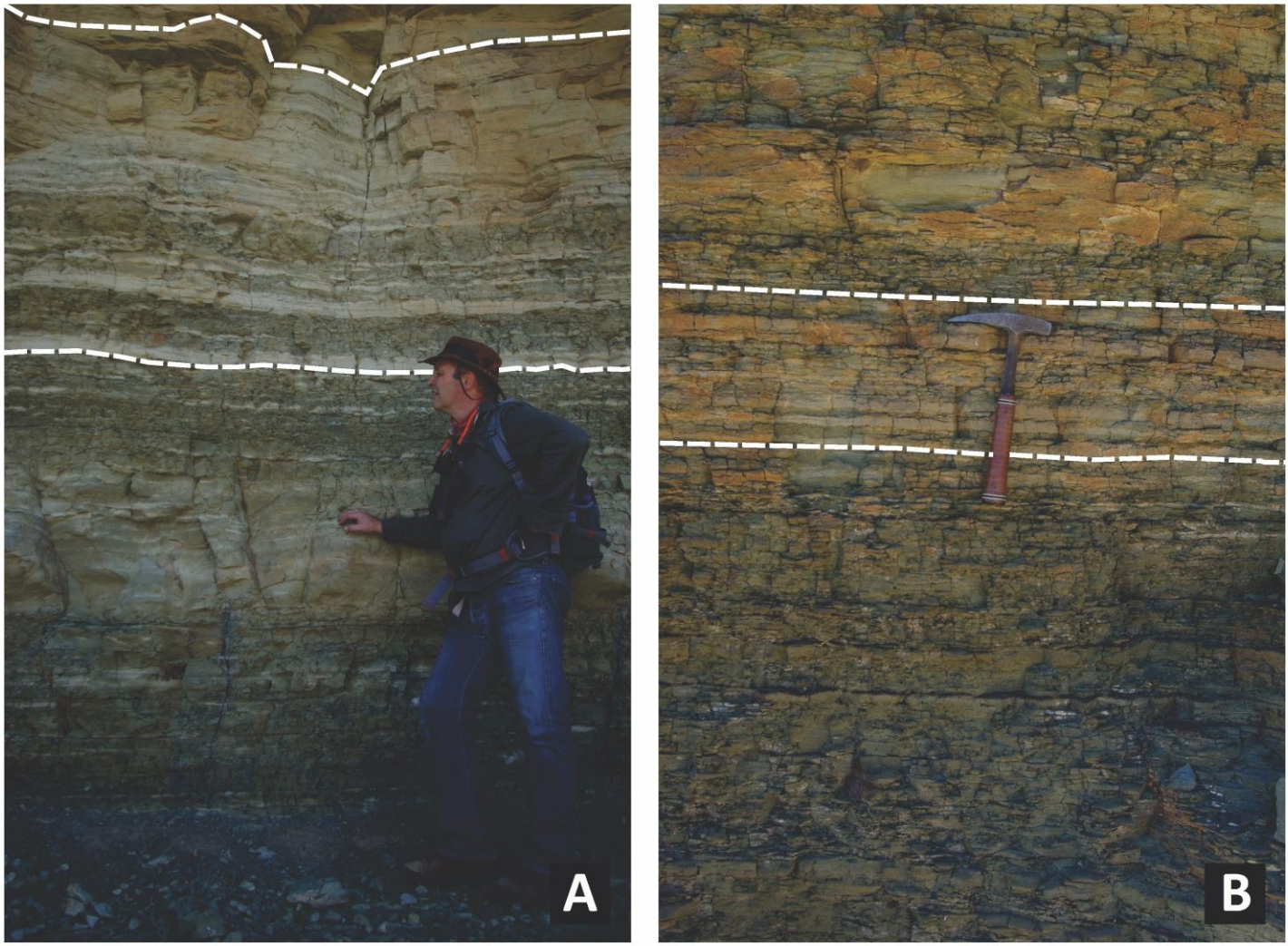


Figure 2.11. Lithofacies 3 – Interbedded sandstone and siltstone. A) Outcrop photo showing the gradual contact between bioturbated siltstones of lithofacies 2 and the heterolithic unit of lithofacies 3. The first continuous sandstone unit occurs at the first hyphenated line. The upper contact with an amalgamated HCS succession (second hyphenated line) is also evident in the upper reaches of the photo (person for scale is 1.8m tall). B) Outcrop photo showing a relatively sharp change in sedimentation between the lower bioturbated siltstone and the interbedded unit of lithofacies 3 (first hyphenated line). The beds are thin (a few cm) and lose their lithological character above the second hyphenated line (hammer is 32cm long).

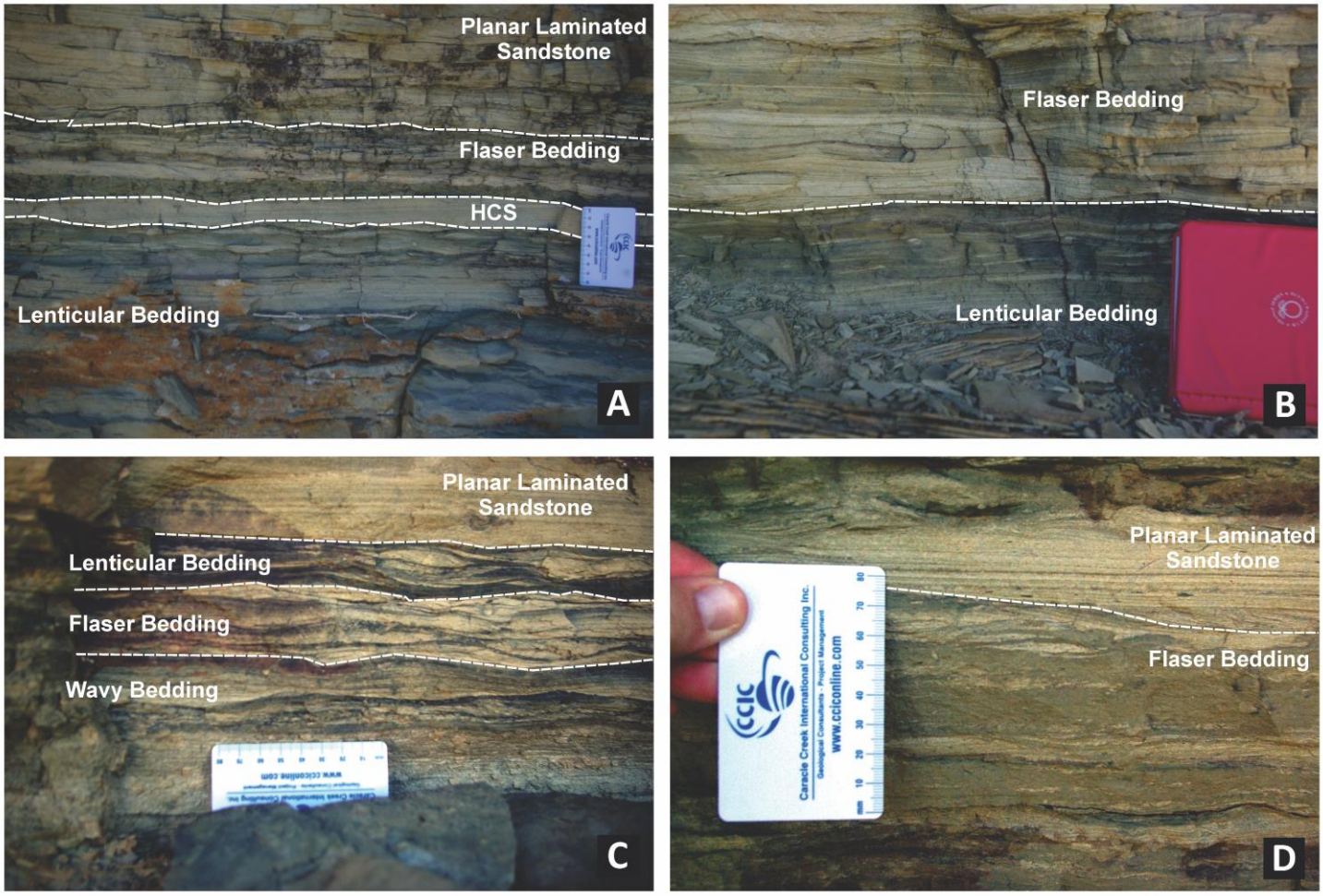


Figure 2.12. Lithofacies 3 – Interbedded sandstone and siltstone. A) Heterolithic unit characterised by lenticular bedding below the first prominent sandstone layer (middle of the photo) and flaser bedding above the sandstone. The middle sandstone displays HCS. This heterolithic unit has a gradual contact with the planar laminated sandstone above (scale left of photo). B) Pronounced contact (hyphenated line) between lower lenticular bedded heterolithic unit and upper flaser bedded heterolithic unit (note book is 19cm in length). C) Close up photo of wavy bedding overlain by flaser bedding below minor lenticular beds sharply overlain by a planar laminated sandstone (scale in lower section of photo). D) Flaser bedding overlain by a planar laminated sandstone with an incisive base indicated by the hyphenated line (scale left of photo).

Interpretation:

The degree of interbedding and the sand/silt ratio suggest an overall depositional trend in offshore transition to upper offshore environment. Interbedding is caused by variability in river floods or storm waves over a variety of different time scales. Waxing/waning currents derived from hyperpycnal flows and/or wave dominated gravity flows resuspended fine-grained material across the shelf. Deposits typical of wave dominated gravity flows (as per Ichaso and Dalrymple, 2009) are absent from this lithofacies indicating hyperpycnal flows as the primary mode of transport and subsequent deposition. Hyperpycnal flows are derived from the flooding of rivers that drain into a body of saline water. These occur when a plume has enough excess density due to high sediment concentration to become negatively buoyant as it leaves the river. This allows the hyperpycnal river plume to flow directly onto the seafloor

and then downslope (Traykovski et al., 2005). Mulder and Syvitski (1995) indicate that many small mountainous streams could produce these hyperpycnal flows in geological time.

Fine-grained (mud/silt) sedimentation was mostly due to suspension fallout with episodic influx of sand transported by offshore currents similar to that seen by Nouidar and Chellai (2002) in the late Barremian succession of the Agadir Basin, Morocco. This type of sedimentation is attributed to intermittent storm-surge ebb currents. An upward increase in depositional energy is inferred from the increase in sandstone:siltstone ratios as well as the upward coarsening trend. Some structures present in this facies (e.g. sharp-based planar laminated and low-angled HCS sandstones) indicate influence from storm-induced geostrophic flow (Clifton, 2006). These structures indicate the presence of moderate to high storm regime and deposition above the storm-wave base (Pattison, 2005a; Pattison, 2005b). Wavy, lenticular and flaser bedding indicate some tidal influence in this facies. The trace fossils identified in this facies are indicative of unstable conditions and are commonly associated with shoreface environments and support the palaeoenvironmental interpretation of this lithofacies.

Overall, an offshore transitional environment is suggested with a river-fed hyperpycnal origin of the sandstone beds coupled with low-energy sediment fallout for the siltstone interbeds.

2.5.4 Lithofacies 4 – Sharp Based, Massive Sandstone

Description:

Sandstones grouped into this facies are structureless (Fig. 2.13C) in most instances although faint laminations are present in the lower portion of these rocks. These rocks are fine- to medium-grained and are internally olive-green and have a dark yellowish orange-red weathering colour. The sandstones are between 0.80m and 3.0m thick, and wave rippled bed surfaces are also present although rarely evident. This facies generally has a sharp base with the underlying and overlying lithologies (Fig. 2.13B). These sandstones are continuous along strike and occur as tabular bodies. This facies occurs as the lower-most sandstone (Fig. 2.13A) in the study area but also occurs

higher up, and in various thicknesses (Fig. 2.13D), in other localities. Trace fossils are observed on upper bed surfaces as well as intraformational rip up clasts (Fig. 2.20C). The lack of structures observable in this facies suggests that these rocks are highly bioturbated (BI=5-6) although weak bedding has been observed. Traces found in this facies include *Skolithos*, *Planolites* and indeterminable short, horizontal to oblique burrows present on upper bedding planes.

Interpretation:

The high degree of bioturbation in this facies indicates that slow deposition in a low energy environment is the likely mechanism for deposition. This must have occurred above the mean storm wave base due to the presence of wave rippled bed tops. Furthermore, the massive appearance of this facies coupled with the non-amalgamated appearance indicates deposition distally on the lower shoreface where organisms were provided suitable conditions to fully rework the sediment. This could only have happened due to a prolonged period of stable conditions to allow organisms to completely rework the relatively thick sandstones in question. Furthermore, oxygen and nutrients would have to be available to allow such reworking of sediment in a marine environment.

2.5.5 Lithofacies 5 – Discrete Hummocky Cross-stratified and Wave Rippled Sandstone

Description:

This facies occurs as isolated, low angle (<10-15^{o}) HCS sandstones often with capping wave ripples and rarely with underlying planar laminations. This facies can be up to three meters thick in places but is generally less than a meter thick. A range of grain sizes are evident for this facies from very fine- to fine-grained sandstones which have a yellowish orange-red weathering colour. Mudstone rip up clasts are present at the base of discrete HCS beds and climbing ripples are evident (Fig. 2.14D). These are often wavy to sharp-based and topped sandstones (Fig. 2.14A) often with minor interbeds of bioturbated siltstone (Fig. 2.14B). However, basal

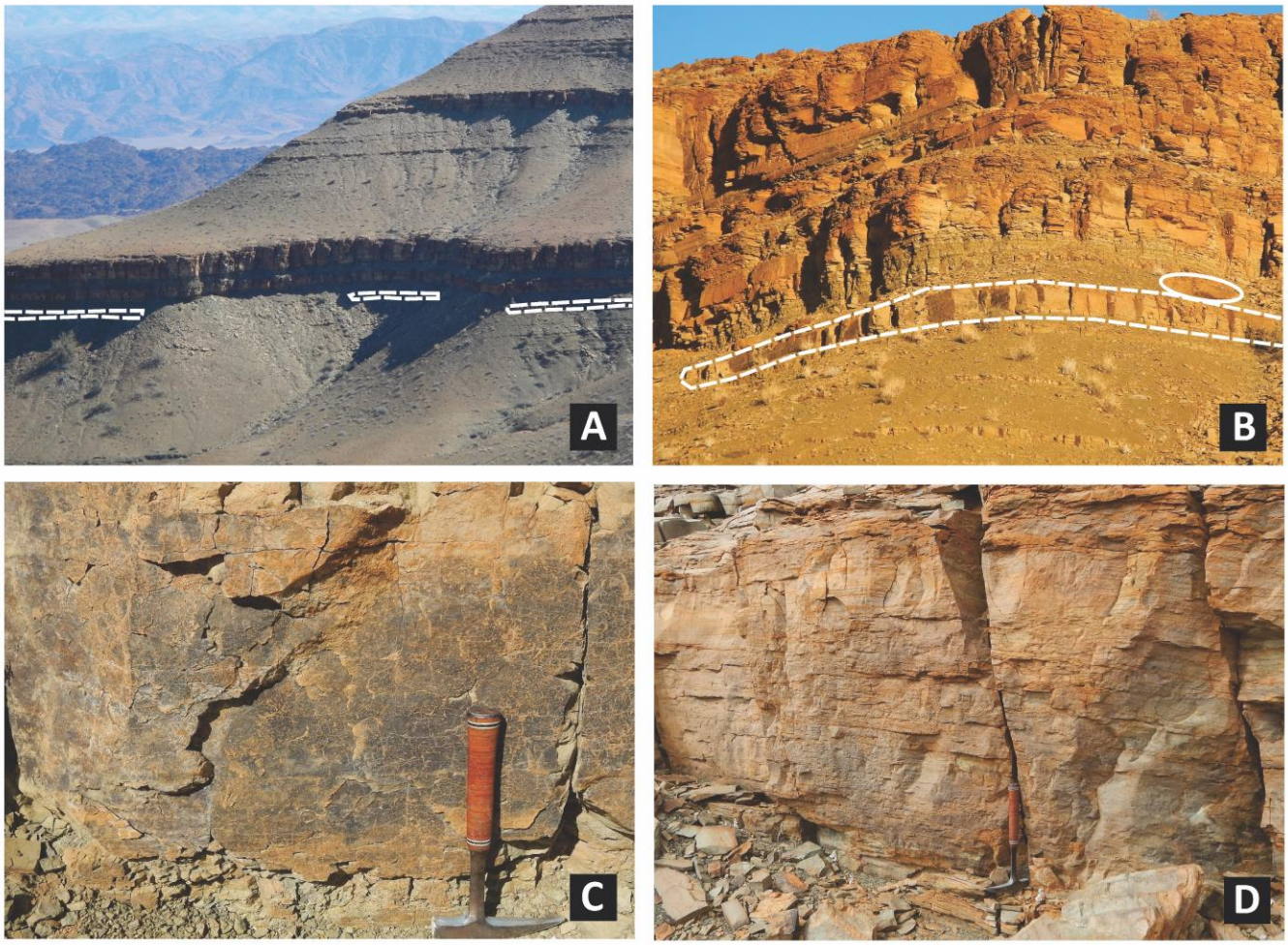


Figure 2.13. Lithofacies 4 – Sharp based massive sandstone**.** A) Photo showing the lateral segmented appearance of lithofacies 4 (outlined) below an amalgamated sandstone unit. This sandstone is 80cm thick and is the lowermost sandstone of the Amibberg Formation. B) Close up of the same 80cm thick lithofacies 4 sandstone along strike on the Amibberg Massif (hyphenated outline) with nodule evident (solid outline). C) Characteristic structureless sandstone with a sharp base (hammer is 32cm). D) Photo showing the thickest sandstone in this facies. Some faint bedding may be observable (hammer is 32cm).

scoured surfaces are present (Fig. 2.14A) and are overlain by HCS and capped by symmetrical wave ripples. In some instances a basal parallel (horizontal to sub horizontal) laminated interval directly overlying the basal erosional surface is present. Zones of convoluted beds (Fig. 2.14C) are also present within this discrete HCS lithofacies. These bodies can be tabular and laterally continuous over large distances whereas some are only observed in a single stratigraphic column. Bioturbation in this facies is usually weak (BI=1-2) but some zones of intense bioturbation (BI=4-5) are present especially in siltstone intervals. No observable grain size change is evident vertically. This lithofacies is distinguished from lithofacies 6 based on thickness and degree of amalgamation. Trace fossils present include *Planolites*, *Skolithos*

Crosspodia, Asterosoma, Helminthopsis Schaubcylidrichnus Thalassinoides and *Monocraterion.*

Interpretation:

Discrete HCS bodies form in deeper water than amalgamated HCS units, due to predominantly muddy background sedimentation. These HCS beds are interpreted as representing a single storm event during which HCS beds are deposited during storms and siltstone interbeds during intervening fair-weather periods (e.g. Dott and Bourgeois, 1982; Duke, 1985). Non-amalgamated hummocky cross-stratified sandstones are interpreted as representing sedimentation in the distal lower shoreface (e.g. Van Wagoner et al., 1990; Kamola and Van Wagoner, 1995; Pattison, 1995; Taylor and Lovell, 1995; Hampson, 2010).

The *Skolithos* ichnofacies present in these amalgamated units indicate storm condition during deposition and the *Cruziana* ichnofacies represents periods of relative calm (e.g. Charvin et al., 2010). These both occur in this lithofacies and point towards a mixed environment in which storm waves were active for periods followed by periods of low energy which allowed the *Cruziana* ichnofacies to become prevalent.

2.5.6 Lithofacies 6 – Amalgamated Hummocky Cross-stratified and Wave Rippled Sandstone

Description:

This facies is characterized by thick (several to tens of metres) amalgamated sandstones (Fig. 2.15A), minor siltstone interbeds and a general lack of mudstone (except as intra formational rip up clasts and minor beds). A range of grain sizes are evident in this facies from very fine- to medium-grained sandstones which have a yellowish orange-red weathering colour. Planar laminations are overlain by low angle (<10-15^{o}) HCS (Fig. 2.15B) which is consequently overlain by wave ripples (Fig. 2.16F) in distinct sequential arrangements. Mudstone partings (Fig. 2.15C), overlying the wave rippled interval, may occur between some HCS units, but are relatively rare

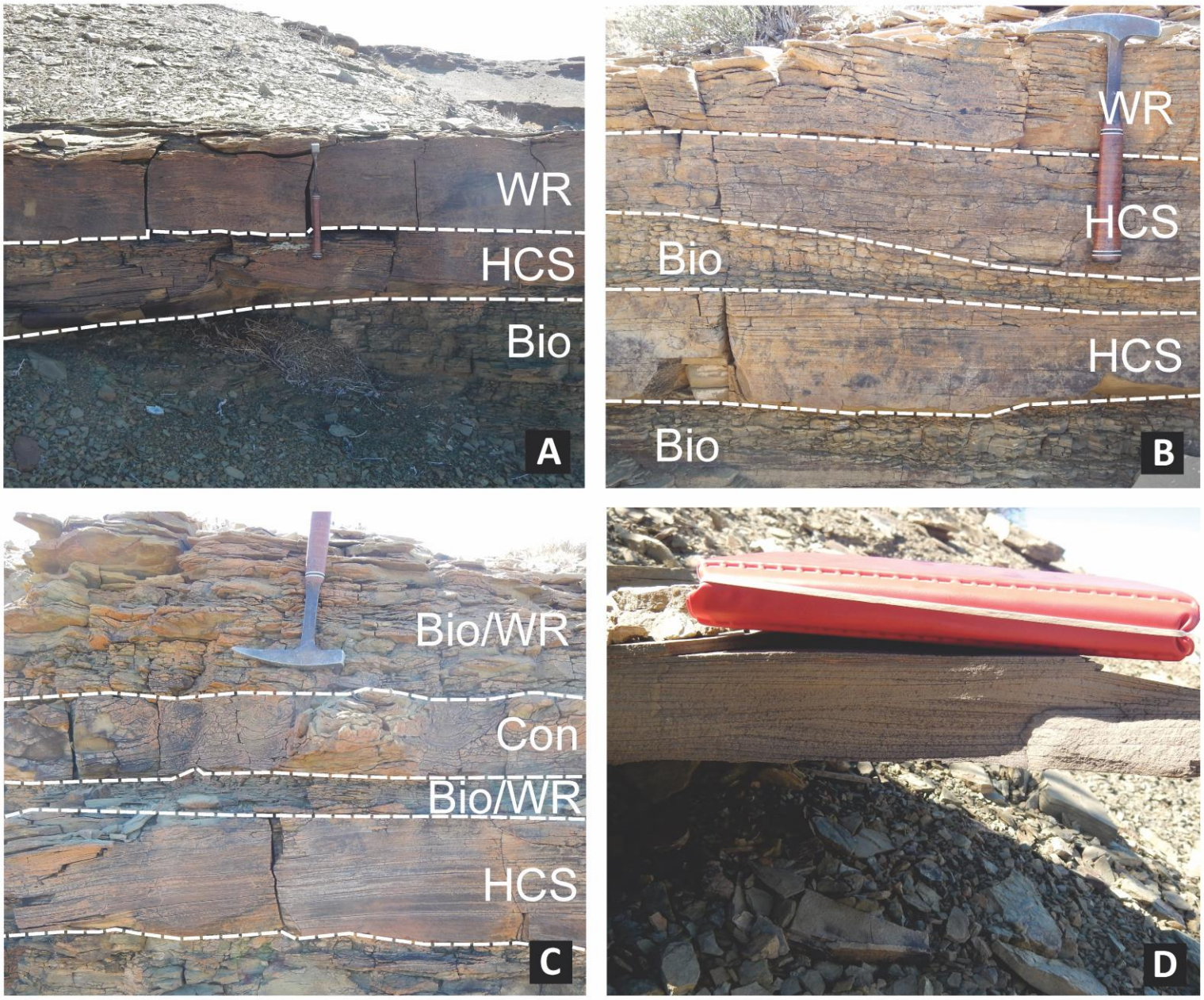


Figure 2.14. Lithofacies 5 – Discrete HCS and wave rippled sandstone. A) Appearance of lithofacies 5 in outcrop underlain by bioturbated siltstone and overlain in succession by a wave rippled sandstone horizon (hammer is 32cm long). B) Lithofacies 5 unit. From bottom to top: thin bioturbated siltstone interval overlain by approximately 12cm thick, low angled HCS sandstone. Overlying this is a bioturbated siltstone interval of varying thickness due to erosive base of overlying HCS sandstone. The uppermost interval is a wave rippled sandstone. Note the hummock in the left hand side of the photo where the second bioturbated siltstone is thickest (hammer is 32cm long). C) Discrete HCS sandstone overlain by a layer of SSD convoluted beds. The uppermost sandstone indicates a minor degree of bioturbation and wave ripples (hammer is 32cm long). D) Climbing ripple cross lamination associated with lithofacies 5 (note book is 19cm long).

whereas siltstone interbeds are present and genetically linked to HCS where they occur on the flanks of low angled hummocks. Individual laminations tend to thicken towards hummocks and swales (Fig. 2.16A). In some instances the low angled HCS even truncates wave ripple laminations or planar laminations and vice versa (Fig. 2.16C). Hummocks and swales, as well as the associated internal laminations, seem to be evident on their own (Fig. 2.15D and Fig. 2.16B, D and E) but whole, large-scale hummock-swale structures are only seen at large outcrop scale. Wave ripples form in finer grained material which has a more negative weathering profile than surrounding HCS strata which forms in the 'cleaner' sandstones which have a less prominent weathering profile. Sandstone bodies that make up this facies show irregularly scoured bases (Fig. 2.15E) due to the presence of hummocks and swales giving these sandstones a wavy lower bounding surface. Other sedimentary structures present are climbing ripples (Fig. 2.15F), convoluted bedding and abundant intra-formational rip up clasts that occur along basal contacts.

In some amalgamated units thin mudstone layers (~5cm) are present (Fig. 2.16A). These mudstone layers are structureless and homogenous with no bioturbation evident. It has a sharp upper and lower contact and very fine-grained sand lenses are present.

This facies is typically tabular and laterally persistent on outcrop scale. Within this facies there are zones of intense bioturbation in which original sedimentary structures are completely obliterated (BI=4-5) and at the top of these units relatively thin upward-finings bioturbated sandstones are present. These are attributed to lithofacies 2 where applicable. Furthermore, SSD structures of lithofacies 7 also occur within these amalgamated units and are described below. These amalgamated bodies generally coarsen upwards and can be thinly to thickly bedded. Generally, the sandstones of this facies are only weakly bioturbated (BI=1-2) with trace fossils found including: Faecal pellets of *Rhizocorallium, Asteriacites, Skolithos, Phycodes, Planolites, Palaeophycus, Cochlichnus, Gyrochorte and Gordia marina.* An unidentified permineralised wood fragment (Fig. 2.20D) was also found *ex-situ* below an amalgamated HCS unit near Norotshama.

For this facies, hummocks and swales are present in unison, hummocks merging into swales laterally and vice versa. Furthermore, there is very little change in the angle of

the bedding and little grain size variation. For this reason hummocky cross-stratification and swaley cross-stratification are not categorized in separate facies. Even though Leckie and Walker (1982) used the term swaley cross-stratification for amalgamated HCS beds with a thickness of more than 2m, the term has been disregarded in this work for the sake of clarity.

Intervals of between 15cm and 50cm of clean, fine- to medium-grained, light grey, quartz-rich sandstone layers form part of this facies. These intervals display HCS, wave rippled surfaces (Fig. 2.17A) and planar laminations (Fig. 2.17B); however, they differ in that they are the coarsest grained of all the observed rocks in the study area and are thinly (3-30cm) to thickly (30-100cm) bedded. These tabular sandstones often have a sharp lower contact whereas the upper contact is slightly wavy or incised (Fig. 2.17A). Bioturbation in these intervals is moderate and variable (BI=2-4). No coarsening/fining trends are observable and these sandstones are extremely hard and difficult to sample. Traces include *Palaeophycus*, *Skolithos* and *Monocraterion*.

Interpretation:

HCS is typically recognized at the transition between nearshore and outershelf facies (e.g.: Duke, 1985) and most commonly between lower shoreface and offshore facies (Harms et al., 1975). In most cases, the sequential distribution of structures present in this facies displays a classic tempestite sequence wherein the planar laminated interval (oscillatory dominant flow) represents storm-wave stirring that was not severe enough to scour the bottom but was still capable of suspending considerable fine sediment; deposition simply draped a flat rather than hummocky bottom surface (Dott and Bourgeois, 1982; Walker et al., 1983). HCS (waning, purely oscillatory flow or very strong oscillatory dominant combined flows) then follows. Dott and Bourgeois (1982) proposed HCS to form by unusual waves beyond the fair-weather wave base and underlined the need of having a first transport of sand offshore either by river flooding events or by wave-surge and wind-driven currents.

Suspension load is the dominant method of transport and deposition in this instance. Following the decrease in wave energy, suspended sediment fallout begins and the

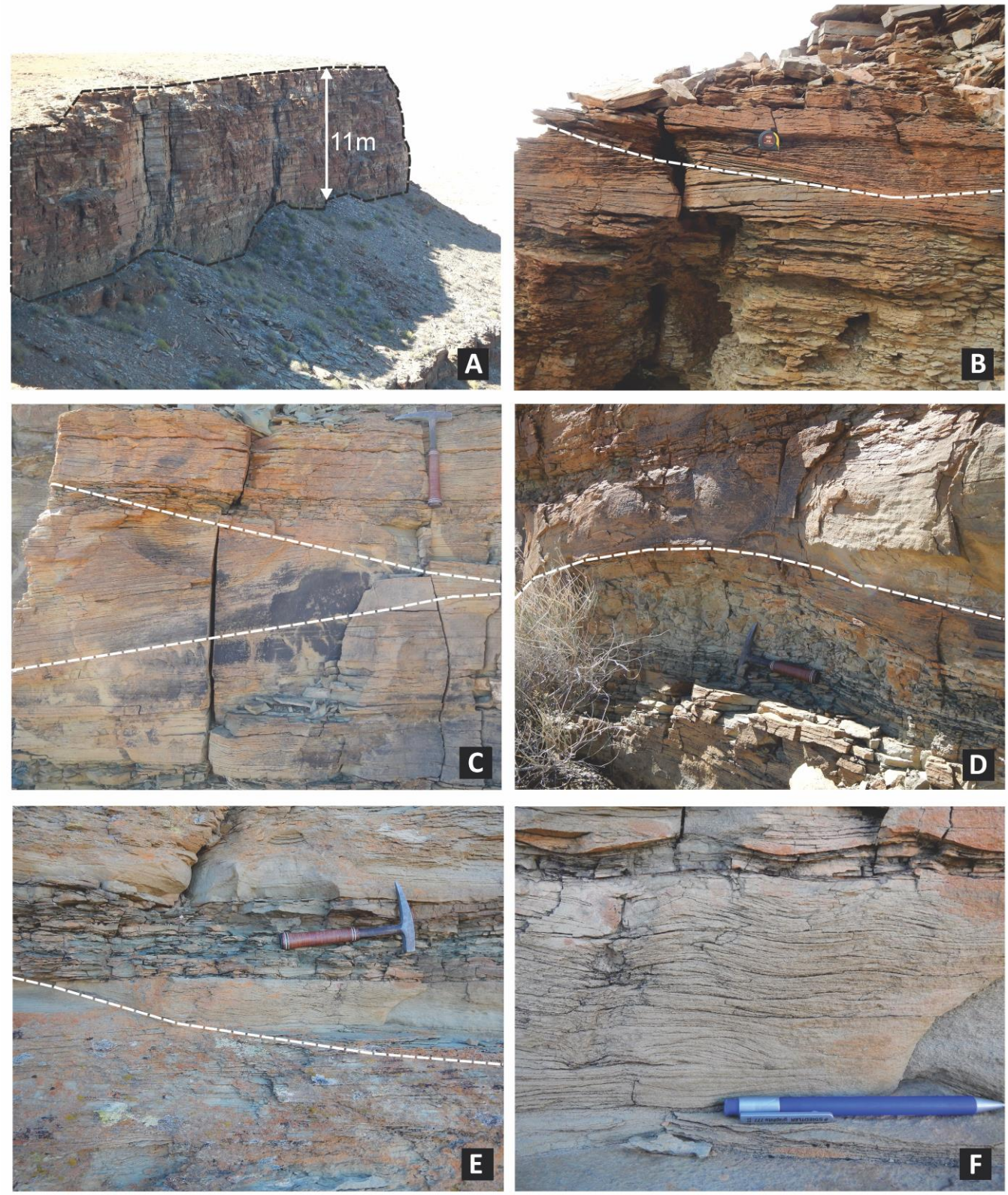


Figure 2.15. Lithofacies 6 – Amalgamated HCS and wave rippled sandstone. A) Appearance of amalgamated HCS sandstone unit in outcrop (outcrop is approximately 11m thick). B) Preserved swale denoted by hyphenated line. Wave ripples cap this sequence (Tape measure for scale is 7cm). C) Hummocks and swales (hyphenated lines) that converge to the right of the photo. Wave rippled sandstones occur in the upper parts. Also note the dipping beds of the swale form a truncation surface (hammer for scale is 32cm long). D) Large wave length hummock (hyphenated line) underlain by convoluted beds (hammer is 32cm long). E) Erosionally scoured base (hyphenated line) in filled with climbing ripples associated with lithofacies 6. This is then overlain by a thin layer of bioturbated siltstone of lithofacies 2 (hammer is 32cm long). F) Close up of E) showing definitive climbing ripples capped by a wave ripples (pencil is 15cm long).

falling grains encounter a zone of intense oscillatory sheet flow, which forms into hummocks and swales (Dott and Bourgeois, 1982). Symmetrical ripples cap the sequence and form when surface waves diminish as the storm wanes. The abundance of mudstone rip up clasts is related to swash and run-up movement of breaking waves (Morsilli and Pomar, 2012). Climbing ripple cross-lamina is formed by waning wave energies. Their occurrence implies that episodic storm- and river-mouth-derived currents were both active during deposition (Hampson and Storms, 2003).

The *Skolithos* ichnofacies present in these amalgamated units indicate storm condition during deposition and the *Cruziana* ichnofacies represents periods of relative calm (e.g. Charvin et al., 2010). These both occur in this lithofacies and point towards a mixed environment in which storm waves were active for periods followed by periods of low energy which allowed the *Cruziana* ichnofacies to become prevalent.

Thick, amalgamated HCS beds are interpreted as proximal storm deposits and record oscillatory and combined flows during successive storms (Cheel and Leckie, 1993). Sustained wave erosion mainly removed mud layers between sandstone beds, with the exception of locally preserved residual mud partings (Brenchley et al., 1993) and siltstone intervals. The thin mudstone intervals present within some amalgamated wave influenced units have the character indicative of a fluid-mud. Fluid-mud transport is initiated by wave-supported turbidity flows generated through the resuspension of sediment on the seafloor (Traykovski et al., 2005) and can result in the transport of sediment further offshore. These flows can occur on low angle slopes where the turbulence from wave energy is able to maintain sediment suspension, unlike shelf-supporting turbidity currents. As shown by Mulder and Syvitski (1995), short steep drainage basins, such as one might expect in an active rift basin, are especially prone to the occurrence of pronounced floods with exceptional suspended-sediment concentrations. These fluid-muds indicate at least minor fluvial transport process influence in this facies.

Amalgamated HCS units commonly occur above the discrete HCS beds in regressive shoreline successions (e.g. Hamblin and Walker, 1979; Leckie and Walker, 1982),

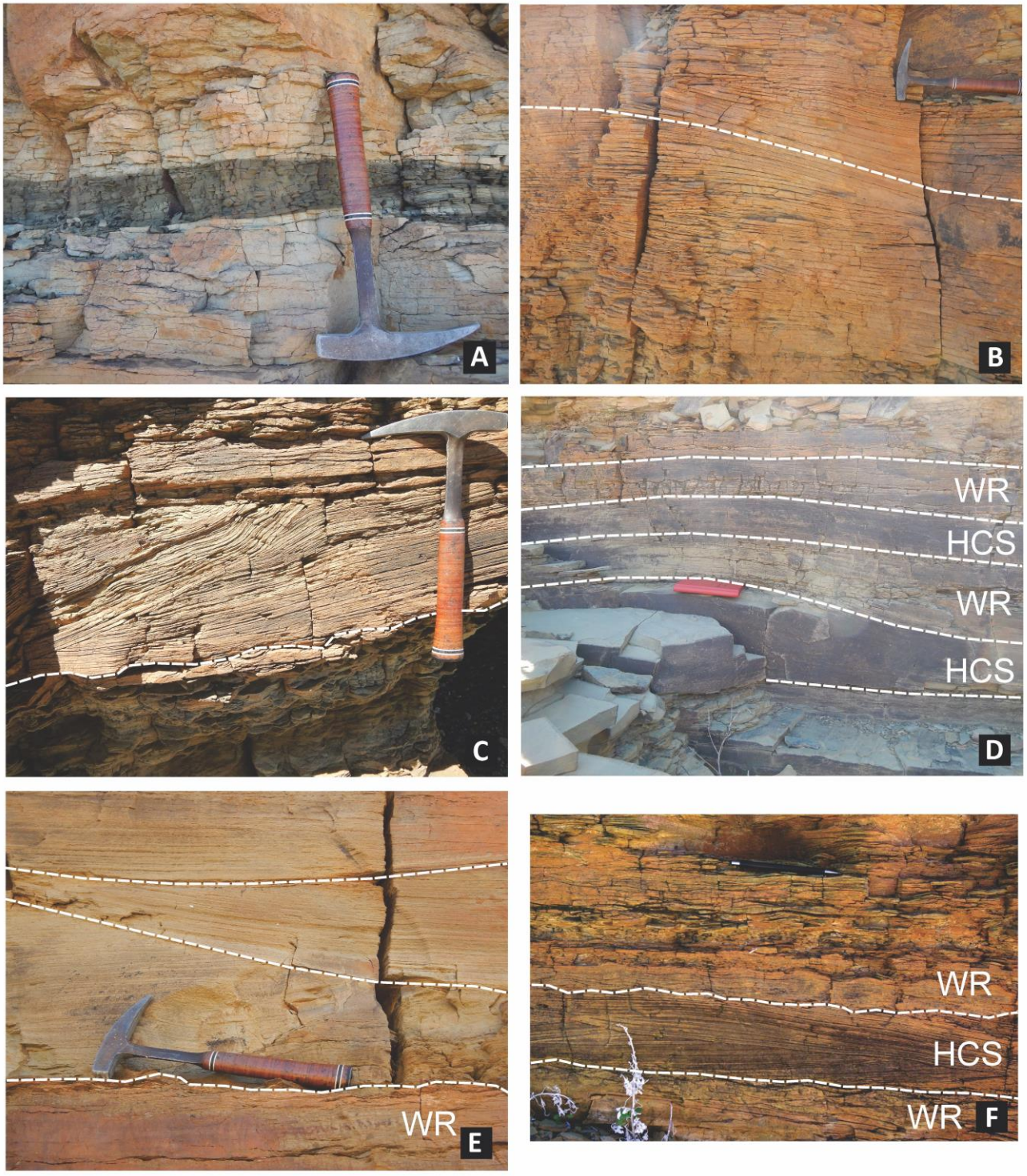


Figure 2.16. Lithofacies 6 – Amalgamated HCS and wave rippled sandstone. A) Close up of a thin mudstone horizon within lithofacies 6. Note the lack of structure in this layer and the fine-grained sandstone lenses on the right hand side of the photo (hammer is 32cm long). B) Preserved hummock (hyphenated line) in outcrop capped by layers of wave ripples. Note the irregularity of the HCS bed surface thus making exact measurement of bed thickness a difficulty (hammer is 32cm long). C) Wavy base (hyphenated line) associated with overlying HCS sandstone. Also note the SSD feature forming on a truncation surface. This gives insight into the mechanisms involved in the formation of SSD structures (hammer is 32cm long). D) Amalgamated HCS succession with large scale hummock overlain by a sequential arrangement of wave ripples (note book is 19cm long). E) Wave rippled sandstone overlain by HCS sandstone in an amalgamated unit. Note the swale in the upper part of the photo indicated by uppermost hyphenated line (hammer is 32cm long). F) Close up of small scale, low angled HCS unit with internally truncated laminae. Note the hummock to the right of the photo (between hyphenated lines). This is then capped by a succession of wave rippled sandstones (pencil is 15cm long).

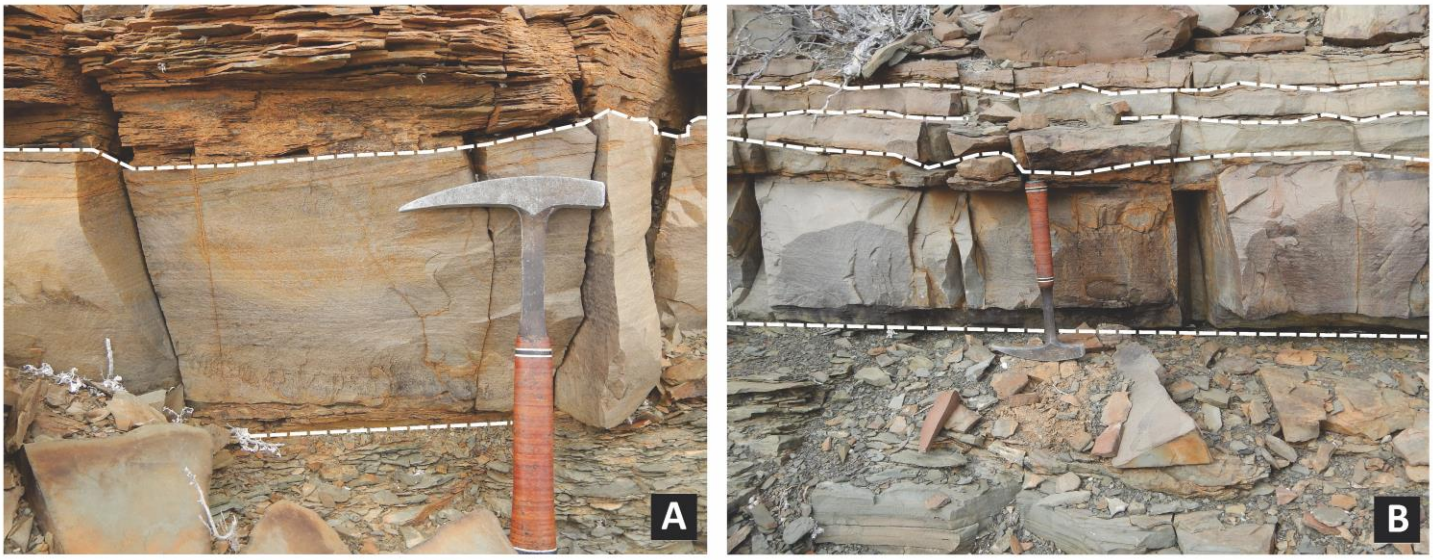


Figure 2.17. Lithofacies 6 – Quartz-rich HCS and wave rippled sandstone. A) Sandstone with sharp base (lowest hyphenated line) and wavy top (upper hyphenated line). HCS and planar laminations also evident (hammer is 32cm long). B) Planar laminated sandstone with wave rippled bed surfaces (hammer is 32cm long).

and due to the amalgamated nature of this facies and the distinctively wave dominated structures inherent in this facies, it is interpreted to represent sedimentation on the proximal lower shoreface.

2.5.7 Lithofacies 7 – Soft-sediment Deformed (SSD) Sandstone and Siltstone

Description:

The sandstones that make up this facies have highly variable thicknesses ranging from 7cm to 55cm. They are fine- to medium-grained and have a dark yellowish orange-red weathering colour. One larger deformed layer is present in the Dickneus and Northern Amibberg stratigraphic columns and is approximately 2m thick (Fig. 2.19A). This layer consists of detached, deformed and folded bodies in the form of large tilted, deformed and even slumped blocks (Fig. 2.19B, D, E and F) making it distinctly different from the other members of this facies. The deformed layer is underlain and overlain by undeformed strata (Fig. 2.19A). The chaotic nature of the bedding makes defining SSD types very difficult (Fig. 2.19C). Apart from the previously mentioned layer, the other sandstones have *in situ* deformation in the form of convoluted bedding and laminations as well as dewatering structures. Ball and pillow (Fig. 2.18C), pseudonodules (Fig. 2.18E) and intraformational rip up clasts are

also present in this facies. Some dewatering structures have not fully developed (Fig. 2.18B) and could possibly be considered as load casts. Other flame structures are upright in orientation (Fig. 2.18D) as are other dewatering structures. These features are normally confined to specific horizons within larger sandstone units and occur in close proximity and in the same stratigraphic horizons as HCS sandstones. The underlying and overlying contacts vary from sharp to largely undulatory. However, large-scale (affecting several layers), meso-scale (affecting one layer) and small-scale (affecting part of a layer) convolutions structures all form part of this facies (Fig. 2.18A and F). Bioturbation is largely absent from this facies or very difficult to distinguish.

Interpretation:

These SSD structures develop due to deformation during or soon after deposition, or when compaction is initiated (Allen, 1982). They are then in effect early diagenetic features (Van Loon, 2009). Convolutions in this facies seem to be syndepositional (during deposition) or metadepositional (after deposition but before the overlying layer was deposited, although sedimentation was apparently uninterrupted) (Van Loon, 2009) whereas the flame structures appear to be metadepositional or postdepositional. The formation of flame structures in this facies is related to density contrasts and fluidization of certain sediment types. These gravity induced structures form as a result of differential vertical movement of sediments due to initiated reverse density gradients (Van Loon, 2009). When a mass of sand is deposited/loaded over unconsolidated mud/silt-rich layers (Allen, 1984) the upper parts of the finer grained material becomes fluidized and is pushed up forming flames between parts that sink down. In this case the movement of the liquefied sediment is vertical as opposed to at an angle/oblique. This may happen when scours or large ripples in fine-grained sediment become filled with sand and create a density contrast that enables the loading process (Van Loon, 2009). There is also the possibility that this occurs together with down slope movements in the form of debris flows or slumps. The causes of external loading may be due to high sedimentation rates, sea-level changes, action of waves/tides or tectonic compression (Oliviera et al, 2011). The presence of SSD features on limbs of hummocks and swales points to minor slope instabilities after the settling of sediment after the conclusion of storm conditions. These sediments on the flanks of hummocks and swales became unstable at such angles and

began to flow forming convolutions. The 2m thick tilted and deformed layer is found along the Amibberg Massif and shows no clear pattern and may be interpreted as a seismite which affected a single stratigraphic horizon.

2.6 Lithofacies Stacking Patterns

The wave-dominated shoreface deposits of the Amibberg Formation are characterised by seven lithofacies which are: 1) Massive, laminated and bioturbated mudstones interpreted as offshore deposits (OS); 2) Bioturbated sandy-siltstones which are representative of offshore-transitional environments (OST); 3) Interbedded sandstones and siltstones also interpreted as offshore-transitional deposits (OST); 4) Sharp based, massive sandstones interpreted as being deposited on the distal lower shoreface (dLSF); 5) non-amalgamated HCS and wave rippled sandstones interpreted as distal lower shoreface-deposits (dLSF); 6) Amalgamated HCS and wave rippled sandstones interpreted as proximal lower shoreface deposits (pLSF); and 7) SSD sandstones and siltstone of no particular depositional environment often occurring in close juxtaposition with dLSF and pLSF deposits.

The vertical arrangement of these lithofacies shows an overall shallowing from offshore, to offshore-transitional, distal lower shoreface and finally proximal lower shoreface deposits. Four major upward-coarsening/shallowing cycles are documented (Fig. 2.33). The lowermost cycle is approximately 14m thick and consists of a 80cm thick, sharp based dLSF sandstone overlain by OS mudstones. However, this upward-coarsening cycle could possible extend into the Aussenkjer Formation below, although this has not been verified. This is then overlain by a thin OST interval and a thick pLSF unit. The second cycle is 75m thick and consists of five dLSF deposits which are underlain by OST and OS deposits respectively. Two dLSF deposits sharply underlain by OS mudstones are also present as is a 4m thick pLSF interval underlain by OST and OS deposits respectively. A highly deformed layer is also present in the upper parts of this cycle although no information of depositional environment can be obtained from this unit. This layer is interpreted to represent a

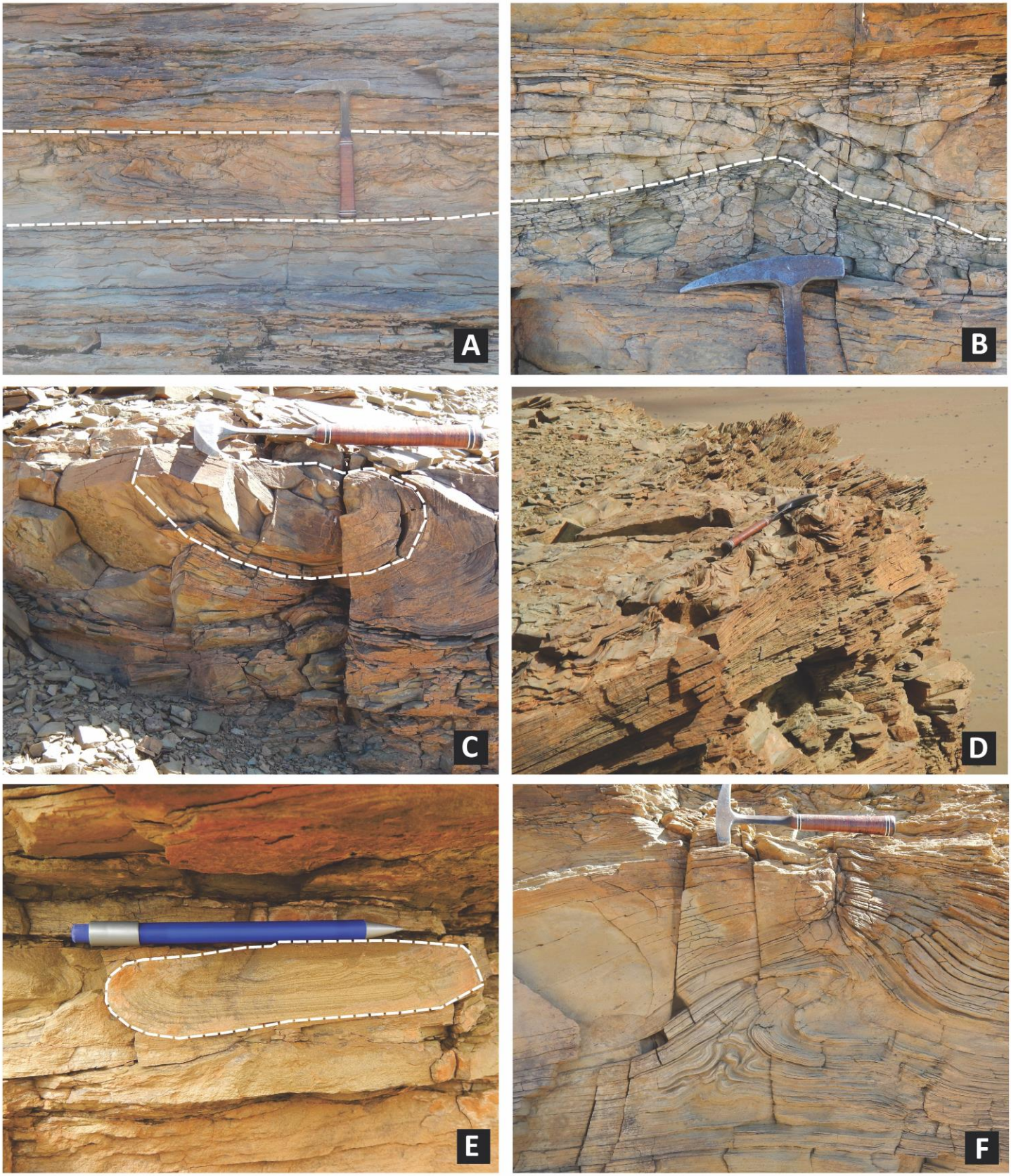


Figure 2.18. Lithofacies 7 – SSD sandstones and siltstones (in-situ). A) Meso-scale convoluted layer in fine-grained sandstone between hyphenated lines (hammer is 32cm long). B) Poorly developed flame structure affecting siltstone and sandstone horizons indicated by hyphenated line (hammer is 32cm long). C) Ball and pillow structure (outlined) in fine-grained sandstone (hammer is 32cm). D) Small scale flame structures that seem to have formed due to sand loading in the troughs of wave ripples (hammer is 32cm). E) Attached pseudonodule (outlined) that appears like a load cast that is still connected to its source bed (pencil is 15cm long). F) Large-scale convoluted beds affecting multiple fine- to medium-grained sandstones (hammer is 32cm long).

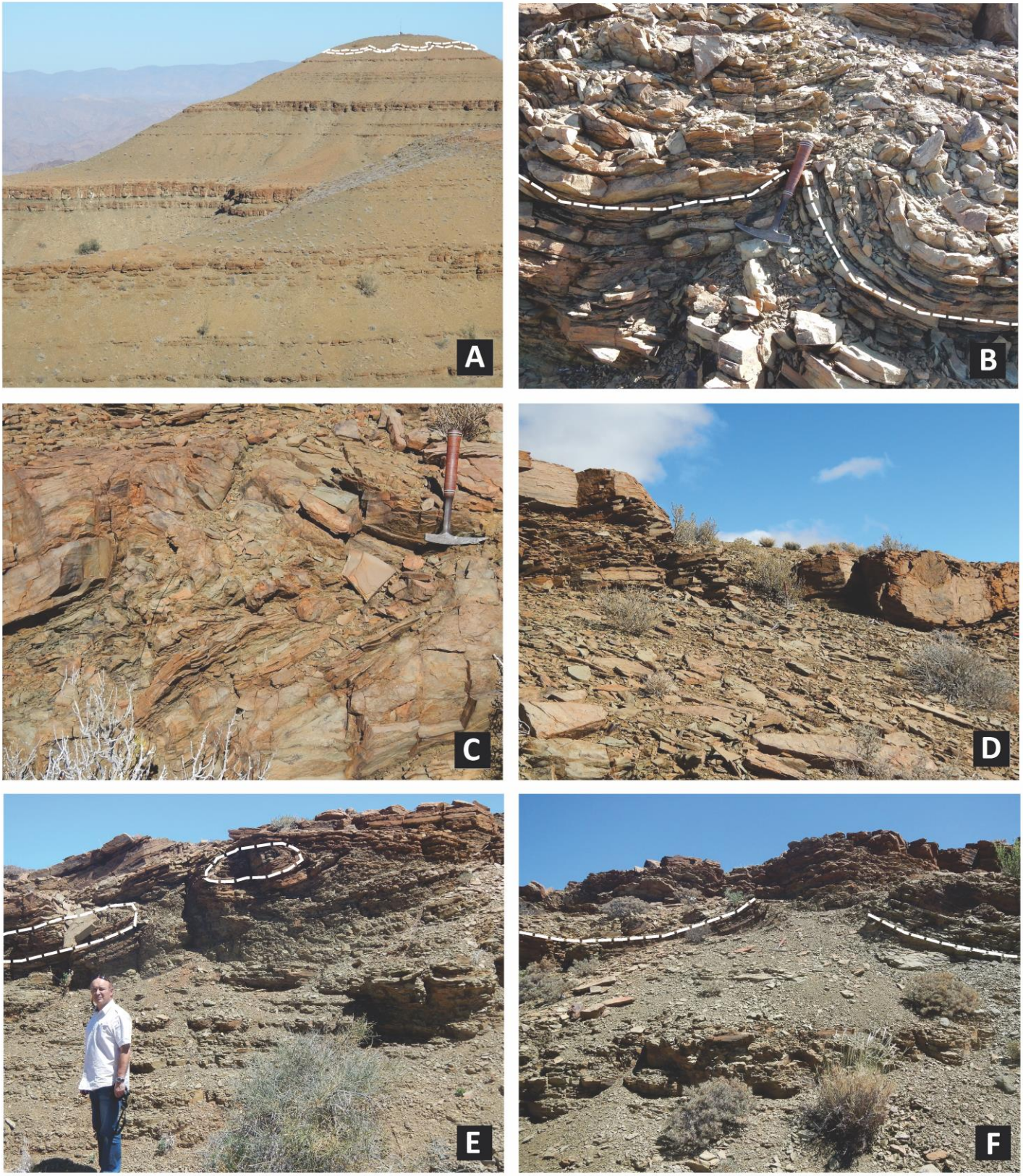


Figure 2.19. Lithofacies 7 – SSD sandstones and siltstones (detached). A) Outcrop locality of the tilted and slumped horizon which is the uppermost sandstone layer on the Dickneus (outlined). B) Large-scale dewatering structure indicated by hyphenated line (hammer is 32cm long). C) Chaotic fabric making SSD classification very difficult (hammer is 32cm). D) Photograph showing the displacement of sandstone layer (hammer is 32cm long). E) The thickness of this layer as well as the chaotic nature of these sandstones exhibited in this photograph. Also present are large ball and pillow structures which are outlined (person for scale is 1.8m tall). F) Deformed limbs (hyphenated lines) of a sandstone showing steepening limbs forming an anticlinal fold structure in the center of the photo (hammer for scale is 32cm long).

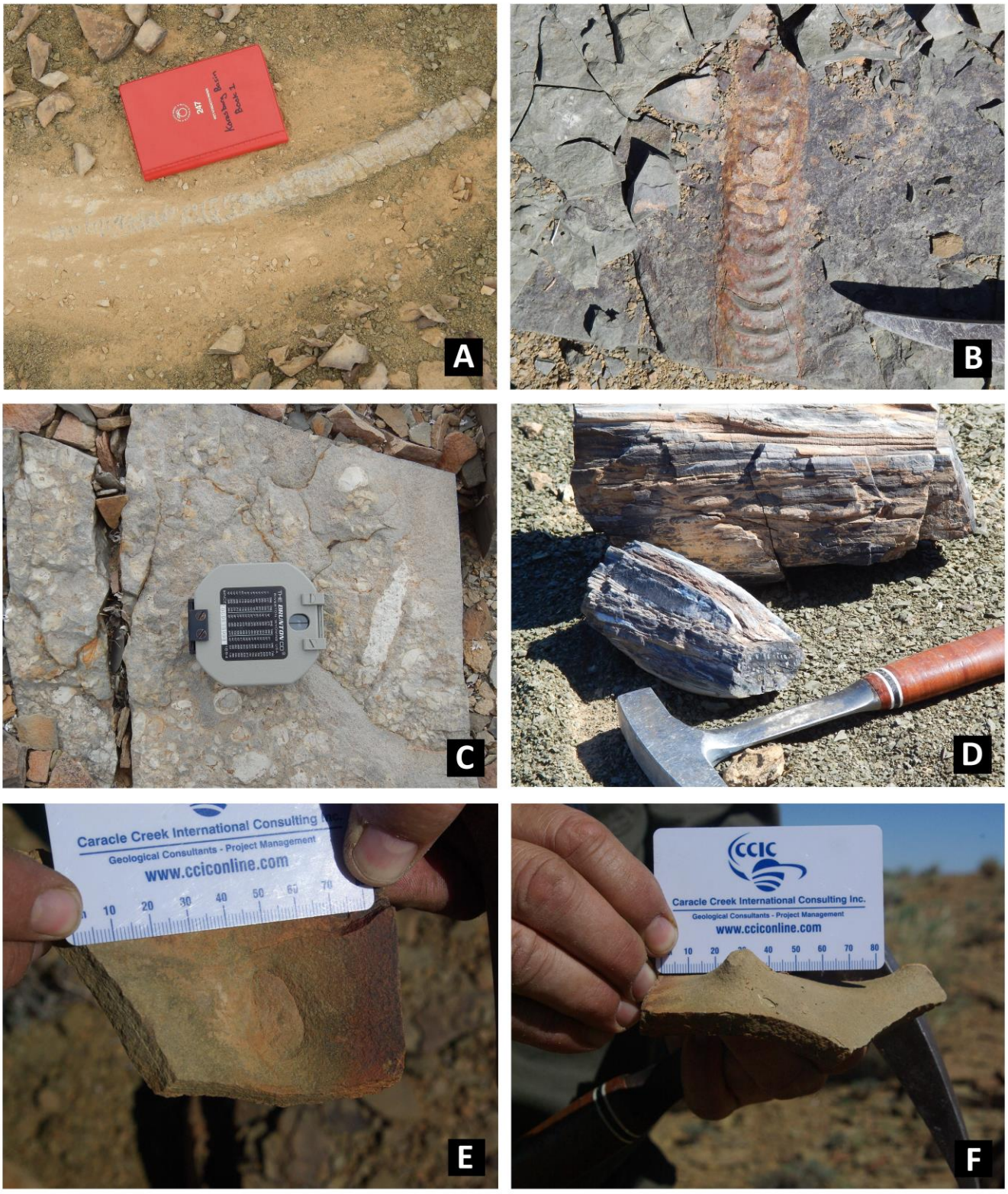


Figure 2.20. Other important photos. A) 1m long, backfilled curved and ribbed *Pseudo-Plagiogmus* trace (note book is 19cm in length). B) Close up of *Pseudo-Plagiogmus* showing a clear row of meniscate bends (hammer for scale is 32cm long). C) Intraformational rip-up clast impressions with a variety of forms and sizes (compass for scale is 7.5cm in length). D) Unidentified permineralized wood fragments found *ex-situ* in the vicinity of the second major sandstone of the Amibberg Formation (hammer for scale is 32cm long). E) Vertically orientated, ovular shaped, infilled burrow set in a depression within fine-grained sandstone seemingly representing *Conichnus conosinus* (scale in upper part of photo). F) Side view of burrow in E) showing funnel-like infill and a gradually decreasing diameter of the burrow with an increase of depth through the sediment (scale evident in photo).

seismite. This cycle is capped by a 15m thick pLSF interval. The third coarsening-upward cycle is approximately 23m thick. This consists of two dLSF deposits underlain by OST and OS intervals respectively. A 10m thick pLSF underlain by OST deposits caps this cycle. The uppermost cycle is 90m thick and consists of three or four dLSF sandstones underlain by OST and OS deposits respectively. Capping this cycle is a 15m thick pLSF unit underlain by OST deposits. A partial cycle forms the uppermost preserved interval in the study area although little environmental data can be obtained by this partially complete unit.

Generally, the pLSF deposits (Fig. 2.21-2.24) are often characterised by a sequential arrangement of HCS, siltstone and wave rippled sandstones (Fig. 2.21). Furthermore, zones of convoluted bedding may also be present in these arrangements. Other times only thin intervals of HCS are present with thicker intervals of wave rippled sandstone present (Fig. 2.22). The thick pLSF units are usually underlain by intervals of OST deposits which in turn are underlain by OS deposits (Fig. 2.23) and represent deposition during the periods of the shallowest water. Immediately overlying these pLSF intervals are bioturbated sandstones (OST) and mudstones (OS) respectively indicating a gradual rise in relative sea level. Distal lower shoreface deposits are underlain by OST and OS deposits respectively. This implies a lesser degree of shallowing during deposition than that which would result in the deposition of pLSF deposits. In some instances dLSF deposits are underlain by OST and other dLSF deposits respectively (Fig. 2.24). This indicates periods of mild shallowing before the depositional environment underwent deepening again. All dLSF deposits are sharply overlain by OS mudstones indicating a rapid rise in relative sea level during the deposition of these sandstones. The above-mentioned arrangement of lithofacies and depositional environments can be seen in the interpreted photomosaics in Figs 2.25, 2.26 and 2.27. These are from various localities in the study area and provide the most useful diagrams to obtain a full interpretive stratigraphic overview of the strata of the Amibberg Formation

In summary, periods of gradual shallowing in the basin resulted in the progradational vertical stacking patterns of these lithofacies. This gradual shallowing is typically terminated by a rapid rise in relative sea level, except after the deposition of pLSF deposits where a gradual rise in sea level is recorded by upward-fining intervals of

bioturbated sandstones. Multiple periods of shallowing are recorded by the coarsening upward character of these lithofacies arrangements (Fig. 2.26 and 2.27).

2.7 Photographic Interpretations

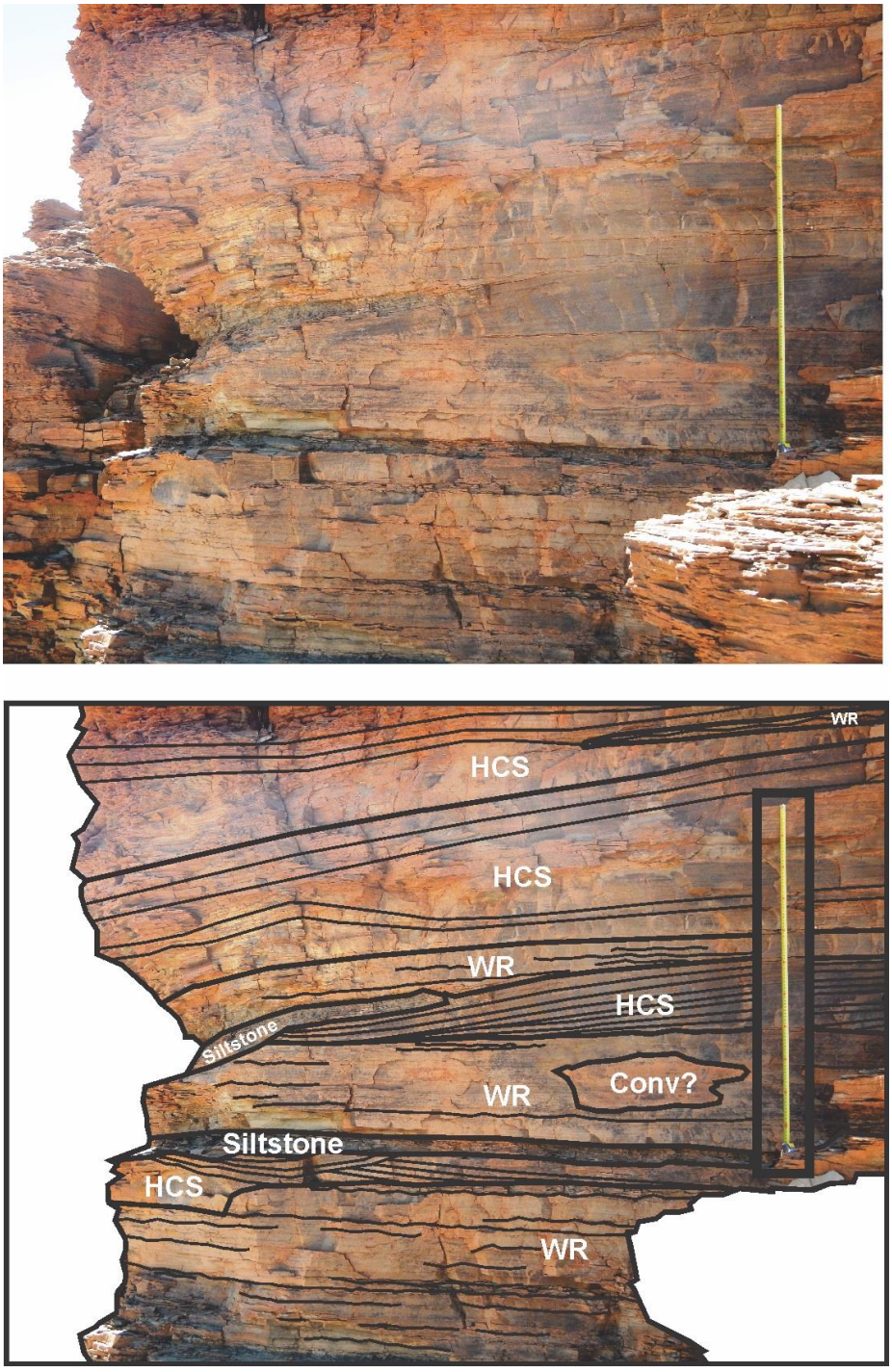


Figure 2.21. Interpreted photograph of an amalgamated HCS and wave rippled unit. Note the relationship between HCS, minor siltstone beds and wave ripples. A zone of possible convolutions is also present (tape measure for scale showing 1.07m).

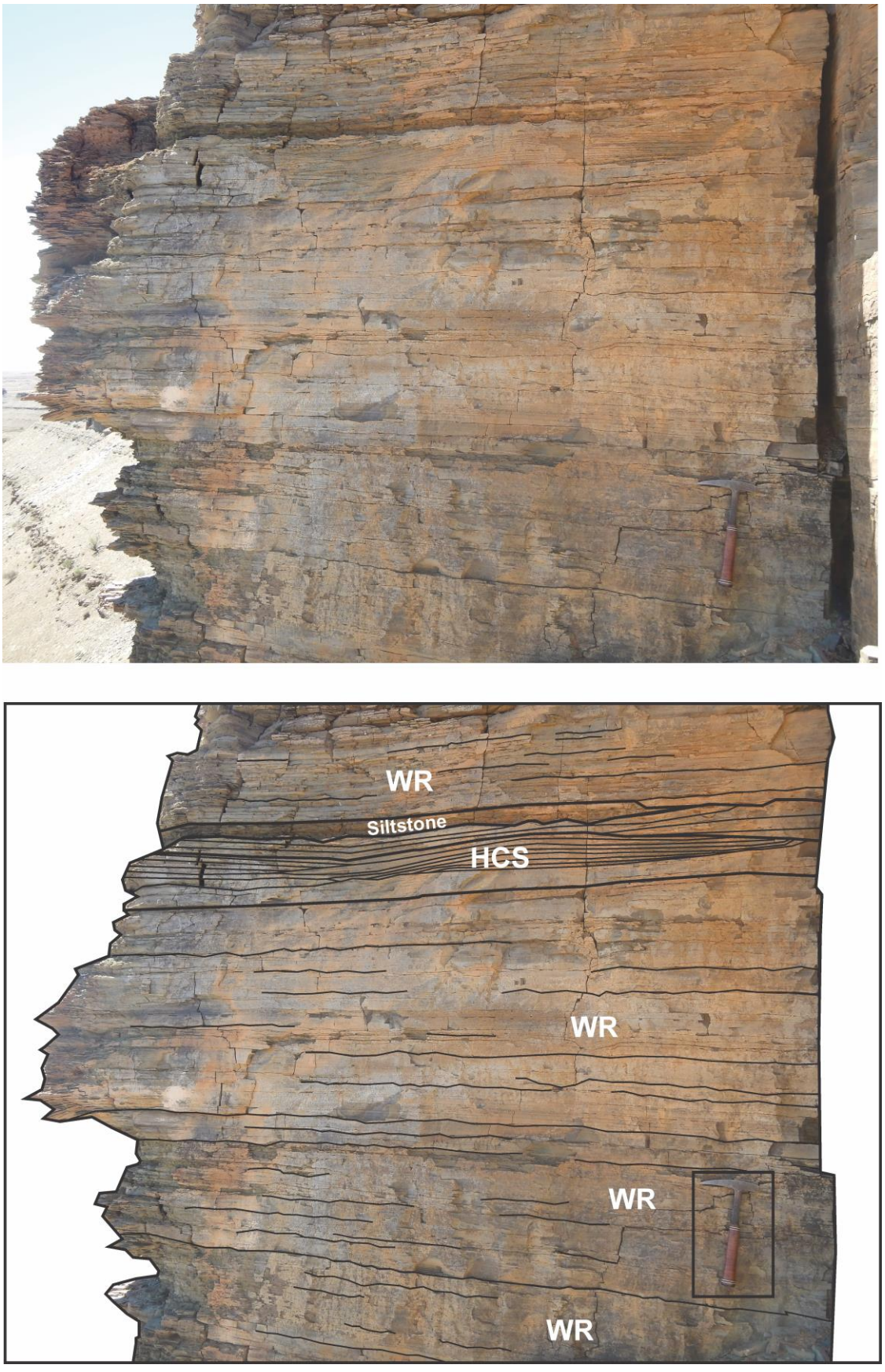


Figure 2.22. Interpreted photograph of an amalgamated HCS and wave rippled unit. 20cm zone of HCS and minor siltstone bed in a unit of amalgamated wave ripples (hammer for scale is 32cm long).

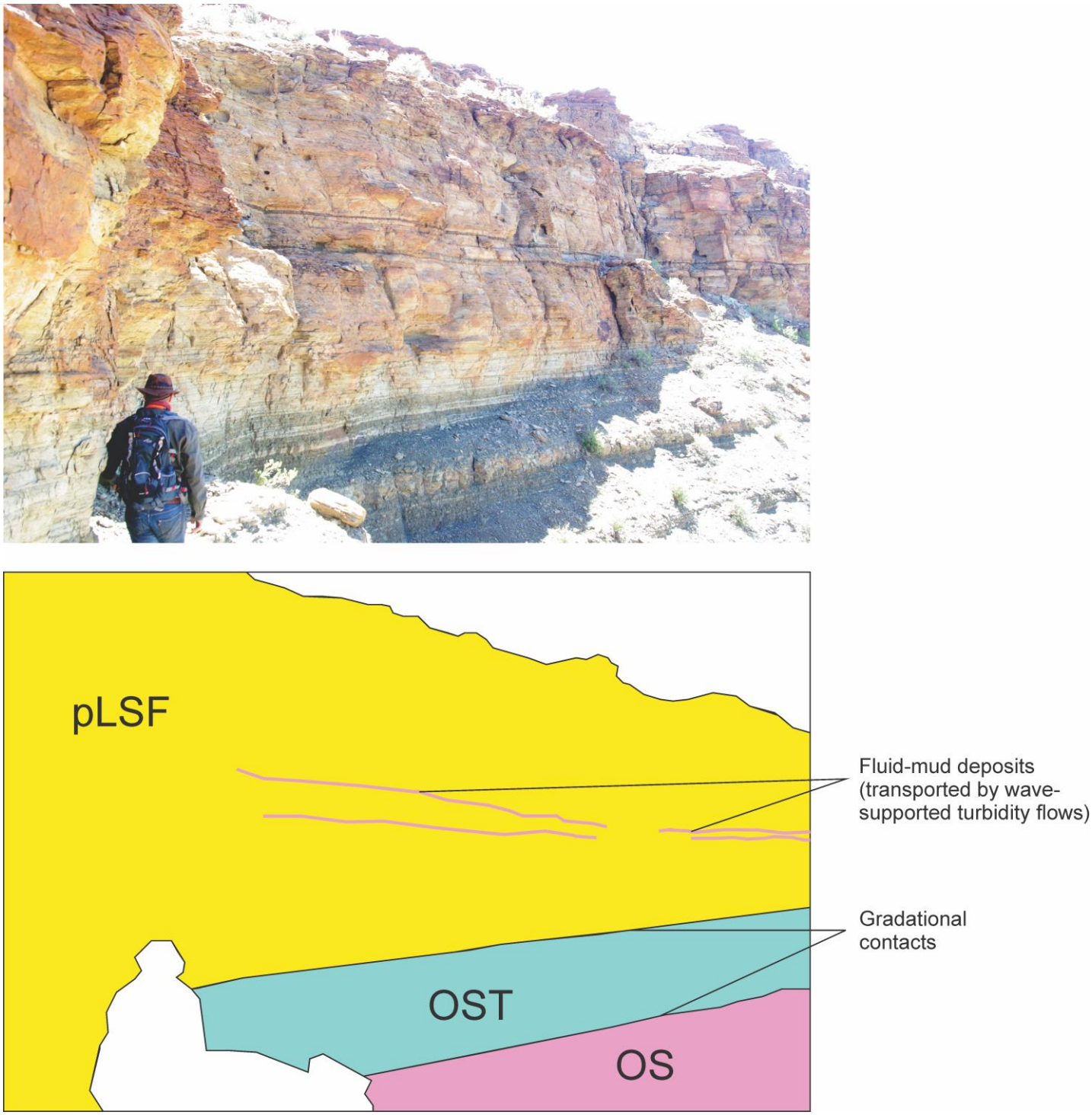


Figure 2.23. Interpreted photograph of the uppermost amalgamated HCS and wave rippled unit in the study area. The sequential relationship between the amalgamated sandstone (yellow), interbedded sandstone and mudstone (blue) and mudstone (pink) is evident (person for scale is 1.8m tall).

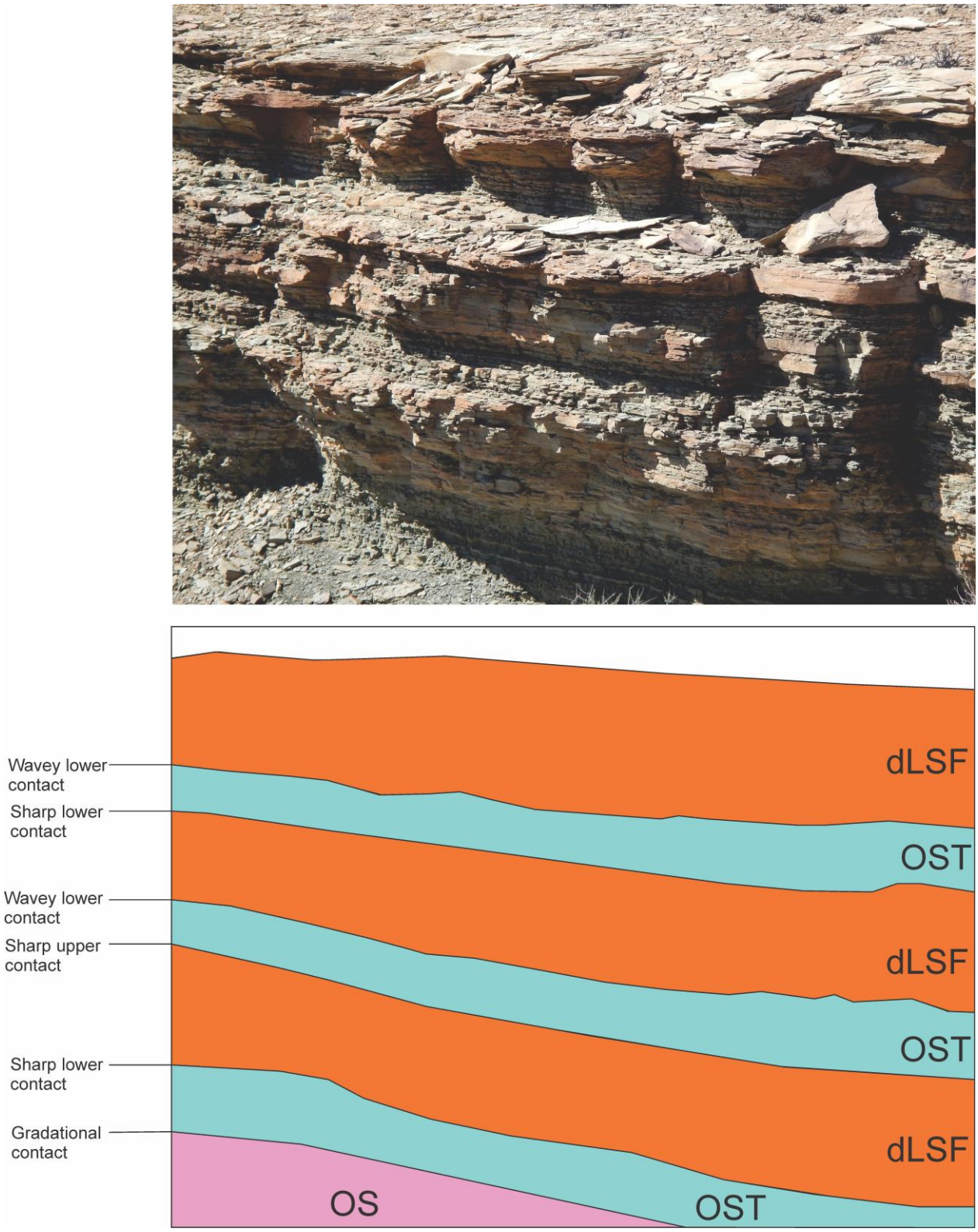


Figure 2.24. Interpreted photograph of an arrangement of discrete HCS and wave rippled intervals. Intervals of distal lower shoreface origin (orange) underlain by offshore transitional strata. This whole interval is underlain by offshore mudstones (outcrop is approximately 10m in height).

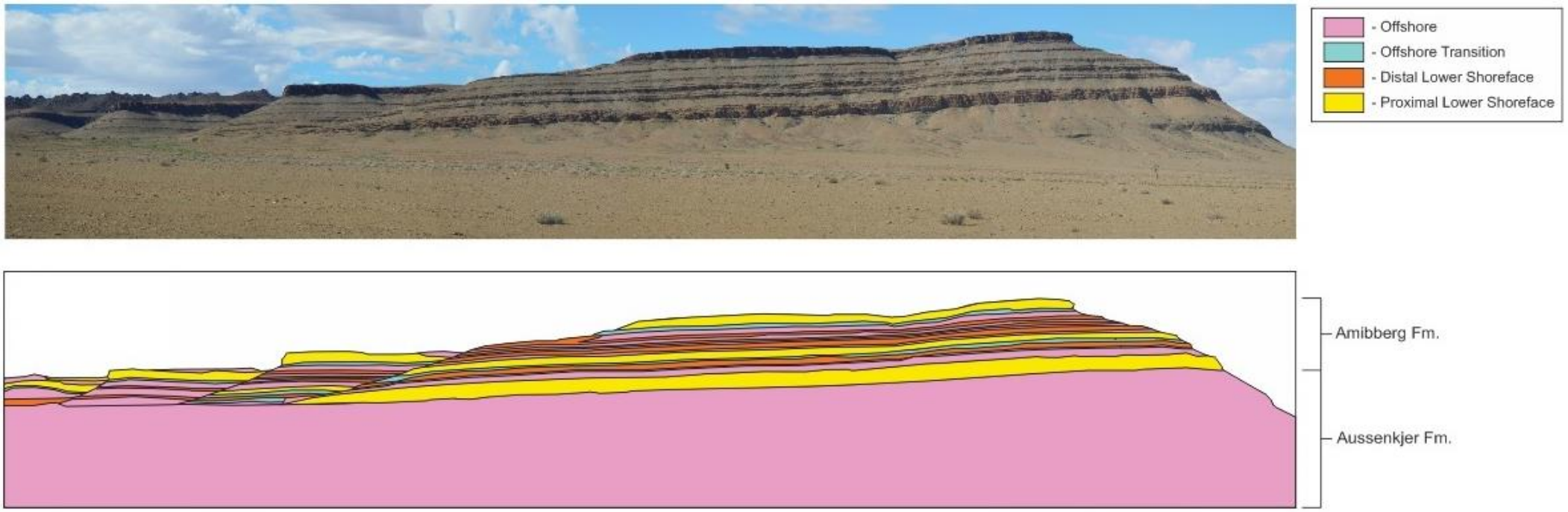


Figure 2.25. Interpreted photomosaic of the Northern Amibberg locality. Slightly tilted strata of the Amibberg and Aussenkjer formations. The Aussenkjer Formation is below the first prominent amalgamated HCS and wave rippled sandstone (yellow) and the Amibberg Formation is defined as anything above this sandstone. Note that the seismite (Fig.2.2) is not clearly defined in side profile as three-dimensional outcrop is required to definitively identify its stratigraphic position (entire Amibberg section approximately 110m thick).

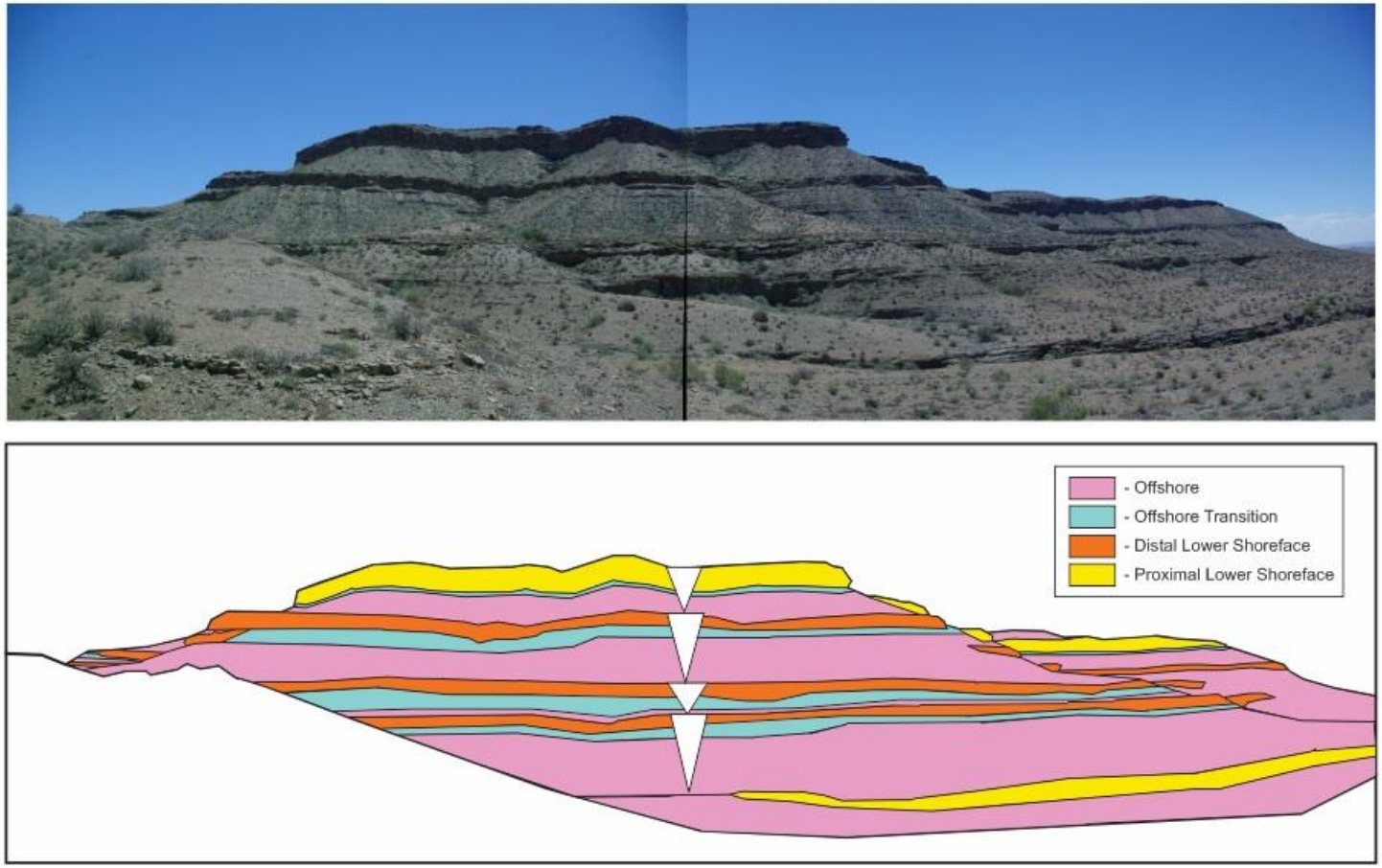


Figure 2.26. Interpreted photomosaic of the Tafelberg locality. Uppermost amalgamated sandstone unit (yellow) in the study area underlain by an interval of interbedded sandstones and mudstones. Underlying this is a thick mudstone interval and sequences of distal lower shoreface and offshore transitional deposits (4 upward-coarsening cycles approximately 80m thick in total).

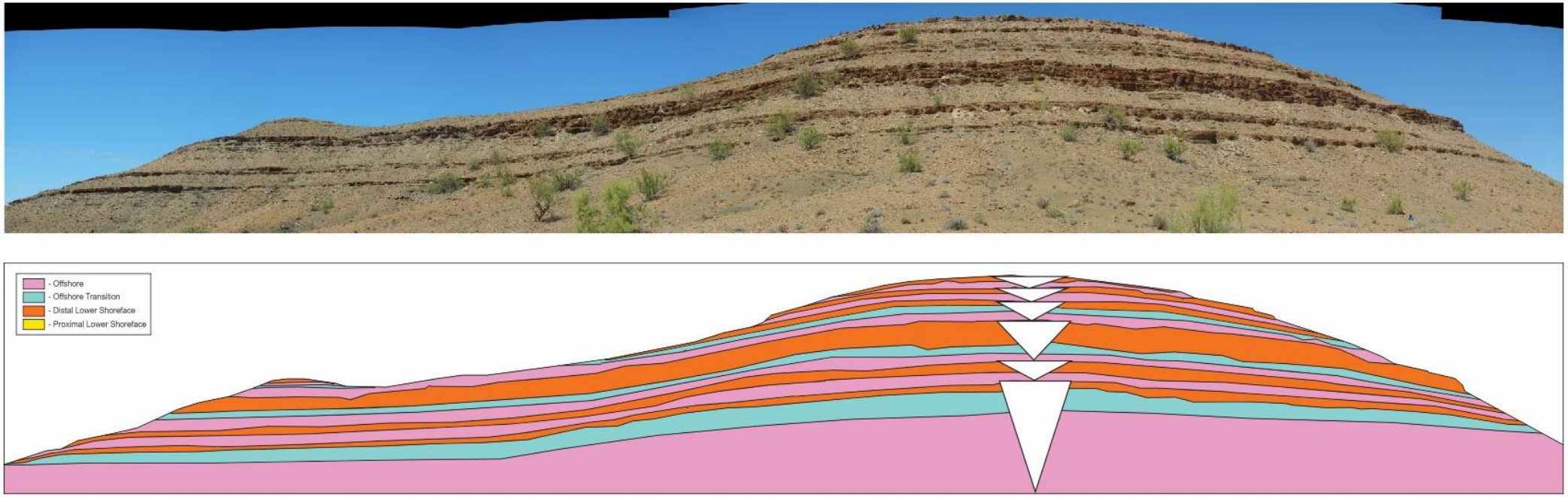


Figure 2.27. Interpreted photomosaic of a section of the Amibberg Massif. Relationship between offshore mudstones (pink), offshore transitional deposits (blue) and distal lower shoreface deposits (orange). 6 upward-coarsening cycles approximately 60m thick in total.

2.8 Ripple Descriptions

Wave ripples from which orientations can be measured are found in lithofacies 3, 5 and 6. A general description of these ripples in required to interpret a palaeoshoreline orientation. Overall the wave ripples in the study area are near symmetric (Fig. 2.31A) to asymmetric (Fig. 2.31B); have slightly rounded crests (Fig. 2.31A) to sharp crests (Fig. 2.31E); have wavelengths of between 11cm and 6cm; have amplitudes of 0.5cm to 0.25cm; are continuous over 25cm to 4m and in some cases show bifurcation. Rounded crests are indicative of combined-flow ripples (Harms, 1969; Yokokawa, 1995) and the symmetrical ripple marks that are discordant with their associated cross-lamination (combined-flow ripples; Harms, 1969) testify to the activity of combined-flow currents. The ripple index [length (crest to crest)/height (crest to trough)], or steepness, of these ripples ranges from 14 to 11 which, coupled with the amplitudes and wavelengths, are indicative of wave ripples (Tanner, 1967). The ripple symmetry index (width of long slope/width of short slope) ranges from 1.75 to almost completely symmetrical values of 1. These symmetrical ripples commonly occur in close vertical juxtaposition with hummocky cross-stratified sandstones (Leckie and Walker, 1982; Leckie, 1985; Wright and Walker, 1981; Cotter 1985; Eyles and Clark, 1986). Such 'capping' wave-ripples are typically straight-crested (Fig. 2.31C and D) with occasional bifurcating patterns, although irregular forms have been observed including: bidirectional (Fig. 2.31F), polygonal, ladderback and box patterns.

2.9 Discussion

2.9.1 Palaeocurrent Interpretation

In terms of using wave ripples to estimate palaeoshoreline, the nature and behaviour of waves must be addressed. Storms approach the coast from different directions and shoaling storm waves become refracted. The resulting wave-ripple crests are approximately parallel to bathymetric contours (Komar, 1976). Also, the internal cross-laminae of symmetrical wave ripples, when present, indicate migration offshore. Therefore, the orientation of wave-ripple crests from the lower shoreface to offshore-

transitional zone of wave-dominated coasts can be used to approximate the local palaeoshoreline trend. Data for wave-ripple crest orientations shown here generally have a spread of a few tens of degrees but some outliers are present within the data set. The general trend would be the result of the varying directions of storm systems and the ensuing waves approaching the palaeoshoreline. Here, it is interpreted that the local palaeoshoreline is perpendicular to the mean palaeocurrent vector.

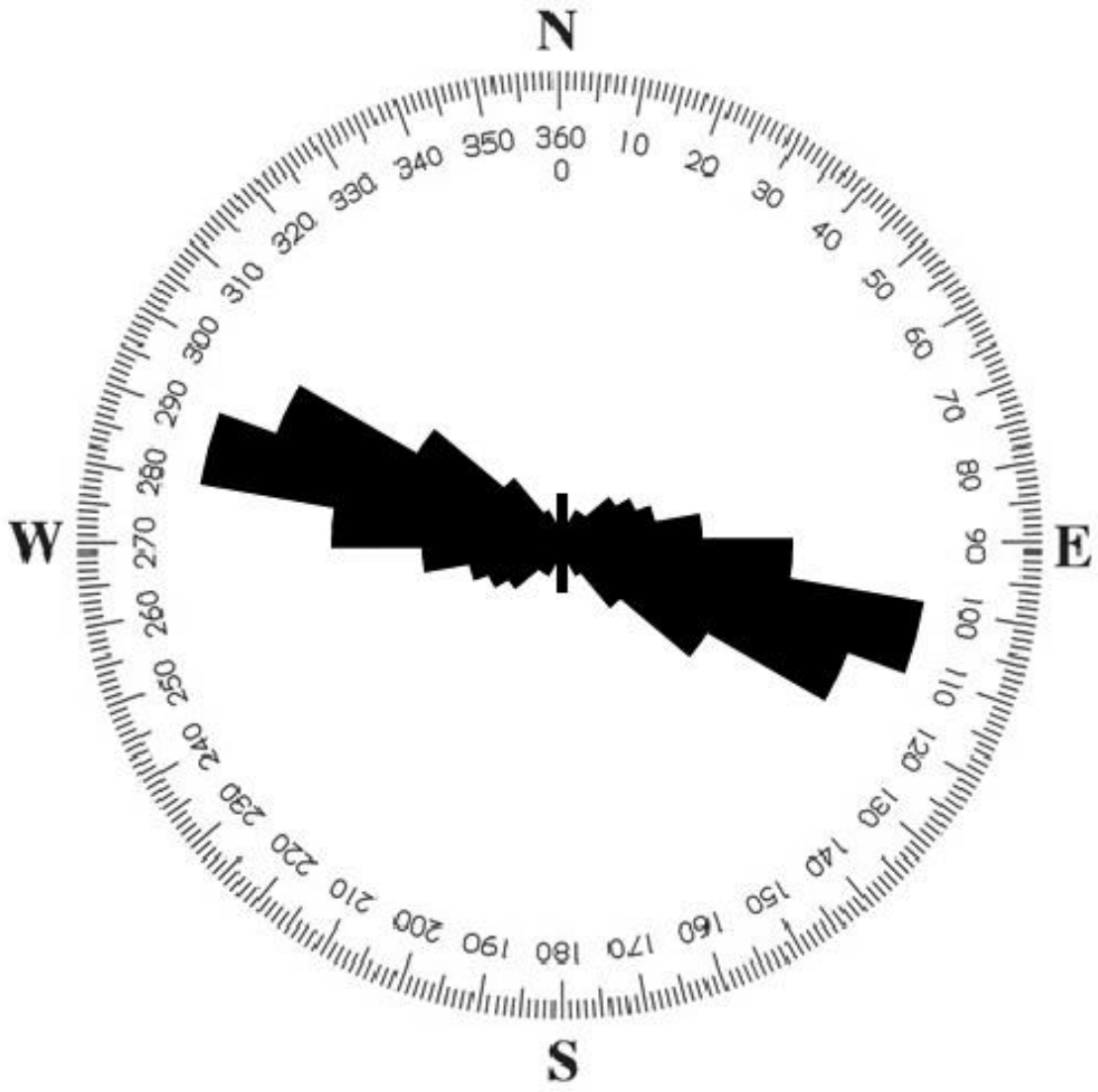


Figure 2.28. Symmetrical wave ripple palaeocurrents. 106 palaeocurrent readings obtained from symmetrical wave ripples and displayed on a rose diagram. A general trend WNW-ESE is observed as well as outliers of the data set.

For symmetrical wave ripples (Fig. 2.28), 106 vector readings (Appendix A) were corrected for dip and magnetic declination, and a mean value for these readings

recorded as 101°-281° (WNW-ESE). From this, the palaeoshoreline is estimated to have trended along 11°-191° (NNE-SSW).

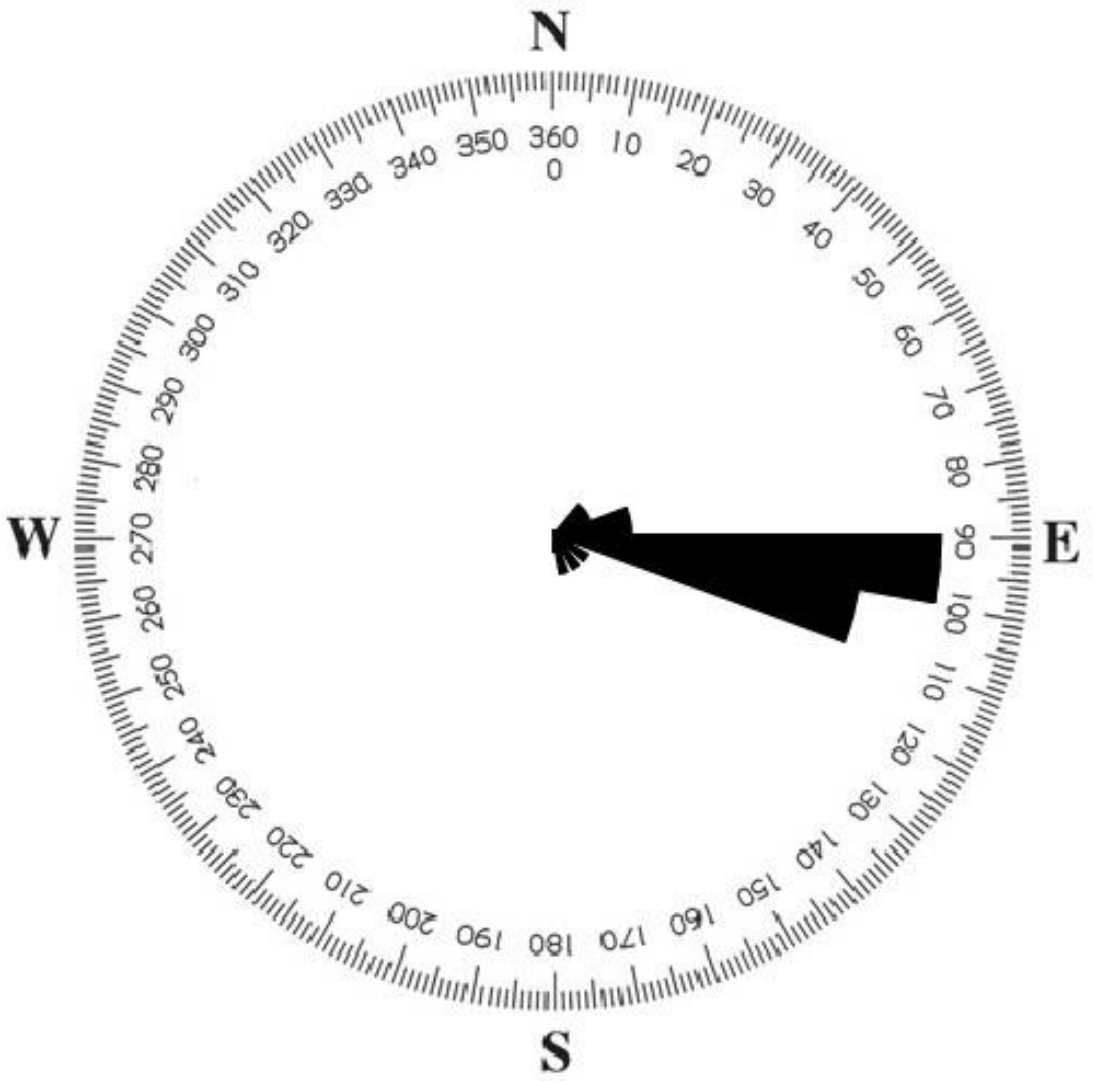


Figure 2.29. Asymmetrical wave ripple palaeocurrents. 28 palaeocurrent readings obtained from asymmetrical wave ripples and displayed on a rose diagram. A general ESE trend is observed as well as outliers of the data set.

In terms of asymmetrical ripples (Fig. 2.29), 28 vector readings (Appendix A) were obtained and corrected for magnetic declination and dip. A mean of 95° has been recorded which indicates a dominant direction of flow towards the ESE during the deposition of these structures.

The main basement feature underlying the Karasburg Basin is the NNW-trending Gariep Belt that has been delineated from geophysical surveys. This tectonic unit should result in a palaeoshoreline parallel to this NNW trend. However, a NNE-SSW trending palaeoshoreline was delineated from this study. This is due to the nature of the Gariep Belt not being wholly continuous over its entire length (Fig. 2.30). Towards the south eastern part of the belt it becomes disaggregated and various splits are present in a north easterly direction. Also in the southeast, various embayments are present from the geophysical delineation of this structure. These various structural features could have acted as bays and sediment traps forming a wave-dominated shoreface with a NNE-SSW trending palaeoshoreline. Furthermore, the approximated palaeoshoreline corresponds to the orientation of the western Cargonian Highlands during the Early Permian. This palaeoshoreline most likely occupied areas of this palaeohigh and was influenced by wave activity from the east, fluvial input from the south as well as tidal processes.

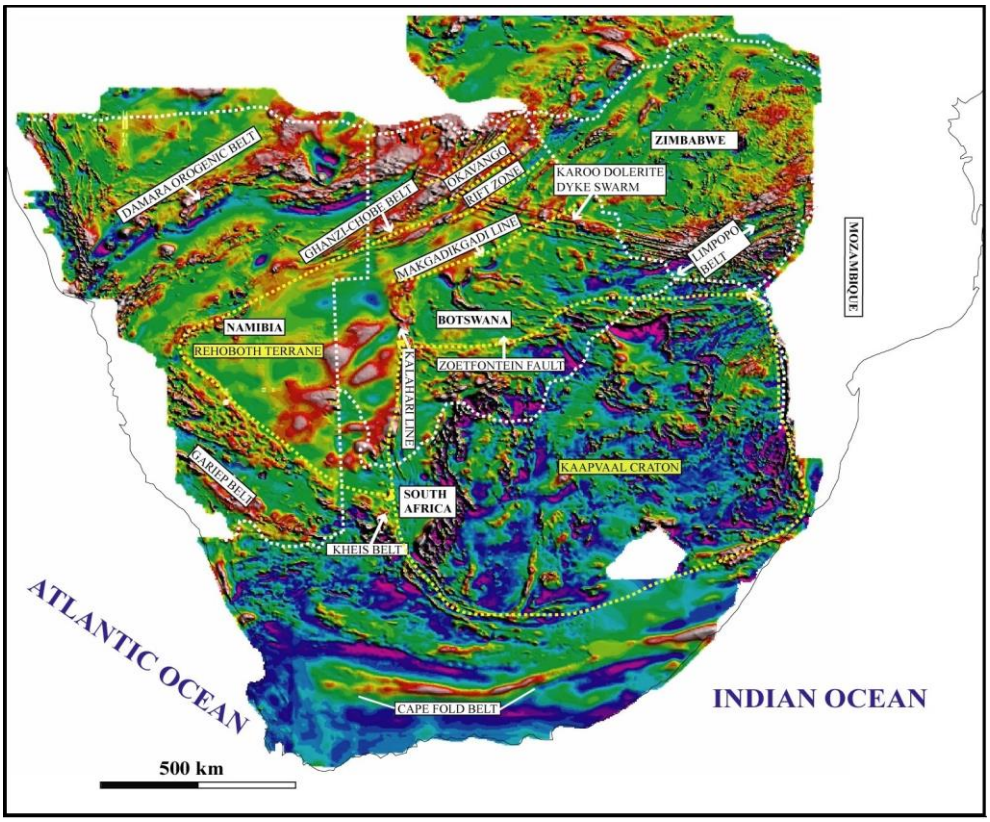


Figure 2.30. Geophysical map of southern Africa indicating major structural features and continental cratons. Note the location of the Gariep Belt along the southern border of Namibia with South Africa [after Nxumalo, 2011 (sourced from the Council of Geoscience)].

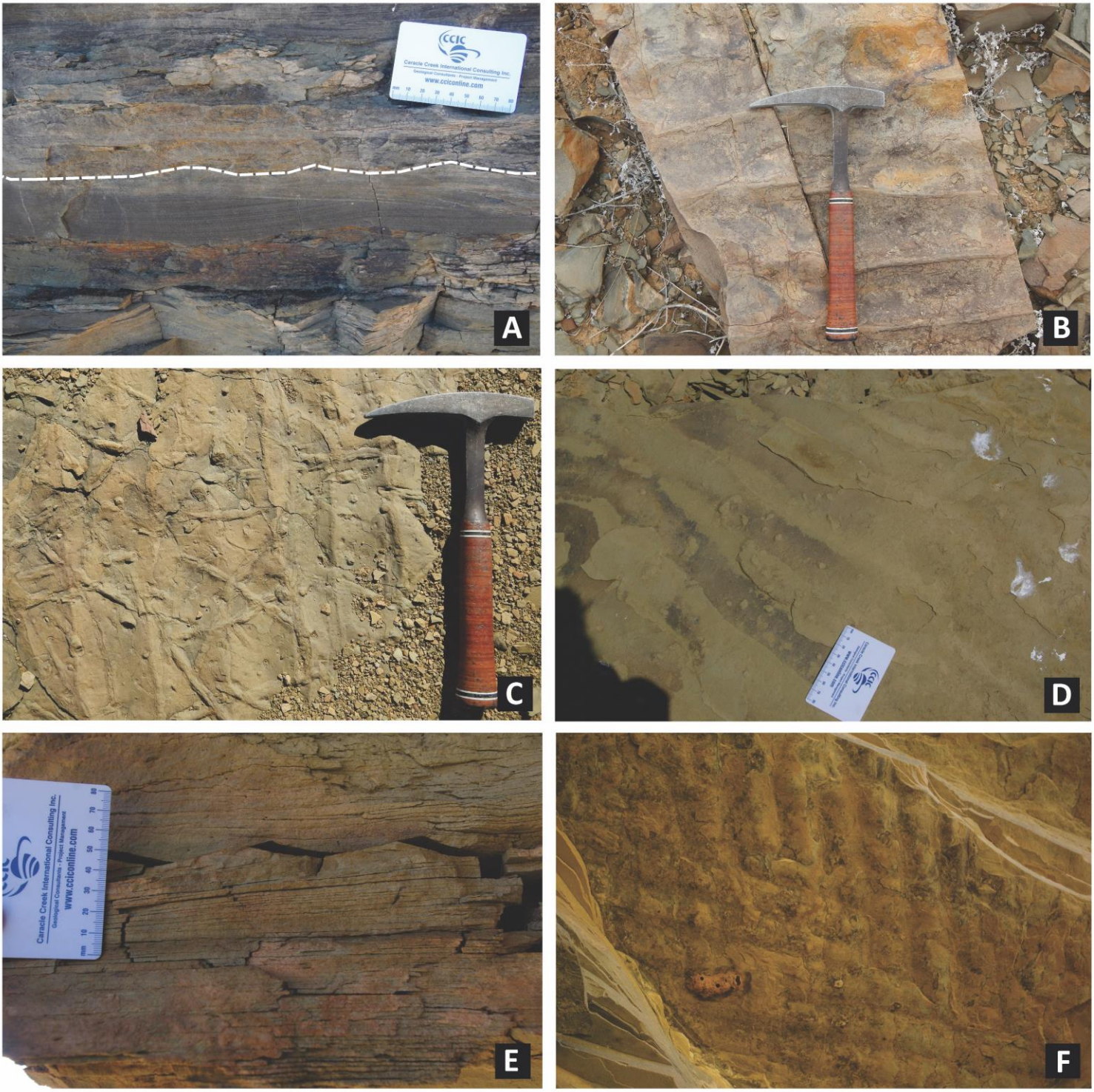


Figure 2.31. Wave ripples. A) Appearance of wave ripples (hyphenated line) with associated ripple cross laminations overlying a HCS bed (scale upper right corner of photo). B) *Ex-situ* wave ripples showing straight to sinuous crests (hammer is 32cm long). C) Wave ripple crests with evidence of biological activity. Overlapping cylindrical burrows interpreted to represent the trace fossil *Palaeophycus* (hammer is 32cm long). D) Wave rippled bed surface with evidence of vertical *Skolithos* burrows (scale bottom center of photo). E) Wave ripples in outcrop with clearly defined shape due to shifting of the rock in recent times (scale left of photo). F) Bidirectional wave ripples on the same lower bedding plane showing distinct interference. One set of ripples trend vertically (N-S) on the photo while the other set trend diagonally across the photo (NW-SE) (wasp nest is approximately 5cm in length).

Table 2.3. Characteristics of lithofacies recognised in the Amibberg Formation.

Lithofacies	**Dimensions and lithology**	**Structures**	**Geometry**	**Bounding surfaces**	**Bioturbation**	**Palaeocurrents**		**Interpretation**
						Var.	**Mean**	
1 Massive to plane-bedded mudstone	1.2 to 39m thick mudstone	Rare planar laminations, carbonate nodules	Mostly laterally extensive and tabular, may pinch-out within a few tens-to-hundreds of meters (lenticular)	Sharp to gradational	Intense (BI = 5-6). Traces include: *Rosellia, Palaeophycus, Paleodictyon, Thalassinoides* and *Pseudo-Plagiogmus.*	NA	NA	Suspension fall out in low energy settings (OS)
2 Bioturbated siltstone and sandstone	0.35 to 4.0m thick sandy-siltstone	Rare planar laminations and wave rippled surfaces	Lenticular	Sharp or wavy	Intense (BI = 4-6). Traces include *Palaeophycus* and *Planolites.*	NA	NA	Low energy environment for prolonged periods of time (OST)
3 Interbedded sandstone and siltstone	0.35m to 7.0m thick interbedded and mixed fine-to medium-grained sandstone and siltstone	Planar and cross laminations, HCS, wave ripples, flaser, wavy and lenticular bedding	Laterally extensive and tabular. Can also be lenticular	Sharp or wavy base to gradational, rare erosional base	Weak to moderate (BI = 1-3). Trace include: *Palaeophycus, Skolithos* and *Arencolites*.	69° to 284°	88° to 268°	Pulsatory type hyperpycnal flows followed by periods of suspension fallout (OST)
4 Sharp based, massive sandstone	0.75 and 3.0m thick fine- to medium-grained sandstone	Weak planar laminations and wave rippled surfaces	Typically continuous along strike, occasionally laterally segmented	Sharp	Intense (BI = 5-6). Traces include *Skolithos* and *Planolites.*	NA	NA	Low energy environment (dLSF)
5 Discrete HCS and wave rippled sandstone	0.25 to 3.0m thick fine- to medium-grained sandstone with siltstone	Planar laminations, HCS, wave ripples, climbing ripples	Typically tabular and laterally persistent	Sharp, wavy to erosional	Sandstones have low bioturbation (BI = 1-2) and siltstones are moderate to intensely bioturbated (BI = 4-5). Traces include: *Planolites, Skolithos Crosspodia, Asterosoma, Helminthopsis, Schaubcylidrichnus, Cochlichnus, Thalassinoides* and *Monocraterion.*	93^{o} to 304^{o}	107^{o} to 287^{0}	Tempestitic origin (dLSF)

6 Amalgamated HCS and wave rippled sandstone	3.0 to 14.10m thick fine- to medium-grained sandstone. Minor mudstone and siltstone	Planar laminations, HCS, wave ripples, climbing ripples	Tabular and laterally persistent	Sharp, wavy to erosional	Sandstones weakly bioturbated (BI =1-2) with other sandstone and siltstone intensely bioturbated (BI=4-5). Traces include: *Rhizocorallium, Asteriacites, Skolithos, Phycodes, Planolites, Palaeophycus, Monocraterion, Cochlichnus, Gyrochorte* and *Gordia.*	34^{o} to 329^{o}	86^{o} to 256^{o}	Tempestitic origin (pLSF)
7 SSD sandstones and siltstone	0.07 to ~2.0m medium- to fine-grained sandstone and minor siltstone	Convoluted bedding, flames, ball and pillows, pseudonodules and possible load casts	Tabular and discordant in some cases	Sharp to wavy	Absent. No trace fossils observed.	NA	NA	Gravity induced structures form as a result of differential vertical movement of sediments. Associated with deposition on the p/dLSF.

Table 2.3. (Continued)

2.9.2 Ichnology

The abundance and rich diversity of trace fossils present in the Amibberg Formation indicates that communities of organisms thrived during the time of deposition. The importance of this biogenic diversity is that it provides valuable insight into the palaeoenvironment at the time of deposition. As stated by various researches (MacEachern et al., 2005; Buatois et al., 2008; MacEachern and Bann, 2008; Bhattacharya and MacEachern, 2009; Carmona et al., 2009; Buatois and Mángano, 2011; Buatois et al., 2011) it is possible to use the ichnological information gathered as well as the changes and behaviours of benthic fauna to provide a better understanding of depositional regimes. For example the presence of traces associated with the *Skolithos* ichnofacies represent opportunistic colonization during or very soon after storm conditions prevailed, whereas *Cruziana* ichnofacies traces are indicative of stable palaeoenvironments (Tiwari et al., 2011). These are the dominant trace fossil suites with regard to a wave dominated shoreface. However, tidal-influenced shallow-marine sandstones have sparse to intense levels of bioturbation by a diverse trace fossil assemblage that constitutes a mixture of *Skolithos* and *Cruziana* ichnofacies (Pemberton et al., 1992). Therefore an introduction of a tidal signature of a wave dominated shoreface may induce the mixed nature of *Skolithos* and *Cruziana* assemblages. Contrary to this, Cheel and Leckie (1993) suggested that after rapid emplacement of sand, the original resident community or a subsequent one may overprint the *Skolithos* ichnofacies resulting in a mixed *Skolithos-Cruziana* ichnofacies. In this case, vertical escape burrows represent the traces of organisms suddenly buried by sand in an attempt to rise to the new substrate following a storm.

In general in this study area the offshore to offshore transitional environments yield more abundant bioturbation whereas the shoreface deposits yield a lower intensity of bioturbation. This may be due to the high intensity and high frequency of storms (Buatois et al., 2012).

The tempestites of the Amibberg Formation generally show a low-diversity suite of trace fossils. These all display characteristic activity on soft ground substrate as no members of the *Glossifungites* ichnofacies have been identified. Figure 2.32 shows an

idealised HCS tempestite deposit and the associated ichnofacies and individual trace fossils that may colonise these substrates (after Ekdale et al., 1984). The *Cruziana* ichnofacies (Fig. 2.34-2.38) is by far the most abundant within the study area. The *Skolithos* ichnofacies (Fig. 2.33) is present to a lesser degree as is the *Nerites* ichnofacies. Typically these ichnofacies (*Skolithos* and *Cruziana*) occur in isolation but there are examples where there is a mixing of these ichnofacies (Fig. 2.39). This may be due to the influence of tidal regimes or due to rapid emplacement of sand as previously mentioned. Trace fossils from the study area are described below.

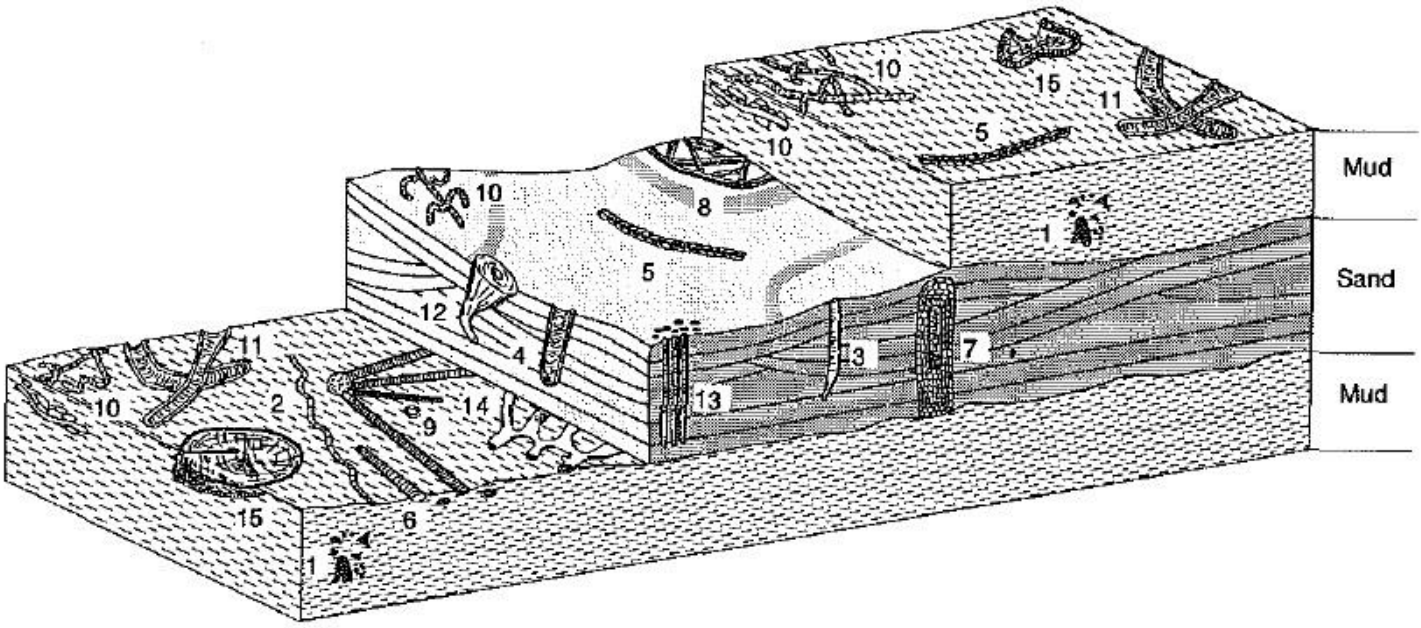


Figure 2.32. Distribution of trace fossils occurring in HCS tempestite deposits. 1, *Chondrites;* 2, *Cochlichnus;* 3, *Cylindrichnus;* 4, *Diplocraterion;* 5, *Gryochorte;* 6, *Muensteria;* 7, *Ophiomorpha;* 8, *Palaeophycus;* 9, *Phoebichnus;* 10, *Planolites;* 11, *Rhizocorallium;* 12, *Rosselia;* 13, *Skolithos;* 14, *Thalassinoides;* 15, *Zoophycos.* (From Ekdale et al., 1984.)

Monocraterion and *Skolithos* are the members of the *Skolithos* ichnofacies which is a high energy, shallow marine substrate and associated with storm influenced deposits. *Skolithos* trace fossils in the study area consist of straight vertical to slightly inclined cylindrical tube burrows (Fig. 2.33B and 2.33D). Burrows are usually parallel and are unbranching and do not cross cut. These burrows are smooth, with massive infill (Fig. 2.33B). When these burrows are found on bedding planes they are circular and approximately 1cm in diameter (Fig. 2.33C). In side profile they range in width from 10mm to 2mm and in vertical height from 7mm to 80mm. This type of trace is typical

of dwelling or suspension feeding of organisms (Bromley, 1996). *Monocraterion* is a dwelling or deposit feeding burrow that are vertical funnel shaped structures penetrated by a central straight tube (Fig. 2.33A). In most cases the gross diameter of these burrows does not exceed 10mm with the central tube having a diameter of approximately 5mm in the study area. *Monocraterion* from upper bedding planes can be misinterpreted as *Rosselia*, while eroded specimen may be mistaken for *Skolithos* (Fillion and Pickerill, 1990; Jensen, 1997).

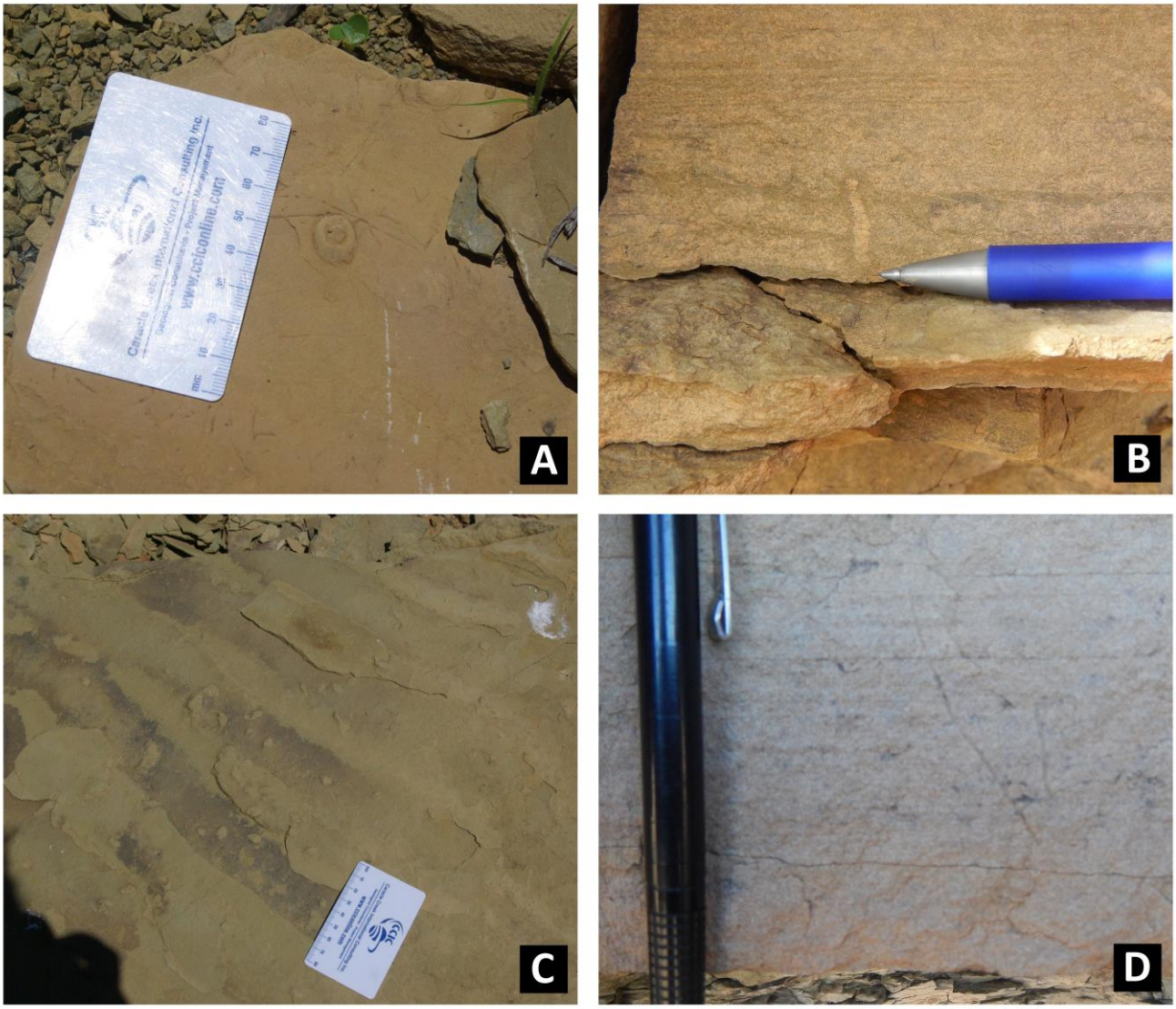


Figure 2.33. *Skolithos* ichnofacies. A) *Monocraterion*. A dwelling or feeding burrow with a single vertical, funnel-like structure penetrated by a central curved tube. The whole structure is approximately 1cm in diameter (scale left of trace fossil). B) *Skolithos*. 3mm wide and 14mm long unbranching vertical burrow. This burrow displays no internal structure (pencil for scale). C) Series of vertical burrows on the upper bedding plane of a wave-rippled surface interpreted to represent *Skolithos* (scale in the lower portion of the photo). D) Close up photo of a series of thin vertical to slightly inclined, unbranching burrows of the trace fossil *Skolithos* (pencil for scale on left hand side of the photo).

Palaeophycus, *Planolites*, *Cochlichnus*, *Rosselia*, *Arenicolites*, *Gyrochorte*, *Schaubcylindrichnus*, *Gordia*, *Asteriacites*, *Phycodes*, *Crossopodia*, *Helminthopsis*, *Asterosoma* and *Thalassinoides* are grouped into the *Cruziana* ichnofacies which is lower energy than *Skolithos* and associated with stable circalittoral substrates (Pemberton et al., 1992).

Arenicolites are indicative of suspension feeding or dwelling burrows (Wilson, 1971). They are vertical to slightly oblique U-shaped burrows (can be J-shaped) that lack spreiten (Fig. 2.34A). Tubes are cylindrical, smooth walled and can have flared openings or funnel-shaped apertures. These burrows are thin (<3mm) and not very long (<70mm). Depth to width ratios vary as does the distance between openings (Fig. 2.34B). *Asteriacites* are star-shaped resting impressions with transversely sculptured arms, preserved in negative relief (Seilacher, 1953a). Only one type of this trace fossil was observed in the study area. It has five (1mm wide) arms radiating from a central node and is present on an upper bedding plane (Fig. 2.34C). *Cochlichnus* manifests as a small, sinuous or meandering, smooth horizontal burrow that resembles a sine curve (Fig. 2.34D). Burrows typically have negative hyporelief, 2mm wide and continuous for only about 5cm on upper bedding planes. The locomotive trace *Crossopodia* manifests as a meandering, curved, or straight trail with a central median furrow (Hattin and Frey, 1969) (Fig. 2.34E). These traces are approximately 10mm wide and occur on upper bedding planes. This trace commonly occurs in high energy marine settings (Hattin and Frey, 1969). Long, slender, unlined, smooth trails of uniform thickness that are mostly bent but sometimes wind and curve irregularly are representative of the trace fossil *Gordia* (Wang et al., 2009) (Fig. 2.34F). These traces are unbranching, smooth, cylindrical or subcylindrical burrows often with a nub on the end. *Gordia* traces are often thin (<2mm) and continuous on bedding planes over 20cm. These horizontal burrows often self-cross. These were probably formed by an organism that was probing the sediment for food and is therefore a grazing or feeding trace (Wang et al., 2009).

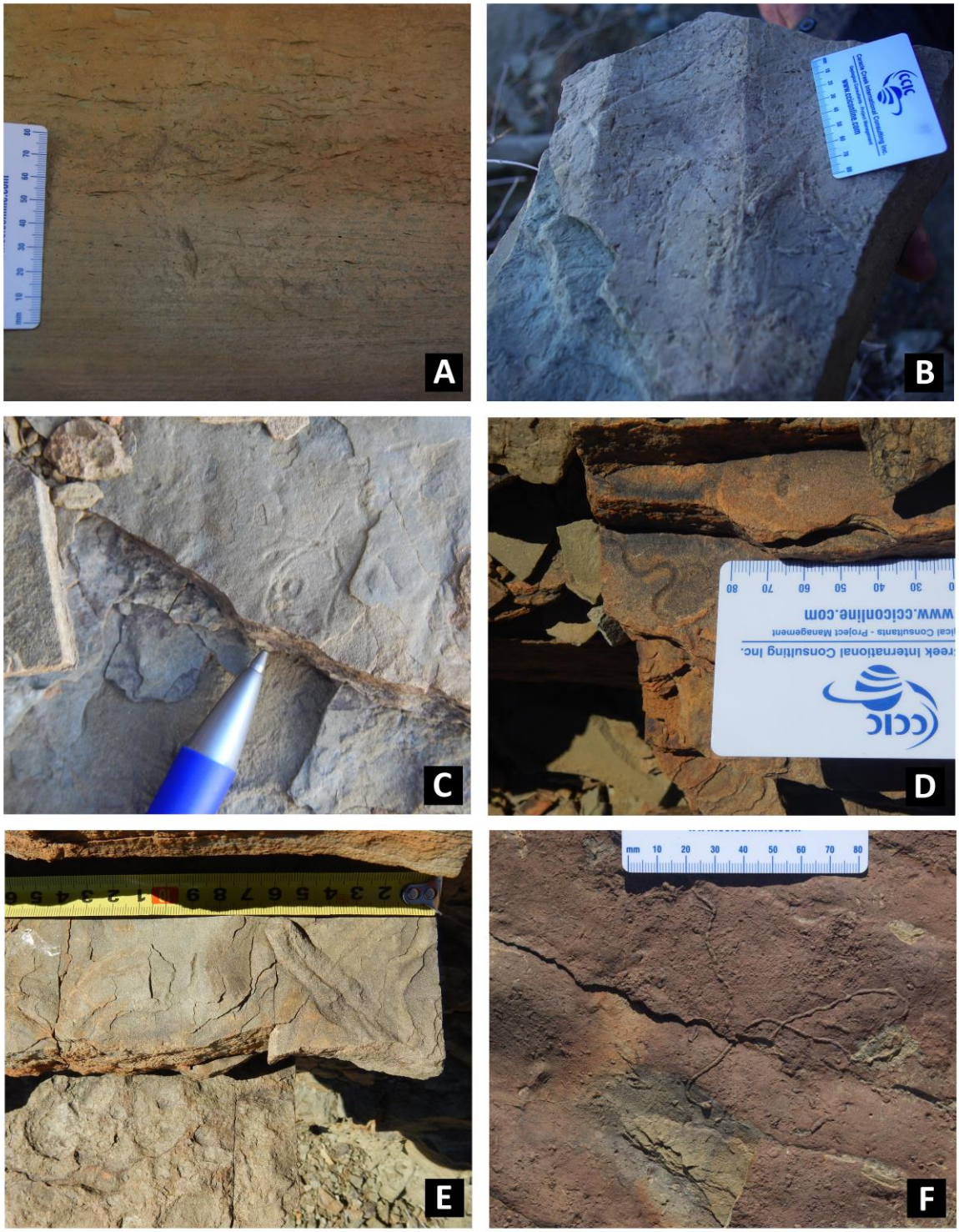


Figure 2.34. *Cruziana* ichnofacies 1. A) *Arencolites* displaying vertical to oblique U and J-shaped burrows. These burrows have no spreiten and are cylindrical in nature (scale to the left of the photo). B) Vertical to oblique *Arencolites* burrows with varying distance between openings. These display typical sprietenless U-shapes in side profile (scale upper right corner). C) Trace fossil identified as *Asteriacites*. This trace has negative hyporelief and a five-limbed star impression radiating from a central node (pencil for scale). D) *Cochlichnus*. A locomotive trace that is sinuous or meandering and smoothly unlined in nature. Trace is present on an upper bedding plane and is little disturbed by bioturbation. E) Trace fossil identified as *Crossopodia*. This is a straight trail with a central median furrow (scale in upper reaches of the photo). F) A grazing or feeding trace fossil. Long, slender, meandering trace of uniform thickness representing *Gordia* (scale in the upper reaches of the photo).



Figure 2.35. *Cruziana* ichnofacies 2. A) *Phycodes*. Appears as a splayed pattern of vertical to oblique cylindrical burrows originating from a central point and radiating out in a linear fashion. These are interpreted to represent feeding probes by an organism (pencil for scale). B) Feeding or locomotive trace of horizontal or sub-horizontal (often convex down) burrow with no cross cutting relationships interpreted to represent *Helminthopsis* (pencil for scale). C) Positive epirelief traces on the upper bedding plane of wave-rippled surface interpreted to represent *Gyrochorte*. These are often low, winding ridges with a median furrow (bottle lid for scale). D) Faint depression vertical burrow with concentric infill (outlined) interpreted to be *Rosselia* (pencil for scale). E) *Schaubcylindrichnus*. Sub-horizontal, oblong, ellipsoidal well-lined sediment filled tube. These are generally U-shaped and wider than traces such as *Diplocraterion*. Above this, traces of *Helminthopsis* are evident (scale lower left of the photo). F) Series of branched, cylindrical burrows interconnected by vertical shafts and displaying characteristic Y-shaped branches typical of *Thalassinoides*. This trace is present of a nodule surface (scale to the right of the photo).

Phycodes occur as a series of cylindrical, 10mm diameter burrows aligned with irregular spacing (Fig. 2.35A). These are a set of vertical to sub-vertical burrows originating from a central base point that fans outward in a linear fashion. These represent distal tunnels that divide at acute angles into several free cylindrical tunnels and are commonly thought to be made by feeding organisms probing the sediment (Bromley and Asgaard, 1972). *Helminthopsis* are irregularly winding to meandering, unbranched, horizontal burrows or trails that do not touch or crosscut each other with massive fill. These often occur as upside down U-shaped burrows of <1mm in width and 10-20mm long (Fig. 2.35B). Burrows of this trace fossil may represent either a feeding burrow or trail of a deposit-feeding organism (Dam, 1989). *Gyrochorte* are positive epirelief burrows consisting of a low, winding ridge with a central median furrow which is only preserved on the bottom side (negative hyporelief) of the trace (Heinberg, 1973) (Fig. 2.35C). Normally these traces have an irregular meandering course although it can rarely be straight to gently curved. *Rosselia* are conical, funnel-shaped, vertical, concentric burrows. The diameter of the burrow is about 30mm with a central cylindrical pencil-thick tube (Dahmer, 1937) (Fig. 2.35D). This trace is present on nodule surfaces and occurs with *Palaeophycus* in outcrop**.** These are dwelling and feeding burrows of a filter- or suspension-feeding organism (Netto, 2014). *Schaubcylindrichnus coronus* are vertical to sub horizontal, oblong, ellipsoidal well-lined sediment filled burrows. The trace wall surface is smooth and can occur as singular tubes or occur in closely-spaced clusters. In outcrop these appear as low amplitude U-shaped burrows 30-70mm wide and are thin (approximately 2mm) in appearance (Fig. 2.35E**).** These are dwelling or feeding burrows that commonly occur in shoreface settings slightly seaward of true high-energy environments (Löwemark and Nara, 2013). *Thalassinoides* consists of a three-dimensional framework of branched cylindrical burrows which are typically Y-shaped when they branch horizontally (Howard and Frey, 1984) (Fig. 2.35F). Traces are never more than 10mm wide and poorly preserved on bedding planes bar a few instances**.** These represent deposit-feeding and dwelling burrows. Faecal pellets of *Rhizocorallium* have been identified. These appear as pockmarks on dune crests and are difficult to determine the true appearance of individual traces. Traces appear to be small 1mm rounded holes that may coalesce. *Asterosoma* trace fossils are present in outcrop. They are bulb-like swelling burrows from a circular central axis (Bromley and Uchman, 2003). The central axes of these burrows are vertical and cause a mild bending of the

bedding. 10mm below where the initial bedding bends there is a sand sphere (approximately 8mm in diameter) often surrounded by mud (Fig. 2.36A). The concentric nature of these spheres are often obscured by outcrop weathering although they are present on closer inspection. Generally, these burrows are variable in dimension, number and may show faint wall ornamentation. *Asterosoma* trace fossils represent deposit feeders in shallow marine settings.

A vertically orientated, ovular shaped, infilled burrow set in a depression within fine to medium-grained sandstone representing *Conichnus conosinus* (Nielsen et al., 1996) was found *ex-situ* below the thick mudstone unit on Norotshama peak. This shows a funnel-like infill and a gradually decreasing diameter of the burrow with an increase of depth through the sediment (Fig. 2.20E and F).

Palaeophycus is a trace fossil that represents multiple behaviours including burrowing and dwelling. Burrows are unbranched, cylindrical, smooth, predominantly horizontal but can be sub-horizontal (Fig. 2.37A), straight to sinuous (Fig. 2.37B), with variable diameter and typically structureless fill similar to host rock (Pemberton and Frey, 1982) (Fig. 2.37C and F). The diameters of these burrows range from 3-10mm and are elliptical to circular in transverse cross section (Fig. 2.37E). These trace fossils are often present on bedding planes in high abundance giving the appearance that they are branched (Fig. 2.37D). *Palaeophycus* is an opportunistic, facies-crossing, low-diversity trace fossil (Archer and Maples, 1984). Opportunistic organisms are present under conditions that discourage or exclude most other organisms (Ekdale, 1985; Martino, 1989).

Planolites are abundant in the Amibberg Formation and occur as simple, unlined, unbranched cylindrical or subcylindrical infilled burrows (Fig. 2.38A and B). These are straight to gently curved and horizontal to oblique to bedding planes. Burrows often cross-over (Fig. 2.38C). Occasionally these burrows take the form of small knobs or discontinuous segments on bedding planes. The burrows vary in width (2-5mm) and are usually continuous along bedding planes for meters (Fig. 2.38D). They can be found as negative hyporelief structures or positive epirelief ones on bedding surfaces. It is often difficult to distinguish between *Palaeophycus*, a passively filled

burrow, and *Planolites*, a burrow formed by active backfill (Pemberton and Frey, 1982). These two similar trace fossils can be of a similar size, shape and orientation (Pemberton and Frey, 1982; Buckman, 1995; Keighley and Pickerill, 1995).

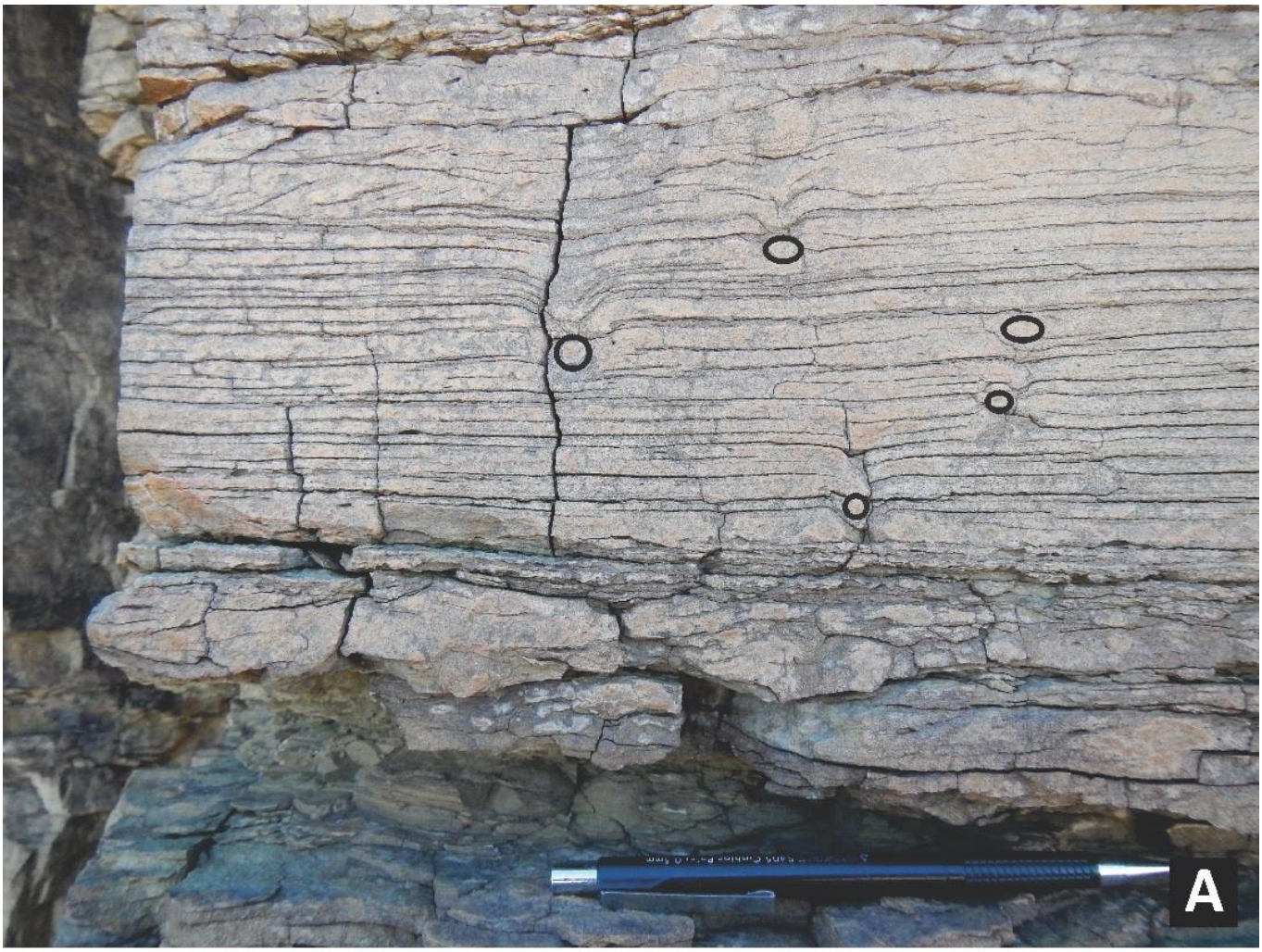


Figure 2.36. *Asterosoma.* A) Bulb-like swelling burrows from a circular central axis (outlined). Note the mild bending of the bedding and the sand sphere 10mm below where the initial bedding bends (pencil for scale).

As mentioned previously, *Paleodictyon* is a member of the *Nerites* ichnofacies which is a bathyal to abyssal, low energy marine substrate. This form of *Paleodictyon* has an irregular, incomplete network of honeycombs (Fig. 2.8C). This trace can further be classified as *Paleodictyon imperfectum* (Seilacher, 1977) due to the nature of the burrows not having perfect hexagonal appearance. There seems to be an 8mm thick main chamber whereby all secondary burrows branch off usually in a pitch-fork shape. The secondary burrows are usually angular where they branch but in some instances they have a more gradual, rounded branch. The ridges are usually

cylindrical or ellipsoid in cross-section. This trace fossil is continuous over about 20cm on the surface of the conspicuous marker nodule horizon mentioned in lithofacies 1.

One interesting trace fossil of note, although observed in the mudstones of the Amibberg Formation, was predominantly observed in the underlying Aussenkjer Formation. These traces occur in abundance about 20m below the Amibberg Formation. This was referred to by Werner (2006) as *Pseudo-Plagiogmus* (Fig. 2.20A and B) which belongs to the ichnogenous *Psammichnites*. These trace fossils are significantly different from Cambrian examples of *Plagiogmus* and are hence assigned the name *Pseudo-Plagiogmus* for practical purposes (Werner, 2006). These traces are on average 5cm in width, 40cm – 1m long backfilled burrows with slightly convex sedimentation and a regularly ribbed row of meniscate bends and/or row of bended knobs which appear to be covered by scratch marks.

The often intensely bioturbated mudstones of lithofacies 1 consist of the trace fossils: *Rosselia, Palaeophycus, Paleodictyon, Thalassinoides and Pseudo-Plagiogmus.* *Paleodictyon* is a deep sea trace fossil and supports the offshore interpretation of this lithofacies. *Rosselia* is a suspension feeder which further supports the stable condition and slow accumulation of mudstones as does the presence of *Pseudo-Plagiogmus*. *Palaeophycus* and *Thalassinoides* are facies-crossing taxa and are less useful in supporting an offshore setting.

Bioturbated sandstones of lithofacies 2 consist of the trace fossils *Palaeophycus* and *Planolites*. These trace fossils support the prolonged periods of low energy conditions to allow for the reworking of the sediment of this facies.

The rhythmically interbedded nature of lithofacies 3 suggests periods of low energy with intermittent periods of pulsatory flow form river-floods. The trace fossils assemblages support this due to the mixing of *Skolithos* and *Cruziana* (*Arencolites* and *Palaeophycus*) ichnofacies.



Figure 2.37. *Palaeophycus*. A) Unbranched, cylindrical, massive filled burrows that are sub-horizontal interpreted to represent the trace fossil *Palaeophycus* (scale left of the photo). B) Positive epirelief, sinuous, smooth walled *Palaeophycus* burrows with the same fill as the host rock (pencil for scale). C) Positive epirelief, sinuous, smooth walled *Palaeophycus* burrows with the same fill as the host rock. Large burrow below the scale is different from the normal *Palaeophcus* burrows but is difficult to classify (lighter for scale). D) Dense network of horizontal to sub-horizontal *Palaeophycus* burrows on the upper bedding plane of a wave-rippled sandstone. These represent opportunistic, facies-crossing ichnotaxa that thrived in environments with alternating periods of rapid sand deposition followed by periods of very low rates of mud deposition under quiet-water conditions (hammer tip for scale in upper right hand side of the photo). E) Close up of rock fragment with abundant *Palaeophycus* trace fossils. Note the same fill as the host rock (hand sample is approximately 10cm long). F) Network of primarily horizontal *Palaeophycus* burrows on the lower bedding plane of a sandstone (scale in upper part of the photo).

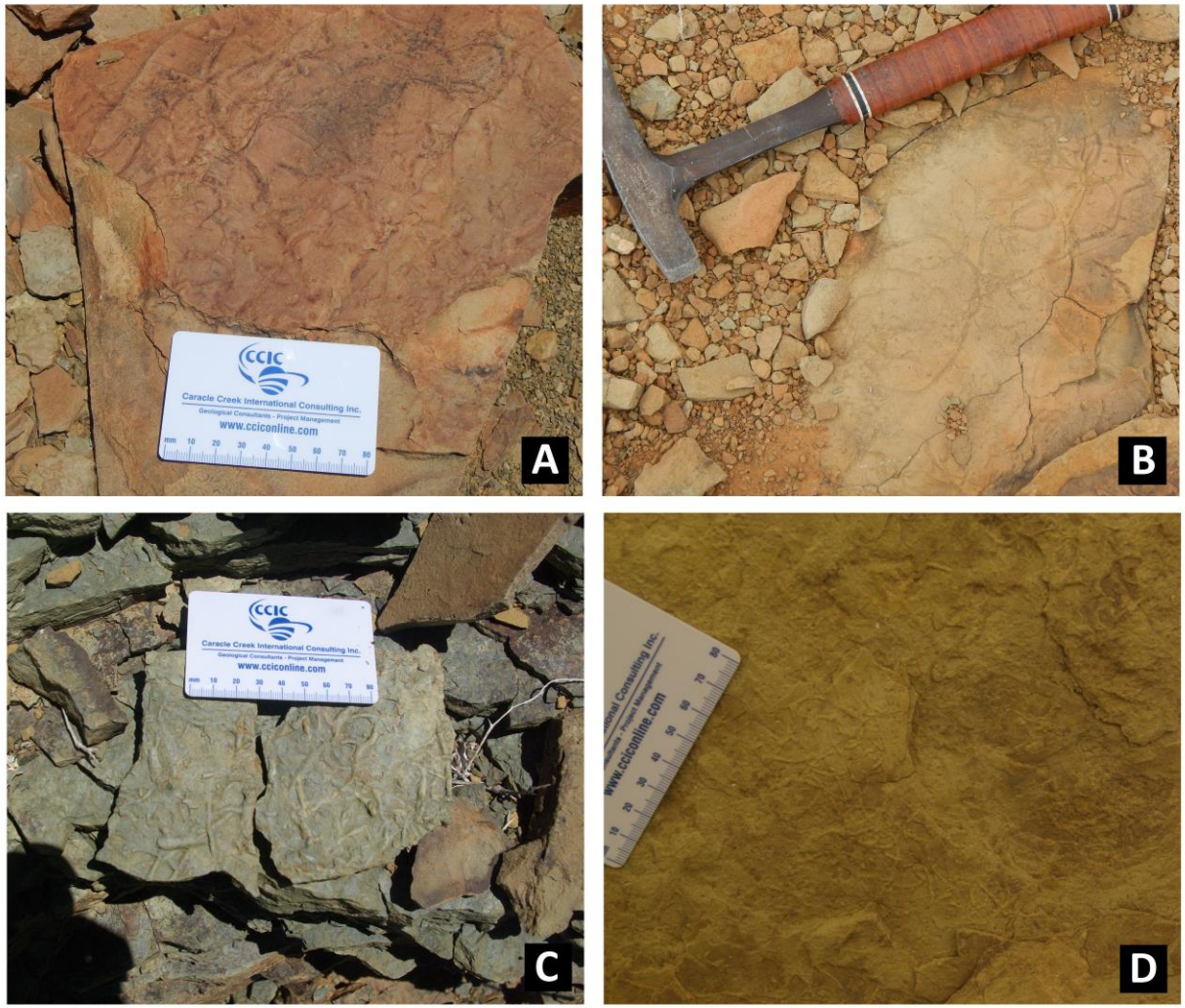


Figure 2.38. *Planolites*. A) Negative hyporelief, simple, unlined, unbranched, curved, cylindrical infilled burrows of *Planolites*. They often cross cut each other (scale in the lower part of the photo). B) Sinuous and undulatory, negative hyporelief *Planolites* burrows (hammer is 32cm long). C) Positive epirelief, infilled burrows that appear as small knobs or disaggregated segments on bedding planes (scale in upper part of the photo). D) Active backfilled burrows on the lower bedding plane of a sandstone (scale left of the photo).

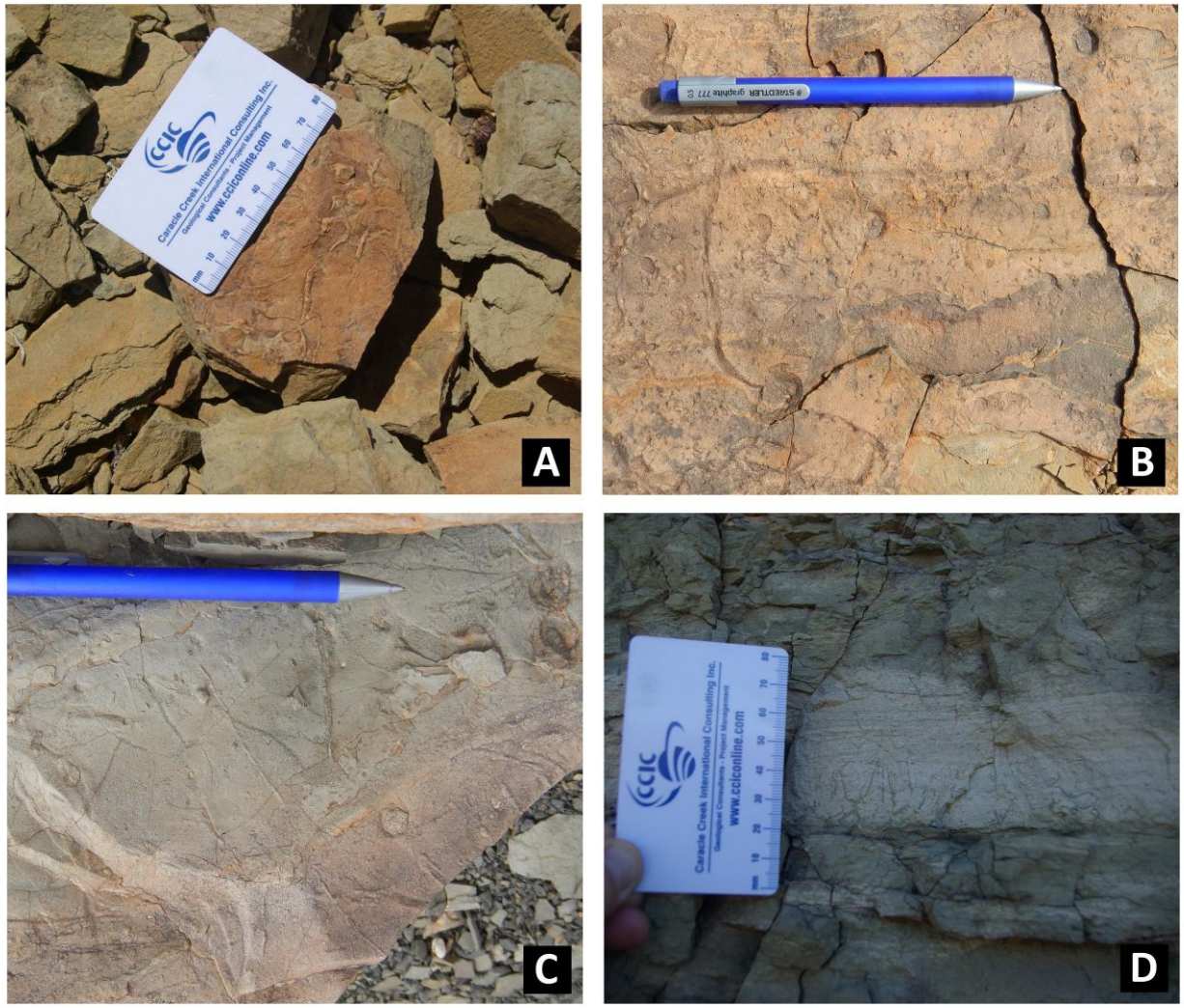


Figure 2.39. Mixed ichnofacies. A) The trace fossil assemblage in this sandstone is diverse. Vertical *Skolithos* traces are present in the upper reaches of the photo. Straight to curved, meandering horizontal *Planolites* burrows are present in abundance and a slender, meandering and curved *Gordia* burrow is evident in the lower left of the photo (scale central in the photo). B) *Skolithos* and *Planolites* occurring together in the same bedding plane (pencil for scale). C) *Skolithos* burrows (throughout photo) and *Monocraterion* burrows (upper right hand corner) as well as horizontal negative hyporelief and positive epirelief burrows of *Palaeophycus* on the same bedding plane (pencil for scale). D) Vertical *Skolithos* burrows occurring in the same stratigraphic interval as J-shaped *Arencolites* burrows (scale left of the photo).

Sharp based, bioturbated sandstones of lithofacies 4 also display mixing of ichnotaxa consisting of *Skolithos* and *Planolites*. *Planolites* are present throughout this facies indicating a prolonged period of stable conditions whereas *Skolithos* are only present in the upper intervals of this facies where conditions became unstable as indicated by wave rippled bed surfaces.

Tempestitic deposits of lithofacies 5 and 6 contain similar trace fossil assemblages. A distinct mixing of the *Skolithos* and *Cruziana* ichnofacies is also evident. *Skolithos* and *Monocraterion* represent unstable, high energy storm wave conditions whereas the presence of the *Cruziana* ichnofacies represent low energy, stable conditions that allowed for the colonization of the sediment after large storm events. *Cruziana* trace fossils present in these lithofacies include: *Planolites, Crosspodia, Astersoma, Helminthopsis, Schaubcylidrichnus, Cochlichnus, Thalassinolites* and *Rhizocorallium, Asteriacites, Phycodes, Palaeophycus, Gyrochorte* and *Gordia.*

2.9.3 Lithostratigraphic Correlation

Units of similar depositional regime, stratigraphic position and thickness are used to correlate the strata of the Amibberg Formation in the Karasburg Basin (Fig. 2.40). In some instances sandstones are classified as bioturbated or interbedded due to the poor outcrop preservation and covering by scree. Along strike these do tend to show undulatory surfaces and some characteristics of discrete HCS sandstone deposits. However, these are classified by their appearance and distinguishing factors as they appear in outcrop. For this reason some distal lower shoreface deposits will become offshore transitional deposits along strike. Other times thin mudstone intervals are present between sandstones in a certain stratigraphic column where they are absent or obscured in others resulting in some mild distortion of the lithostratigraphic correlation. Generally, the thick amalgamated HCS sandstone units are the most useful in ascertaining a broad correlation of the strata in the study area. The four most distinctive units are easily correlated and all the minor strata in between can more readily be correlated due to a more clearly definable stratigraphic position. Some sandstone bodies seem to be lenticular in geometry due to their presence in one stratigraphic column and absence in others.

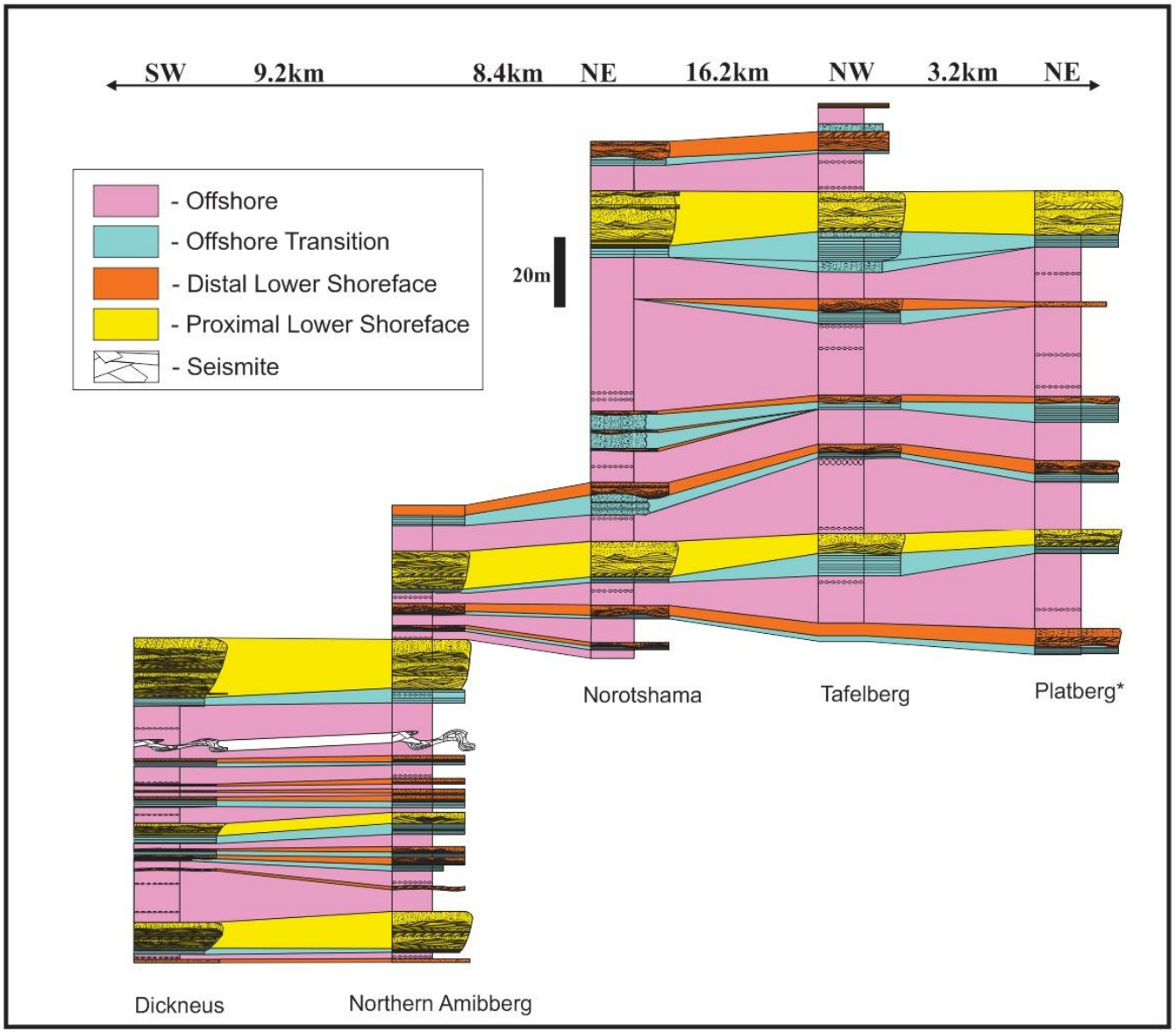


Figure 2.40. Lithostratigraphic correlation. Along strike correlation of strata of the Amibberg Formation in the Karasburg Basin (* denotes informal locality name).

Chapter 3: Petrography and Provenance

3.1 Introduction

Conducting a petrographic analysis of sedimentary rocks from a sedimentary basin is critical to the understanding of the palaeoenvironment at the time of deposition. The mineralogical composition and textures of sandstones generally reflects the provenance, mode of transport and environmental conditions during deposition, all of which can be studied and subsequently interpreted from petrographic analysis. Furthermore, the mineralogical and chemical composition of fine-grained mudstones can also be used as indicators of provenance, weathering conditions and tectonic settings (Cullers, 2000; Nesbitt et al., 1996; Cox et al., 1995; Taylor and McLennan, 1985; Taylor and McLennan, 1991). No previous petrographic study of the Amibberg Formation has been conducted and it is evident that petrophysical analyses are essential in order to understand the palaeoenvironments and the source area for the sandstones and mudstones that constitute this formation in the Karasburg Basin.

3.2 Methodology

45 sandstone samples (Table 3.1) were collected from 4 separate localities during the conduct of fieldwork. These samples were collected from well-defined amalgamated and discrete bodies and are representative of all possible lithofacies and stratigraphic intervals. Samples were then cut perpendicular to bedding and prepared into thin sections. The thin sections were then described in detail in terms of: mineral composition, grain-size, grain textures and fabrics, grain contacts, sorting, roundness and porosity. The grain roundness and sorting was measured semi-qualitatively using the standard charts of Tucker (2011). A 350 point count was then conducted to determine, as accurately as possible, the modal composition and to minimize the effect of grain size (Ingersoll et al., 1984). The constituent minerals of the sandstone were then classified into quartz (monocrystalline quartz), feldspar (K-feldspar and plagioclase) and lithic fragments. Following this, the modal analysis data was recalculated on a matrix-free basis for each sample and then plotted on the QFL (quartz-feldspar-lithic fragments) diagram as per Pettijohn (1975). Further classification of sandstones as per Dickinson and Suczek (1979) and Dickinson et al., (1983) was useful in determining provenance (parent rock assemblage and source area) and tectonic setting of the rocks of the Amibberg Formation. Carbonate nodule samples were analysed under thin section for their

carbonate content. The samples with sufficient carbonate content (>70%) were then crushed for three seconds to a fine powder and sent to iThemba labs. The samples were then run on a DELTA V Advantage Mass Spectrometer with a Gas Bench II interface and sample preparation device including GC PAL auto-sampler. This measures $^{13}C/^{12}C$ isotopic ratios of $CaCO_3$ which is mostly in the form of calcite. This data aids in determining primary biological activity and tracing carbonate production in the basin. 5 mudstone samples were crushed and milled to a fine powder and sent for analysis at the XRF lab at the school of geoscience, University of the Witwatersrand. At this laboratory the fine powdered material was then pressed and analysed for trace elements on the Axios machine with the Protrace programme. Further samples used for major element analysis were fused with tetra-borate Flux and analysed on the same machine. The XRF methods were used to characterise provenance and palaeoclimatic factors involved with the deposition of sediments in the Karasburg Basin**.** All of the gathered and interpreted data is then used to further enhance the palaeoenvironmental reconstruction provided in Chapter 2.

3.3 Petrography of Sandstones

The grain size (Fig. 3.1A and B) of these thin sections varies from very fine sandstones (0.063-0.125mm) to medium sandstones (0.250-0.500mm). Silt sized particles, clay matrix and clay clasts (Fig. 3.2E and F) are also present in the studied samples. Rarely, some calcite cement is evident but only in minor amounts and in a select few samples (Fig. 3.3D). The majority of thin sections consist of moderately well-sorted and well-sorted particle arrangements (Fig. 3.1C and D). However, one of the carbonate samples displays poor sorting. Samples show a clear majority of angular/subangular to subrounded grain shapes (Fig. 3.1C and D) although rounded and very angular grains are present to a lesser degree. Observable grain contacts are usually point to point or concavo-convex in nature (Fig. 3.1C and D). Other contacts of a sutured nature exist if the rock has undergone a high degree of compaction. Sedimentary structures that are observable under the microscope consist of fine, horizontal laminations and obliquely orientated fine-grained drape-like structures. Bioturbation is also evident occasionally where quartz grains and clay matrix become heavily mixed (Fig. 3.1E and F). Burrows made by organisms are also relatively common. These are usually vertical to oblique in orientation and consist of unlaminated, fine-grained backfill (Fig. 3.2A and B). Some algal features are also observed in carbonate samples (Fig. 3.12). Porosity is rare and mostly absent in most samples. Pore space, when present, is typically

found in areas where fractures have occurred (Fig. 3.5A and B). These pore spaces are typically unfilled but occasionally have siliclastic grains present (Fig. 3.5C and D). Other individual pore spaces are present, generally found around and centred in a rounded clay or oxide mineral grain that has undergone dissolution (Fig. 3.2C and D). Lithic fragments are extremely rare in these thin sections with only one polycrystalline quartz lithic observed. Other intrabasinal mudstone lithics are present in these sections.

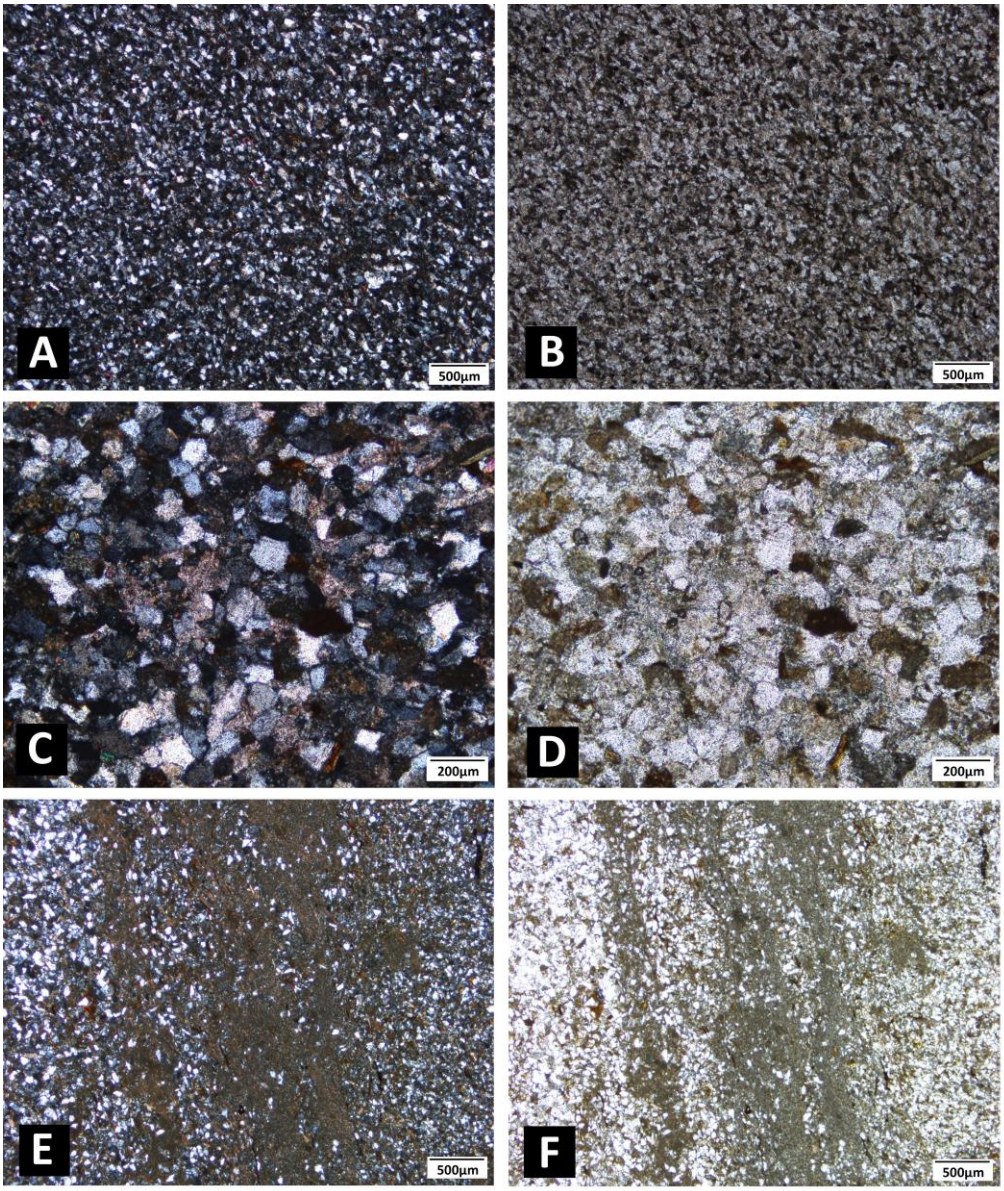


Figure 3.1. Photo micrographs. A and B) Representative sample indicating the fine-grained nature of the sandstones in the study area at a magnification of 4X (A under XPL; B under PPL). C and D) Representative sample indicating subangular to subrounded grain shapes, point to point and concavo-convex grain contacts as well as moderate-well sorting (C under XPL; D under PPL). E and F) Sample showing bioturbation with mud-sized particle burrow fill with spreite and coarser sand-sized particles orientated parallel to bedding (E under XPL; F under PPL).

Sample Number	Lithofacies	Grain Size (μm)	Sorting	Roundness	Sandstone Classification
148SSA	7	50-200	Well sorted	Subangular to subrounded	Quartz wacke
148SSB	6	71-167	Moderately well sorted	Angular to subrounded	Feldspathic wacke
148SSC	6	59-143	Moderately well sorted	Angular to subrounded	Feldspathic wacke
148SSD	6	63-182	Moderately well sorted	Angular to subrounded	Quartz wacke
148SSE	6	56-182	Moderately well sorted	Angular to subrounded	Feldspathic wacke
148SSF	6	83-200	Well sorted	Subangular to subrounded	Feldspathic wacke
148SSG	4	111-333	Well sorted	Angular to subrounded	Quartz wacke
148CCB	6	111-333	Well sorted	Subangular to subrounded	Feldspathic wacke
148SIS	3	33-125	Moderately well sorted	Angular to subrounded	Quartz wacke
14811MLM/STN	1	26-83	Moderately well sorted	Angular to subrounded	NA
14811MLMSTN	1	26-71	Moderately well sorted	Angular to subrounded	NA
158PLATSSTOP1	6	53-250	Well sorted	Angular to subrounded	Quartz wacke
DIKCNEUSLIMESTONE	1	16-56	Moderately well sorted	Angular to subrounded	NA
228DNEUS2SS1	6	167-333	Well sorted	Subangular to subrounded	Feldspathic wacke
228DNEUS2SS2	6	77-182	Moderately well sorted	Angular to subrounded	Feldspathic wacke
SAMPLE178	6	43-118	Moderately well sorted	Angular to subrounded	Quartz wacke
178JAGDSS1	3	100-333	Moderately well sorted	Subangular to subrounded	Feldspathic wacke
178JAGDSS2	4	53-125	Moderately well sorted	Angular to subrounded	Quartz wacke
178JAGDSS3	6	77-200	Moderately well sorted	Angular to subrounded	Quartz wacke
178JAGDSS4	6	63-200	Moderately well sorted	Angular to subrounded	Feldspathic wacke
178JADGSS5	6	60-154	Well sorted	Subangular to subrounded	Quartz wacke
178JAGDSS6	6	100-400	Moderately well sorted	Angular to subrounded	Feldspathic wacke
178JAGDSS7	6	77-143	Well sorted	Angular to subrounded	Feldspathic wacke
178JAGDSS8	6	67-250	Moderately well sorted	Angular to subrounded	Feldspathic wacke
178JAGDSS9	3	63-143	Moderately well sorted	Angular to subrounded	Quartz wacke
178JAGDSS10	6	63-154	Moderately well sorted	Angular to subrounded	Quartz wacke
178JAGDSS11	6	53-143	Moderately well sorted	Angular to subrounded	Quartz wacke
178JAGDSS12	6	71-143	Moderately well sorted	Angular to subrounded	Quartz wacke
178LMBALL1	1	66-1000	Poorly sorted	Angular to subrounded	NA
178LMBALL2	1	31-286	Moderately well sorted	Angular to subrounded	NA
208TAFELSS1	5	100-182	Well sorted	Angular to subrounded	Quartz wacke
208TAFELSS2	6	91-200	Well sorted	Subangular to subrounded	Feldspathic wacke
208TAFELSS3	6	48-167	Moderately well sorted	Angular to subrounded	Quartz wacke
208TAFELSS4	6	83-143	Moderately well sorted	Angular to subrounded	Quartz wacke
208TAFELSS5	2	83-167	Moderately well sorted	Angular to subrounded	Quartz wacke
218NOROSS1	5	53-133	Moderately well sorted	Angular to subrounded	Feldspathic wacke
218NOROSS2	6	63-133	Moderately well sorted	Angular to subrounded	Quartz wacke
218NOROSS3	2	48-125	Moderately well sorted	Angular to subrounded	Feldspathic wacke
218NOROSS4	5	45-105	Moderately well sorted	Subangular to subrounded	Quartz wacke
218NOROSS5	6	53-111	Moderately well sorted	Angular to subrounded	Quartz wacke
218NOROSS6	6	125-333	Well sorted	Subangular to subrounded	Quartz wacke
218NOROSS7	6	100-333	Well sorted	Subangular to subrounded	Quartz wacke
218NOROSS8	6	59-133	Moderately well sorted	Angular to subrounded	Quartz wacke
218NOROSS9	6	71-154	Moderately well sorted	Angular to subrounded	Quartz wacke
218NOROEX1	6	91-400	Well sorted	Angular to subrounded	Feldspathic wacke

Table 3.1. Table showing the characteristics of each sample as well as their classification and appropriate lithofacies.

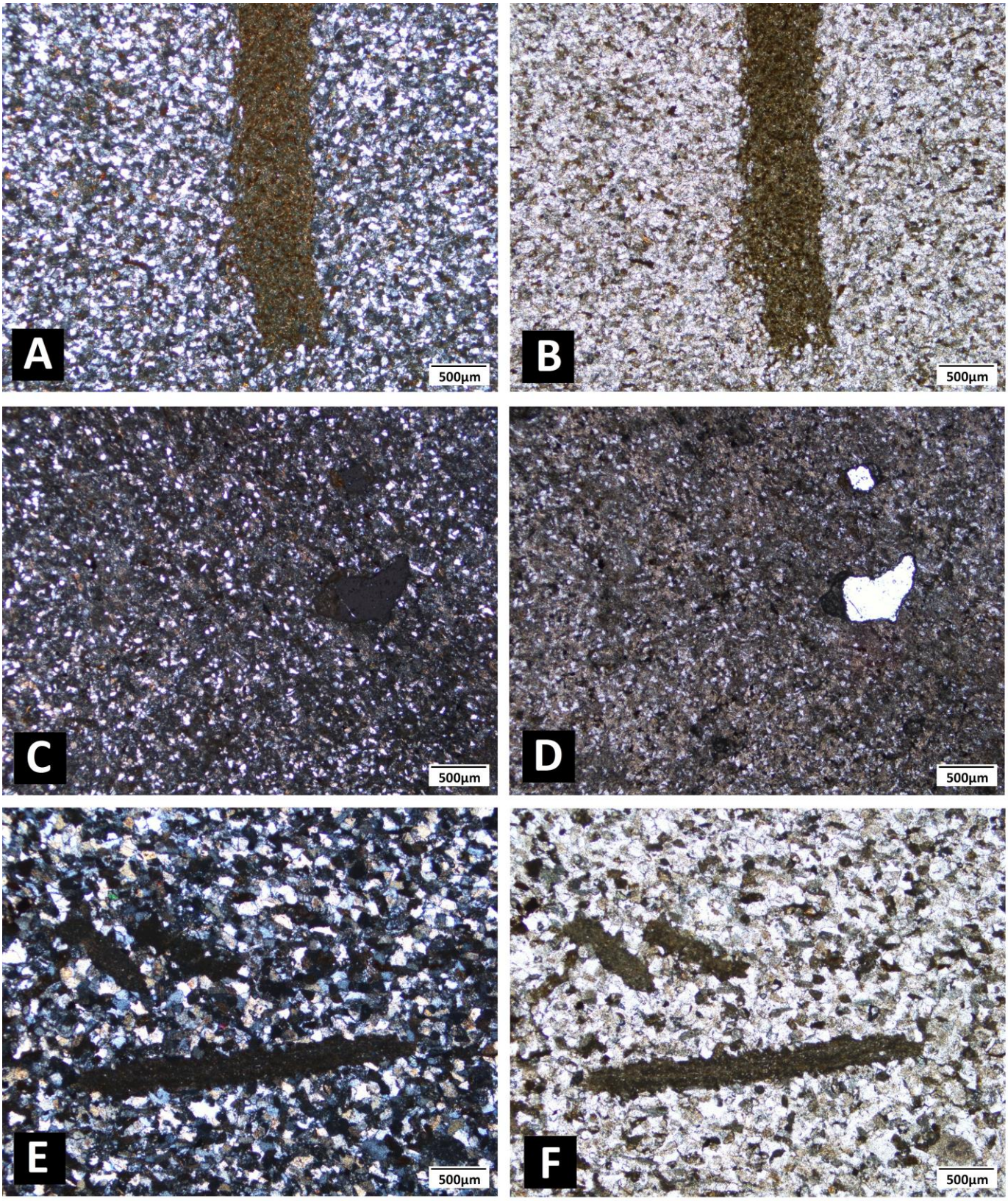


Figure 3.2. Photo micrographs. A and B) Sample displaying vertically orientated burrow with unlaminated, fine-grained backfill (A under XPL; B under PPL). C and D) Sample with clearly defined pore spaces which has formed as a result of dissolution (C under XPL; D under PPL). E and F) Large mudstone clasts in medium-grained sandstone sample. Note the indentation of the grain boundary of the large mudstone fragment (E under XPL; F under PPL).

3.4 Detrital Framework Grains

3.4.1 Quartz

Quartz (Fig. 3.4A and B) displays low 1st order yellow-grey-white interference colours; no preferred orientation and low relief with moderate-high relief in certain grains that have heavy clay alteration at grain boundaries. Some grains have point contacts and others have concavo-convex contacts with some quartz grains displaying inclusions. In these sections quartz is predominantly monocrystalline with grain shapes that vary from subangular to subrounded and anhedral. No undulose extinction is exhibited by individual quartz grains and only one polycrystalline quartz lithic is present in the studied samples.

3.4.2 Plagioclase

The most common plagioclase grain in these sections is albite (Fig. 3.4C and D) which displays distinctive polysynthetic twinning with low to moderate relief and inclined extinction. These grains are colourless in PPL and often the individual grains appear dirty and overgrown due to alteration. This may be due to the process of kaolinitization whereby most feldspars are completely replaced or dissolved into clay minerals (Haszeldine et al., 1984).

3.4.3 Orthoclase

Orthoclase is difficult to distinguish from quartz in thin sections without the aid of a staining technique due to the fine-grained nature of the majority of samples. However, Carlsbad (simple) twinning, which is common in orthoclase, has been observed in a number of grains. Orthoclase also has parallel extinction which distinguishes it from quartz. These grains are typically euhedral, colourless and have low 1st order interference colours.

3.4.4 Micas

Four types of micas are present in the studied samples. Biotite and muscovite (Fig. 3.4E and F) are by far the most abundant and are described below. Minor occurrences of chlorite and phlogopite have also been observed.

3.4.4.1 Biotite

Biotite grains range in shape from straight, crenulated or bent (120^{o}) laths and generally display well pronounced fabric in a direction parallel to the bedding planes. The bending of

these grains is usually due to compaction processes. These grains display cleavage, are pleochroic from light brown to dark brown/ red and have low 2nd order interference colours.

3.4.4.2 Muscovite

Muscovite laths are colourless in PPL; have low relief; cleavage in one direction and high 3rd order anomalous interference colours; and unlike biotite display no pleochroism. These grains typically have a preferred orientation in the direction of the bedding plane but do branch in some cases.

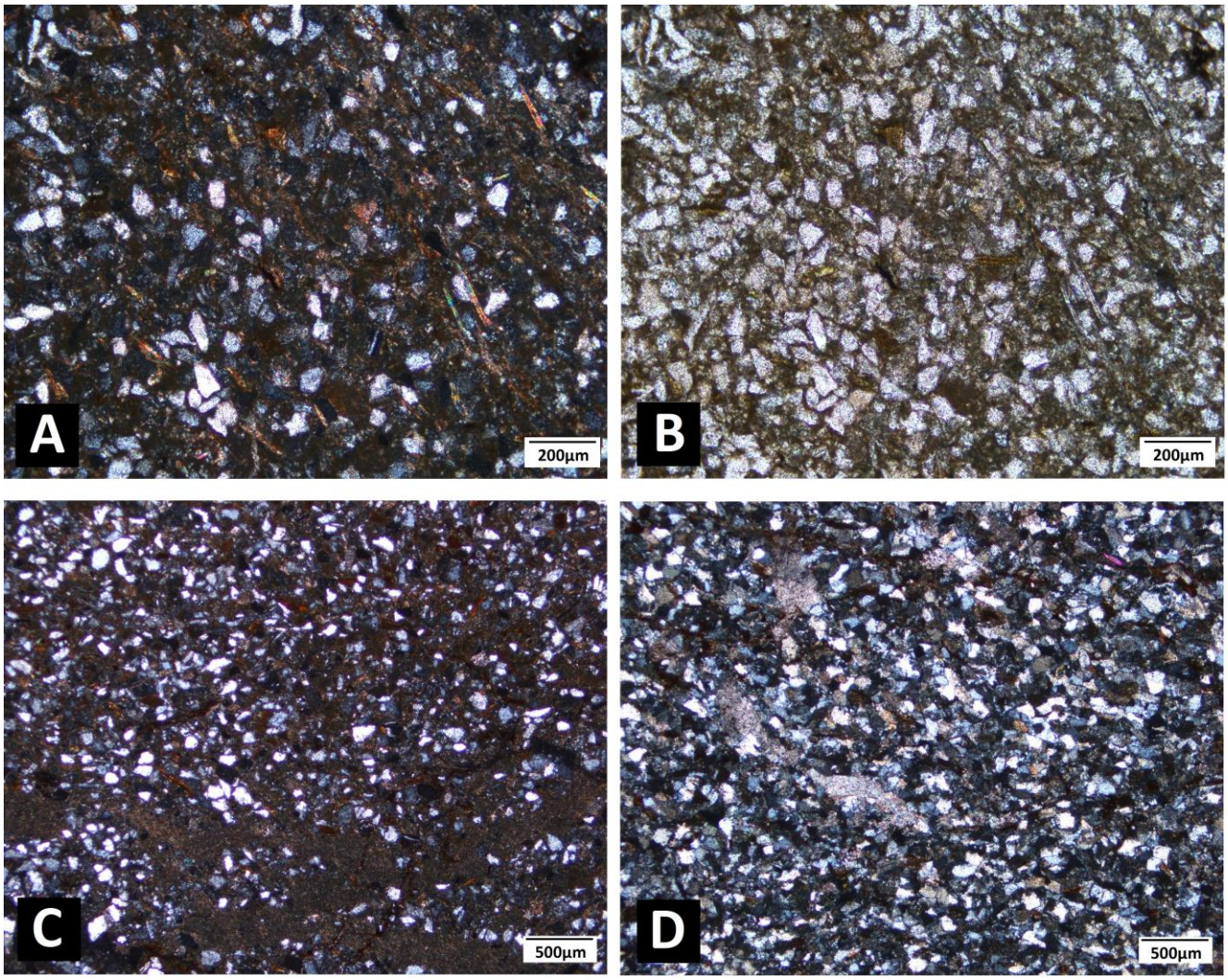


Figure 3.3. Photo micrographs. A and B) Representative sample showing the dirty/dusty, grey-brown appearance of clay minerals in thin section. Note how the clay matrix is interspersed with quartz and mica grains (A under XPL; B under PPL). C) Sample which shows a high percentage of clay matrix to quartz in terms of area (under XPL). D) Sample showing fine calcite cement in between coarser quartz grains (under XPL)

3.4.5 Clay Minerals

Clay minerals in the various thin sections take up a variety of appearances. In general however, they appear dirty/dusty, fine-grained, and grey-brown in both PPL and XPL with only minor colour changes between the two optical realms (Fig. 3.3A, B and C). Often these occur as coalesced clay clasts that appear as individual rounded or angular grains often with concavo-convex contacts with quartz grains; as large fill patterns in between quartz grains; as alterations around individual quartz grains; or as having replaced a whole quartz grain and containing quartz inclusions. The more richly coloured, darker brown-red appearance of the clays may be due to haematite staining (Fig. 3.4E).

3.4.6 Heavy Minerals

Heavy minerals (Fig. 3.4B) are abundant in the studied sandstone samples. These are usually derived from the source of the sediment and can be used to indicate source rock types. The heavy minerals present in the sandstones of the Amibberg Formation each have defining characteristics and are as follows: zircon (Fig. 3.6A, B, E and F; Fig. 3.7A, B, E and F), garnet, epidote, glauconite, rutile, tourmaline, glaucophane, diopside (Fig. 3.6C and D), apatite, actinolite (Fig. 3.6A, B, C and D; Fig. 3.7C and D), titanite/sphene, kyanite and oxide minerals (magnetite, ilmenite and pyrite). Oxide minerals are opaque in thin sections (Fig. 3.5E and F) and are difficult to correctly classify using reflected light microscopy.

3.5 Detrital Modes and Sandstone Classification

Results of point counting of sandstone are shown in Table 3.2 and point count data for carbonate samples are shown in Table 3.3. Point counts of the detrital grains like quartz, feldspar and lithic fragments were recalculated into a percentage and then plotted into a triangular diagram (Fig. 3.8 and 3.9) for classification as per Pettijohn (1975). This classification scheme is used due to the amount of clay matrix present in these thin sections, using 30 µm as upper limit for matrix. The large amount (>15%) of fine-grained matrix results in all of the samples falling into the realm of wackes. Typical wackes have angular quartz, detrital mica and albite as the dominant feldspar with hazy grain margins as though encroached on by the matrix (Pettijohn, 1987). All of these can be seen in the samples from

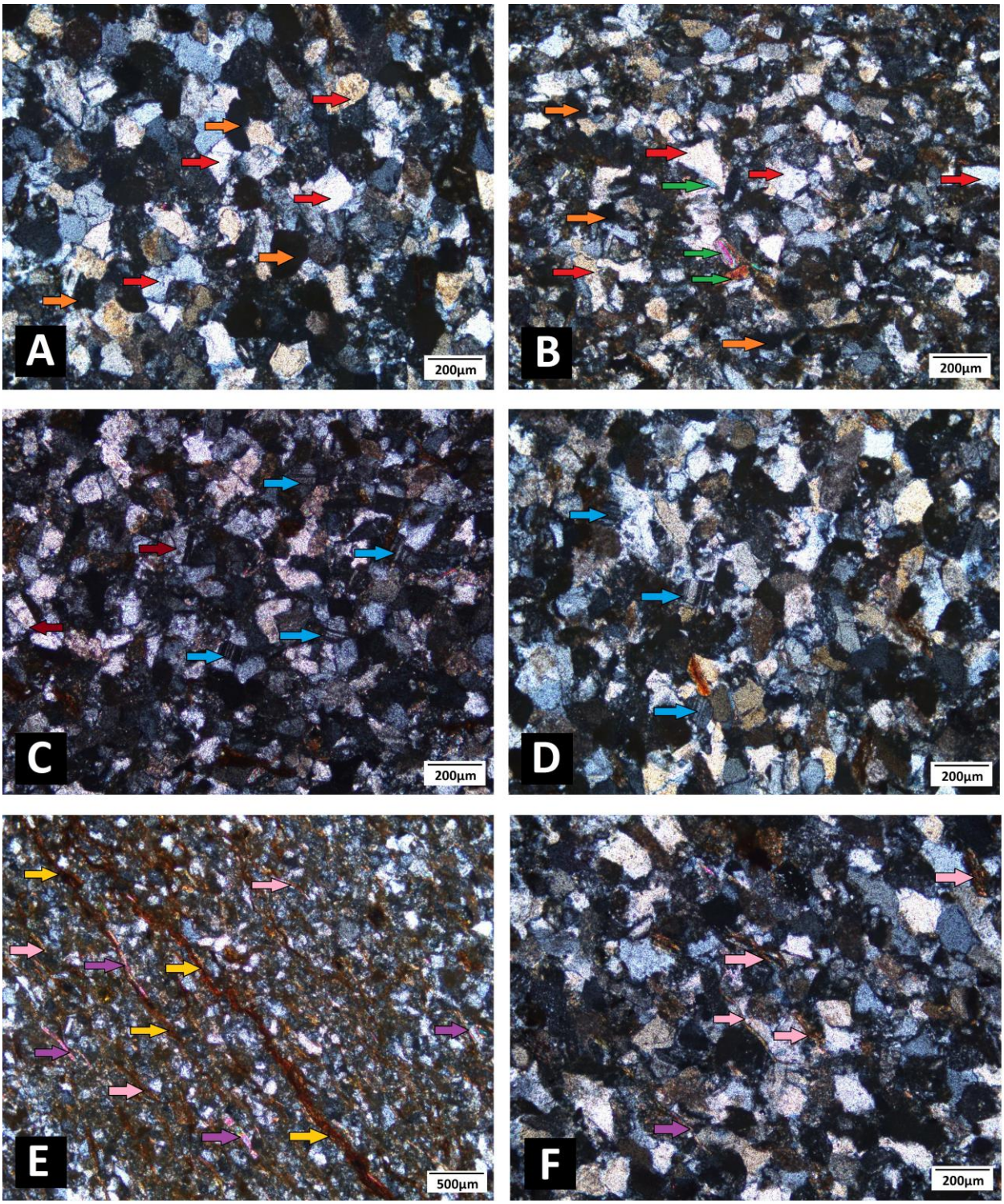


Figure 3.4. Photo micrographs. A) Representative sample displaying the appearance of mostly subrounded quartz grains in thin section. Red arrows indicate quartz at non-extinction angle and orange arrows indicate quartz at extinction (under XPL). B) Representative sample displaying the appearance of mostly angular and subangular quartz grains in thin section. Red arrows indicate quartz at non-extinction angle and orange arrows indicate quartz at extinction. Green arrows show interspersed heavy minerals (under XPL). C) Representative sample displaying the appearance of plagioclase in thin section. Blue arrows indicate albite with polysynthetic twinning whereas the maroon arrows indicate orthoclase with Carlsbad twinning (under XPL). D) Representative sample displaying the appearance of plagioclase in thin section. Blue arrows indicate albite with polysynthetic twinning (under XPL). E) Sample showing the appearance of various micas in thin section. Note the continuous to discontinuous iron-oxide rich laminae. Purple arrows indicate muscovite, pink arrows represent biotite and yellow arrows indicate haematite (under XPL). F) Sample showing the appearance of various micas in thin section. Purple arrows indicate muscovite and pink arrows represent biotite (under XPL).

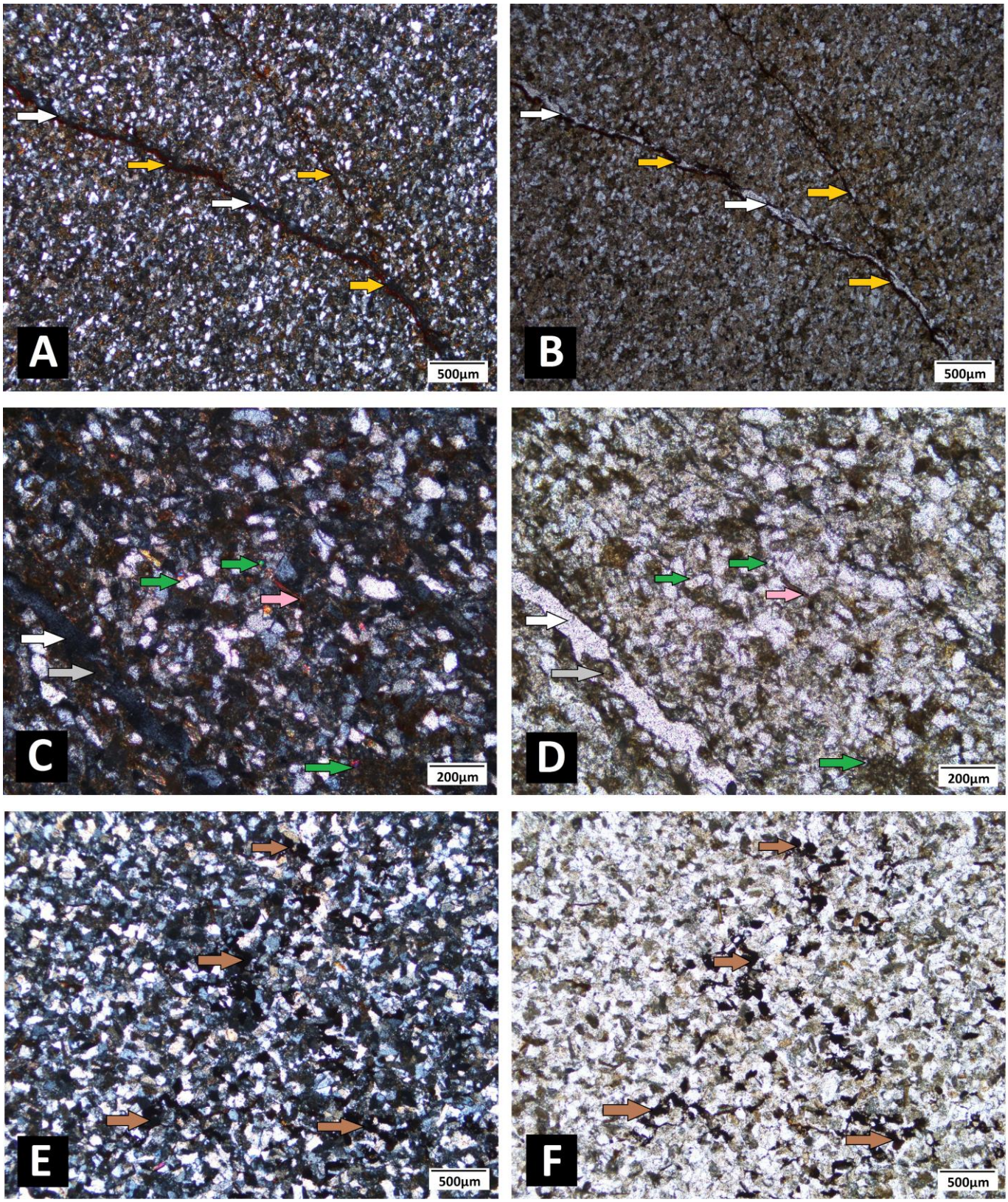


Figure 3.5. Photo micrographs. A and B) Sample showing unfilled fracture porosity in sandstone with a hematite lining. White arrows indicate fracture and yellow arrows indicate hematite (A under XPL; B under PPL). C and D) Sample showing fracture porosity with some siliciclastic infill. White arrow indicates fracture; grey arrow indicates siliciclastic infill; pink arrow indicates biotite and green arrows show distribution of heavy minerals within the sample (C under XPL; D under PPL). E and F) Sample showing a high concentration of oxide minerals within siliciclastic groundmass. Brown arrows indicate oxide minerals (E under XPL; F under PPL).

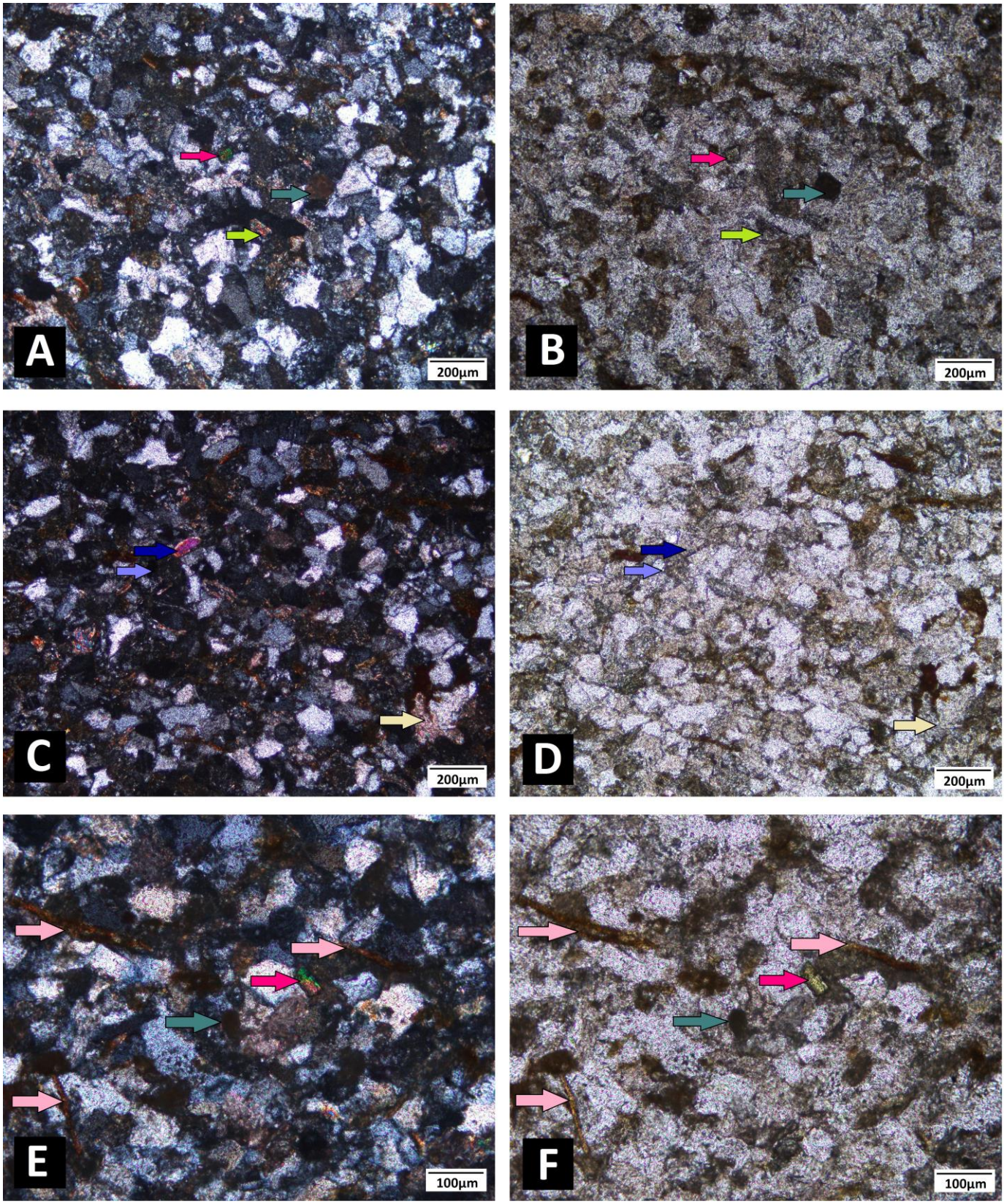


Figure 3.6. Photo micrographs. A and B) Sample showing the appearance of heavy minerals in thin section. Pink arrow indicates zircon; lime arrow indicates actinolite and lilac arrow indicates clay clast (A under XPL; B under PPL). C and D) Sample showing heavy minerals in thin section. Blue arrow indicates actinolite; light blue arrow indicates diopside and white arrow indicates calcite cement (C under XPL; D under PPL). E and F) Sample showing the appearance of heavy minerals in thin section. Pink arrow indicates zircon; lilac arrow indicates clay clast and pink arrow indicates biotite (E under XPL; F under PPL).

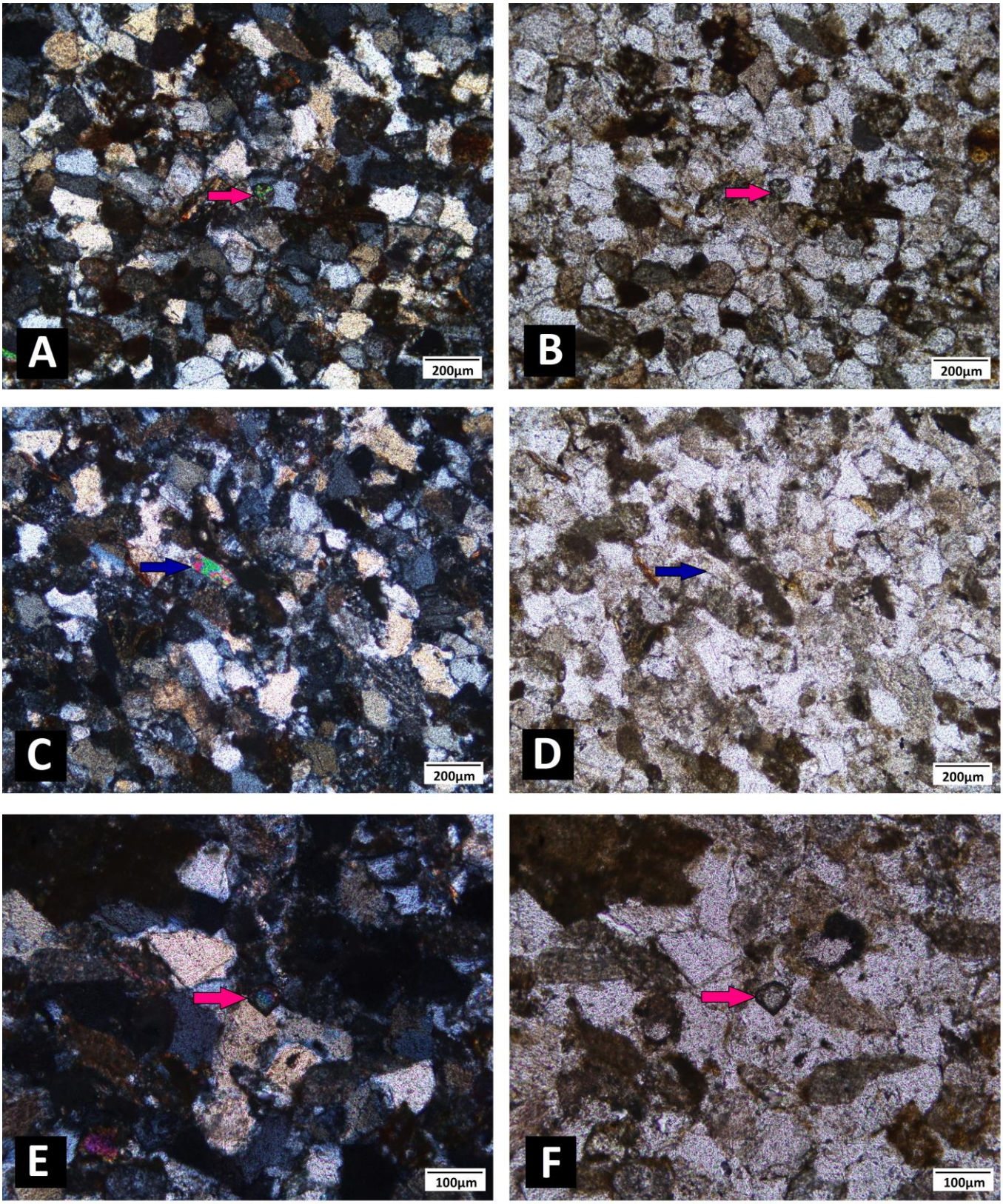


Figure 3.7. Photo micrographs. A and B) Sample showing the appearance of heavy minerals in thin section. Pink arrow indicates zircon (A under XPL; B under PPL). C and D) Sample showing heavy minerals in thin section. Blue arrow indicates actinolite (C under XPL; D under PPL). E and F) Sample showing the appearance of heavy minerals in thin. Pink arrow indicates zircon (E under XPL; F under PPL).

	Quartz	Clay (Cement)	Clay (Rounded)	Clay (Angular)	Clay (Clast)	Orthoclase	Plagioclase	Mica	Heavy Minerals	Oxide Minerals	Pore Space	Calcite Cement	Hematite	Burrow Fill	Total
Sample Number															
148SSA	197	104	8	6	0	5	3	5	5	5	8	0	4	0	**350**
148SSB	173	88	16	14	0	10	5	10	6	5	0	0	23	0	**350**
148SSC	181	96	12	12	1	9	3	8	4	5	0	2	17	0	**350**
148SSD	201	84	5	14	0	6	2	8	2	3	0	2	23	0	**350**
148SSE	164	94	12	13	0	12	4	12	6	10	4	0	19	0	**350**
148SSF	191	100	3	6	0	18	3	11	3	1	2	0	12	0	**350**
148SSG	227	80	2	3	3	7	5	5	3	1	0	0	14	0	**350**
148CCB	211	95	5	6	0	12	4	7	5	5	0	0	0	0	**350**
148SIS	148	138	8	3	26	3	3	6	4	7	2	0	2	0	**350**
158PLATSSTOP1	212	97	5	10	0	6	4	5	4	3	0	0	4	0	**350**
228DNEUS2SS1	188	92	10	4	0	26	8	8	7	1	0	0	6	0	**350**
228DNEUS2SS2	176	108	12	20	0	11	7	6	4	3	0	0	3	0	**350**
SAMPLE178	105	178	4	0	19	0	0	3	0	16	0	0	25	0	**350**
178JAGDSS1	220	74	12	7	2	13	4	9	5	0	0	0	4	0	**350**
178JAGDSS2	207	98	5	4	1	6	3	5	3	4	8	0	6	0	**350**
178JAGDSS3	189	112	6	6	6	4	3	3	3	2	2	0	14	0	**350**
178JAGDSS4	174	99	13	5	1	11	1	4	4	7	7	0	24	0	**350**
178JADGSS5	194	102	6	10	10	7	2	7	5	3	0	0	4	0	**350**
178JAGDSS6	196	85	0	7	23	12	4	5	4	5	0	1	8	0	**350**
178JAGDSS7	206	94	3	8	0	14	2	5	3	1	1	0	13	4	**350**
178JAGDSS8	189	102	11	6	1	9	4	7	4	2	1	3	11	0	**350**
178JAGDSS9	168	112	2	4	35	3	2	10	3	5	0	0	6	0	**350**
178JAGDSS10	176	130	4	4	2	6	4	4	4	8	0	0	8	0	**350**
178JAGDSS11	137	161	18	11	0	4	1	2	4	7	1	0	4	0	**350**
178JAGDSS12	187	126	2	3	0	3	2	2	3	11	0	0	11	0	**350**
208TAFELSS1	186	79	7	8	44	6	2	5	1	1	0	0	11	0	**350**
208TAFELSS2	195	103	8	4	0	9	3	12	4	1	0	0	11	0	**350**
208TAFELSS3	188	135	1	1	8	3	1	4	2	2	2	0	3	0	**350**
208TAFELSS4	210	93	5	4	0	7	2	11	4	3	0	2	9	0	**350**
208TAFELSS5	171	105	4	5	37	3	2	8	2	4	0	0	9	0	**350**
218NOROSS1	171	56	8	6	74	11	0	12	5	4	0	0	3	0	**350**
218NOROSS2	207	96	4	3	0	6	3	7	9	4	0	0	11	0	**350**
218NOROSS3	202	104	6	5	0	12	1	14	2	3	0	0	1	0	**350**
218NOROSS4	175	128	6	7	6	7	2	5	3	7	0	0	4	0	**350**
218NOROSS5	203	107	2	3	2	6	3	9	5	2	2	0	6	0	**350**
218NOROSS6	237	53	4	19	0	8	3	8	1	5	0	0	12	0	**350**
218NOROSS7	236	72	8	2	0	7	5	7	2	4	1	0	6	0	**350**
218NOROSS8	181	113	4	13	0	5	1	4	0	11	0	0	18	0	**350**
218NOROSS9	212	98	6	10	0	6	3	6	3	5	0	0	1	0	**350**
218NOROEX1	207	82	9	12	0	18	4	6	6	2	0	0	4	0	**350**

Table 3.2. Point count data from sandstone samples.

	Quartz	Clay (Cement)	Plagioclase	Mica	Oxide Minerals	Pore Space	Calcite Cement	Hematite	Muddy Sphere	Shadow Around Muddy Spheres	Lithic Fragment	Unidentified Fibrous Mineral	Hematite Ball	**Total**
Sample Number														
DIKCNEUSLIMESTONE	55	0	0	0	8	0	285	2	0	0	0	0	0	**350**
14811MLM/STN	55	0	0	1	0	0	279	11	0	0	0	0	4	**350**
14811MLMSTN	54	0	1	1	8	0	271	13	0	0	0	0	2	**350**
178LMBALL2	133	140	0	0	1	1	23	1	36	15	0	0	0	**350**
178LMBALL1	41	0	0	0	0	0	8	17	275	0	1	8	0	**350**

Table 3.3. Point count data from carbonate nodule samples.

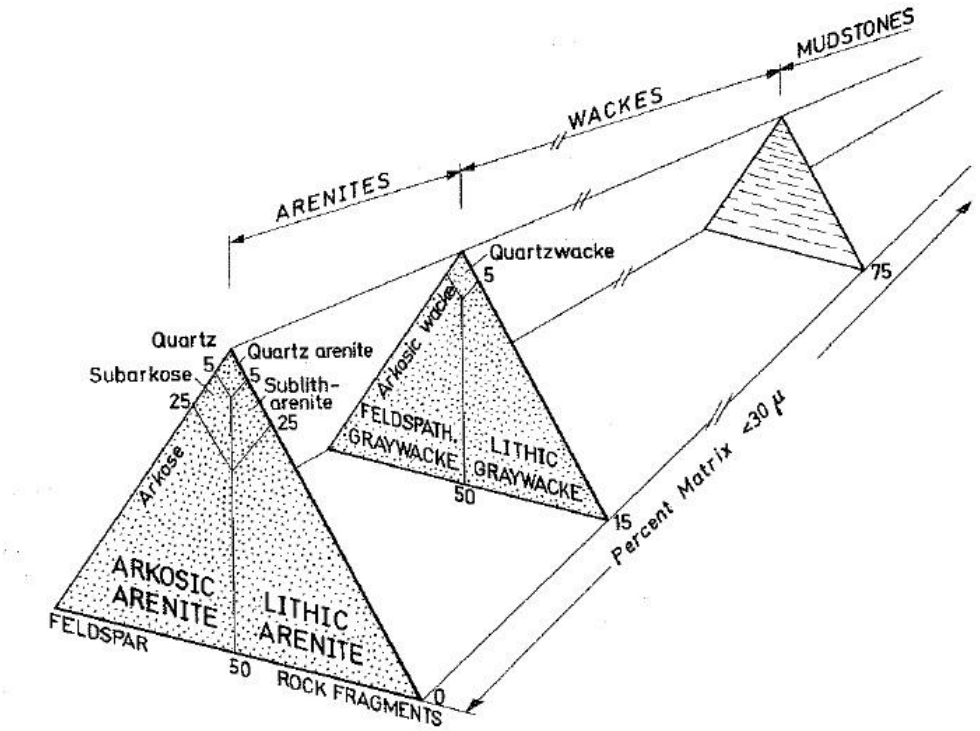


Figure 3.8. QFL diagram. Showing the classification scheme used in this work. All samples contain more than 15% matrix and are therefore classified as wackes (after Pettijohn, 1975).

the study area. In argillaceous sandstones there is great difficulty in distinguishing matrix and detrital grain boundaries because of the recrystallization of matrix. This may lead to an overestimation of the abundance of matrix (de Booy, 1966). The problem of the matrix is that mud and sand are not usually deposited simultaneously. The mud has been suggested to have precipitated by the flocculation of electrolytes in seawater (Woodland, 1938) but evidence for this is lacking and few modern shallow-marine sands have the character (i.e. interstitial mud) to become wackes on lithification (Pettijohn, 1987). Matrix is generally derived from the weathering and reworking of unstable framework grains (Pettijohn, 1987) such as feldspars. Matrix formation is accompanied by albitization of feldspar minerals and diagenetic changes, which can leach framework grains and thus alter the perception of their provenance (Pettijohn, 1987). It is possible that the high clay content in these sandstone samples is climatically controlled as temperate climate conditions favour chemical feldspar weathering. This can lead to the increasing clay and quartz contents in the sediments. The term "greywackization" suggests matrix was formed by the transformation of argillaceous and volcanic rock fragments after deposition (Cummins, 1962a; Kuenen, 1966). The presence of matrix where calcite cement is absent suggests a diagenetic origin. Due to the concentration of samples in a relatively confined space on the QFL diagram a general delineation of the samples has been classified (Fig. 3.8 and 3.9). Out of the 45 studied samples 24 are classified as quartz wackes and the remaining 21 are classified as feldspathic wackes/arkosic wackes.

3.6 Lithofacies Based Petrographic Descriptions

3.6.1 Lithofacies 1 – Mudstone

This lithofacies was not sampled for thin sections analysis due to the fine-grained and cleaved nature of these rocks, but was sampled for geochemical analysis. The nodules that are present within this facies were sampled and thin sections were prepared. Photo micrographs of these samples are shown in Figure 3.10, 3.11 and 3.12. Two samples (178LMBALL1 and 178LMBALL2) obtained near a volcanic sill intrusion have been heavily metamorphosed and have a different mineralogical assemblage than the unmetamorphosed nodules. Of the unmetamorphosed nodules, three samples (14811MLMSTN, 14811MLM/STN and DICKNEUSLIMESTONE) were analysed. Generally these samples have 81-77% micrite matrix (>30μm) and approximately 15% quartz grains that range in size from 56μm to 83μm.

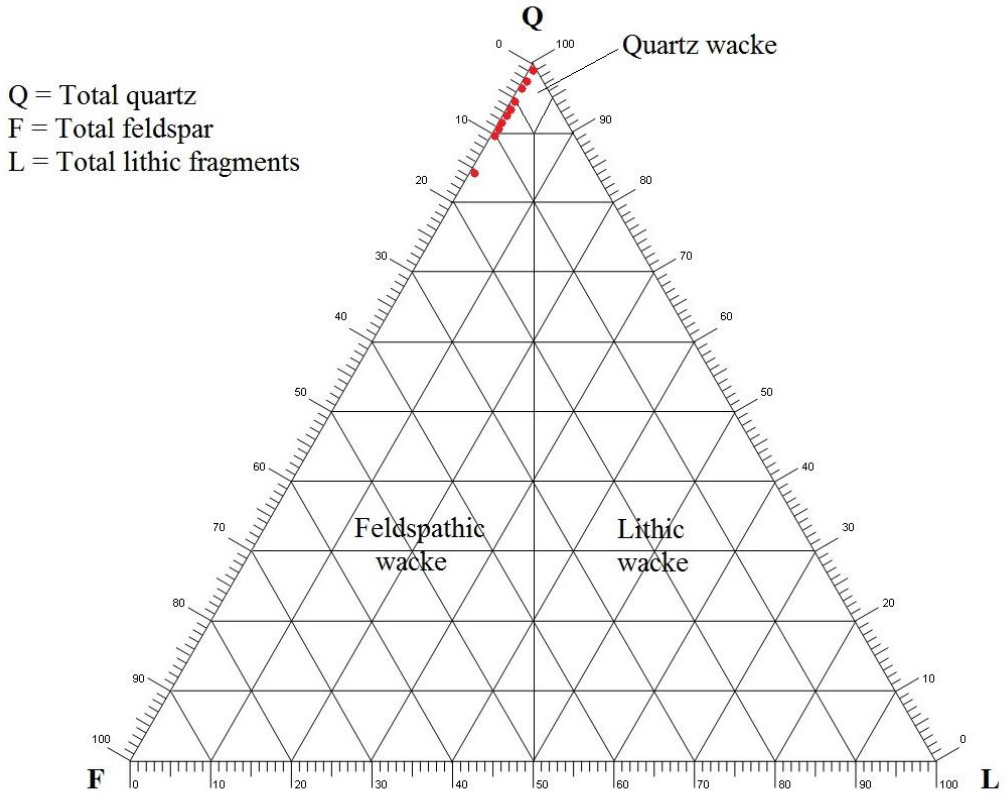


Figure 3.9. QFL diagram of the wacke field [(>15% matrix) after Pettijohn (1975)]. Red dots indicate sample plots. The absence of lithic fragments as well as the low proportion of feldspar allow for the majority of samples from the study area to be classified as quartz wackes. Samples with more than 5% feldspars fall into the feldspathic wacke field.

Minor amounts of mica, plagioclase and oxide minerals are present. Hematite is also present in various amounts as altered grains and nodules with a central nucleus and outer halo. These samples are moderately-well sorted with quartz grains being subangular to subrounded. Another, sample AM002, which was analysed for d13C, clearly shows biogenic textures in the form of algal mats (Fig. 3.12). The metamorphosed nodules provide little in the way of palaeoenvironmental information but are still interesting in terms of mineralogical assemblage. Sample 178LMBALL2 contains 38% quartz, 40% clay matrix, approximately 7% micrite, approximately 15% muddy spheres (of unidentified mineral) and minor amounts of hematite, oxide minerals and pore spaces. Samples 178LMBALL1 consists of approximately 79% muddy spheres (of unidentified mineral), approximately 12% quartz, 2% calcite cement, 5% hematite and minor amounts of polycrystalline quartz and an unknown fibrous mineral. It is possible that the unidentified fibrous mineral is actinolite that formed close to the intrusion, at high temperatures (>250°C). Whereby, bundles of acicular needles

of actinolite protrude into open pores spaces. These nodules do not fall into the QFL classification or the provenance classification of Dickenson and Suczek (1979) and are therefore not plotted.

3.6.2 Lithofacies 2 - Bioturbated sandy-siltstone

Two samples (208TAFELSS5 and 218NOROSS3) were collected from this lithofacies. These samples show a range of grain sizes from coarse silt (48µm) to fine sand (167µm) and are moderately well sorted with angular to subrounded grain shapes. These prepared thin sections contain between 49% and 58% quartz; 30% clay matrix; up to 11% orthoclase as well as minor amounts of plagioclase, mica, heavy minerals, oxide minerals and hematite. These samples plot as both quartz wackes and feldspathic wackes on the QFL diagram and fall into the realm of continental block provenance as per Dickenson and Suczek (1979). Photomicrographs of sample 208TAFELSS5 are given in Figure 3.1.E and F and sample 218NOROSS3 in Figure 3.13.A and B.

3.6.3 Lithofacies 3 - Interbedded sandstone and siltstone

Two samples (148SIS1 and 178JAGDSS9) were collected and analysed from this lithofacies. These samples show a range of grain sizes from coarse silt (33µm) to medium sand (143µm) and are moderately well-sorted with angular to subrounded grain shapes. These two samples consist of between 42% and 48% quartz; 32% and 39% clay matrix; between 7% and 10% clay clasts as well as minor amounts of orthoclase, plagioclase, mica, heavy minerals, oxide minerals, pore spaces and hematite. These samples plot as quartz wackes on the QFL diagram and fall into the realm of continental block provenance as per Dickenson and Suczek (1979). Photo micrographs of this facies are shown in Figure 3.13 C-F.

3.6.4 Lithofacies 4 - Structureless sandstone

Two samples (148SSG and 178JAGDSS2) were analysed for this facies. These samples range from being well-sorted to moderately well-sorted with angular to subrounded grain shapes. The grain size variation in this facies is from coarse silt (53µm) to medium sand (333µm). These two samples consist of between 59% and 65% quartz; 23-28% clay matrix with minor amounts of orthoclase, plagioclase, mica, heavy minerals, oxide minerals, pore

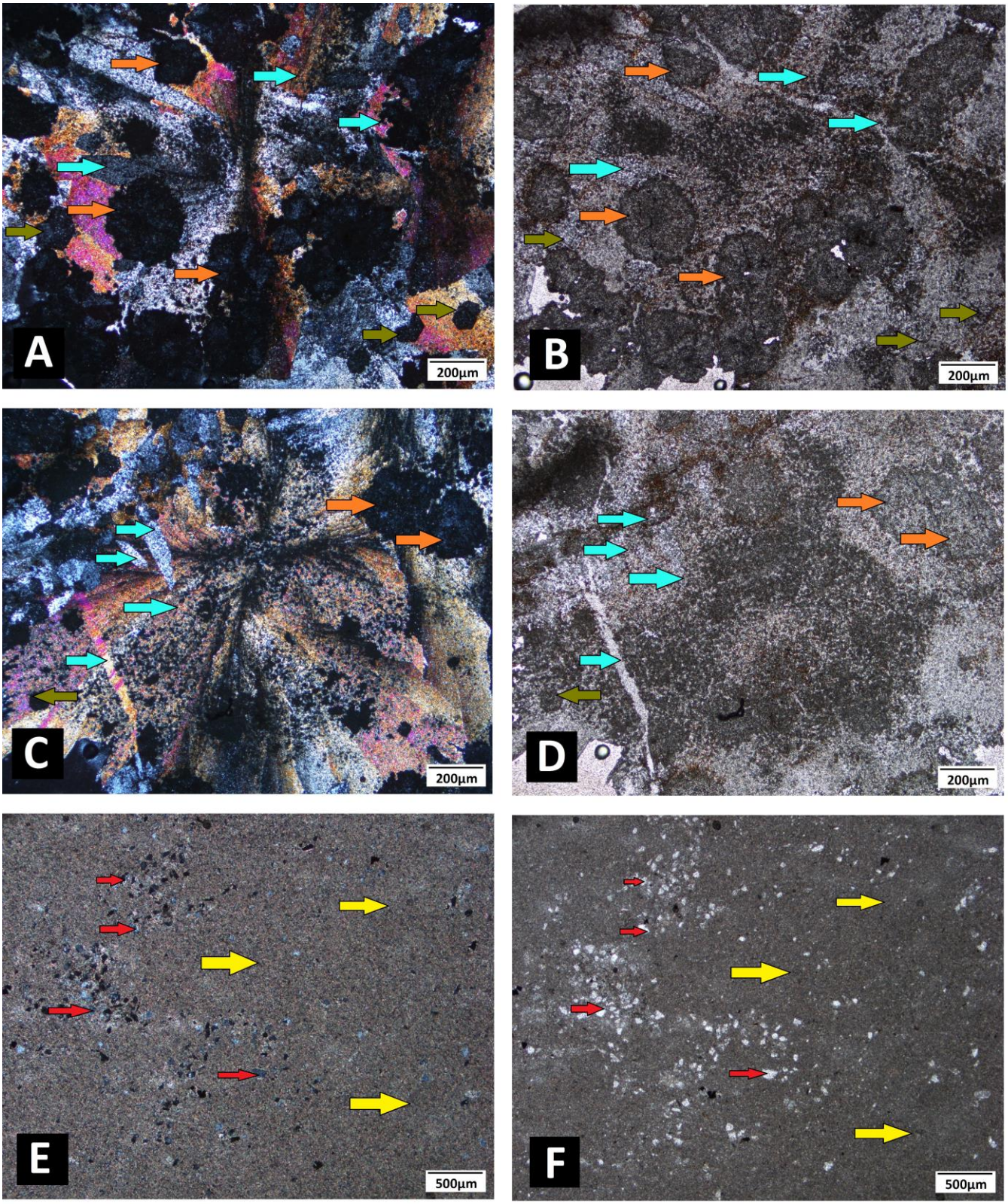


Figure 3.10. Photo micrographs. A and B) Sample showing mineral assemblage of a nodule due to contact metamorphism. Off-yellow/green arrow indicates unknown mineral; orange arrow indicates ball-like structure of unknown composition and light blue arrow indicates unknown mineral (A under XPL; B under PPL). C and D) Sample showing mineral assemblage of a nodule due to contact metamorphism. Off-yellow/green arrow indicates unknown mineral, orange arrow indicates ball-like structure of unknown composition and light blue arrow indicates unknown mineral (C under XPL; D under PPL). E and F) Shows nodule sample unaffected by contact metamorphism. Red arrow indicates siliciclastic grains set in a fine-grained micrite matrix indicated by the yellow arrows. (E under XPL; F under PPL).

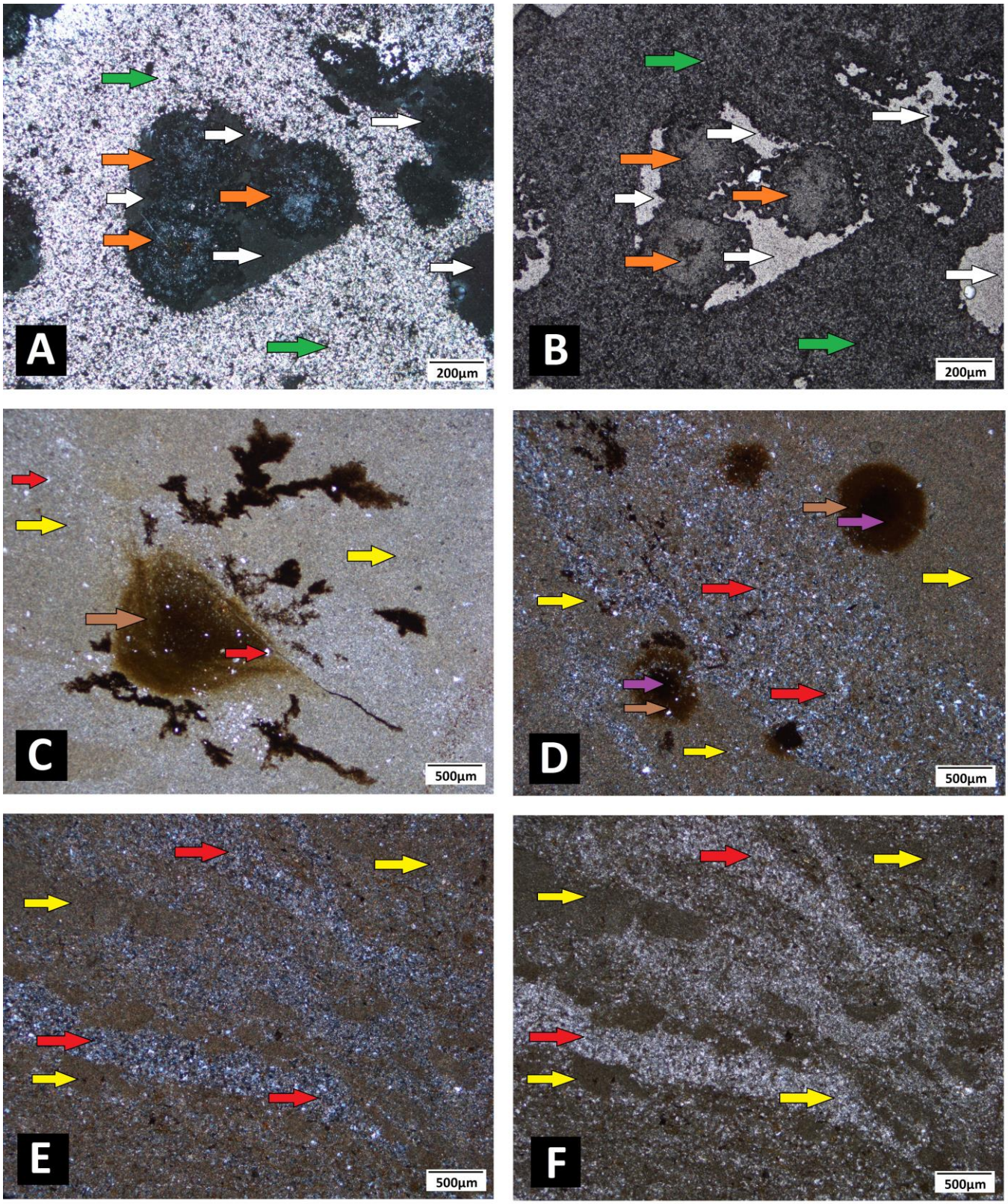


Figure 3.11. Photo micrographs. A and B) Sample showing mineral assemblage in nodule due to contact metamorphism. Orange arrow indicates ball-like structure of unknown composition; white arrow indicates pore space and green arrow indicates fine-grained matrix of unknown composition (A under XPL; B under PPL). C) Sample showing hematite nodule in a fine-grained micritic groundmass. Brown arrow indicates hematite nodule, red arrow indicates siliciclastic grains and yellow arrow indicates micrite (under XPL). D) Sample showing hematite nodule in a fine-grained micritic groundmass. Brown arrow indicates hematite nodule halo; purple arrow indicates hematite nodule nucleus; red arrow indicates siliciclastic grains and yellow arrow indicates micrite (under XPL). E and F) Sample showing the mixed siliciclastic-micritic nature of carbonate nodules in the study area. Red arrow indicates siliciclastic grains and yellow arrow indicates micrite (E under XPL; F under PPL).

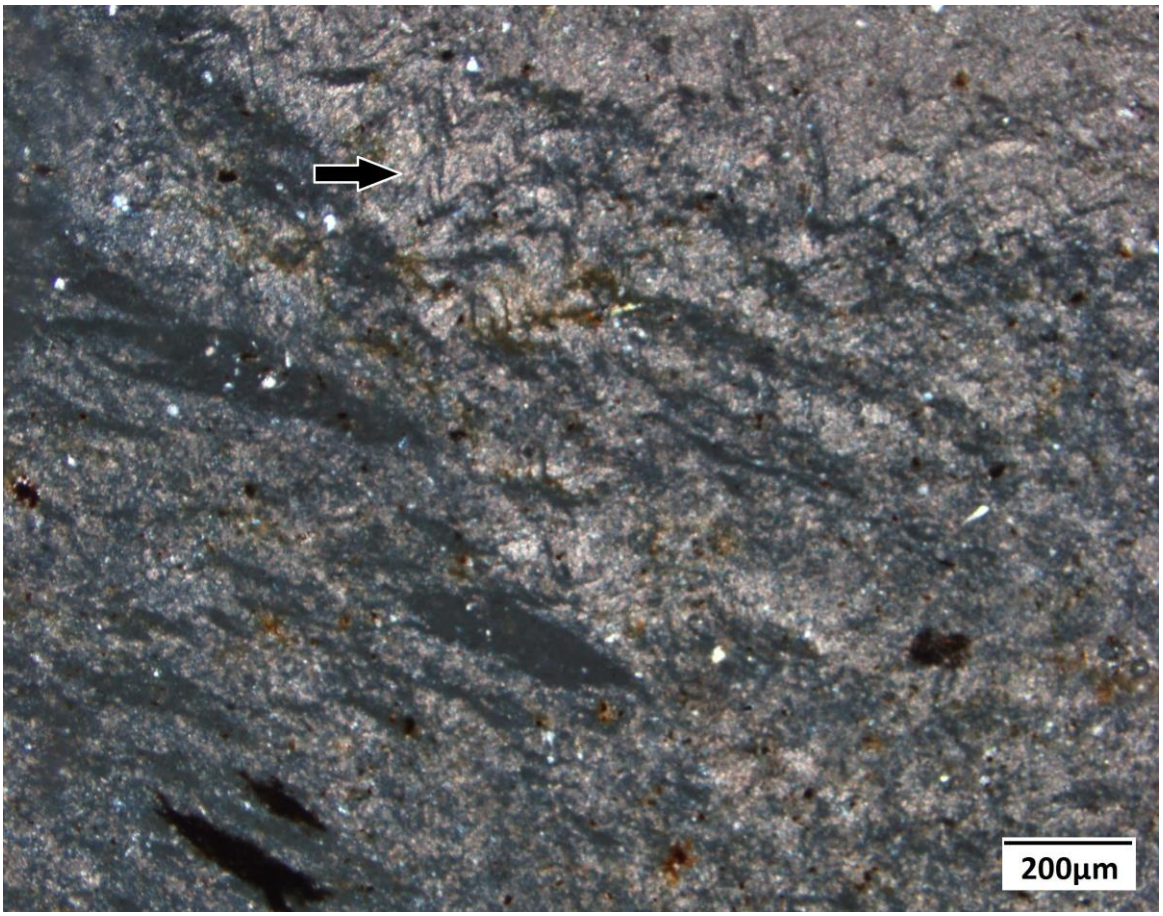


Figure 3.12. Photo micrograph. Sample AM002 under PPL which displays biogenic textures associated with algal mats (black arrow with white outline).

spaces and hematite. These samples plot as quartz wackes on the QFL diagram and as continental block provenance as per Dickenson and Suczek (1979). Photo micrographs of this facies are shown in Figure 3.14 A and B.

3.6.5 Lithofacies 5 - Discrete HCS sandstone

Six samples (208TAFELSS1, 2, 3; 218NOROSS1, 4 and 9) were collected and analysed from this lithofacies. These samples range from being well-sorted to moderately well-sorted with angular to subrounded grain shapes. The grain size variation in this facies is from coarse silt (45µm) to fine sand (182µm). The mineralogy of these samples is as follows: 49%-60% quartz; 16%-36% clay matrix; 13%-21% clay clasts and minor amounts of orthoclase, plagioclase, mica, heavy minerals, oxide minerals and hematite. These samples also contain a high frequency of burrows with fine-grained sediment infill. These plot as both quartz

wackes and feldspathic wackes on the QFL diagram and as continental block provenance as per Dickenson and Suczek (1979).). Photo micrographs of this facies are shown in Figure 3.14 C-F.

3.6.6 Lithofacies 6 - Amalgamated HCS sandstone

This lithofacies was the most abundantly sampled of all facies due to the lateral continuity and general thickness of the amalgamated sandstone packages. Sixteen samples were collected and analysed. The samples are:

1) 148SSC
2) 148SSD
3) 148SSE
4) 148SSF
5) 158PLATSSTOP1
6) 178JAGDSS3
7) 178JAGDSS4
8) 178JAGDSS5
9) 178JAGDSS6
10) 178JAGDSS7
11) 178JAGDSS8
12) 178JAGDSS10
13) 178JAGDSS11
14) 208TAFELSS4
15) 218NOROSS2
16) 218NOROSS5

These samples are generally moderately-well sorted although a few samples are well sorted and the majority of grain shapes are angular to subrounded. The grain sizes vary from coarse silt (48µm) to medium sand (400µm). These samples generally have between 50% and 60% quartz; 25-40% clay matrix; 1-7% hematite as well as minor amounts of orthoclase, plagioclase, mica, heavy minerals, oxide minerals, pore space and burrow fill. Some calcite cement has also been observed in two samples. Of the sixteen samples, ten plot as quartz

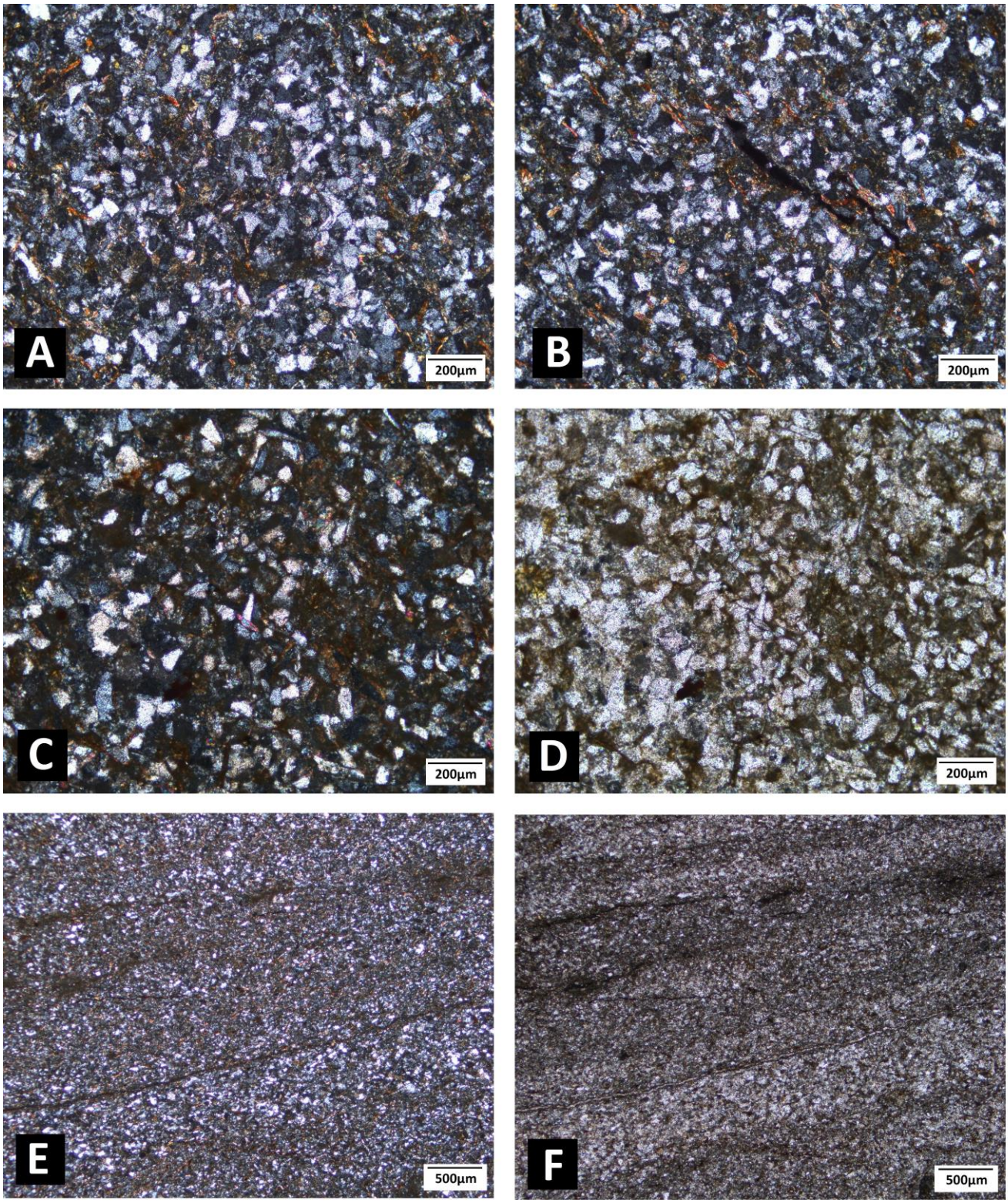


Figure 3.13. Photo micrographs. A and B) Sample 218NOROSS3 representing lithofacies 2 and showing the relatively fine-grained nature of this facies as well as moderate-well sorting. Also displayed is the high quartz to clay matrix ratio. Minor orthoclase, mica, heavy minerals, oxide minerals and hematite also shown (A and B under XPL). C and D) Representative sample showing the grain size, sorting and relatively equal quartz to clay matrix ratio of lithofacies 3. Clay clasts and other accessory minerals also present (C under XPL and D under PPL). E and F) Representative sample of lithofacies 3, showing the fine-grained nature of the sandstone as well as fine-grained inclined laminations within the coarser-grained faction of the rock. Often fracture porosity is observed within the laminations (E under XPL and F under PPL).

wackes and the remaining six plot as feldspathic wackes on the QFL diagram. All these samples fall into the continental block provenance as per Dickenson and Suczek (1979). Photo micrographs of this lithofacies are shown in Figure 3.15 A-F and 3.16 A-D.

Six samples (148SSB, 218NOROSS6, 218NOROSS7, 218NOROEX1, 228DNEUS2SS1 and 228DNEUS2SS2) of the apparently quartz-rich sandstone intervals were collected and analysed from amalgamated HCS packages. The grain size of these samples vary from very-fine sand (77µm) to medium sand (400µm) and are predominantly well-sorted although there are a few samples that display moderate-well sorting. The grain shapes range from angular to subrounded. These samples contain 49-68% quartz; 15-31% clay matrix; 1-6% angular clay fragments; 2-7% orthoclase; 1-7% hematite as well as trace amounts of mica, plagioclase, heavy minerals, pore space and oxide minerals. Four samples plot as feldspathic wackes of the QFL diagrams whereas the other two samples are so quartz-rich that they plot on the cusp of quartz wackes and feldspathic wackes. All of these samples plot as continental block provenance as per Dickenson and Suczek (1979). Photo micrographs of this facies are shown in Figure 3.17 C-F.

3.6.7 Lithofacies 7 - SSD sandstones and siltstone

Only one sample (148SSA) was collected for this lithofacies. The sample was obtained from the highly tilted and deformed layer observed in the Dickneus VS. However, in many stratigraphic intervals of lithofacies 6 SSD features occur and laterally become HCS structures. Therefore it is difficult to fully obtain a sample that is representative of this facies. This sample ranges in grain size from coarse silt (50µm) to fine sand (200µm) and is well-sorted and has subangular to subrounded grains. Mineralogically, this sample contains 56% quartz, 30% clay matrix and minor amounts of orthoclase, plagioclase, mica, heavy minerals, oxide minerals, pore spaces and hematite. This sample plots as a quartz wacke on the QFL diagram and falls into the realm of continental block provenance as per Dickenson and Suczek (1979). Photo micrographs of this facies are shown in figure 3.17 A and B.

A few samples have been omitted from the petrographic study of this due to factors such as a high degree of metamorphism and due to collection from the Aussenkjer Formation rather than the Amibberg Formation.

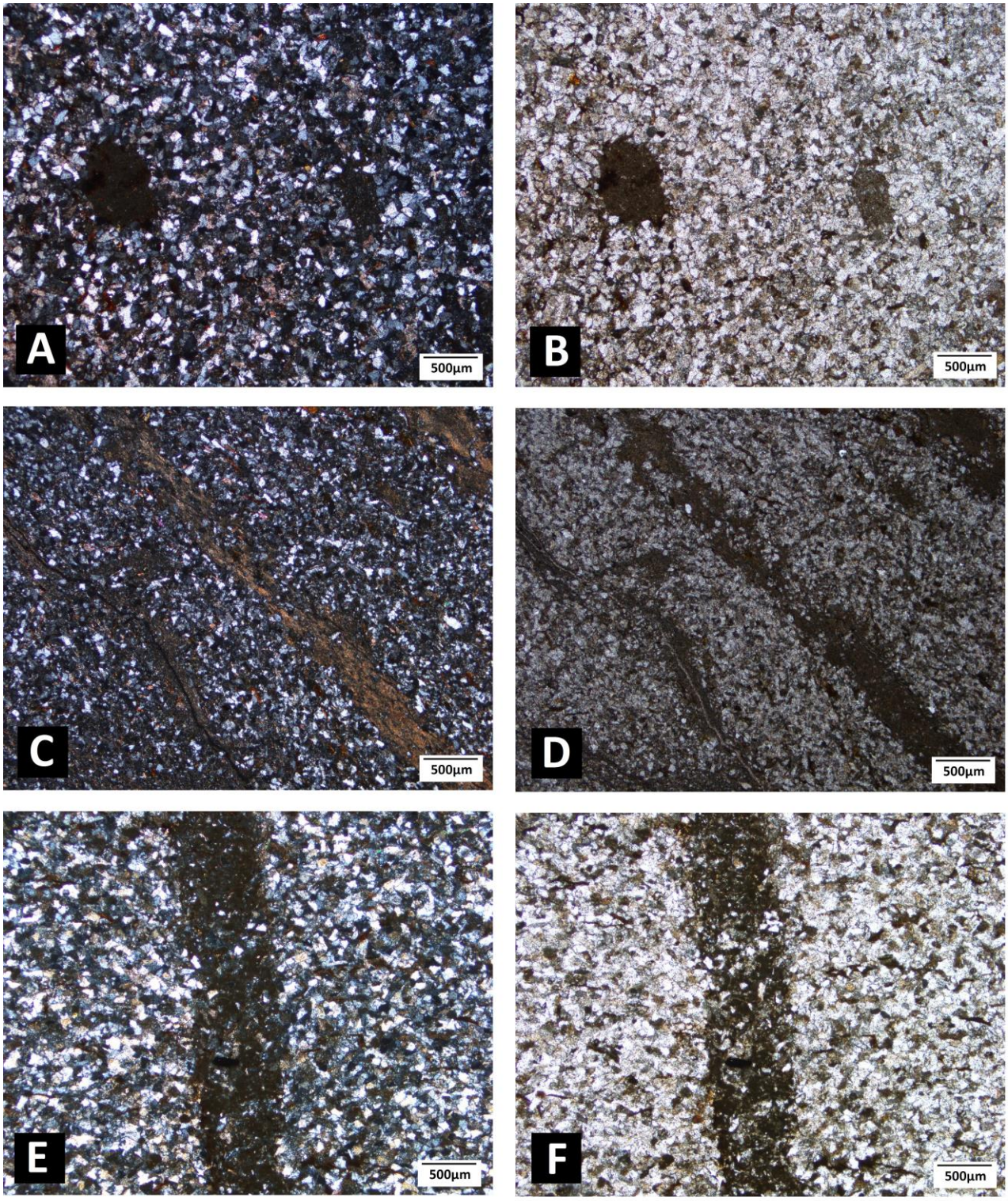


Figure 3.14. Photo micrographs. A and B) Samples from lithofacies 4 showing the variation in grain size from coarse silt (53µm) to medium sand (333µm). Also displayed is the high percentage of quartz and the relatively low clay matrix percentage. In the centre left and right of the slide are mudstone rip-up clasts. The well-sorted nature and angular to subrounded grain shapes are also typical of this facies (A under XPL and B under PPL). C and D) Representative sample of lithofacies 5 showing obliquely orientated burrows with mixed silt sized and fine-grained sand sized particles. Also shown is the generally fine-grained nature of this facies and minor amounts of orthoclase, plagioclase, mica, heavy minerals, oxide minerals and hematite (C under XPL and D under PPL). E and F) Sample from lithofacies 5 showing vertically orientated burrow structures with fine-grained sediment infill. Also evident is the high proportion of clay clasts relative to the other facies (E under XPL and F under PPL).

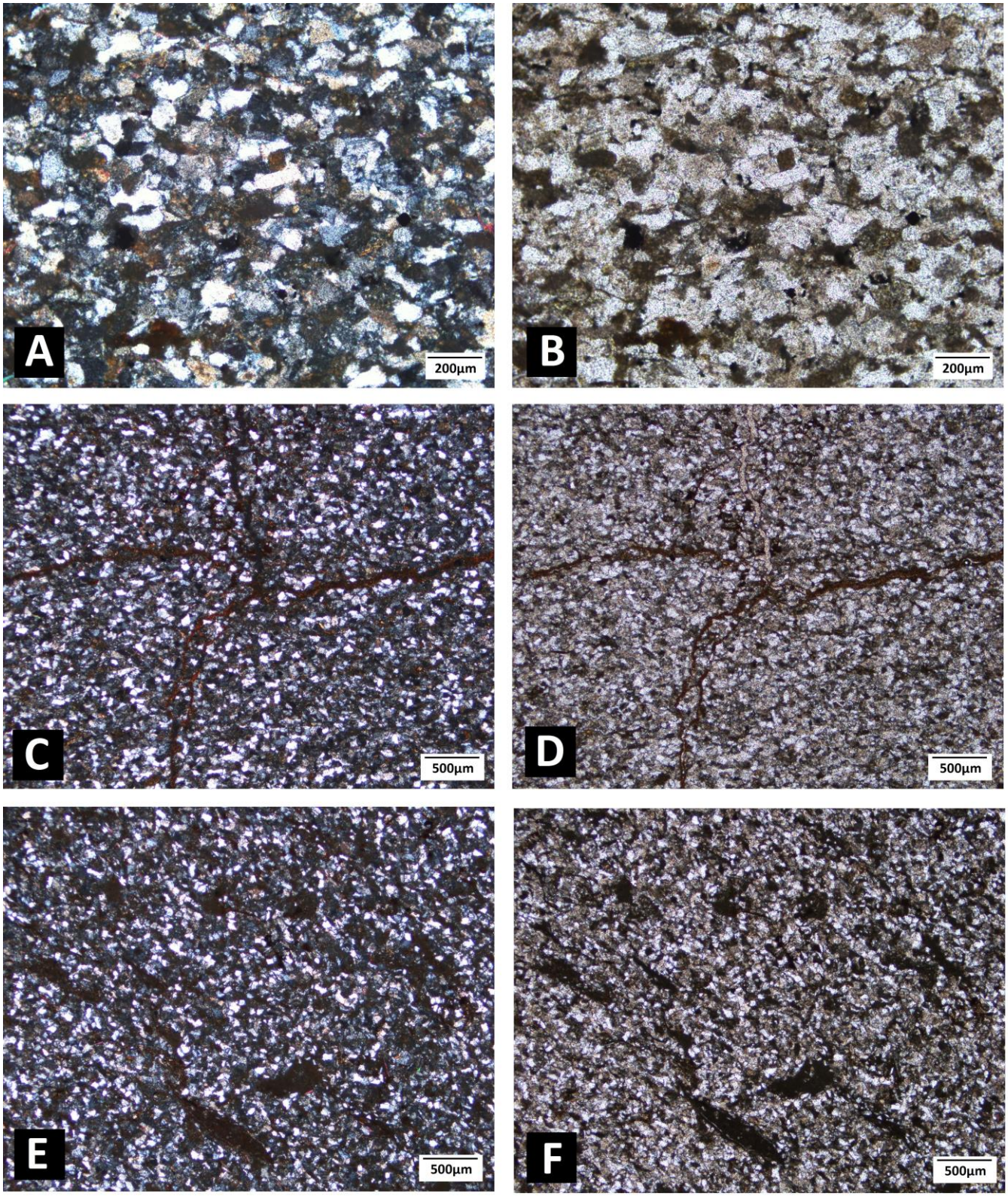


Figure 3.15. Photo micrographs of lithofacies 6. A and B) Sample of lithofacies 6 showing the grain size variation from coarse silt (48µm) to medium sand (400µm). The high percentage of both quartz and clay matrix is also evident with some rounded clay clasts present. The well-sorted nature of these rocks is also displayed as well as the angular to subrounded grain boundaries (A under XPL and B under PPL). C and D) Sample from lithofacies 6 showing hematite filled and unfilled fracture porosities (C under XPL and D under PPL). E and F) Representative sample of lithofacies 6 showing the high frequency of mudstone rip-up clasts set into the fine- to medium-grained groundmass (E under XPL and F under PPL).

3.7 Sandstone Provenance and Tectonic Setting

The composition of detrital sediments is primarily controlled by the source rock composition whereby weathering and diagenetic processes have a minor influence (e.g., Armstrong-Altrin, 2009). Compositional characteristics of source rocks are reflected in their sedimentary products and provide valuable information about nature of source rocks and the tectonic setting of their emplacement (Van de Kamp and Leake, 1995; Joo et al. 2005; Armstrong-Altrin et al. 2004; Armstrong-Altrin and Verma, 2005; Wanas and Abdel-Maguid, 2006; Liu et al. 2007; Sinha et al. 2007; Nagarajan et al. 2007a; Nagarajan et al. 2007b; Maravelis and Zelilidis, 2009). Therefore, provenance studies are mainly based on modal analysis of detrital framework grains (Dickinson and Suczek, 1979; Dickinson et al., 1983) and bulk rock geochemistry (Bhatia, 1983; Bhatia, 1985; Bhatia and Crook, 1986; Roser and Korsch, 1986).

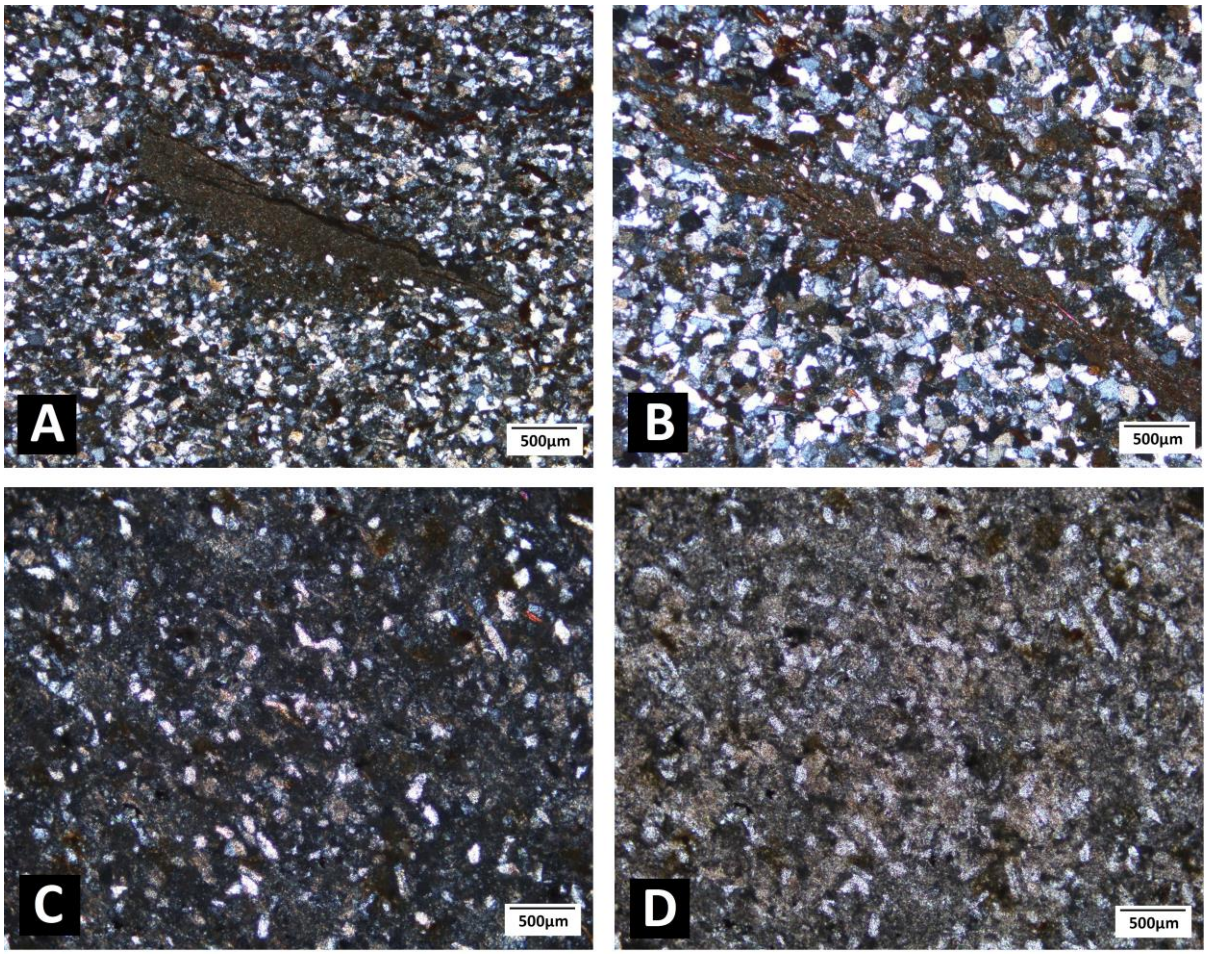


Figure 3.16. Photo micrographs of lithofacies 6. A) Sample displaying fine-grained mudstone clast. Hematite is present as a filled fracture within the rip-up clast. Fracture porosity can be seen in the upper parts of the section (under XPL). B) Mudstone rip-up clast in a fine to medium-grained sandstone sample. Micas as well as quartz grains are seen interspersed within the clast (under XPL). C and D) Representative sample showing a high proportion of clay matrix to detrital quartz (C under XPL and D under PPL).

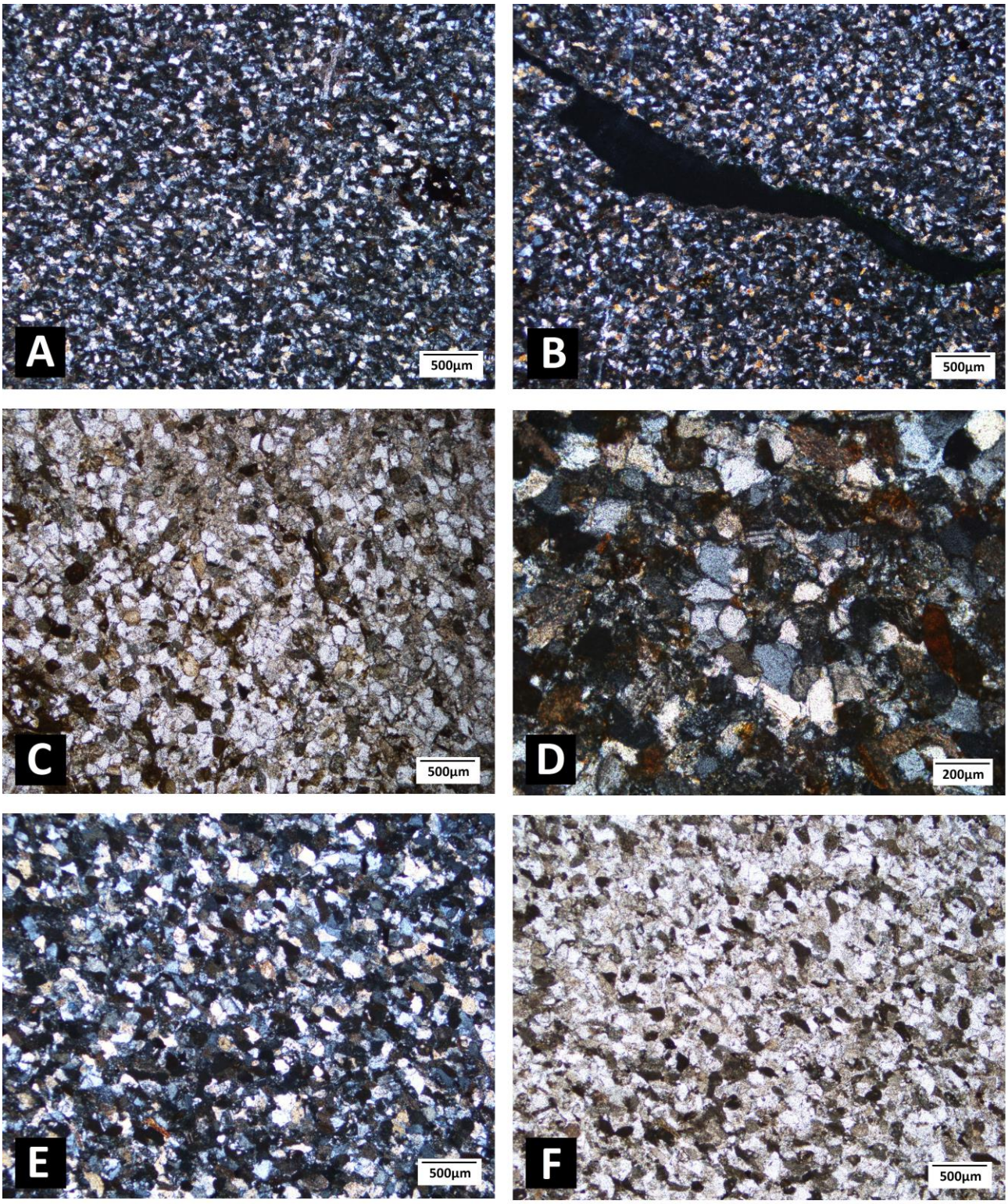


Figure 3.17. Photo micrographs. A) Sample 148SSA from lithofacies 7 showing grain size variation from coarse silt (50µm) to fine sand (200µm) and subangular to subrounded grains that are well-sorted. Mineralogically, this sample contains 56% quartz, 30% clay matrix and minor amounts of orthoclase, plagioclase, mica, heavy minerals, oxide minerals, pore spaces and hematite (under XPL). B) Sample 148SSA from facies 7 displaying a large unfilled pore space (under XPL). C) Apparent quartz-rich sample from lithofacies 6 indicating the coarsest rocks present ranging from very-fine sand (77µm) to medium sand (400µm) and are predominantly well-sorted. This sample shows a higher proportion of rounded and angular clay fragments than the other sandstones. This sample shows between 49-68% quartz and 15-31% clay matrix as well as other trace minerals (under XPL). D) Representative sample of quartz-rich sandstone showing the angular to subrounded shapes of the quartz grains as well as the well-sorted nature of this sample. Minor amounts of hematite and plagioclase can be seen centrally in this sample (under XPL). E and F) This sample of quartz-rich sandstone again shows the grain size, high quartz proportion and high concentration of angular and rounded clay fragments (E under XPL and F under PPL).

Detrital modes of sandstone also provide information about the tectonic settings of basins of deposition (Dickinson et al., 1983). Provenances and derivative sandstone suites were grouped into three general groups by Dickenson and Suczek (1979), one of which is the continental block provenance in which the samples from the study area fall (Fig. 3.18). Sediment is sourced from shields and platforms or in faulted basement blocks. If rifting of the continental block occurs, the sands will be quartzo-feldspathic with high ratios of alkali feldspar to plagioclase. If the sands are derived from high topographic areas located long distances from the depositional areas, the sands will be more quartz rich, showing a higher degree of mineralogical maturity.

The maturity of sandstones coupled with mineral composition provides information concerning the sediment source area(s) (Flesch and Wilson, 1974). In terms of maturity, the three useful stages of maturing sandstones are: 1) the removal of clays 2) rounding, and 3) sorting. In the case of these samples, it is evident that with a high percentage of clay matrix, the generally angular to subrounded grain shapes and moderate-well sorting, these samples are only submature or even immature. Furthermore, maturity can be compositional and expressed in chemical or mineralogic terms. A 100% pure quartz concentration is the ultimate sand. This is because quartz is the only physically and chemically durable constituent of plutonic rocks common enough to be accumulated in great volume (Pettijohn, 1954). A measure of mineralogical maturity, therefore, is given by its quartz content. As most quartz was originally plutonic and closely associated with feldspar, the maturity may also be expressed by the disappearance of feldspar (Dott, 1964). However, polycrystalline quartz and quartz with undulatory extinction are less stable in the sedimentary environment than monocrystalline non-undulatory quartz. Thus, sandstones consisting of monocrystalline quartz that does not show undulatory extinction are mineralogically the most mature.

In terms of mineralogy, the presence of biotite in the studied samples suggests either a plutonic igneous or schistose metamorphic provenance. The presence of zircon and sphene weigh in favour of plutonic granitic provenance (Basu, 1976). Detrital quartz grains are the most abundant constituent in the cratonic sandy deposits (Krynine, 1948; Folk, 1951; Folk, 1980; Basu, 1985). Monocrystalline quartz grains are of volcanic origin as these grains exhibit non-undulose extinction and are free of inclusions (Asiedu et al., 1996). Various authors also indicate that the abundance of non-undulatory monocrystalline quartz suggests plutonic provenance (Blatt, 1967; Basu et al., 1975; Suttner et al., 1981; Tortosa et al., 1991), though it may also be a reflection of grain size. Varieties that exhibit undulose extinction and

inclusions are generally rare in these samples. Furthermore, the absence of polycrystalline quartz in these sandstones rules out a metamorphic province as a source area.

The high amount of mica and primary matrix, high frequency of angular detrital grains all point to a near source derivation of detritus and rapid deposition. The moderate to well-sorted nature of the samples, however, indicate that significant reworking took place. The mudstone rip-up clasts and clay fragments are considered to be sourced intrabasinally.

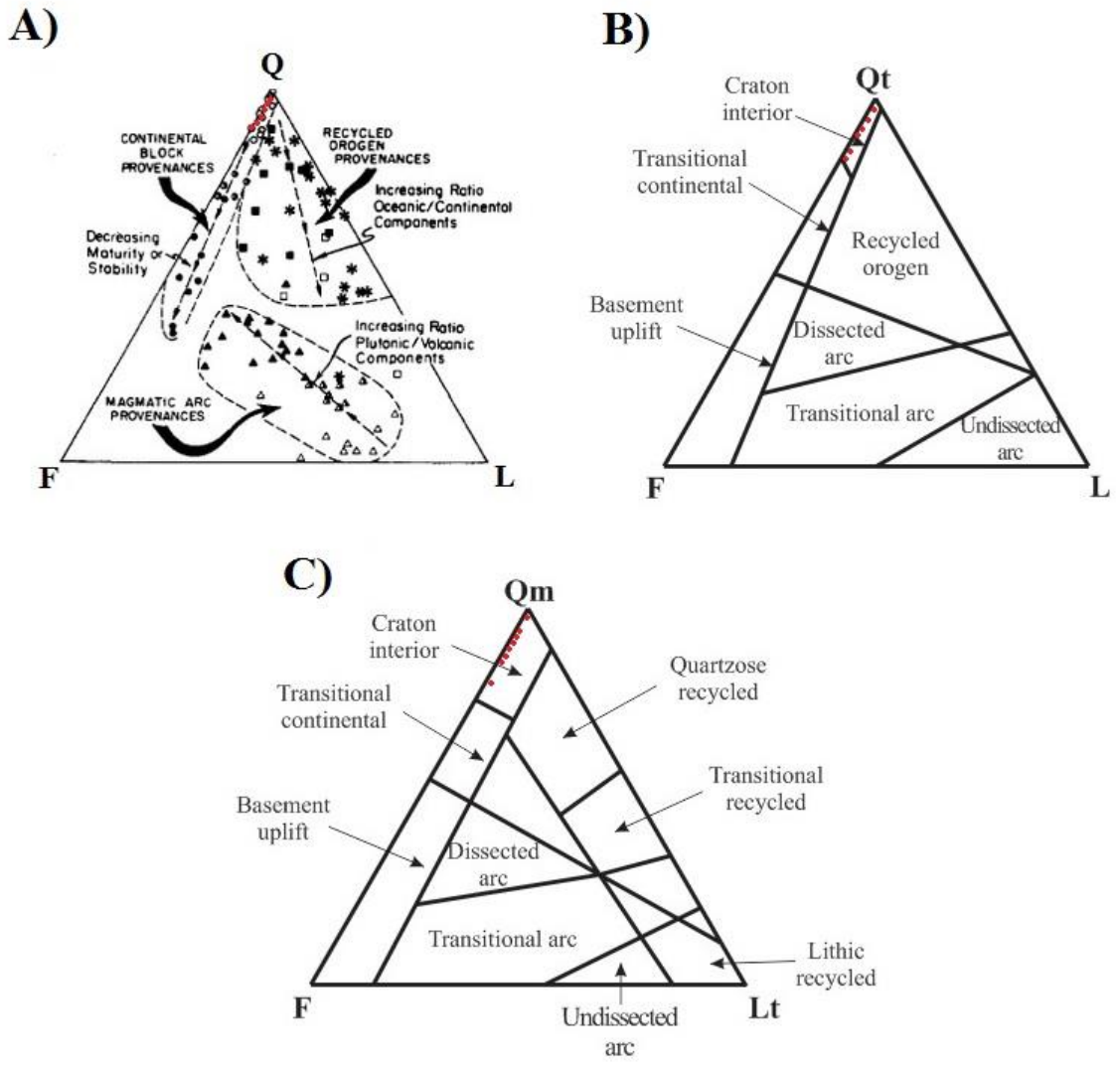


Figure 3.18. QFL ternary diagrams. Red dots indicate sample plots. A) QFL plot showing mean framework modes for sandstones from different provenances. Q is total quartz; F is total feldspars and L is all lithic fragments excluding polycrystalline quartz fragments (after Dickenson and Suczec, 1979). B) QtFL plot showing clearly delineated provenance types. The samples from this study area fall into the craton interior provenance (modified after Dickenson et al., 1983). C) QmFLt plot showing clearly delineated provenance types. The samples from this study area fall into the craton interior provenance (modified after Dickenson et al., 1983

Crook (1970b) recognized three major wacke classes attributed to different provenances. The studied samples fall into the intermediate class (between 15% and 65% quartz) which has a mixed provenance between volcanic and sedimentary sources. This class has been attributed to tectonically active margins of continents and microcontinents. (Pettijohn, 1987). Wackes are characteristically found in Alpine-type orogenic belts (but are known to form elsewhere) and are absent in undeformed, stable or platform areas and are typically marine (Pettijohn, 1987).

3.8 Carbon Isotope Data for Nodules

The d13C values of organic carbon in the sedimentary rocks are used to infer climate changes (Scheffler et al., 2003). Carbon isotopes record local and global variations because of isotopic exchange between carbon reservoirs (Hayes et al., 1999). In shallow water settings photosynthetic activity of cyanobacteria remove CO_2, raising the saturation state of $CaCO_3$ and inducing carbonate precipitation. Eventually, cyanobacteria are starved of Fe which results in the reduction of carbonate precipitation. The high FeO (Fe^{+2}) content of the sediment as well as the negative d13C values (Table 3.4) indicate that algal activity may have been the primary factor for inducing the formation of the carbonate nodules in the study area. Furthermore, trace fossils found on the surfaces, as well as other biogenic structures present, also point towards these nodules as possible microbial mounds that acted as food sources for organisms. Additionally, Scheffler et al. (2003) indicate that organic matter in the central Karoo Basin was primarily of algal origin and that d13C values are controlled by global mechanisms instead of local ones.

Sample Number	δ13C (ppt)
NOD001	-3.16
NOD002	-11.29
NOD003	-6.49
NOD004	-6.07

Table 3.4. δ13C data for nodules of the Amibberg Formation.

3.9 Geochemistry of Mudstones

The study of major and trace elements (Appendix C) is conducted to geochemically identify source rock composition and gain insight into palaeoredox conditions during the deposition of mudstones of the upper Aussenkjer Formation and the Amibberg Formation. Through the use of independent geochemical proxies (Table 3.5), it is possible to reconstruct the depositional environment and climate changes within a sedimentary basin. As ancient climatic or environmental conditions cannot be directly measured, the information obtained from geochemical proxies has to be used determine depositional conditions (Scheffler et al., 2006). For provenance studies, trace elements such as Sc, Cr, Th, Zr and TiO_2 are most useful because of their low mobility during sedimentary processes (McLennan et al., 1983). For palaeoredox conditions Mo, U/Th, Th/U, V/Cr, V/(V+Ni), Ni/Co and V/Sc are used. These ratios are used because redox-sensitive trace metals tend to be more soluble under oxidizing conditions and less soluble under reducing conditions. This elemental behaviour makes U, V and Mo, and to a lesser extent certain other trace metals such as Cr and Co, useful as paleoredox proxies (Tribovillard et al., 2006).

Mudstones of the upper Aussenkjer Formation and Amibberg Formation display high SiO_2 values (72%-77%) due to a high proportion of silt particles in these mudstones. This is due to the near shore position during deposition and high detrital run off from rivers (Bangert, 2000). Other major element data of importance are the high Al_2O_3 values (11.57-14.32); FeO (2.23-3.41); Na_2O (~3); MgO (~1); CaO (~2) and K_2O (2.12-3.84). The other values of major elements are low to negligible.

The Th/U ratio has been used as a proxy for the redox condition (Fig. 3.23) at the time of deposition of ancient sediment (Myers and Wignall, 1987; Wignall, 1994). Reducing conditions lead to an accumulation of U in sediment whereas oxidizing conditions lead to a loss of U from sediments. The mudstone samples show low to moderate U content (0.81-4.05). These low to moderate contents of U are generally found in sediments which were deposited under oxygenated marine conditions (Somayajulu et al., 1994; Madhavaraju and Ramasamy, 1999). Wignall and Twitchett (1996) indicate that anoxic conditions yielded

Sample Number	Fe2O3/K2O	Al2O3/TiO2	TiO2/Ni	Th/U	V/Cr	V/Sc	V/(V+Ni)	Ni/Co	Cu/Zn	log(Fe2O3/K2O)	log(SiO2/Al2O3)	U/Th	Authigenic U
AM002 (dark blue)	0.154	24.19	0.037	3.51	2.36	5.14	0.80	1.24	0.22	-0.813	0.73	0.28	-0.53
AM003 (red)	0.096	31.05	0.031	5.47	2.42	6.01	0.79	1.79	0.25	-1.016	0.70	0.18	-1.37
AM005 (green)	0.134	27.94	0.036	2.29	2.89	7.22	0.82	1.68	0.28	-0.872	0.73	0.44	0.96
NR001 (purple)	0.137	23.38	0.038	3.95	1.53	7.99	0.79	2.06	0.28	-0.864	0.81	0.25	-0.92
NR002 (light blue)	0.128	27.11	0.042	11.31	0.92	7.47	0.82	1.58	0.33	-0.891	0.83	0.09	-2.24

Table 3.5. Calculated geochemical proxies for mudstones of the upper Aussenkjer Formation and the Amibberg Formation.

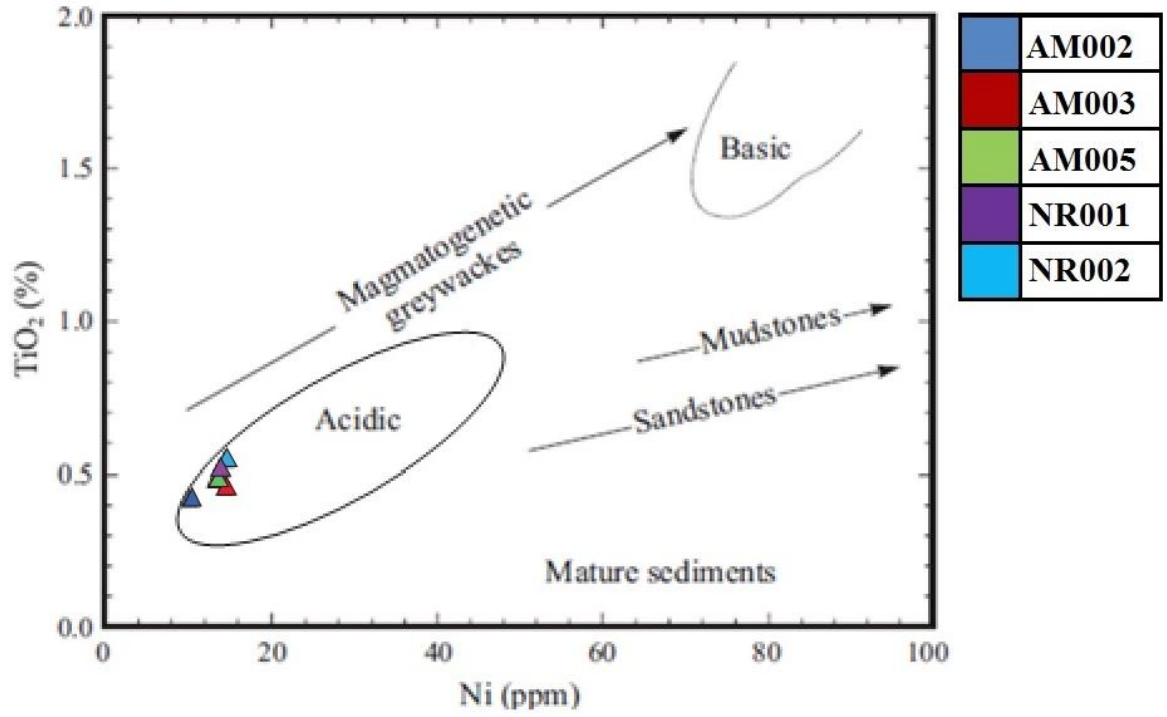


Figure 3.19. TiO_2 vs Ni bivariate plot for the mudstones of the upper Aussenkjer Formation and the Amibberg Formation (fields after Floyd et al., 1989). Triangles indicate plotted samples.

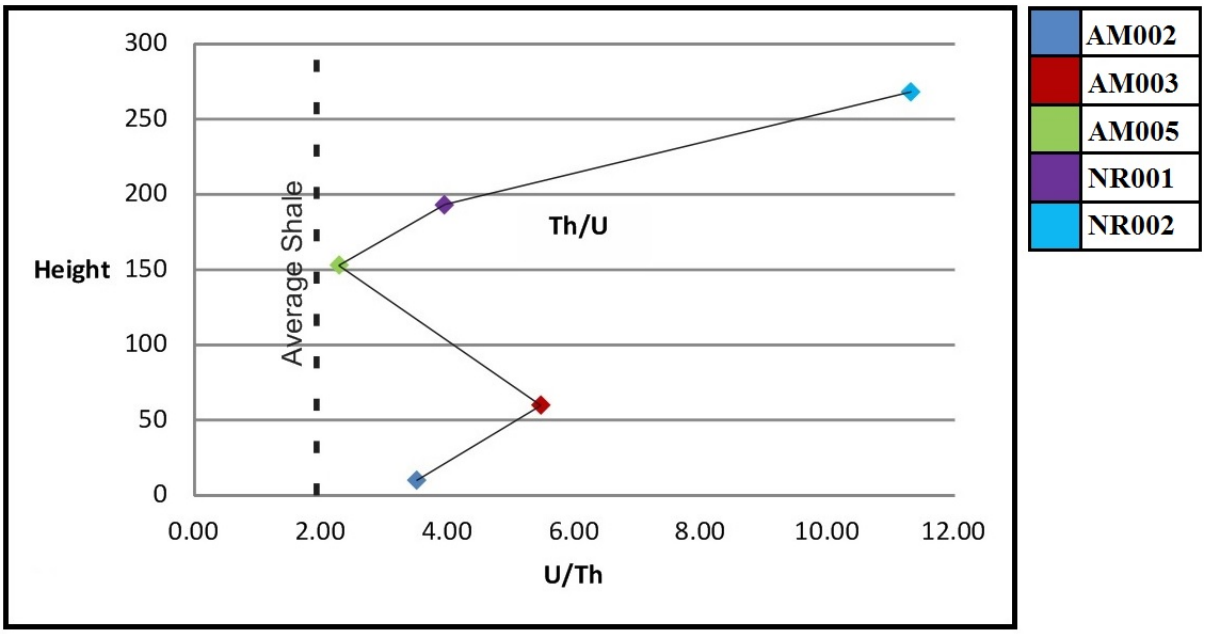


Figure 3.20. Th/U trend with increasing height in the Aussenkjer and Amibberg formations. Note that the trend falls outside of the value for average shales.

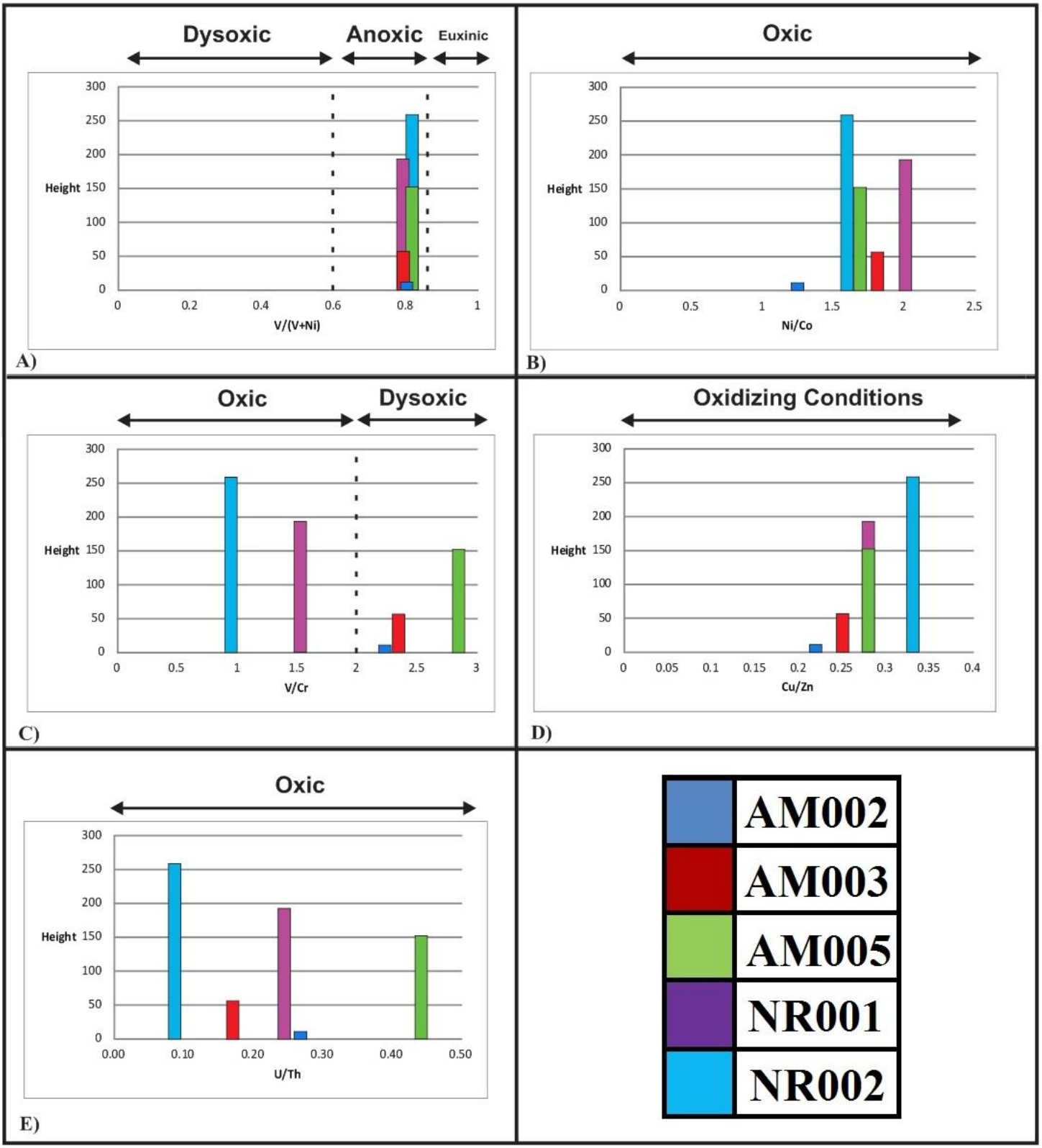


Figure 3.21. Relationship of stratigraphic height and certain palaeoredox proxies. Ranges for V/Cr and Ni/Co are from Jones and Manning (1994); ranges for V/(V + Ni) are from Hatch and Leventhal (1992). A) V/(V+Ni). B) Ni/Co. C) V/Cr. D) Cu/Zn. E) U/Th.

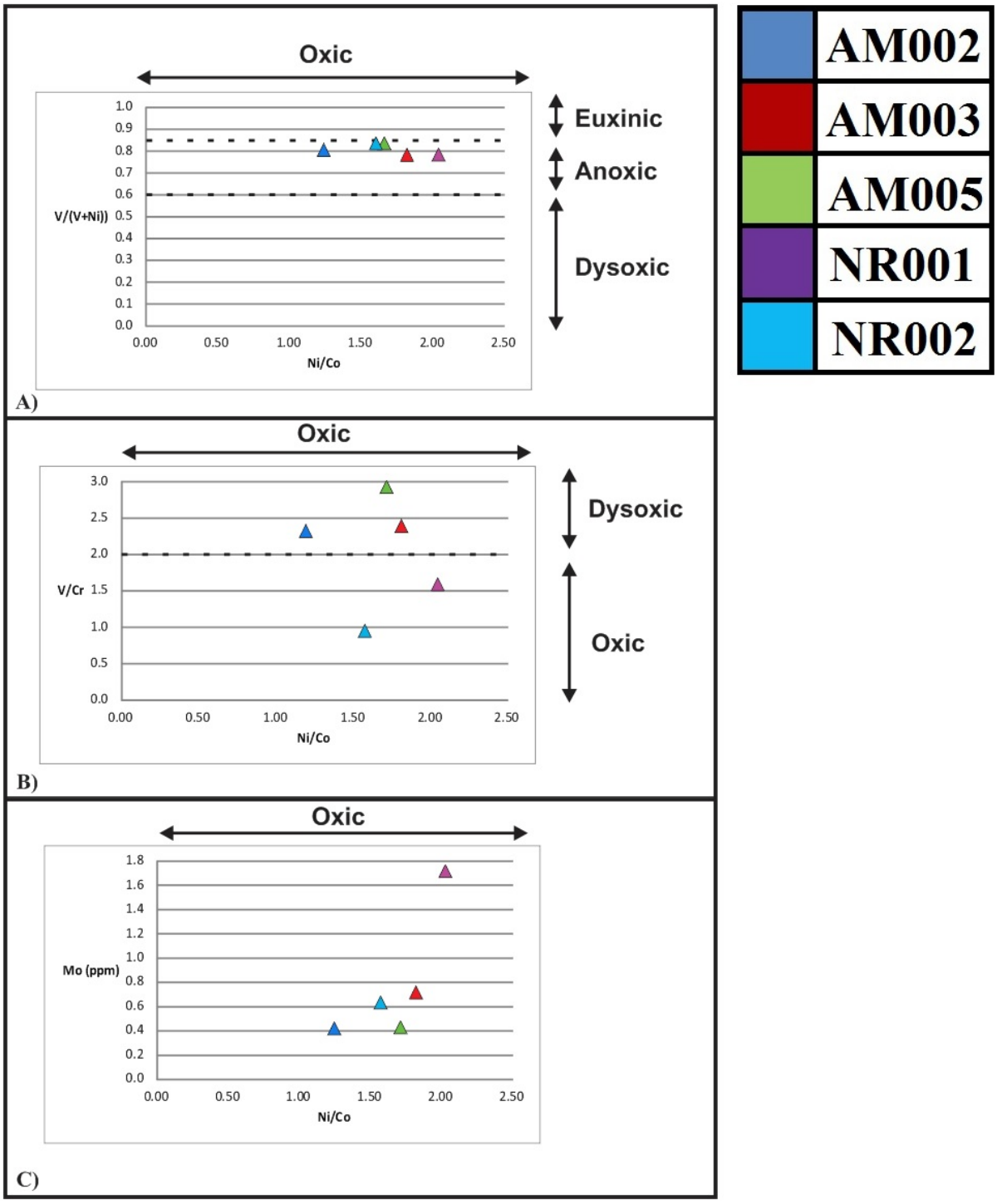


Figure 3.22. Crossplots of various trace element ratios used as palaeoredox proxies. A) Ni/Co vs V/(V+Ni). B) Ni/Co vs V/Cr. C) Ni/Co vs Molybdenum (in parts per million).

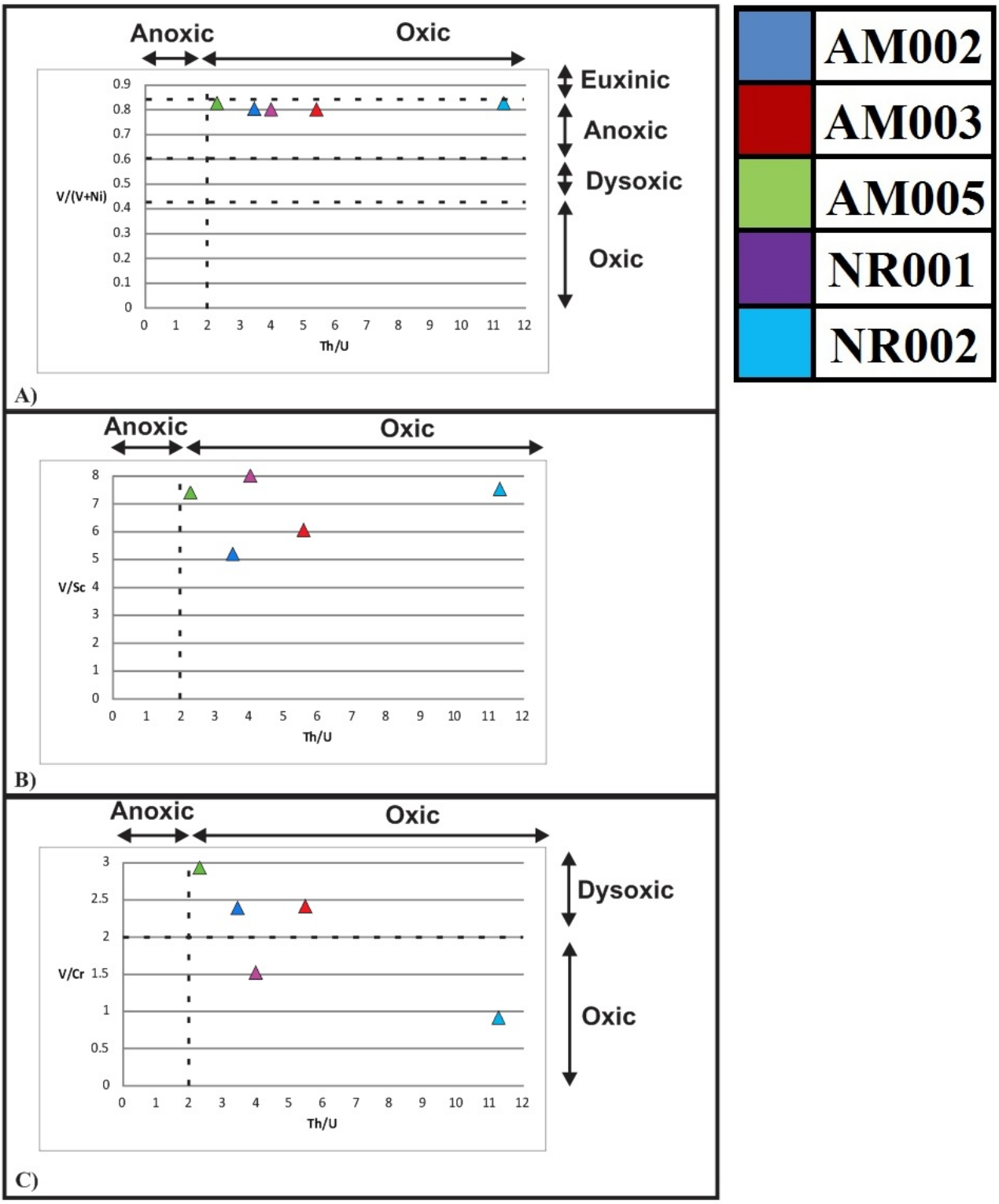


Figure 3.23. Crossplots of various trace element ratios used as palaeoredox proxies. A)Th/U vs V/(V+Ni). B) Th/U vs V/Sc. C) Th/U vs V/Cr.

Th/U ratios of 0 to 2 in the average shale whereas values greater than 2 indicate oxic conditions as seen in these samples (Fig. 3.23B). Figure 3.20 shows the change in Th/U ratios through the stratigraphic succession. Note that although the Th/U ratios vary through stratigraphy these ratios are always outside of the ratio for average shales. Furthermore, based on the geochemical facies of Adams and Weaver (1958) of thorium and uranium determinations it is possible to state that these sediments were sourced from rapidly deposited igneous rock detritus mixed with a variety of sedimentary sources.

The ratio of uranium to thorium has been used as a redox indicator with U/Th ratio being higher in organic rich mudstones (Jones and Manning, 1994). U/Th ratios below 1.25 suggest oxic conditions of deposition, whereas values above 1.25 indicate suboxic and anoxic conditions (Nath et al., 1997). The U/Th ratios of the mudstone samples from the study area range from 0.09 to 0.44 (Fig. 3.21E) and therefore suggest deposition in oxic environments.

The authigenic uranium content is also considered as a proxy for bottom water conditions at the time of deposition (Wignall and Myers, 1988). The authigenic uranium content is calculated as: (authigenic U) = (total U) – Th/3. Values of authigenic U below 5 represent oxic depositional conditions, while values above 5 are indicative of suboxic and anoxic conditions. Thus, the observed low U/Th ratios and low authigenic U content (-2.24-0.96) in the studied mudstones further support deposition in an oxic environment.

Vanadium is also a redox-sensitive element that is concentrated in sediments associated with mostly anoxic waters (Rimmer, 2004; Emerson and Huested, 1991). Jones and Manning (1994) proposed that V/Cr ratios less than 2 pointed to oxic conditions, ratios of 2−4.25 to dysoxic conditions, and any ration above 4.25 to suboxic to anoxic conditions (Fig. 3.21C, 3.22B and 3.23C). Hatch and Leventhal (1992) demonstrated that V/(V+Ni) ratios 0.46−0.60 for dysoxic conditions, 0.54−0.82 for anoxic conditions, and >0.84 for euxinic conditions (Fig. 3.21A, 3.22A and 3.23A). The studied samples have V/Cr ratios between 0.92 and 2.89, which imply that these mudstones were deposited in oxic and dysoxic depositional environment. The V/V+Ni ratios (0.79-0.82) suggest anoxic conditions during deposition of these mudstones.

Kimura and Wantanabe (2001) indicate that normal shales/mudstones yield V/Sc ratios between 4.7 and 9.1 under oxic conditions. The values of mudstones from the study area conform to this “normal” shale index as the ratios range between 5.14 and 7.99 (Fig. 3.23B).

Jones and Manning (1994) proposed that Ni/Co ratios below 5 indicate oxic environments, whereas ratios of 5-7 suggest dysoxic conditions and ratios above 7 are due to suboxic or anoxic environments (Fig. 3.21B and Fig. 3.22). The Ni/Co ratios of these samples range between 1.24 and 2.06 indicating oxic conditions for these mudstones.

The Cu/Zn ratio is also used as a redox indicator (Hallberg, 1976). According to Hallberg (1976) high Cu/Zn ratios indicate reducing depositional conditions, while low Cu/Zn ratios suggest oxidizing conditions as seen in the low Cu/Zn ratios of these samples (Fig. 3.21D).

Mudstones deposited under anoxic conditions tend to be enriched in molybdenum (Fig. 3.22C); however, in oxygenated seawater molybdenum occurs as unreactive MoO_2^{-4} and therefore will not be concentrated in sediment as seen in the low Mo concentration in these samples (0.3 – 1.6 ppm).

Overall, the trends observed through the use of the various geochemical proxies it is evident that the deposition of these mudstones occurred in oxic settings. However, samples do plot in the anoxic and dysoxic fields in some proxies.

In terms of using geochemical data for provenance studies the Al_2O_3/TiO_2 ratios in clastic sedimentary rocks can be used to infer the source rock compositions. Al_2O_3/TiO_2 ratios for mafic igneous rocks range from 3 to 8; intermediate rocks from 8 to 21 and for felsic igneous rocks a range from 21 to 70 (Hayashi et al., 1997). In this studied samples have a range of Al_2O_3/TiO_2 ratios from 23 to 31. These then fall into the realm of felsic igneous rocks. This is further supported by the TiO_2 *vs.* Ni bivariate plot (Fig. 3.19), which also indicate that these mudstones were mainly derived from an acidic source and hence are derived from felsic igneous source rocks.

Chapter 4: Sequence Stratigraphy

4.1 Introduction

Sequence stratigraphy is the "recognition and correlation of stratigraphic surfaces which represent changes in depositional trends in the rock record. Such changes, which are the product of the interplay of sedimentation, erosion and shifting of base level, are now recognised by sedimentological criteria and geometric relationships" (Embry et al., 2007 pg.5). The use of sequence stratigraphy and facies analysis can be useful in deciphering the palaeogeographic evolution and depositional history of sedimentary basins.

Over the past fifty years many different "schools" of sequence stratigraphy have developed. It is outside of the scope of this work to evaluate each on their merits and pitfalls; however, it is critical to choose one which works best for this study area. In this case the use of the empirical approach is best suited (Fig. 4.1). This method advocates the use of four material based sequence stratigraphic surfaces of Embry et al. (2007) which are: subaerial unconformity (SU); shoreline ravinement (SR); maximum regressive surface (MRS) and the maximum flooding surface (MFS). These are based on vertical changes within a stratigraphic package, which allow for the delineation of stratigraphic surfaces on a physical basis. These changes in depositional trend can be used to define stratigraphic boundaries which are useful for correlation purposes. The previously mentioned surfaces are then used to define sequence stratigraphic units such as the T-R sequence (Embry and Johannessen, 1992), also termed a genetic stratigraphic sequence (Galloway, 1989), in this instance with maximum flooding surfaces as its boundaries. This unit can further be defined in terms of system tracts [regressive system tract (RST) and transgressive system tract (TST)] which form the subdivision of a sequence (Brown and Fisher, 1977) and allow for the correlation of depositional systems. An evaluation of T-R sequences is necessary to fully understand relative sea-level fluctuations within marginal marine systems (Allen and Johnson, 2011).

Of the four material based surfaces, the SR is absent due to the lack of regional truncation surfaces and the SU is not present in the study area as no nonmarine or brackish strata are present. However, the SU may be present as a correlative conformity (CC) as some forced regressions will not have a great effect on offshore facies (Jinnah, pers. Comm.).

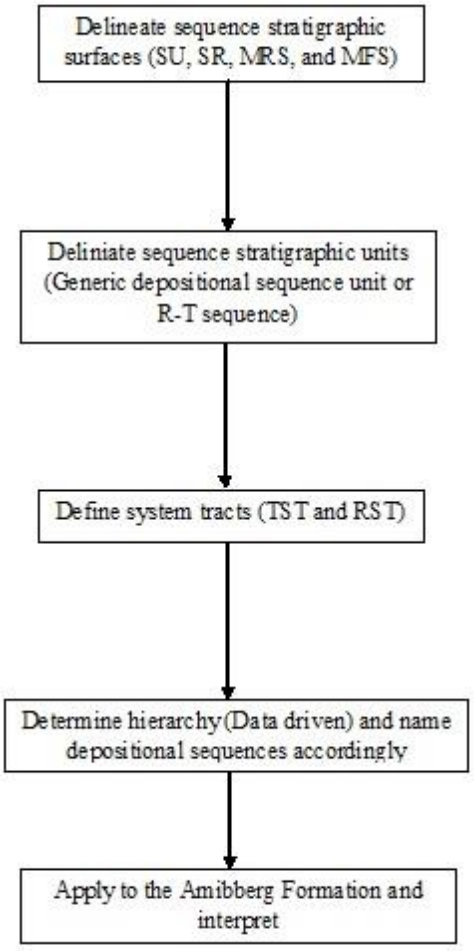


Figure 4.1. Empirical approach. Depiction of the steps to taken to classify sequence boundaries and sub-classes to allow for a useful interpretation of base-level changes within the study area (SU - subaerial unconformity; SR – shoreline ravinement; MRS – maximum regressive surface; MFS – maximum flooding surface; TST – transgressive system tract; RST – regressive system tract; R-T – regressive-transgressive).

The presence of MFS and MRS allow for the delineation of TST and RST and hence T-R sequences. The MRS is identified by the change in trend from coarsening-upward to fining-upward. This mostly coincides with a change from shallowing-upwards to deepening-upwards. In terms of stacking pattern, the MRS separates a progradational system tract from a retrogradational one. This surface is associated with the end of shoreline regression. The MFS can be recognised in siliciclastic strata by a change from fining-upward to coarsening-upward, which in a nearshore environment is a change from deepening to shallowing upward.

In offshore areas this is not true and the deepest water horizon can lie above the MFS (Embry, 2009). In terms of stacking pattern, this surface is underlain by a retrogradational package and overlain by a progradational one.

Transgressive intervals (TST) are typically represented by thin bioturbated sandstones, associated with flooding surfaces which bound thicker progradational facies successions (Allen and Johnson, 2011). When sea-level rise overcomes sediment supply, during a net relative sea-level rise, transgressive deposits are thin and comprise a minor fraction of the overall stratigraphy (e.g. retrogradational parasequence set; Van Wagoner et al., 1990; Posamentier and Allen, 1999). This system tract is characterised by retrogradational stacking patterns and fining-upwards strata. This system tract is bound by the MRS below and the MFS above and encompasses all strata deposited during transgression (Embry et al., 2007).

Regressive intervals (RST) are characterised by coarsening-upward strata with progradational stacking patterns. The earliest (and latest) deposits of marine coarsening-upwards successions are likely to accumulate in deepening water (Galloway, 1989; Naish and Kamp, 1997; Catuneanu et al., 1998). This system tract is bound by the MFS below and the MRS above and encompasses all strata deposited during regression (Embry et al., 2007).

4.2 Hierarchy

It is important that sequence stratigraphic surfaces be assigned a hierarchy to enable these surfaces to be useful for regional correlation and mapping purposes (Embry, 1993; Embry, 1995). Generally, the largest magnitude boundaries are categorised as 1st order surfaces and the smallest magnitude boundaries would be assigned to higher orders (e.g. 4, 5 or 6). The larger magnitude boundaries (1, 2 or 3) are usually correlatable throughout a sedimentary basin. These are interpreted to have been generated by tectonic forces, whereas smaller magnitude boundaries are driven by glacio-eustasy. These high order, low magnitude boundaries exhibit no change in tectonic or depositional regime and allow only for local correlation. Furthermore, sequences generated by eustasy are relatively thin in shelfal areas, and numerous, very similar sequences are stacked upon each other (Embry et al., 2007). Boundaries generated by tectonically driven base-level changes are widely spaced and overlain by thin intervals of transgressive strata. Transgressive strata are in turn overlain by thick intervals of regressive strata (Embry et al., 2007). In contrast, it is possible for high-frequency, tectonically driven sequence boundaries to develop in tectonically active settings such as foreland basins (Catuneanu et al., 1997) and rift basins (Gawthorpe et al., 1994).

Substantial angularity between an unconformity and the underlying sequence stratigraphic surfaces is indicative of tectonic activity. Other changes across sequence boundaries associated with changes in tectonics are changes in deposition regime and changes in sediment composition and source (Embry et al., 2007).

In the Amibberg Formation there is little change in depositional regime across sequence boundaries. The only apparent change is one from proximal lower shoreface deposits to a distal lower shoreface or offshore-transitional one. This cannot be driven by tectonic forces and is rather interpreted to be of eustatic origin. Furthermore, the petrography (Chapter 3) across these sequence boundaries differs very little and hence there is no change in sediment composition and source area. Furthermore, tectonically dominated base level curves are indicated by slow rise punctuated by short intervals of rapid fall followed by rapid rise, whereas a eustatic curve is dominated by long, slow falls and short intervals of fast rise (Embry et al., 2007). This eustatic type succession is evident in the Amibberg Formation (Fig. 4.2). Therefore, there is sufficient evidence for eustatic processes to have formed the sequence boundaries in the study area. These sequence units are either 3rd or 4th order cycles. Due to the lack of petrographic or depositional change across a boundary these units are classified as 4th order cycles due to the nature of the strata above and below the boundary. This is also due to the lack of major changes in palaeocurrent trend across sequence boundaries and throughout the stratigraphic succession.

4.3 Base Level Curves

Tectonically dominated base level curves are indicated by slow rise punctuated by short intervals of rapid fall followed by rapid rise, whereas a eustatic curve is dominated by long, slow falls and short intervals of fast rise (Embry et al., 2007).

At the large scale, base level changes seen in the study area are characterised by four short intervals of rapid base level rise followed by long intervals of base level fall (Fig. 4.5) reinforcing the large scale influence of eustasy on the basin. Large scale regressions are punctuated by small scale base level changes (Fig 4.5) due to increased sediment supply to the basin.

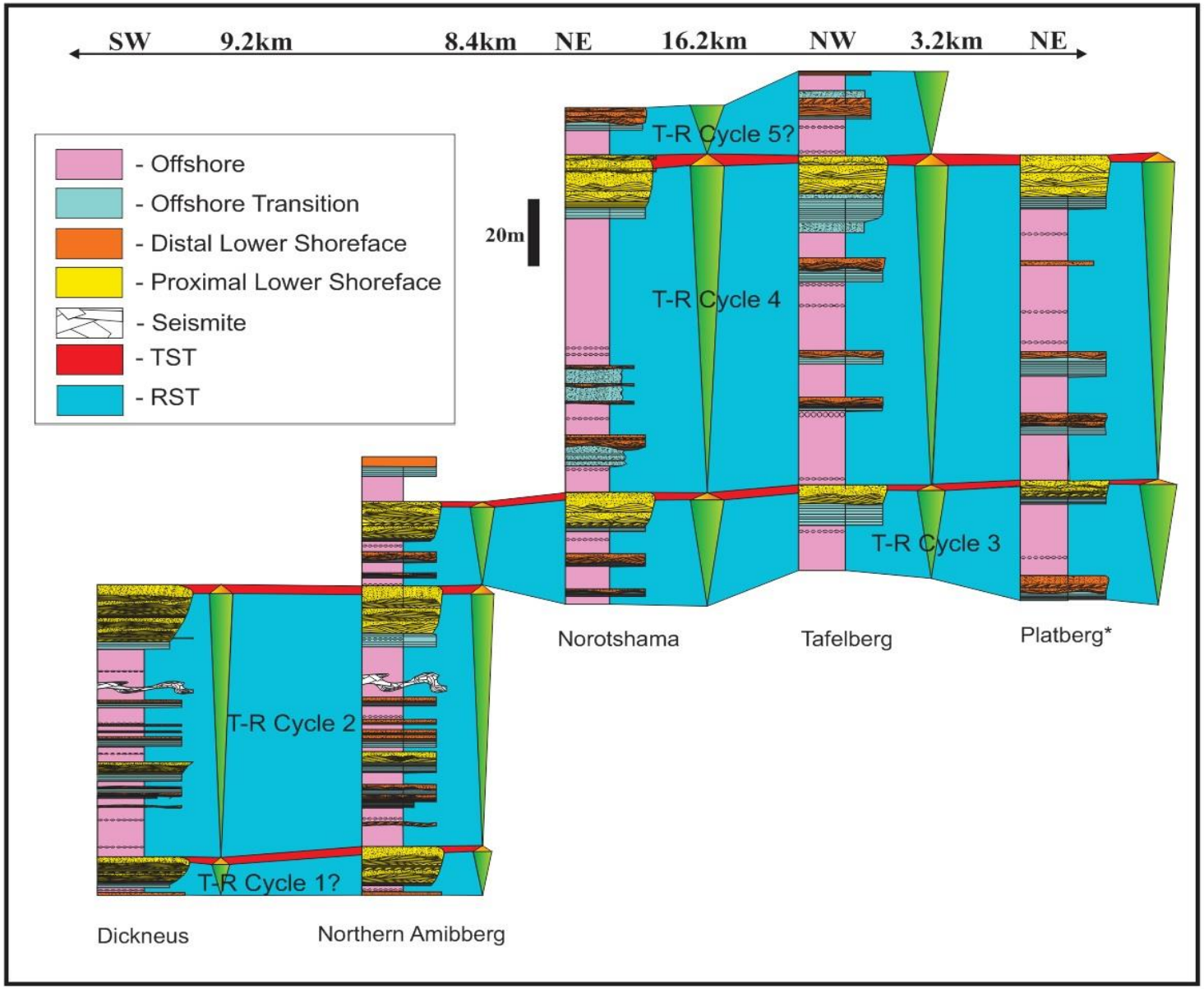


Figure 4.2. Sequence stratigraphic correlation. Note, on the large scale, the thin transgressive intervals (red) and the thick regressive intervals (blue). * denotes informal locality name.

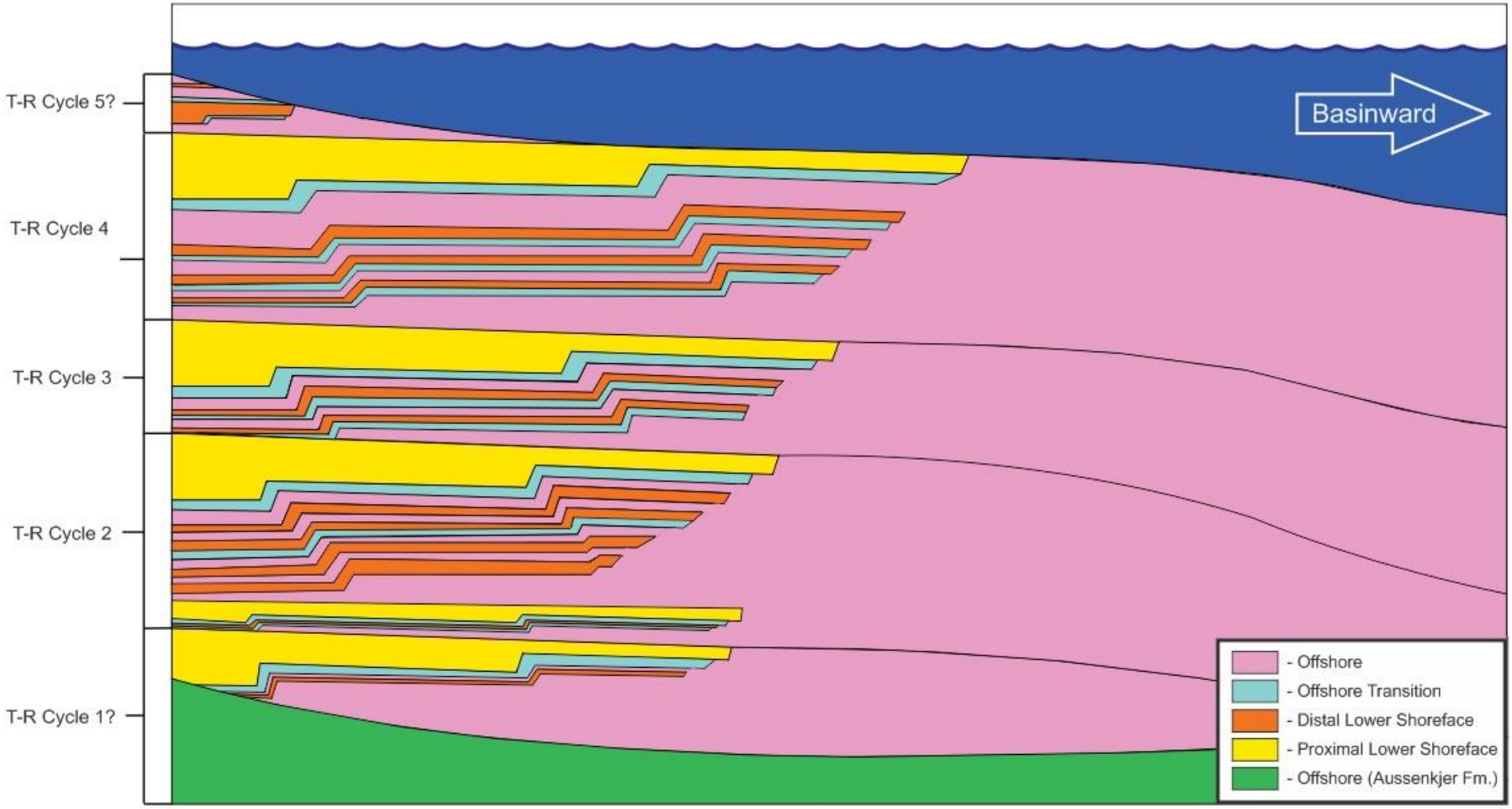


Figure 4.3. Idealised shoreline profile showing strata prograding into the basin in a WNW direction. Note that the large scale trend of this depositional system is largely aggradational.

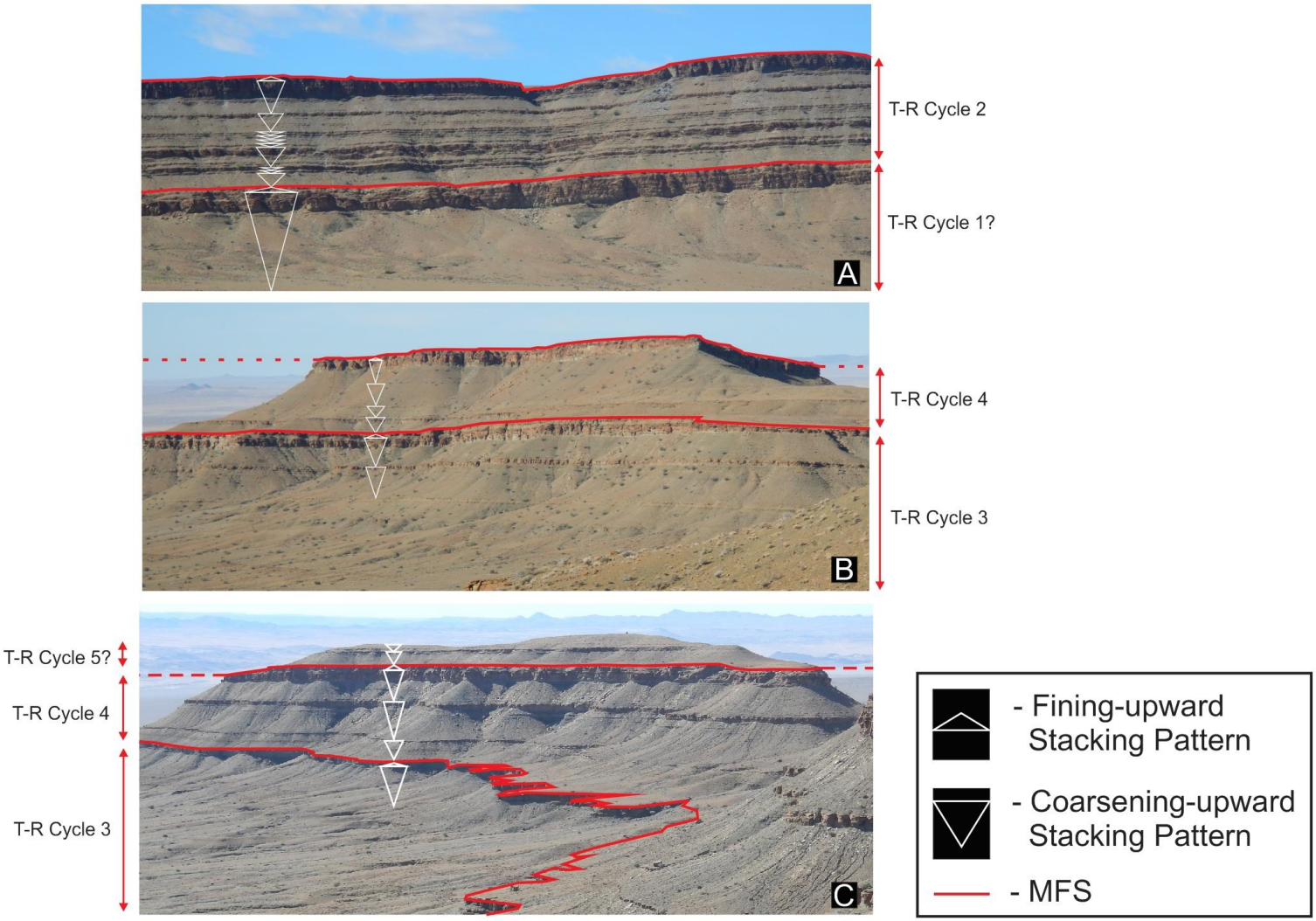


Figure 4.4. Sequence stratigraphic interpretation of outcrop. A) Northern Amibberg locality. B) Platberg locality. C) Tafelberg locality. Note the generally incomplete large scale T-R cycles and well as the upward-coarsening stacking patterns (MFS – maximum flooding surface).

4.4 Sequence Stratigraphic Interpretation

Ancient regressive wave-dominated shoreface deposits are characterized by laterally continuous sandstone bodies (T-R cycles) that are bounded by marine flooding surfaces (Van Wagoner et al., 1990; Reynolds, 1999). In a vertical stratigraphic column these shorelines are represented by coarsening-upward and shallowing-upward successions (e.g. Elliott, 1986; Walker and Plint, 1992; Bhattacharya, 2006; Clifton, 2006). These shorefaces result from sediment supply exceeding the rate of sea level change and therefore typically coarsen upward (Bernard et al., 1962; Davies et al., 1971; Harms et al., 1975). Progradation into water shallower than normal wave base can result in the absence of fine-grained shoreface deposits and forms relatively sharply rather than gradationally based regressive sands (Oomkens, 1970; Meckel, 1975). Furthermore, in regressive shorelines the preservation of upper shorefaces deposits may be minimal due to their deposition and subsequent erosion during sea level low stands. This lack of upper shoreface deposits is observed in the study area where lower shoreface deposits are excellently preserved and middle to upper shoreface deposit are absent. The occurrence of amalgamated hummocky cross-stratified sandstone strata above discrete HCS beds in a coarsening-upward lithofacies sequential arrangement is indicative of typical regressive shoreface successions (Leckie and Walker, 1982).

In the studied stratigraphic interval there are three clearly distinguishable T-R cycles, with two cycles only partially distinguishable (Fig 4.2 and 4.4). T-R cycle 1 cannot be definitively constrained due to the lack of a corresponding MFS in the upper reaches of the Aussenkjer Formation. However, there may be a MFS lower down in stratigraphy and this should be verified in future. Similarly, due to erosion of overlying strata, T-R cycle 5 cannot be delineated due to the lack of an upper MFS to be used in conjunction with a lower MFS that is present. The three distinguishable T-R cycles are characterised by thick regressive intervals and thin transgressive intervals. Of the three defined T-R cycles, 2 and 4 are both approximately 70m thick whereas T-R cycles 3 is much thinner, not exceeding 30m.

One stratigraphic interval of interest is the seismite (Fig 4.5) observed throughout the Amibberg Massif. This unit implies that tectonic activity has a large influence after deposition of this stratum and does not fit in with the overall eustatic interpretation of the Amibberg Formation. Furthermore, this unit does not conform to a sequence boundary although it is unclear if this was deposited during a forced regression. The overlying strata

had not yet been deposited and hence it is unaffected. The underlying couple of meters of mudstone strata have also been affected whereas the sandstone units below this mudstone are unaltered. A mild earthquake occurring before the sediment has time to lithify would explain the formation of this unit. The force of this seismic event is only enough to have altered unlithified sediment and not enough to have caused large-scale subsidence or elevation in the basin and hence generate a sequence boundary.

The MFS has been interpreted to have formed due to a change from decreasing sediment supply to increasing sediment supply, often associated with the onset of regression (Embry, 2009) at the end of shoreline transgression. Normal regression implies that sediment supply is the main control whereas forced regression implies that basin tectonics or eustasy is the controlling factor. Sharp based dLSF deposits present in the Amibberg Formation would imply that forced regression was the dominant effect leading to deposition. However, tidal influence in wave-dominated shoreface deposits would result in the presence of these sharp based dLSF deposits without implying forced regression. This has already been determined (Chapter 2) and hence sediment supply was the main control on the formation of maximum flooding surfaces in the study area.

Roughly the same facies are present in each T-R cycle in the Amibberg Formation although in T-R cycle two there is a high frequency of facies variation which represents increasing sediment supply to the basin. In T-R cycles three and four there is a lower frequency in terms of facies changes. Furthermore, along strike, only minor variations in facies are observed with the majority of facies being correlatable over large distances. All of this indicates an overall aggradational stacking pattern (Fig. 4.3) which develops as a result of equal rates of accommodation and sedimentation.

Visser (1993) determined a global eustatic signal in the Karoo Basin above the "noise" generated by isostatic and tectonic effects during the Early Permian. Furthermore, he stated that the major regression in the basin was controlled by high rates and volume of sediment input exceeding the rate of basin subsidence during the late Permian. This reinforces the eustatic interpretation for the Amibberg Formation in the Karasburg Basin as well as the aggradational nature of these T-R cycles.

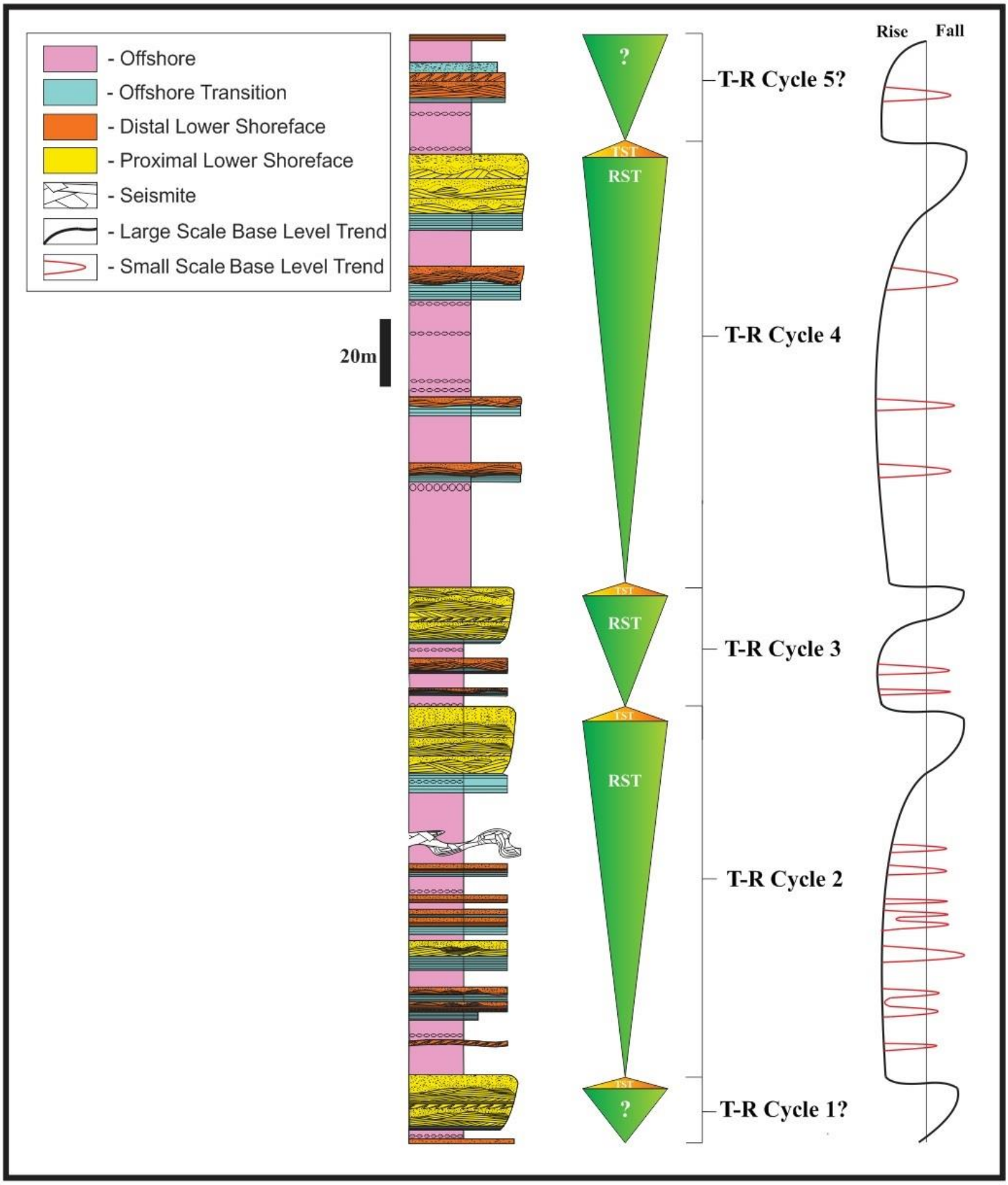


Figure 4.5. Idealised stratigraphic section with interpreted base level curve. Note the large scale regressive intervals punctuated by short, rapid transgressions. Also note the high frequency small scale base level rises and falls (TST – transgressive system tract; RST – regressive system tract).

Chapter 5: Discussion and Conclusions

5.1 Palaeogeographic Reconstruction and Provenance Discussion

The evolution of these wave-dominated shoreline systems through time is characterised by the upward-coarsening, progradational nature of these successions. Four thick amalgamated HCS and wave rippled pLSF deposits record progradation into shallow waters and represent the most proximal deposits in the study area. The upward thickening and upward amalgamation of beds within the study area are also interpreted to represent increasing proximity to the shoreface, which was the source of the episodic unidirectional flows, during an overall shallowing (Hampson and Stroms, 2003).

Discrete HCS and wave rippled dLSF deposits record a lesser degree of shallowing whereas sharp based dLSF deposits are interpreted to reflect the propensity for wave-dominated, tide-influenced systems to prograde into shallow basins where storm waves can effectively rework sediment long distances from the shoreline without a drop in relative sea level (Vakarelov et al., 2012). Tidal signatures are absent in these facies as passing storm waves would obliterate any previous tidal induced structures.

Heterolithic OST deposits typically underlie dLSF and pLSF and indicate gradually shallowing conditions during deposition. The presence of lenticular, wavy and flaser bedding in certain stratigraphic positions and geographical locations indicate a proximity to the shoreline. The arrangement of these structures in the heterolithic lithofacies are identical to the "tidal bedding" of Wunderlich (1970), although this type of bedding is not diagnostic of significant tidal influence. However, tidal amplification which can lead to the preservation of such structures is common in embayments (Collins et al., 2014). Further evidence for tidal influence in these deposits is the mixing of trace fossils assemblages and the lack or poorly developed cross-stratified upper shoreface intervals (without implying forced regression) typical of microtidal systems. Other OST deposits are heavily bioturbated indicating opportunistic colonization by organisms during intermittent periods of calm. Reworked, bioturbated and wave rippled bed tops are interpreted to record episodic deposition from unidirectional flows fed by river flooding events (Hampson and Storms. 2003). Further

evidence for fluvial transport processes is present in the heterolithic nature of OST deposits as well as the presence of fluid-muds in pLSF deposits.

OS mudstone deposits are typically intensely bioturbated due to the prolonged period of suspension settling. These mudstones typically have a uniform thickness although in certain stratigraphic intervals they do thicken towards the north and thin towards the south. Locally, thinning and thickening of mudstone units can be explained by scouring of the overlying shoreface deposits. However, at a basin scale the thicker mudstone units are due to tidal and long-shore drift influences that may have resulted in the transportation of suspended sediment towards the north. Overall, the rocks of the Amibberg Formation were deposited as a wave-dominated shoreface with some degree of tidal influence and river-fed processes.

These wave dominated shoreface environments display a well-defined decrease in wave-energy with an increase in water depth (Dalrymple and Choi, 2007). Therefore, there is a predictable correlation between water depth and lithofacies that is represented by an upward-coarsening succession. This 'classic' succession passes from mudstones (offshore); through deposits with interbedded sandstones and siltstones with wave ripples and HCS (offshore transition); into discrete HCS sandstone (distal lower shoreface); into amalgamated sandstones with HCS (proximal lower shoreface); into amalgamated sandstones with swaley cross-stratification and eventually into trough-cross bedded sandstones (upper shoreface) (e.g., Walker and Plint, 1992; Hampson and Storms, 2003; Charvin et al., 2010; Hampson, 2010; Vakarelov et al., 2012). This vertical succession is so predictable that even slight differences can be used to infer forced regressions (Dalrymple and Choi, 2007). This type of predictable vertical succession of lithofacies is evident in the Amibberg Formation, although no cross-bedded upper shoreface deposits are present.

In terms of changes in stratigraphy, there is evidently a high frequency of changes in depositional conditions between the lower two prominent pLSF deposits. Multiple, thin sharp based dLSF deposits are present, most of which are underlain by OST heterolithics. One other pLSF deposit is present as well as a seismite. This implies various changes in sediment accumulation between the shoreface and offshore environments. Either frequent rises and falls in relative sea level occurred or a large tidal influence enabled the transport of sediment deeper into the basin. Higher up in the stratigraphic succession thicker mudstone

intervals are evident and the frequency of sharp based dLSF deposits decreases. This implies a more gradual and cyclic sea level rise/fall trend indicated by thicker OST heterolithics and bioturbated sandy-siltstones.

The characteristics of recent wave dominated shorelines are influenced by geography and physical processes; therefore ancient deposits are useful in determining palaeogeographical reconstructions (Heward, 1981). Palaeotopography is an important control on location and preservation of shoreline deposits. The geometry of ancient accumulations typically reflects the underlying topography in a basin (Busch, 1959; McCubbin, 1969; Berg, 1976). Most modern shorelines are oriented alongshore perpendicular to palaeoslope which indicates that ancient linear sand bodies are useful in determining the palaeoslope direction (Heward, 1981).

All this information has a significant influence in terms of understanding the palaeogeography of the Karasburg Basin at the time of deposition of the Amibberg Formation. A low angle slope on which the sediments of the Amibberg Formation were deposited can be inferred from the presence of fluid-muds generated by wave-supported turbidity flows on low angle slopes (Traykovski et al., 2005); the effect of tidal influences in allowing sediment to be bypassed across a low angle shelf (Vakarelov et al., 2012) and the lack of distinctive clinoforms. Furthermore, wave-dominated shorelines with significant tidal influence are associated with either open shorelines facing wide shelves or shorelines adjacent to large sea ways (Vakarelov et al., 2012) such as the Ecca interior sea way.

In terms of palaeotopography, many recent and ancient beaches formed or were stabilised on topographic highs, whilst wave-dominated deltas occupy structural depressions (Weimer, 1970; Hobday and Orme, 1974; Home et al., 1974; Halsey, 1979). Shorelines of the Ecca interior sea way transgressed up to the palaeo-escarpment along the west coast of Namibia. This shoreline of the Ecca interior sea way was very irregular and resulted in linear fjords extending for hundreds of kilometres into the Cargonian Highlands (Martin, 1975; Visser and Kingsley, 1982). The Ecca interior sea way breached these mountainous highlands creating large, partially emergent islands known as the Karasburg Ridge (a part of the larger Cargonian Highlands) (Visser, 1983a).The shoreline of the Amibberg Formation therefore must then have occupied a palaeohigh such as emergent parts of the Cargonian Highlands. Additionally, Stollhofen et al (2008) indicate that basement ridges such as the Cargonian

Highlands would have acted as high points in inter-rift areas and been on the periphery of marine systems that occupied rift basins. Furthermore, based on palaeoice-flows and the distribution of sandstone bodies associated with the Dwyka Group, Visser (1987) states that the Karasburg Basin was bounded at least on three sides by mountainous highlands.

These highlands would have been dissected by multiple, steep mountainous river systems which drained into the Ecca interior sea way. This sea way extended northwards into southwestern Gondwana (Visser, 1983a). The proximity of these highland regions would have led to an increase in terrigenous sediment supply and rate of sedimentation to the basin, during a period of relative tectonic inactivity. Mulder and Syvitski (1995) also indicate that short steep drainage basins with multiple mountainous streams, such as one might expect in an active rift basin, are especially prone to the occurrence of pronounced floods with exceptional suspended-sediment concentrations. This would allow for the deposition of heterolithic bedding of OST deposits over geological time as well as the thin bioturbated OST deposits which overlie pLSF intervals. Furthermore, if the detritus was derived from high topographic areas located long distances from the depositional areas, the sands would be more quartz rich, showing a higher degree of mineralogical maturity. The composition of sandstones is to a certain degree controlled by the environment during the time of deposition. For example, detrital matrix would be present in minor amounts or even completely absent from high energy environments. Furthermore, a high wave energy shoreline should have more compositionally mature sands than one of lower energy. High mineralogical maturity of sandstones from wave-dominated shoreface environments may be a result of high energy marine reworking on the shoreface where the detritus could be winnowed several times before deposition (Cotter, 1983). However, effective grain rounding by surf action is doubtful (Pettijohn, 1987) and the relatively low mineralogical maturity of these sandstones points towards a near source area for the sediment. This is supported by the high amount of mica and the high frequency of angular detrital grains which all point to a near source derivation of sediment as well as rapid deposition. The moderate to well sorted nature of the samples are related to significant reworking on the shoreface.

Matrix is a result of the decomposition of detrital grains such as feldspars and lithic fragments as mentioned previously. Quartz is the most abundant siliciclastic grain across all facies (Fig. 5.1A), whereas feldspars are relatively uncommon. These sandstones that contain an abundance of detrital clay (Fig. 5.1B) preserve little altered orthoclase and microcline

feldspars as also seen by Haszeldine et al. (1984). Lamination seen in thin sections could probably reflect sorting processes during deposition through the boundary layer of a turbulent flow (Stow and Bowen, 1978). The presence of glauconite in some sandstone samples indicates shallow marine environments (Bakkiaraji et al., 2010) and these sandstones conform to an idealized regressive shoreline as per Heward (1981), which are moderately sorted consisting of sand, silt, clay, carbonate particles, heavy minerals and glauconite.

All the studied sandstones fall into the continental block realm in terms of provenance. Continental block provenance sediments are believed to have been sourced from shields and platforms or in faulted basement blocks. Point count data which shows high quartz (Fig. 5.1A) to feldspar ratios indicate that the source was a stable craton as opposed to a faulted block as per Dickenson and Suczek (1979).

Based on palaeocurrent directions and provenance data a southerly source area for these rocks is supported. This information coupled with the supporting evidence for a near source derivation would entail that the sediment input into the Karasburg Basin came from the Cargonian Highlands which Visser (1987) proposed consisted of Precambrian Witwatersrand and Olifantshoek Supergroup quartzites. The rocks of the Witwatersrand Supergroup were deposited in a large basin on the Kaapvaal Craton whereas the quartzites of the Matsap Subgroup (Olifantshoek Supergroup) were part of a clastic wedge that extended along the western edge of the craton (Moen, 2006). However, various geochemical proxies indicate some influence from a felsic igneous source. Mineralogically, the presence of zircon and sphene weigh in favour of plutonic granitic provenance (Basu, 1976) as does the abundance of detrital biotite and the abundance of non-undulatory monocrystalline quartz (Blatt, 1967; Basu et al., 1975; Suttner et al., 1981; Tortosa et al., 1991). Furthermore, based on the proposed geochemical facies of Adams and Weaver (1958), Th/U-ratios between 2 and 7 are evident in the mudstones of the upper Ecca Group which reflect partly weathered and rapidly deposited igneous rock detritus mixed with a variety of sedimentary sources. A metamorphic source can be discounted due to the lack polycrystalline quartz. Contrary to this, the studied samples fall into the intermediate class of wackes suggested by Crook (1970b) which has mixed provenance between volcanic and sedimentary. It is evident that the interpretation of data by various means is conflicting and leads to the delineation of a mixed (plutonic igneous,

volcanic and sedimentary) source. Therefore, unless the rocks of the Amibberg Formation reflect the provenance of the rocks of the Cargonian Highlands there must at least be a secondary plutonic source for the rocks of the Amibberg Formation.

In terms of the character of the Cargonian Highlands at the time of deposition of the Amibberg Formation it is evident that these highlands were at least partially emergent. Evidence to support this is the presence of fossil wood in the study area. This suggests rapid transgression of the surrounding area followed by the transportation of the dead wood basinwards (Visser, 1993) and a transgression along the western margin of the Cargonian Highlands. A regressive phase during the deposition of the Ecca Group delivered abundant plant material in tempestitic sediments to the Amibberg Formation in the Karasburg Basin. This required a vegetated land area in the proximity of the basin, probably in the area of the Cargonian Highlands (Werner, 2006).

The interpreted palaeoshoreline of this study generally conforms to the NE-SW orientation of the western portion, and northern side of the Cargonian Highlands. This means that the shoreline successions of the Amibberg Formation were prograding in an overall north-westerly direction from the Cargonian Highlands rather than southward from the Aranos Basin. Furthermore, palaeocurrent data obtained from unidirectional structures indicate an overall flow from the ESE which coincides with the open end of a partially enclosed Ecca interior sea way.

5.2 Basin Connectivity Discussion

To establish environmental variability and connectivity across Karoo basins at the time of the deposition of the Amibberg Formation, similar lithological elements must be present in the same stratigraphic interval as this formation in other basins. Grill (1997) indicates that the Nossob Sandstone in the Aranos Basin is a south-westerly prograding, fluvial and wave-dominated delta. Furthermore, it is proposed that this model of delta progradation into a southward deepening basin is enforced by the sedimentary succession in the Karasburg Basin whereby Martin (1981a) and Visser (1983a) indicate that the entire preserved Ecca Group in the Karasburg Basin represents offshore and distal turbidite sediments. This is not wholly the case as wave-dominated shoreface strata are present in the Karasburg Basin. Grill (1997)

also indicates that the other major sandstone member in the Aranos Basin (the Auob Sandstone) represents a wave-dominated shoreline that prograded in a south-westerly

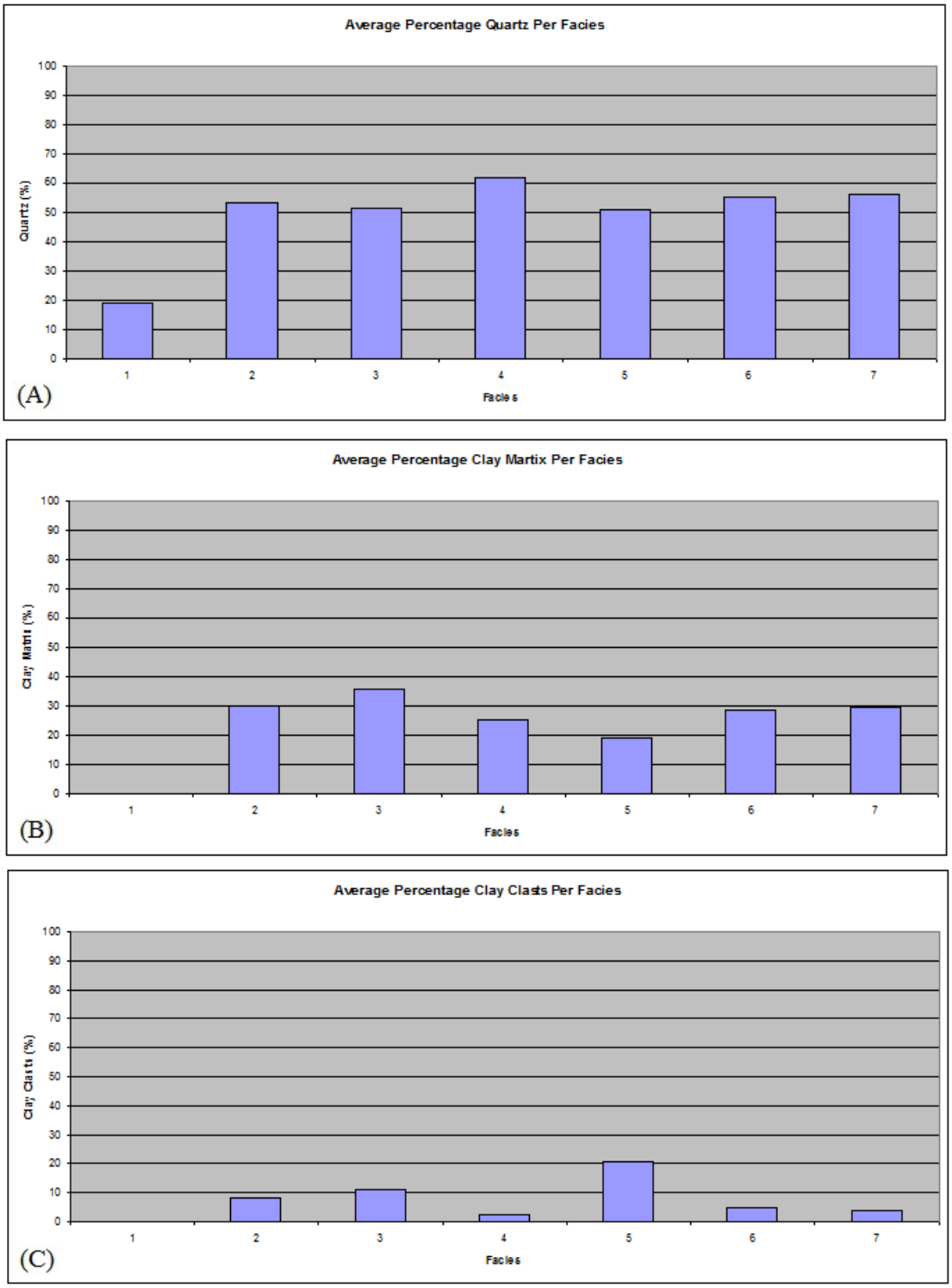


Figure 5.1. Relative Mineral Percentage Graphs. A) Graph shows the average percentage of quartz per facies. Lithofacies 4 is the most quartz rich. However, the percentage quartz per facies fluctuates very little in general. B) Graph shows the average percentage of clay matrix per facies. Lithofacies 3 is the most rich in clay matrix while lithofacies 5 is the matrix most poor. C) Graph shows the average percentage of clay clasts per facies. Lithofacies 5 contains the most clay clasts of any facies. The other facies only have low percentages of clay clasts.

direction towards the centre of the depositional basin. These postglacial deltas and shorelines prograded in an overall southerly direction parallel to the axis of this Carboniferous-Permian rift-basin (Stollhofen et al., 2008). The sandstone members in the Aranos Basin are not present in the corresponding Prince Albert Formation in the Karasburg Basin. However, interpreted sequence boundaries deduced by Werner (2006) show a distinct correlation between the Prince Albert formations in the Aranos and Karasburg Basins. The correlative sequence boundaries and lack of sandstones equivalents in the Karasburg Basin indicate that the strata of the Karasburg Basin are deeper water facies than the Aranos Basin rocks. All this data indicates that the Aranos and Karasburg basins were connected during the Early Permian and that the rocks of the Karasburg Basin were deposited distally in a large, generally north-south trending basin whereas the rocks of the Aranos Basin were deposited more proximally.

The Auob and Nossob sandstones are not equivalents of the Amibberg Formation as these stratigraphically underlie the Whitehill Formation and the Amibberg Formation occurs higher up in stratigraphy, overlying the Whitehill and Aussenkjer formations respectively. Therefore, the proximal equivalents of the Amibberg Formation in the Aranos Basin are absent as Jurassic volcanics rest disconformably on top of the Whitehill Formation and in some instances the Dwyka Group (Grill, 1997). Cenozoic Kalahari sediments also overly Karoo Supergroup rocks in the Aranos Basin. The lack of preserved upper Ecca Group rocks in the Aranos Basin is probably due to a depositional hiatus during which deposition in the proximal reaches of the basin would have ceased while in the distal reaches sedimentation would have continued. This would support the proposal that the Karasburg Basin was a distal, marine portion of a larger basin that included the present day Karasburg and Aranos basins. Additionally, this would have enabled the northerly progradation of the Amibberg shoreface successions from the Cargonian Highlands as opposed to the southerly progradation from the Aranos Basin.

No stratigraphic equivalents of the Amibberg Formation are present in the various Kalahari sub-basins. Petrography and geochemical studies on sandstones of the Ecca Group in the Gemsbok Sub-basin conducted by Nxumalo (2011) suggest that the source areas for these rocks were dominated by metamorphic and felsic igneous or acidic magmatic rocks with lesser influence from sedimentary source rocks located adjacent to the basin. Smith (1984) suggested that the Precambrian granite and gneiss complex to the south probably acted as a source of detritus for the Ecca Group in the Central Kalahari Sub basin with minor input from

the Waterberg Group situated to the south of Botswana. A further source area, based on thinning patterns of the Ncojane Sandstone Member of the Ecca Group, has been indicated to the north or northwest in Namibia (Smith, 1984). Furthermore, the strata of the Karoo Supergroup in the eastern Kalahari Karoo Basin was predominantly derived from the Cargonian Highlands in the south with minor contributions from the eastern and the northern highlands (Scheffler et al., 2006). Palaeocurrent data obtained from Nossob Member in the Aranos Basin show source directions from the north and the northwest (Stollhofen et al., 2000) indicating that the Windhoek Highlands was most likely the source for this basin.

It has been speculated that a transpressive ridge (Karasburg Ridge) could have separated formerly contiguous sedimentary environments, for instance the Karasburg Basin from the Aranos Basin (Visser, 1983). However, the fault pattern for the Karasburg Basin published by Visser (1983a) represents influence by the Gariep Mobile Belt (Daly et al., 1989; Gresse and Germs, 1993). The presence of the Karasburg Ridge is now considered highly unlikely and should be disregarded in future palaeogeographical reconstructions of southwestern Gondwana. This indicates that no obvious structural separation existed between the Aranos and Karasburg Basins. Therefore, palaeogeographic maps (Fig. 5.2) suggest that the Karasburg, Aranos and Main Karoo basins were all connected by the Ecca interior sea way during the Early Permian. This sea way extended throughout southwestern Gondwana and was connected with the palaeo-Pacific Ocean by breaches in the Southern Highlands. The evidence for this sea way is based on (1) facies changes in the Dwyka Group diamictite facies along the western margin of the Karoo basin (Visser, 1983a); (2) the presence of marine fossils in the Kalahari, Main Karoo and Karasburg basins (Martin and Wilczewsky, 1970; McLachlan and Anderson, 1973; Martin, 1975; Pickford, 1995); and (3) the necessity for a large body of water to provide the moisture for the growth of ice sheets on the Windhoek and Cargonian highlands (Frakes and Crowell, 1972) which were at least 1500 km from the nearest ocean. The same fossils found in both Namibia and in Argentina coupled with corresponding glacial striations support this idea (Santos et al., 1996). The Cargonian Highland must have played at least a minor part in the separation of the Main Karoo and Karasburg basins.

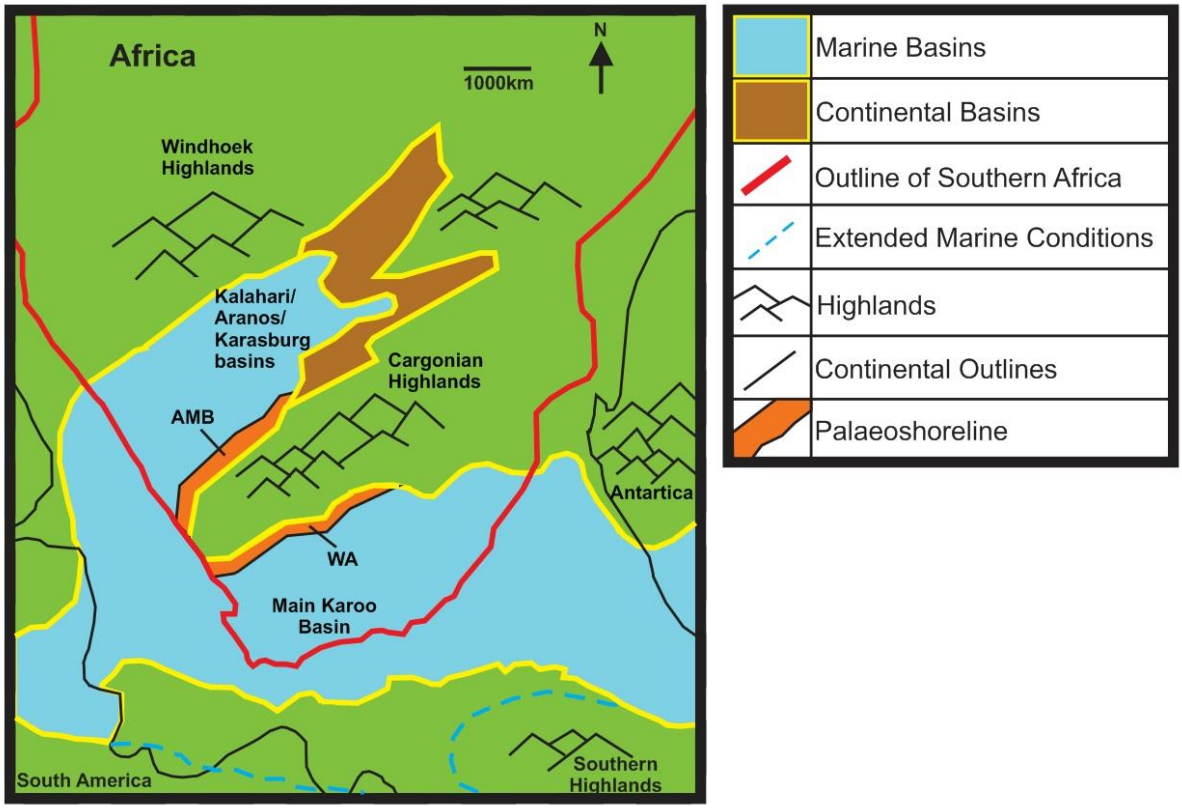


Figure 5.2. Palaeogeographic reconstruction of southern Gondwana during the Late Palaeozoic (based on Visser and Praekelt, 1996 and Scheffler et al., 2006). Note the connectivity of the Aranos, Karasburg and Main Karoo basins as well as shoreline orientations along the Cargonian Highlands (AMB – Amibberg Formation; WA – Waterford Formation).

5.3 Stratigraphic Correlation Discussion

The Dwyka Group, Prince Albert Formation and Whitehill Formation all have corresponding equivalents and namesakes in the Main Karoo Basin. Werner (2006) indicates that the Collingham Formation is present in the Karasburg Basin, although this could not be verified in this study, and this also has a name equivalent in parts of the Main Karoo Basin and its sub-basins. The Aussenkjer Formation is a correlative of the Tierberg Formation in the northwestern part of the Main Karoo Basin. In the east of the Main Karoo Basin the major part of the Volksrust Formation is most probably a correlative of the Aussenkjer Formation and hence the Tierberg Formation (Johnson et al., 1997).

Miller (1992) correlates the Amibberg Formation with the Waterford Formation in the Main Karoo Basin, but Veevers et al. (1994c) introduced the correlation with the Ripon Formation in the Southern Sub-basin. Smith et al. (1993) equated the Amibberg Formation to both Fort

Brown and Waterford Formation. Moreover, the Amibberg Formation is considered to reach into the Beaufort Group (Smith et al., 1993). Another correlation by Johnson et al. (1996), placed the Amibberg Formation at the same stratigraphic position as the Waterford Formation, whereas Werner (2006) equates the Amibberg Formation to the Carnarvon Formation (which is now included in the Waterford Formation).

In terms of stratigraphic position the logical progression would be that the Waterford Formation is the equivalent of the Amibberg Formation in the Main Karoo Basin. However, in the Tanqua and Laingsburg sub-basins this does not hold true. In the Tanqua Sub-basin the Tierberg Formation is overlain by the Skoorsteenberg, Kookfontein and Koedoesberg formations respectively (Fig. 5.3). Similarly in the Laingsburg Sub-basin the Vischkuil Formation (an equivalent of the Tierberg Formation) is overlain by the Laingsburg, Fort Brown and Waterford formations respectively (Fig. 5.3). The Skoorsteenberg and Laingsburg formations in the Tanqua and Laingsburg sub-basins are not an option for correlation as these rocks were deposited in deep-water conditions as submarine fan complexes and are sufficiently different in terms of stratigraphic position. However, these submarine fan complexes contain five T-R cycles similar to the Amibberg Formation (Catuneanu et al., 2002). These are of much larger thickness than the Amibberg Formation and are interpreted to have been generated due to subduction underneath the retroarc foreland system (Mitrovica et al., 1989; Gurnis, 1992; Holt and Stern, 1994). These T-R cycles are thus of tectonic origin and sufficiently different from the eustatic T-R cycles of the Amibberg Formation. Therefore, there are no equivalents of the Laingsburg and Skoorsteenberg formations in the Karasburg Basin. Furthermore, on the evidence from this work it is not possible that the Amibberg Formation extends upwards into the Beaufort group. This is due to the fact that the Beaufort group consists of fluvially deposited sediments whereas the Ecca Group consists predominantly of marine sediments. Apart from depositional changes, distinct colour changes occur in the shale units from the Ecca to Beaufort groups and these are not recognized. No equivalents of the Amibberg Formation have been identified in the Aranos or Kalahari basins.

The Amibberg Formation and each of the remaining possible equivalents of the Amibberg Formation will be assessed on their merits and pitfalls.

5.3.1 Amibberg Formation

SACS (1980) described the Amibberg Formation as a 140m thick succession of alternating sandstone and shale with no upper contact preserved and an age-equivalent of some part of the Ecca Group in South Africa. The lower contact of the Amibberg Formation is placed at the base of the first prominent sandstone layer overlying the Aussenkjer Formation (SACS, 1980). This study shows that the actual thickness of the Amibberg Formation is more likely in the region of 250m as does Werner (2006). This formation consists of alternating sequential arrangements of sandstone, siltstones and mudstones. Sedimentary structures include HCS, wave ripples, ripple cross-stratification, climbing ripples, planar laminations, flaser/lenticular/wavy bedding, soft sediment deformation structures and carbonate nodules. Trace fossil assemblages include *Skolithos, Cruziana* and more rarely *Nerites* isp. as well as a mixing of these assemblages resulting from tidal influences. Fossil wood, fish scales and more rarely bivalves are present in this formation. This formation consists of five poorly defined upward coarsening successions. Three major regressive intervals capped by thin transgressive intervals have been documented in this study. Overall the rocks of this formation can be classified as shallow-marine, prograding, regressive, wave-dominated shoreface deposits. Petrographically the sandstone samples are very-fine to medium-grained quartz wackes or feldspathic wackes. This work shows average palaeocurrent direction of WNW-ESE and a palaeoshoreline has been ascribed to trend NE-SW.

5.3.2 Ripon Formation

The Ripon Formation in the Southern Sub-basin is generally 600-700m thick, with fine- to very fine-grained lithofeldspathic sandstones, dark-grey clastic rhythmite and mudrock (Johnson et al., 2006). Sedimentary structures include: nodules, deformation structures, horizontal laminations, ripple lamination, low-amplitude ripples, groove casts and graded bedding (Johnson et al., 2006). This formation consists of two well defined cycles and has few trace fossils. The absence of any shallow-water indicators reflect deposition by gravity flows on the slope of advancing submarine fan complexes (Kingsley, 1981). This formation is also an equivalent of the Laingsburg and Skoorsteenberg formations. This coupled with its stratigraphic position (underlying the Fort Brown and Waterford formations respectively) makes correlation with the Amibberg Formation improbable.

5.3.3 Fort Brown Formation

This formation is confined to the southern margin (Laingsburg Sub-basin) of the Main Karoo Basin and has an average thickness of 1000m consisting of rhythmite, mudrock and minor sandstones (Johnson et al., 2006) which display an overall coarsening upward trend. Sedimentary structures include: oscillation ripples, ripple cross-lamination, wavy bedding/laminations, horizontal laminations, ball-and-pillow deformation structures and calcareous concretions (Johnson et al., 2006). Towards the top of the formation, *Cruziana* and *Skolithos* trace fossil assemblages occur as well as wave ripples attesting to the decrease in water depth (Kingsley, 1977). Isolated fish scales and abundant plant material are present in this formation (Rubidge et al., 2000). According to Reineck and Singh (1973), the coarser strata could represent "Storm-sand layers". Mean ripple crest orientations from the central outcrop area indicates WNW-ESE palaeocurrent trend (Ryan, 1967). This formation consists primarily of mudrock with only minor sandstones present making it distinctly different to the Amibberg Formation. Furthermore, the Fort Brown Formation has been correlated with the Volksrust Formation (Johnson et al., 2006) making the correlation with the Amibberg Formation improbable. However, the upper, sand dominant parts of this formation may be incorporated as equivalents of the lower sandstones of the Amibberg Formation.

5.3.4 Kookfontein Formation

The Kookfontein Formation is 250m thick in the Tanqua Sub-basin (Wickens, 1994) and overlies the submarine fans of the Skoorsteenberg Formation. This formation is also not suitable for correlation as the lower cycles (1-5) lack any indication of storm influence in shallow-water. The upper cycles (6-13) do in fact show similar sedimentary structures (HCS, wave ripples and deformation structures), palaeocurrent data (NW-SE trend) and coarsening upward trends. These rocks contain an abundance of wave ripples and *Cruziana* trace fossils indicating an upward shallowing during deposition. These deposits are interpreted to represent deposition in a shelf-type setting (Wild, 2005). However, this upper interval of the Kookfontein Formation shows a distinct thickness contrast between the Tanqua Sub-basin (50m) and the Karasburg Basin (250m).

5.3.5 Koedoesberg/Waterford Formation

In the Tanqua Sub-basin the Kookfontein Formation is overlain by the Koedoesberg/Waterford Formation which is approximately 330m thick (Fildani et al., 2007). These rocks have a gradational contact with lower Kookfontein Formation and sharp upper contact with Abrahamskraal Formation and consist of fine- to medium-grained tabular sandstones, siltstones, rhythmites and shales. Structures include: HCS, horizontal laminations, ball-and-pillow deformation structures and wave ripples. This formation consists of four upward coarsening cycles (Visser, 1993). *Cruziana* is the most common trace fossil assemblage with *Skolithos* being more rare. Palaeoniscid fish scales, bivalves, and fossil wood with *Glossopteris* and *Schizoneura* leaves have been recorded within the Koedoesberg Formation (Rubidge et al., 2000). Palaeocurrent directions for the sedimentary system of the Tanqua sub-basin area indicate an overall progradation to the north and east (Wickens, 1994; Hodgson et al., 2006; Johnson et al., 2006; Wild et al., 2009). Based on thickness, lithology, sedimentary structures, stacking pattern, progradational trend, trace fossil assemblages, stratigraphic position and other fossil indicators it is possible to propose that the Koedoesberg/Waterford Formation is at least a partial equivalent of the Amibberg Formation in the Tanqua Sub-basin. Furthermore, due to the gradational contact between the Koedoesberg and Kookfontein formations it is possible that the upper parts of the Kookfontein Formation (cycles 1-5) and the lower parts of the Koedoesberg Formation are equivalent of the Amibberg Formation.

5.3.6 Waterford Formation (Laingsburg Sub-basin)

In the southern area (Laingsburg Sub-basin) of the Main Karoo Basin this formation has a variable thickness from 200-800m and consists of alternating very fine-grained lithofeldspathic sandstones, mudrocks and clastic rhythmite units (Johnson et al., 2006), with four defined upwards coarsening cycles observed (Visser, 1993). Sedimentary structures include: horizontal laminations, HCS, oscillation ripples, rare cross-bedding, ball-and-pillow deformation structures, calcareous concretions as well as a variety of trace fossils (Johnson et al., 2006). Due to the abundance of wave ripples this formation is interpreted to have formed in relatively shallow water (Johnson et al., 2006). Petrographically these rocks indicate a magmatic arc provenance. This southern portion of the Waterford Formation shows

similarities with the Amibberg Formation in terms of sedimentary structures, stacking pattern and depositional environment and can also be considered as an equivalent of the Amibberg Formation.

5.3.7 Carnarvon/Waterford Formation

Although the Carnarvon Formation is not a recognisable unit of SACS (1980) it was put forward by Terblanche (1979) as being separate from the Waterford Formation. Rocks of this formation occur along the northwestern margin of the Main Karoo Basin (Johnson et al., 2006) and consist of interbedded sandstones, siltstone and shales. This succession attains a thickness of 250m with primary sedimentary structures including: HCS, ripple cross-stratification, wave ripples, bioturbation and load structures (Siebrits, 1987). Trace fossil suites include *Skolithos* isp., *Cruziana* isp. and what Siebrits (1987) incorrectly described as *Scoyenia* which is in fact *Palaeophycus* or *Halopoa* which is easily confused with *Scoyenia*. The entire succession is characterised as an upward-coarsening (6 poorly defined cycles), prograding (regressive), wave dominated, shallow sea deposit influenced by periodic storms (Siebrits, 1987). Petrographically the sandstones from this formation are fine to very fine-grained lithic wackes and lithic arenites. Siebrits (1987) places the lower contact of the Carnarvon Formation at the lowermost continuous, horizontal sandstone above the mudstone dominated Tierberg Formation. The uppermost contact is placed where marine sandstones lose their distinctive character and are replaced by fluvially dominated rocks (as per Terblanche, 1979). Siebrits (1987) shows average palaeocurrent directions of NNW-SSE and similarly Terblanche (1979) shows average wave ripple orientation of NW-SE which he equates to the orientation of the palaeoshoreline. However, the shoreline should be approximated as being perpendicular to the mean palaeocurrent vectors. This would indicate a shoreline roughly trending NE-SW. This is also supported by the palaeogeographic maps (Fig. 5.2) as the palaeoshoreline is orientated parallel to the southern side of the western Cargonian Highlands. However, lithologically the Waterford Formation is not identical to that of the Amibberg Formation. This is due to different conditions and sedimentological processes operating from the open end of the Ecca interior sea way. Based on stratigraphic position, thickness, sedimentary structures, trace fossil assemblages, palaeocurrent trends and stacking patterns it is strongly supported that the Carnarvon/Waterford Formation is an equivalent of the Amibberg Formation in the northwestern part of the Main Karoo Basin.

5.4 Conclusions

The main aim of this project has been to delineate lithofacies to enable a reconstruction of depositional environments and to enable a correlation with both the Aranos and Main Karoo basins. Further emphasis has been placed on palaeogeographical reconstruction of the Karasburg Basin at the time of deposition of the Amibberg Formation and the role of the Cargonian Highlands during the Early and Middle Permian.

The detailed stratigraphic outcrop logging conducted in this study has shown that it is possible to correlate lithofacies across the Amibberg Formation. Seven lithofacies and two ichnofacies (*Cruziana* and *Skolithos*) were identified and used for correlation purposes and to document changes in depositional environments. These include: 1) Massive, laminated and bioturbated mudstones interpreted as offshore deposits (OS); 2) Bioturbated sandy-siltstones which are representative of offshore-transitional environments (OST); 3) Interbedded sandstones and siltstones also interpreted as offshore-transitional deposits (OST) and generated by river-fed hyperpycnal plumes; 4) Sharp based, massive sandstones interpreted as being deposited on the distal lower shoreface (dLSF); 5) non-amalgamated HCS and wave rippled sandstones interpreted as distal lower shoreface-deposits (dLSF); 6) Amalgamated HCS and wave rippled sandstones interpreted as proximal lower shoreface deposits (pLSF); and 7) SSD sandstones and siltstone occurring in close juxtaposition with dLSF and pLSF deposits.

The vertical arrangement of these lithofacies shows an overall coarsening and shallowing upward trend indicating a prograding shoreline. Fluvial processes are interpreted from the heterolitihic nature of OST deposits and the presence of fluid-muds in pLSF deposits. Tidal influence manifests in the rock record by the mixing of trace fossils assemblages in various lithofacies: the presence of wavy, lenticular and flaser bedding in OST deposits; sharp and scoured dLSF deposits immediately overlying OS mudstones and the lack of cross-stratified upper shoreface intervals. Overall the rocks of the Amibberg Formation consist of wave-dominated shoreface deposits with significant influence by tidal and fluvial processes.

Petrographically, the sandstone samples contain a high percentage of subangular to subrounded monocrystalline quartz indicating a short transport distance before deposition. High concentrations of clay matrix in these sandstone samples are climatically controlled as temperate climate conditions favour chemical feldspar weathering. This can lead to the increasing clay and quartz contents in the sediments as seen in these samples. The moderately well-sorted nature of these samples is due to mild degrees of sorting due to tidal and wave activity on the shoreface. Sandstones fall into the class of quartz and feldspathic wackes and are sourced from craton interior and continental block provenances. Geochemical analysis of mudstones and nodules indicates high levels of microbial activity under oxic conditions during the deposition of the Amibberg Formation. Data obtained through the use of various geochemical proxies provide significant overlap in the type of source rocks. This conflicting data has led to the delineation of a mixed (plutonic igneous, volcanic and sedimentary) source.

Five poorly defined 4th order T-R cycles are observable within the strata of the Amibberg Formation. Large regressive intervals are capped by thin transgressive ones and these cycles are interpreted to have formed due to eustatic processes. At the basin scale, four rapid periods of base-level rise occurred after three gradual periods of base-level fall. Coarse-grained material was delivered to the shoreface by high rates of sediment supply where reworking by waves, tides and organisms occurred. Overall, this represents a eustatically controlled regressive shoreline.

The stated hypotheses (Chapter 1) can now be scrutinised in terms of their respective merits:

5.4.1 The Karasburg Basin and Aranos Basin were connected at the time of deposition, and the Karasburg Basin contains a more distal set of palaeoenvironments than the Aranos Basin.

Palaeotransport indicators and Karoo Supergroup lithologies do not indicate an obvious structural separation between the Aranos and Karasburg basins. Fossil remains also indicate that the Main Karoo Basin and Karasburg Basin were at least partially connected during the Permian. The environmental variability across the Aranos - Karasburg - Main Karoo basins was investigated.

No obvious structural separation existed between the Aranos and Karasburg Basin. This is based on the lack of evidence for the existence of the Karasburg Ridge as well as the presence of the same marine fossils in both basins. In addition, the presence of the same deepwater facies in the Karasburg Basin and shallower water facies in the Aranos Basin, as well as the same sequence boundaries indicates the connectivity of the two basins. The Cargonian Highlands played an active role in determining environmental variation along the western margin of the Ecca interior sea way even though it played no definitive role in separating the Aranos and Karasburg basins. Based on palaeogeographic maps (Fig. 5.2) the Cargonian Highlands only partially separated the Main Karoo Basin from the more northerly Namibian Karoo basins.

5.4.2 The Amibberg Formation correlates to the Waterford Formation in the Main Karoo Basin.

The Amibberg Formation in the Karasburg Basin has been equated with various formations in the Main Karoo Basin. Lithostratigraphy and sequence stratigraphy will be used to provide a concrete stratigraphic correlation between the Amibberg Formation and its equivalents in the Main Karoo Basin.

The Ripon Formation is not a likely correlation for Amibberg Formation based on T-R cycle order and stratigraphic position. The upper reaches of the Kookfontein Formation do show some similarities with the Amibberg Formation, and due to the gradational contact between the Kookfontein and Koedoesburg formations and the generally shallowing upward trend, it is possible that the upper cycles of the Kookfontein Formation and the Koedoesberg Formation are Amibberg Formation equivalents in the Tanqua Sub-basin. This also holds true in the Laingsburg Sub-basin where sand-dominated upper intervals of the Fort Brown Formation and the whole of the Waterford Formation are considered equivalents of the Amibberg Formation. More concrete is the correlation of the Amibberg Formation with the Waterford Formation in the Southern Sub-basin and the Carnarvon Formation on the northwestern margin of the Main Karoo Basin (Fig 5.3). The Carnarvon Formation is almost identical in characteristics except for the increase of sandstone amalgamation towards the top of this formation which is absent in the Karasburg Basin.

5.4.3 The western Cargonian Highland was subaerial during deposition of the Amibberg Formation, and acted as a major sediment source in the Karasburg Basin.

Lithofacies analysis, petrography, and shoreline orientation will be used to investigate the nature of the Cargonian Highland and the role it played in the separation of the Karasburg Basin from the Main Karoo Basin.

The Cargonian Highlands were at least partially emergent during the deposition of the Amibberg Formation. This is recognised because of the presence of fossil wood in this strata and due to wave-dominated shoreface deposits and the associated palaeoshoreline being orientated perpendicular to this palaeohigh. Furthermore, the Cargonian Highlands acted as a major source for the sediment of the Amibberg Formation although evidence for a secondary plutonic source has been identified.

5.5 Concluding Remarks

This study has provided a lithostratigraphic and palaeoenvironmental framework for the upper Ecca Group strata in the Karasburg Basin and has enabled a palaeogeographic reconstruction to be carried out. This has been useful in assessing the role of the Cargonian Highlands as a sediment source for the Karasburg Basin as the role it played in separating the Karasburg-Aranos basins from the Main Karoo Basin. A definitive correlation for the Amibberg Formation has been determined as the Waterford Formation in the Main Karoo Basin and various subsidiary basins. Furthermore, the recognition of the Amibberg Formation as a wave-dominated shoreface with significant tidal and fluvial influence allows for future researchers to compare ancient and modern deposits by using this work for comparative studies.

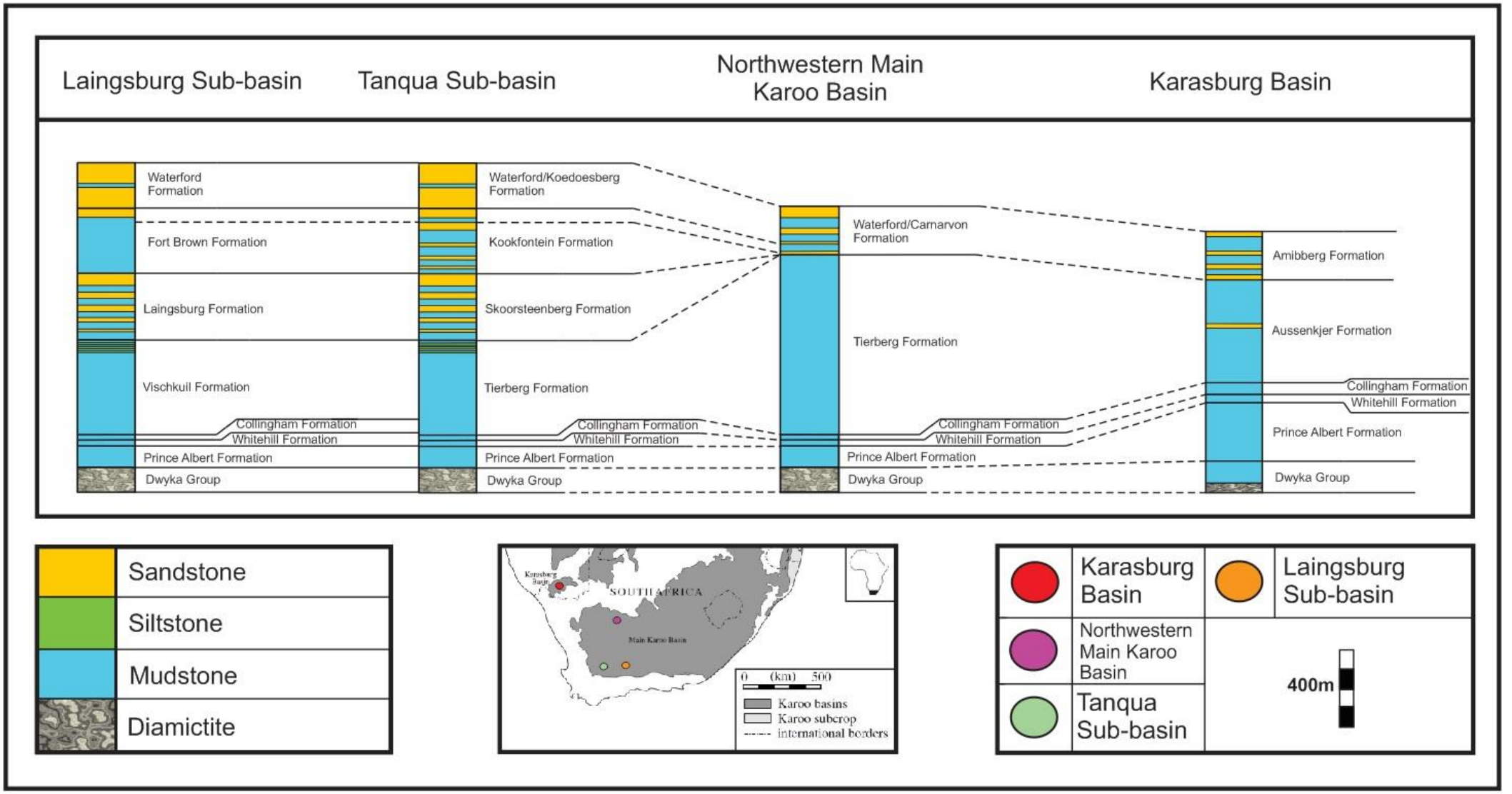


Figure 5.3. Final lithostratigraphic correlation between the Karasburg and Main Karoo basins as well as the Tanqua and Laingsburg sub-basins. Inset map of southern Africa displays the location of the various stratigraphic sections. Note that thickness of formations may vary within a given basin.

5.6 Recommendations

One recommendation is that detrital zircon dating be carried out on sandstone samples from the Amibberg Formation. This would provide the necessary data to definitively determine the source area/areas of the sediment in question as well as providing age constraints for the formation. Furthermore, due to the abundance and variety of trace fossils present in the Amibberg Formation and underlying formations, a detailed ichnological study should be carried out to gain insight into and understanding of the behaviour of organisms and how these reflect different depositional environments.

Chapter 6: References

Adams, J. A. S. and Weaver, C. E. (1958). Thorium-to-uranium ratios as indicators of sedimentary processes: example of concept of geochemical facies. *American Association of Petroleum Geologists Bulletin*, 42(2), pp. 387- 430.

Allen, J.R.L. (1982). Sedimentary Structures: Their Character and Physical Basis. *Developments in Sedimentology*, 30.

Allen, J.R.L. (1984). Wrinkle marks: an intertidal sedimentary structure due to aseismic soft-sediment loading. *Sedimentary Geology*, 41, pp. 75–95.

Allen, J.L. and Johnson, C.L. (2011). Architecture and formation of transgressive–regressive cycles in marginal marine strata of the John Henry Member, Straight Cliffs Formation, Upper Cretaceous of Southern Utah, USA. *Sedimentology*, 58, pp. 1486–1513.

Anderson, A.M. (1975). Turbidites and arthropod trackways in the Dwyka glacial deposits (Early Permian) of southern Africa. *Transactions of the Geological Society of South Africa*, 78, pp. 265-273.

Archer, A. W. and Maples, C. G. (1984). Trace-fossil distribution across a marine-to-nonmarine gradient in the Pennsylvanian of southwestern Indiana. *Journal of Paleontology*, 58, pp. 448–466.

Armstrong-Altrin, J.S. (2009). Provenance of sands from Cazones, Acapulco, and Bahía Kino beaches, Mexico. *Revista Mexicana de Ciencias Geológicas*, 26 (3), pp. 764-782.

Armstrong-Altrin, J.S. and Verma, S.P. (2005). Critical evaluation of six tectonic setting discrimination diagrams using geochemical data of Neogene sediments from known tectonic setting. *Sedimentary Geology*, 177, pp. 115-129.

Armstrong-Altrin, J.S., Lee, Y.I., Verma, S.P. and Ramasamy, S. (2004). Geochemistry of sandstones from the upper Miocene Kudankulam formation, Southern India: Implications for provenance, weathering, and tectonic setting. *Journal of Seimentary Research*, 74 (2), pp. 285-297.

Asiedu, D.K., Suzuki, S. and Shibata, T. (1996). Provenance of Lower Cretaceous sediments in the Nariwa and Hokubo areas, Okayama Prefecture, deduced from detrital modes and geochemistry of sandstones. *Okayama University Earth Science Reports*, 3(1), pp. 1-17.

Bakkiaraj, D., Nagendra, R., Nagarajan, R. and Armstrong-Altrin, J.S. (2010). Geochemistry of Sandstones from the Upper Cretaceous Sillakkudi Formation, Cauvery Basin, Southern India: Implication for Provenance. *Journal of the Geological Society of India*, 76, pp. 453-467.

Bamford, M.K. (2000). Fossil wood of Karoo age deposits in South Africa and Namibia as an aid in biostratigraphical correlation. *Journal of African Earth Science*, 31, pp. 119–132.

Bangert, B., Stollhofen, H., Lorenz V. and Armstrong, R. (1999). The geochronology and significance of ash-fall tuffs in the glaciogenic Carboniferous-Permian Dwyka Group of Namibia and South Africa. *Journal of African Earth Science*, 29, pp. 33-49.

Bangert, B. (2000). Tephrostratigraphy, petrography, geochemistry, age and fossil record of the Ganigobis Shale Member and associated glaciomarine deposits of the Dwyka Group, Late Carboniferous, southern Africa. Unpublished PhD thesis, University of Würzburg, pp. 243.

Basu, A. (1976). Petrology of Holocene fluvial sand derived from plutonic source rocks: implications to paleoclimatic interpretation. *Journal of Sedimentary Petrology*, 46, pp. 694–709.

Basu, A. (1985). Reading provenance from detrital quartz; In: Provenance of Arenites (Ed. G.G. Zuffa), Reidel Publishing Co., pp. 231–247.

Basu, A., Young, S.W., Suttner, L.J., James, W.C. and Mack, G.H. (1975). Re-evaluation of the use of undulatory extinction and polycrysrtallinity in detrital quartz for provenance interpretation. *Journal of Sedimentary Petrology*, 45, pp. 873–882.

Berg, R.R. (1976). Highlight Muddy field - Lower Cretaceous transgressive deposits in the Powder River basin, Wyoming. *Mountain Geol*ogy, 13, pp. 33-45.

Bernard, H.A., Le Blanc, R.J. and Major, C.F. (1962). Recent and Pleistocene geology of southeast Texas: field excursion 3. In: Geology of the Gulf Coast and Central Texas, a Guidebook of Excursions. *Annual Meeting of The Geological Society of America Guidebook*, pp. 175-224.

Bhatia, M. R. (1983). Plate tectonics and geochemical composition of sandstones. *Journal of Geology*, 91, pp. 611-627.

Bhatia, M.R. (1985). Rare earth element geochemistry of Australian Paleozoic greywackes and mudstones: provenance tectonic control. *Sedimentary Geology*, 45, pp. 97-113.

Bhatia, M. R. and Crook, K. A. W. (1986). Trace element characteristics of graywackes and tectonic setting of Miocene sandstones in the Bengal Basin. *Contributions to Mineralogy and Petrology*, 92, pp. 181–193.

Bhattacharya, J.P. (2006). Deltas. In: Facies Models Revisited (Eds. H.W. Posamentier and R.G. Walker), *Society for Sedimentary Geology Special Publication*, 84, pp. 237–292

Bhattacharya, J.P. and MacEachern, J.A. (2009). Hyperpycnal rivers and prodeltaic shelves in the Cretaceous seaway of North America. *Journal of Sedimentary Research*, 79, pp. 184–209.

Blatt, H. (1967). Provenance determinations and recycling of sediments. *Journal of Sedimentary Petrology*, 37, pp. 1031-1044.

Bordy, E.M., Hancox, P.J. and Rubidge, B.S. (2005). The contact of the Molteno and Elliot formations through the main Karoo Basin, South Africa: a second-order sequence boundary. *South African Journal of Geology*, 108, pp. 351-364.

Bordy, E.M., Segwabe, T. and Makuke, B. (2010). Sedimentology of the Upper Triassic - Lower Jurassic (?) Mosolotsane Formation (Karoo Supergroup), Kalahari Karoo Basin, Botswana. *Journal of African Earth Sciences*, doi:10.1016/j.jafrearsci.2010.02.006

Bouma, A.H. and Wickens, H. de V. (1991). Permian passive margin submarine fan complex, Karoo Basin, South Africa: possible model to Gulf of Mexico. *Transactions of the Gulf Coast Association of Geological Societies*, 41, pp. 30-42.

Brenchley, P.J., Pickerill, R.K. and Stromberg, S.G. (1993). The role of wave reworking on the architecture of storm sandstone facies, Bell Island Group (Lower Ordovician), eastern Newfoundland. *Sedimentology*, 40, pp. 359–382.

Bristow, J.W. and Saggerson, E.P. (1983). A review of Karoo vulcanicity in South Africa. *African Bulletin of Volcanology*, 46, pp. 135–159.

Bromley, R.G. (1996). Trace fossils – Biology, taphonomy and applications. Chapman and Hall, London, pp. 361.

Bromley, R. G. and Asgaard, U. (1972). Notes on Greenland trace fossils. I—III. *Rapport Grønlands geologiske Undersøgelse*, 49, 30 p.

Bromley, R.G. and Uchman, A. (2003). Trace fossils from the Lower and Middle Jurassic marginal marine deposits of the Sorhat Formation. Bornholm, Denmark. *Bulletin of the Geological Society of Denmark*, 52, pp. 185-208.

Brown, L.F. Jr. and Fisher, W.L. (1977). Seismic stratigraphic interpretation of depositional systems: examples from Brazilian rift and pull apart basins. In: Seismic Stratigraphy - Applications to Hydrocarbon Exploration (Ed.C.E. Payton). *American Association of Petroleum Geologists Memoir*, 26, pp. 213-248.

Buatois, L.A., Santiago, N., Parra, K. and Steel, R. (2008). Animal-substrate interactions in an Early Miocene wavedominated tropical delta: delineating environmental stresses and depositional dynamics (Tácata Field, Eastern Venezuela). *Journal of Sedimentary Research*, 78, pp. 458–479.

Buatois, L.A., Saccavino, L.L. and Zavala, C. (2011). Ichnologic signatures of hyperpycnal-flow deposits in Cretaceous river-dominated deltas, Austral Basin, southern Argentina. In: Sediment transfer from shelf to deep water – revisiting the delivery system (Eds. R.M. Slatt and C. Zavala). *American Association of Petroleum Geologists Studies in Geology*, 61, pp. 153-170.

Buatois, L.A., Santiago, N., Herrera, M., Plinkbjörklund, P., Steel, R., Espin, M. and Parra, K. (2012). Sedimentological and ichnological signatures of changes in wave, river and tidal influence along a Neogene tropical deltaic shoreline. *Sedimentology*, 59, pp. 1568–1612.

Buatois, L.A. and Mángano, M.G. (2011). Ichnology: Organism- Substrate Interactions in Space and Time. Cambridge University Press, Cambridge, 358.

Buckman, J. O. (1995). A comment on annulate forms of Palaeophycus with particular reference to P. 'annulatus' sensu Pemberton and Frey 1982 and the erection of P. crenulatus ichnosp. *Ichnos*, 4, pp. 131–140.

Bumby, A.J. and Guiraud, R. (2005). The Geodynamic setting of the Phanerozoic basins of Africa. *Journal of African Earth Sciences*, 43, pp. 1-12.

Busch, D.A. (1959). Prospecting for stratigraphic traps. *American Association of Petroleum Geologists Bulletin*, 43, pp. 2829-2843.

Cairncross, B. (2001). An overview of Permian (Karoo) coal deposits of southern Africa. *Journal of African Earth Sciences*, 33, pp. 529-562.

Cairncross, B. and Cadle, A.B. (1988). Paleoenvironmental and quality in the Permian Vryheid Formation, East Witbank Coalfield, South Africa. *International Journal of Coal Geology*, 9, pp. 343-370.

Carmona, N.B., Buatois, L.A., Ponce, J.J. and Mángano, M.G. (2009). Ichnology and sedimentology of a tide-influenced delta, Lower Miocene Chenque Formation, Patagonia, Argentina: trace-fossil distribution and response to environmental stresses. *Palaeogeography, Palaeoclimatology, Palaeoecology*, 273, pp. 75–86.

Carney, J. N., Aldis, D. T. and Lock, N. P. (1994). *The Geology of Botswana*, 37, pp. 113.

Catuneanu, O. (2004a). Basement control on flexural profiles and the distribution of foreland facies: the Dwyka Group of the Karoo Basin, South Africa. *Geology*, 32, pp. 517–520.

Catuneanu, O., Sweet, A.R. and Miall, A.D. (1997). Reciprocal architecture of Bearpaw T–R sequences, uppermost Cretaceous, Western Canada Sedimentary Basin. *Bulletin of Canadian Petroleum Geology*, 45, pp. 75–94.

Catuneanu, O., Hancox, P.J. and Rubidge, B.S. (1998). Reciprocal flexural behaviour and contrasting stratigraphies: a new basin development model for the Karoo retroarc foreland system, South Africa. *Basin Research*, 10, pp. 417-439.

Catuneanu, O., Willis, A.J. and Miall, A.D. (1998). Temporal significance of sequence Boundaries. *Sedimentary Geology*, 121, pp. 157-178.

Catuneanu, O., Hancox, P.J., Cairncross, B. and Rubidge, B.S. (2002). Foredeep submarine fans and forebulge deltas: orogenic off-loading in the underfilled Karoo Basin. *Journal of African Earth Sciences*, 35, pp. 489–502.

Catuneanu, O., Wopfner, H., Eriksson, P.G., Cairncross, B., Rubidge, B.S., Smith, R.M.H. and Hancox, P.J. (2005). The Karoo basins of south-central Africa. *Journal of African Earth Sciences*, 43, pp. 211-253.

Catuneanu, O. and Elango, H.N. (2001). Tectonic control on fluvial styles: the Balfour Formation of the Karoo Basin, South Africa. *Sedimentary Geology*, 140, pp. 291- 313.

Chaiwongsaen, N. (2007). Sedimentology and stratigraphy of the Prairie Canyon Member, Salt and Bootlegger Washes, Thompson Spring, Eastern Utah. Unpublished MSc Thesis, Colorado School of Mines.

Charvin, K., Hampson, G.J., Gallagher, K.L. and Labourdette, R. (2010). Intra-parasequence architecture of an interpreted asymmetrical wave-dominated delta. *Sedimentology*, 57, pp. 760–785.

Cheel, R.J. and Leckie, D.A. (1993). Hummocky cross-stratification. In: Sedimentology Review (Ed. V.P. Wright), 1, pp. 103–122.

Clifton, H.E. (2006). A re-examination of facies models for clastic shorelines. In: Facies Models Revisited (Eds. H.W. Posamentier and R.G. Walker). *Society for Sedimentary Geology Special Publication*, 84, pp. 293–337.

Collins, D.S., Allison, P.A., Johnson, H.D., Avdis, A., Hill, J. and Piggot, M. (2014). Integrating Tidal Modeling and Facies Analysis for the Miocene, Northwest Borneo, South China Sea. *Search and Discovery*, 50990.

Cotter, E.C. (1983). Shelf, paralic and fluvial environments and eustatic sea-level fluctuations in the origin of the Tuscarora Formation (Lower Silurian) of central Pennsylvania. *Journal of Sedimentary Petrology*, 53, pp. 25–49.

Cotter, E. C. (1985). Gravel-topped offshore bar sequences in the Lower Carboniferous of southern Ireland. *Sedimentology*, 32, pp. 195-213.

Cox, R., Low, D.R. and Cullers, R.L. (1995). The influence of sediment recycling and basement composition on evolution of mudrock chemistry in the southwestern United States. *Geochimica et Cosmochimica Acta*, 59(14), pp. 2919-2940.

Crook, K.A.W. (1970b). Geotectonic significance of graywackes: Relevance of recent sediments from Niugini. 42nd ANZAAS Congress, Port Moresby, Niugini.

Cullers, R. L. (2000). The geochemistry of shales, siltstones and sandstones of Pennsylvanian–Permian age, Colorado, USA: Implications for provenance and metamorphic studies. *Lithos*, 51, pp. 181–203.

Cummins, W.A. (1962a). The greywacke problem. *Geological Journal*, 3, pp. 51–72. doi: 10.1002/gj.33500301053.

Dahmer, G. (1937). Lebensspuren aus dem Taunusquarzit und den Siegener Schichten (Unterdevon). *Preussische Geologische Landesanstalt zu Berlin*, 57, pp. 523-539.

Dalrymple, R.W. and Choi, K. (2007). Morphologic and facies trends through the fluvial–marine transition in tide-dominated depositional systems: A schematic framework for environmental and sequence-stratigraphic interpretation. *Earth-Science Reviews*, 81, pp. 135–174.

Daly, M.C., Chorowicz, J. and Fairhead, J.D. (1989). Rift basin evolution in Africa, the influence of reactivated steep basement shear zones. In: Inversion Tectonics (Eds. M.A. Cooper and G.D. Williams). *Special Publication of the Geological Society of London*, pp. 309-334.

Dam, G. (1989). Taxonomy of trace fossils from the shallow marine Lower Jurassic Neill Klinter Formation, East Greenland. *Bulletin of the Geological Society of Denmark*, 38.

Davies, D.K., Ethridge, F.G. and Berg, R.R. (1971). Recognition of barrier environments. *American Association of Petroleum Geologists Bulletin*, 55, pp. 550-565.

de Booy, T. (1966). Petrology of detritus in sediments, a valuable tool. *Koninklijke Nederlandse akademie van wetenschappen. Series B, Physical sciences*, 69 (2), pp.277-282.

de Villiers, J. and Söhnge, P.G. (1959). The Geology of the Richtersveld. *Geological Survey of South Africa Memoir*, 48, pp. 295.

de Wit, M.J.d. and Ransome, I.G.D. (1992). Regional inversion tectonics along the southern margin of Gondwana. In: Inversion Tectonics of the Cape Fold Belt, Karoo and Cretaceous Basins of Southern Africa (Eds. M.J.d. Wit and I.G.D. Ransome), pp. 15-21.

Dickinson, W. R. and Suczek, C. A. (1979). Plate tectonics and sandstone compositions. *American Association of Petroleum Geologists Bulletin*, 63, pp. 2164–2182.

Dickinson, W. R., Beard, L. S., Brakenridge, G. R., Erjavec, J. L., Ferguson, R. C., Inman, K. F., Knepp, R. A., Lindberg, F. A. and Ryberg, P. T. (1983). Provenance of North American Phanerozoic sandstones in relation to tectonic setting. *Geological Society of America Bulletin*, 94, pp. 222–235.

Dingle, R.V. and Scrutton, R.A. (1974). Continental break-up and the development of Post-Palaeozoic sedimentary basins around Southern Africa. *Geological Society of America Bulletin*, 85, pp. 1467-1474.

Dong, J., Zhang S.H., Jiang G.Q., Zhao, Q.L., Li, H.Y., Shi, X.Y. and Liu, J.L. (2008). Early diagenetic growth of carbonate concretions in the upper Doushantuo Formation in South China and their significance for the assessment of hydrocarbon source rock. *Science in China Series D-Earth Science*, 51, 9, pp. 1330-1339**.**

Dott, R.H. Jr. and Bourgeois, J. (1982). Hummocky stratification; significance of its variable bedding sequences. *Geological Society of America Bulletin*, 93, pp. 663–680.

Dott, R. H. Jr. (1964). Wacke, Graywacke and Matrix - What Approach to Immature Sandstone Classification? *Journal of Sedimentary Research*, 34(3).

Duke, W.L. (1985). Hummocky cross-stratification, tropical hurricanes, and intense winter storms. *Sedimentology*, 32, pp. 167–194.

Duncan, R.A., Hooper, P.R., Rehacek, J., Marsh, J.S. and Duncan, A.R. (1997). The timing and duration of the Karoo igneous event, southern Gondwana. *Journal of Geophysical Research*, 102, pp. 18127–18138.

du Toit, A.L. (1921). The Carboniferous glaciation of South Africa. *Transactions of the Geological Society of South Africa*, 24, pp. 188-227.

du Toit, A.L. (1927). Geological Comparison of South America with South Africa: with a Palaeontological Contribution by F.R. Cowper Reed, Carnegie Institute Publication, 381, pp. 1–157.

du Toit, A.L. (1954). The Geology of South Africa, 3rd ed. Oliver and Boyd, Edinburgh, pp. 611.

Ekdale, A.A. (1985). Paleoecology of the marine endobenthos. *Palaeogeography, Palaeoclimatology, Palaeoecology*, 50, pp. 63–81.

Ekdale, A.A., Bromley, R.G. and Pemberton, S.G. (1984). Ichnology: Trace fossils in sedimentology and stratigraphy. *Society for Sedimentary Geology Short Course*, 15, pp. 317.

Elliott, T. (1986). Clastic shorelines. In: Sedimentary Environments and Facies, 2nd ed. (Ed. H.G. Reading), pp. 143–177.

Embry, A.F. (1993). Transgressive-regressive (T-R) sequence analysis of the Jurassic succession of the Sverdrup Basin, Canadian Arctic Archipelago. *Canadian Journal of Earth Sciences*, 30, pp. 301-320.

Embry, A.F. (1995). Sequence boundaries and sequence hierarchies: problems and proposals. In: Sequence stratigraphy on the northwest European margin (Eds. R.J. Steel, F.L. Felt, E.P. Johannessen and C. Mathieu). *Norwegian Petroleum Society Special Publication*, 5, pp. 1-11.

Embry, A.F. (2009). Practical sequence stratigraphy. *Canadian Society of Petroleum Geologists*, Online at www.cspg.org, pp. 79.

Embry. A.F. and Johannessen, E.P (1992). T-R sequence stratigraphy, facies analysis and reservoir distribution in the uppermost Triassic-Lower Jurassic succession, western Sverdrup Basin, Arctic Canada, In: Arctic Geology and Petroleum Potential (Eds. T. Vorren, E. Bergsager, O.A. Dahl-Stamnes, E. Holter, B. Johansen, E. Lie and T.B. Lund). *Norwegian Petroleum Society Special Publication*, 2, pp. 121-146.

Embry, A., Johannessen, E., Owen, D., Beauchamp, B. and Gianolla, P. (2007). Sequence Stratigraphy as a "Concrete" Stratigraphic Discipline - Report of the ISSC Task Group on Sequence Stratigraphy.

Emerson, S. R. and Huested. S. S. (1991). Ocean anoxia and the concentrations of molybdenum and vanadium in seawater. *Marine Chemistry*, 34, pp. 177－196.

Exploration Consultants Limited, (1998). Petroleum Potential of the Karoo of Botswana. Report - Volume 1. Department of Geological Survey, Botswana, GC 122/2/1a.

Eyles, N. and Clark, B. M. (1986). Significance of hummocky and swaley cross-stratification in late Pleistocene lacustine sediments of the Ontario basin, Canada. *Geology*, 14, pp. 679-682.

Fildani, A., Drinkwater, N.J., Weislogel, A., McHargue, T., Hodgson, D.M. and Flint, S.S. (2007). Age controls of the the Tanqua and Laingsburg deep-water systems: new insights on the evolution and sedimentary of the Karoo Basin, South Africa. *Journal of Sedimentary Research*, 77, pp. 901-908.

Fillion, D. and Pickerill, R.K. (1990). Ichnology of the Lower Ordovician Bell Island and Wabana Groups of eastern Newfoundland. *Palaeontographica Canadiana*, 7, pp. 1-119.

Flesch, G.A. and Wilson, M.D. (1974). Petrography of the Morrison Formation (Jurassic) Sandstone of the Ojito Spring Quadrangle, Sandoval County, New Mexico. *New Mexico Geological Society Guidebook*, 25th Field Conference.

Floyd, P.A., Winchester, J.A. and Park, R.G. (1989). Geochemistry and tectonic setting of Lewisian clastic metasediments from the Early Proterozoic Loch Maree Group of Gairloch, N.W. Scotland. *Precambrian Research*, 45(1-3), pp. 203-214.

Folk, R. L. (1951). Stages of textural maturity in sedimentary rocks. *Journal of Sedimentary Petrology*, 21, pp. 127–130.

Folk, R. L. (1980). Petrology of Sedimentary Rocks. Hemphill Publication Co., Austin, Texas. 182.

Frakes, L.A. and Crowell, J.C. (1970). Late Paleozoic glaciation: II, Africa exclusive of the Karroo Basin. *Geological Society of America Bulletin*, 81, pp. 2261-2286.

Frakes, L.A. and Crowell, J.C. (1972). Late Paleozoic Glaciation; Part V, Karroo Basin, South Africa. *Geological Society of America Bulletin*, 83, pp. 2887-2912.

Galloway, W. (1989). Genetic stratigraphic sequences in basin analysis I: architecture and genesis of flooding surface bounded depositional units. *American Association of Petroleum Geologists Bulletin*, 73, pp. 125-142.

Gawthorpe, R., Fraser, A. and Collier, R. (1994). Sequence stratigraphy in active extensional basins: implications for the interpretation of ancient basin fills. *Marine and Petroleum Geology*, 11, pp. 642- 658.

Geiger, M. (1999). An explanation of the Geological Map 1:10000 of the Namibian borderland along the Orange River at Zwartbas, Warmbad District, Karas Region, Namibia. Unpublished Diploma Thesis, University of Würzburg.

Geiger, M., (2000). The geology of the southern Warmbad basin margin – tephrostratigraphy, age, fossil record and sedimentary environment of Carboniferous-Permian glacigenic deposits of the Dwyka Group, Zwartbas, southern Namibia. Unpublished Diploma Thesis, University of Würzburg.

Genis, G. and Schalk, K.E.L. (1984). The geology of area 2618: Keetmanshoop. Explanation of sheet 2618 scale 1:250000. Geological Survey of South West Africa/Namibia, 12.

Geological Survey of Namibia (1999). Geological map of Namibia, sheet 2816 – Oranjemund, 1:250 000 series. Ministry of Mines and Energy.

Gresse, P.G. and Germs, G.J.B. (1993). The Nama foreland basin: sedimentation, major unconformaty bounded sequences and multisided active margin advance. *Precambrian Research*, 63, pp. 247-272.

Grill, H. (1997). The Permo-Carboniferous glacial to marine Karoo record in southern Namibia: sedimentary facies and sequence stratigraphy. *Beringeria*, 19, 98.

Gurnis, M. (1992). Rapid continental subsidence following the initiation and evolution of subduction. *Science*, 255, pp. 1556–1558.

Hallberg, R.O. (1976). A geochemical method for investigation of palaeoredox conditions in sediments. *Ambio Special Report*, 4, pp. 139-147.

Halsey, S.D. (1979). Nexus: new model of barrier island development. In: Barrier Islands - From the Gulf of St. Lawrence to the Gulf of Mexico (Ed. S.P. Leatherman). Academic Press, New York, pp. 185-210.

Hamblin, A.P. and Walker, R.G. (1979). Storm dominated shallow marine deposits: the Fernie-Kooteney (Jurassic) transition, southern Rocky Mountains. *Canadian Journal of Earth Science*, 16, pp. 1676–1690.

Hampson, G.J. and Storms, J.E.A. (2003). Geomorphological and sequence stratigraphic variability in wave-dominated, shoreface-shelf parasequences. *Sedimentology*, 50, pp. 667– 701.

Hampson, G.J., Procter, E.J. and Kelly, C. (2008). Controls on isolated shallow-marine sandstone deposition and shelf construction: late Cretaceous Western Interior Seaway, northern Utah and Colorado. In: Recent Advances in Models of Siliciclastic Shallow-Marine Stratigraphy (Eds. G.J. Hampson, R.J. Steel, P.M. Burgess and R.W. Dalrymple). *Society for Sedimentary Geologists Special Publcation*, 90, pp. 355–389.

Hampson, G.J. (2010). Sediment dispersal and quantitative stratigraphic architecture across an ancient shelf. *Sedimentology*, 47, pp. 96–141.

Hancox, P.J. (2000). The Continental Triassic of South Africa. *Zentralblatt für Geologie und Paläontologie*, 1, pp. 1285-1324.

Harms, J.C. (1969). Hydraulic significance of some sand ripples. *Geological Society of America Bulletin*, 80, pp. 363–396.

Harms, J.C., Southard, J.B., Spearing, D.R. and Walker, R.G. (1975). Depositional Environments as Interpreted from Primary Sedimentary Structures and Stratification. *Society of Economic Paleontologists and Mineralogists*, Short Course 2.

Haszeldine, R.S., Samson, I.M. and Cornford, C. (1984). Quartz Diagenesis and Convective Movement: Beatrice Oilfield, UK North Sea. *Clay Minerals*, 19, pp. 391-402.

Hatch, J.R. and Leventhal, J.S. (1992). Relationship between inferred redox potential of the depositional environment and geochemistry of the Upper Pennsylvanian (Missourian) stark shale member of the Dennis Limestone, Wabaunsee County, Kansas, USA. *Chemical Geology*, 99, pp. 65－82.

Hattin, D.E. and Frey, R.W. (1969). Facies relationship of Crossopodia SP., A trace fossil from the upper Cretaceous of Kansas, Iowa and Oklahoma. *Journal of Palaeontology*, 43, pp. 1435-1440.

Haughton, S.H. and Frommurze, H.F. (1927). The Karroo beds of the Warmbad District, South-West Africa. *Transactions of the Geological Society of South Africa*, 30, pp. 133-142.

Haughton, S.H. and Frommurze, H.F. (1936). The geology of the Warmbad district, South West Africa. An explanation of geological sheets Amib (H-33-F), Umeis (H-34-A) and Nakop (H-34-B). *SWA Department of Mines Memoir*, 2, pp. 64.

Hayashi, K., Fujisawa, H., Holland, H. and Ohmoto, H. (1997). Geochemistry of ~1.9 Ga sedimentary rocks from northeastern Labrador, Canada: *Geochimica et Cosmochimica Acta*, 61, pp. 4115-4137.

Hayes, J.M., Strauss, H. and Kaufman, A.J. (1999). The abundance of 13C in marine organic matter and isotopic fractionation in the global biogeochemical cycle of carbon during the past 800 Ma. *Chemical Geology*, 161, pp. 103–125.

Heath, D.C. (1972). Die geologie van die Sisteem Karoo in die gebied Mariental-Asab, Suidwes-Afrika. *Memoir of the Geological Survey of South Africa*, 61, pp. 36.

Hegenberger, W. (1992). Coal. In: The Mineral Resources of Namibia, 1st ed., Ministry of Mines and Energy, Geological Survey, Windhoek, Namibia, pp. 7.2-1–7.2-29.

Heinberg, C. (1973). The internal structure of the trace fossils Gyrochorte and Curvolithos. *Lethaia*, 6, pp. 227-238.

Heward, A.P. (1981). A Review of Wave-Dominated Clastic Shoreline Deposits. *Earth-Science Reviews*, 17, pp. 223-276.

Hobday, D.K. and Orme, A.R. (1974). The Port Durnford Formation: a major Pleistocene barrier-lagoon complex along the Zululand coast. *Transactions of the Geological Society of South Africa*, 77, pp. 141-149.

Hodgson, D.M., Flint, S.S., Hodgetts, D., Drinkwater, N.J., Johannesson, E.J. and Luthi, S.M. (2006). Stratigraphic evolution of fine-grained submarine fan systems, Tanqua depocentre, Karoo Basin, South Africa. *Journal of Sedimentary Research*, 76, pp. 20-40.

Holt, W.E. Stern, T.A. (1994). Subduction, platform subsidence and foreland thrust loading: the late Tertiary development of Taranaki basin, New Zealand. *Tectonic*s, 13, pp. 1068–1092.

Horne, J.C., Ferm, J.C. and Swinchatt, J.P. (1974). Depositional model for the Mississippian-Pennsylvanian boundary in northeastern Kentucky. In: Carboniferous of the Southeastern United States (Ed. G. Briggs). *Special Paper of the Geological Society of America*, 148, pp. 97-114.

Howard, J.D. and Frey, R.W. (1984). Characteristic trace fossils in nearshore to offshore sequences, Upper Cretaceous of east-central Utah. *Canadian Journal of Earth Sciences,* 21, pp. 200–219.

Ichaso, A. A. and Dalrymple, R. W. (2009). Tide-and wave-generated fluid mud deposits in the Tilje Formation (Jurassic), offshore Norway. *Geology*, 37(6), pp. 539-542.

Ingersoll, R.V., Bullard, T.F., Ford, R.L., Grimm, J.P., Pickle, J.D. and Sares, S.W. (1984). The effect of grain size on detrital modes: a test of the Gazzi-Dickenson point-counting method. *Journal of Sedimentary Petrology*, 46, pp. 620-632.

Jensen, S. (1997). Trace fossils from the Lower Cambrian Mickwitzia sandstone, south-central Sweden. *Fossils and Strata*, 42, pp. 1-111.

Johnson, M.R. (1976). Stratigraphy and sedimentology of the Cape and Karoo Sequences in the Eastern Cape Province. Unpublished Ph.D. Thesis, Rhodes University, Grahamstown, pp. 335.

Johnson, M.R., van Vuuren, C.J., Hegenberger, W.F., Key, R. and Shoko, U. (1996). Stratigraphy of the Karoo Supergroup in southern Africa. *Journal of African Earth Science,* 23, pp. 3-15.

Johnson, M.R., van Vuuren, C.J., Visser, J.N.J., Cole, D.I., Wickens, H. de V., Christie, A.D.M. and Roberts, D.L. (1997). The foreland Karoo Basin, South Africa. In: African Basins (Ed. R.C. Selley). *Sedimentary basins of the world*, 3, pp. 269-317.

Johnson, M.R., Van Vuuren, C.J., Visser, J.N.J., Cole, D.I., Wickens, H. de V., Christie, A.D.M., Roberts, D.L. and Brandl, G. (2006). Sedimentary rocks of the Karoo Supergroup. In: The Geology of South Africa (Eds. M.R. Johnson, C.R. Anhaeusser and R.J. Thomas). Geological Society of South Africa/Council of Geoscience, South Africa, pp. 461-499.

Johnson, S.D., Flint, S., Hinds, D. and Wickens, H. de V. (2001). Anatomy, geometry and sequence stratigraphy of basin floor to slope turbidite systems, Tanqua Karoo, South Africa. *Sedimentology*, 48, pp. 987-1023.

Jones, B. and Manning, D.A.C. (1994). Comparison of geochemical indices used for the interpretation of palaeoredox conditions in ancient mudstones. *Chemical Geology*, 111, pp.111-129.

Joo, Y.J., Lee, Y.I. and Bai, Z. (2005). Provenance of the Qingshuijian Formation (Late Carboniferous), NE China: Implications for tectonic processes in the northern margin of the North China block. *Sedimentary Geology*, 177, pp. 97- 114.

Kamola, D. L. and Van Wagoner, J. C. (1995). Stratigraphy and facies architecture of parasequences with examples from the Spring Canyon Member, Blackhawk Formation, Utah. pp. 27-54.

Keighley, G. D. and Pickerill, R. K. (1995). The ichnotaxa Palaeophycus and Planolites in historical perspectives and recommendations. *Ichnos*, 3, pp. 301–310.

Key, R. M., Tidi, J., Mc George, I., Aitken, G., Cadman, A. and Anscombe, J. (1998). The lower Karoo Supergroup geology of the southwestern part of the Gemsbok sub-basin of the Kalahari Basin, Botswana. *South African Journal of Geology*, 101, pp. 225-236.

Kimura, H. and Watanabe, Y. (2001). Ocean anoxia at the Precambrian-Cambrian boundary. *Geology*, 29, pp. 995-998.

Kingsley, C.S. (1977). Straigraphy and sedimentology of the Ecca Group in the Eastern Cape Province, South Africa. Unpublished Ph.D. Thesis, University of Port Elizabeth, 286 pp.

Kingsley, C.S. (1981). A composite submarine fan-delta-fluvial model for the Ecca and lower Beaufort Groups of Permian age in the Eastern Cape Province, South Africa. *Transactions of the Geological Society of South Africa*, 84, pp. 27-40.

Kingsley, C.S. (1985). Sedimentological analysis of the Ecca Sequence in the Kalahari Basin, South West Africa/Namibia. Unpublished report, CDM Mineral Surveys, 39.

Komar, P. D. (1976). Beach Processes and Sedimentation. Englewood Cliffs, N.J., Prentice-Hall, pp. 426.

Krynine, P.D. (1948). The megascopic study and field classification of sedimentary rocks. *Journal of Geology*, 56, pp. 130–165.

Kuenen, Ph.H. (1966). Matrix of turbidites. Experimental approach. *Sedimentology*, 7, pp. 267-297.

Leckie, D. A. (1985). The Lower Cretaceous Notikewin Member (Fort St. John Group), northeastern British Columbia: a progradational burner island system. *Canadian Petroleum Geology Bulletin*, 33, pp. 39- 51.

Leckie, D.A. and Walker, R.G. (1982). Storm and tide dominated shorelines in Cretaceous Moosebar–Lower Gates interval—outcrop equivalents of deep basin gas traps in Western Canada. *American Association of Petroleum Geologists Bulletin*, 18, pp. 138– 157.

Liu, S., Lin, G., Liu, Y., Zhou, Y., Gong, F. and Yan, Y. (2007). Geochemistry of Middle Oligocene-Pliocene sandstones from the Nanpu Sag, Bohai Bay Basin (Eastern China): Implications for provenance, weathering, and tectonic setting. *Geochemical Journal*, 41(5), pp. 359-378.

Loock, J.C. and Visser, J.N.J. (1985). South Africa. In: The Carboniferous of the World II. Australia, Indian Subcontinent, South Africa, South America and North Africa (Ed. C.M. Diaz). *International Union of Geological Sciences Publication of the Institute of Geology*, 20, pp. 167–174.

Löwemark, L. and Nara, M. (2013). Morphological variability of the trace fossil Schaubcylindrichnus coronus as a response to environmental forcing. *Palaeontologia Electronica*, 16 (1), pp. 14. Palaeoelectronica.org/content/2013/382-schaubcylindrichnus

MacEachern, J.A., Bann, K.L., Battacharya, J.P. and Howell, C.D. Jr. (2005). Ichnology of deltas, organism responses to the dynamic interplay of rivers, waves, storms, and tides. In: River Deltas; Concepts, Models and Examples (Eds. L. Giosan and J.P. Bhattacharya). *Society of Sedimentary Geology Special Publication*, 83, pp. 49–85.

MacEachern, J.A. and Bann, K.L. (2008). The role of ichnology in refining shallow marine facies models. In: Recent Advances in Models of Siliciclastic Shallow-Marine Stratigraphy (Eds. G.J. Hampson, R.J. Steel, P.M. Burgess and R.W. Dalrymple). *Society of Sedimentary Geology Special Publication,* 90, pp. 73–116.

MacRae, C.S. (1988). Palynostratigraphic correlation between the lower Karoo sequence of the Waterberg and Pafuri coal-bearing basins and the Hammanskraal plant macrofossil locality, Republic of South Africa. *Memoir of the Geological Survey of South Africa*, 75, pp. 217.

MacRae, C. S. (1992). Age of the Whitehill Formation in the Hopetown area, northeastern Cape Province. *Abstracts of the Seventh Conference of the Paeleontological Society South Africa*, 29.

Madhavaraju, J. and Ramasamy, S. (1999). Rare earth elements in limestones of Kallankurichchi Formation of Ariyalur Group, Tiruchirapalli Cretaceous, Tamil Nadu. *Journal of the Geological Society of India*, 54, pp. 291-301.

Maravelis, A. and Zelilidis, A. (2009). Petrography and geochemistry of the late Eocene-early Oligocene submarine fans and shelf deposits on Lemnos Island, NE Greece. Implications for provenance and tectonic setting. *Geological Journal.* DOI: 10.1002/gj.1183.

Marsh, J.S. (2002). The geophysical mapping of Mesozoic dyke swarms in southern Africa and their origin in the disruption of Gondwana: discussion. *Journal of African Earth Science*, 35, pp. 525–527.

Marsh, J.S., Hooper, P.R., Rehacek, J. and Duncan, A.R. (1997). Stratigraphy and age of Karoo basalts of Lesotho and implications for correlations within the Karoo Igneous Province. In: Large Igenous Provinces: Continental, Oceanic and Planetary Flood Volcanism, Geophysical Monograph (Eds. J.J. Mahoney and M.F. Coffin). *American Geophysical Union*, 100, pp. 247–272.

Martin, H. (1975). Structural and palaeogeographical evidence for an upper Palaeozoic sea between southern Africa and South America. *Proceeding Papers International Union of Geological Sciences 3rd Gondwana Symposium*, pp. 37-51.

Martin, H. (1981a). The Late Palaeozoic Dwyka Group of the South Kalahari Basin in Namibia and Botswana and the subglacial valleys of the Kaokoveld in Namibia. In: Earths pre-Pleistocene glacial record (Eds. M.J. Hambrey and W.B. Harland). Cambridge University Press, New York, pp. 61-66.

Martin, H. (1981b). The Late Palaeozoic Dwyka Group of the Karasburg Basin, Namibia. In: Earths pre-Pleistocene glacial record (Eds. M.J. Hambrey and W.B. Harland). Cambridge University Press, New York, pp. 67-70.

Martin, H. and Wilczewski, N. (1970). Palaeoecology, conditions of deposition and the palaeogeography of the marine Dwyka beds of South West Africa. *Proceeding Papers International Union of Geological Sciences 2nd Gondwana Symposium*, pp. 225-232.

Martino, R. L. (1989). Trace fossils from marginal marine facies of the Kanawa Formation (Middle Pennsylvanian), West Virginia. *Journal of Paleontology*, 63, pp. 389–403.

McCubbin, D.G. (1969). Cretaceous strike-valley sandstone reservoirs, northwestern New Mexico. *American Association of Petroelum Geologists Bulletin*, 53, pp. 2114-2140.

McLachlan, I.R. and Anderson, A.M. (1973). A review of the evidence for marine conditions in Southern Africa during Dwyka times. *Palaeontologia Africana*, 15, pp. 37-64.

McLennan, S.M., Taylor, S.R. and Eriksson, K.A. (1983). Geochemistry of Archaean shales from the Pilbara Supergroup, Western Australia. *Geochimica et Cosmochimica Acta*, 47(7), pp. 1211-1222.

Meckel, L.D. (1975). Holocene sand bodies in the Colorado delta area, northern Gulf of California. In: Deltas Models for Exploration (Ed. M.L. Broussard). *Houston Geological Society*, pp. 239-265.

Miller, R.McG. (1992). Stratigraphy. In: The mineral resources of Namibia, Geological Survey of Namibia, pp. 1.2-1 – 1.2-34.

Miller, R. McG. (2005). Complilation of geological maps of the Stampriet Artisian Basin. Final Report. Ministry of Agriculture, Water and Rural Development, Department of Water Affairs, Republic of Namibia, 20.

Miller, R. McG. (2008). The Geology of Namibia. Palaeozoic to Cenozoic (Volume 3). Ministry of Mines and Energy, Geological Survey, Namibia, pp. 16:1 – 28:13.

Mitrovica, J.X., Beaumont, C., and Jarvis, G.T. (1989). Tilting of continental interiors by the dynamical effects of subduction. *Tectonics*, 8, pp. 1079–1094.

Modie, B.N. (2007). The Palaeozoic Palynostratigraphy of the Karoo Supergroup and palynofacies insight into palaeoenvironmental interpretations, Kalahari Karoo Basin, Botswana. Unpublished PhD Thesis, Universite de Bretagne Occidentale, France, pp. 300.

Moen, H.F.G. (2006). The Olifantshoek Supergroup. In: The Geology of South Africa (Eds. M.R. Johnson, C.R. Anhaeusser and R.J. Thomas). pp. 319-324.

Morsilli, M. and Pomar, L. (2012). Internal waves vs. surface storm waves: a review on the origin of hummocky cross-stratification. *Terra Nova*, 24, pp. 273–282.

Mulder, T. and Syvitski, J.P.M. (1995). Turbidity currents generated at river mouths during exceptional discharges to the ocean: the importance of small mountain rivers. *Journal of Geology*, 100, pp. 525-544.

Myers, K. J. and Wignall, P. B. (1987). Understanding Jurassic organic-rich mudrocks - New concepts using gamma ray spectrometry and palaeoecology: Examples from the Kimmeridge clay of Dorset and the Jet rock of Yorkshire. In: Marine Clastic Sedimentology (Eds. J.K. Leggett and G.G. Zuffa). pp. 1-45.

Nagarajan, R., Armstrong-Altrin, J.S., Nagendra, R., Madhavaraju, J. and Moutte, J. (2007a). Petrography and geochemistry of terrigenous sedimentary rocks in the Neoproterozoic Rabanpalli Formation, Bhima Basin, southern India: Implications for paleoweathering condition, provenance, and source rock composition. *Journal of the Geological Society of India*, 70(2), pp. 297-312.

Nagarajan, R., Madhavaraju, J., Nagendra, R., Armstrong-Altrin, J.S. and Moutte, J. (2007b). Geochemistry of Neoproterozoic shales of Rabanpalli Formation, Bhima Basin, Northern Karnataka, Southern India: Implications for provenance and paleoredox conditions. *Revista Mexicana Ciencias Geológicas*, 24(2), pp. 150-160.

Naish, T. and Kamp, P. (1997), Sequence stratigraphy of 6th order (41 k.y.) Pliocene - Pleistocene cyclothems, Wanganui Basin, New Zealand: a case for the regressive systems tract. *Geological Society of America Bulletin*, 109, pp. 979 – 999.

Nath, B.N., Bau, M., Ramalingeswara Rao, B. and Rao, Ch.M. (1997). Trace and rare earth elemental variation in Arabian Sea sediments through a transect across the oxygen minimum zone. *Geochimica et Cosmochimica Acta*, 61(12), pp. 2375-2388.

Nesbitt, H. W., Young, G. M., McLennan, S. M. and Keays, R. R. (1996). Effects of chemical weathering and sorting on the petrogenesis of siliciclastic sediments, with implications for provenance studies. *Journal of Geology*, 104, pp. 525-542.

Netto, R.G., Tognoli, F.M.W., Assine N.L. and Nara, M. (2014). Crowded Rosselia ichnofabric in the Early Devonian of Brazil: An example of strategic behaviour. *Palaeogeography, Palaeoclimatology, Palaeoecology*, 395, pp. 103-113.

Nielsen, J.K., Hansen, K.S. and Simonsen, L. (1996). Sedimentology and ichnology of the Robbedale Formation (Lower Cretaceous), Bornholm, Denmark. *Bulletin of the Geological Society of Denmark*, 43, pp. 115-131.

North, F.W. (1878). Colonial Mining Engineers Report on the Coalfield of the Stormbergen. Parlimentary Report of the Cape of Good Hope, G47.

Nouidar, M. and Chellai, E.H. (2002). Facies and sequence stratigraphy of a Late Barremian wave dominated deltaic deposit, Agadir Basin, Morocco. *Sedimentary Geology*, 150, pp. 375–384.

Nxumalo, V. (2011). Stratigraphy and basin modelling of the Gemsbok sub-basin (Karoo Supergroup) of Botswana and Namibia. Unpublished MSc Thesis, University of the Witwatersrand, Johannesburg.

Oelofsen, B.W. (1981). An anatomical and systematic study of the family Mesosauridae (Reptilia; Proganosauria) with special reference to its associated fauna and paleoecological environment in the Whitehill Sea. Unpublished PhD Thesis, University of Stellenbosch, Stellenbosch, pp. 163.

Oelofsen, B.W. and Araujo, D.C. (1983). Palaeoecological implications of the distribution of Mesosaurid reptiles in the Permian Irati Sea (Parana Basin), South America. *Revista Brasileira de Geociências*, 13(1), pp. 1-16.

Oelofsen, B. W. and Araujo, D. C. (1987). Mesosaurus tenuidens and Stereosternum tumidum from the Permian Gondwana of both southern Africa and South America. *South African Journal Science*, 83, pp. 370.72

Oomkens, E. (1970). Depositional sequences and sand distribution in the postglacial Rhone delta complex. In: Deltaic Sedimentation Modern and Ancient (Ed. J.P. Morgan). *Society for Sedimentary Geology Special Publication*, 15, pp. 198-212.

Oliveira, C.M.M., David M. Hodgson, D.M. and Flint, S.S. (2011). Distribution of soft-sediment deformation structures in clinoform successions of the Permian Ecca Group, Karoo Basin, South Africa. *Sedimentary Geology*, 235, pp. 314–330.

Pattison, S.A.J. (1995). Sequence stratigraphic significance of sharp-based lowstand shoreface deposits, Kenilworth Member, Book Cliffs, Utah. *American Association of Petroleum Geologists Bulletin*, 79, pp. 444–462.

Pattison, S.A.J. (2005a). Storm-influenced prodelta turbidite complex in the lower Kenilworth Member at Hatch Mesa, Book Cliffs, Utah, USA; implications for shallow marine facies models. *Journal of Sedimentary Res*earch, 75, pp. 420–439.

Pattison, S.A.J. (2005b). Isolated shelf sandstone body of turbiditic origin, lower Kenilworth Member, Cretaceous Western Interior, Book Cliffs, Utah, USA. *Sedimentary Geology*, 177, pp. 131–144.

Pattison, S.A.J., Ainsworth, R.B. and Hoffman, T.A. (2007a). Evidence of across-shelf transport of fine-grained sediments: turbidite-filled shelf channels in the Campanian Aberdeen Member, Book Cliffs, Utah, USA. *Sedimentology*, 54, pp. 1033– 1064.

Pemberton, S.G. and Frey, R.W. (1982). Trace fossil nomenclature and the Planolites-Palaeophycus dilemma. *Journal of Paleontology*, 56, pp. 843-871.

Pemberton, S. G., MacEachern, J. A. and Frey, R W. (1992). Trace fossil facies models: environmental and allostratigraphic significance. In: Facies Models - Response to Sea Level Change (Eds. R.G. Walker and N.P. James). *Geological Association of Canada*, pp. 47-72.

Pettijohn, F.J. (1954). Classification of Sandstones. *The Journal of Geology*, 62 (4), pp. 360-365.

Pettijohn, F.J. (1975). Sedimentary Rocks (3rd ed.) Harper & Bros., New York.

Pettijohn, F.J., Potter, P.E. and Siever, R. (1987). Sand and Sandstone. Springer-Verlag, New York. pp. 533.

Pickford, M. (1995). Karoo Supergroup palaeontology of Namibia and brief description of a Thecodont from Omigonde. *Palaeontologia Africana*, 32, pp. 51-66.

Posamentier, H. and Allen, G. (1999). Siliciclastic sequence stratigraphy - concepts and applications. *Society for Sedimentary Geology Concepts in Sedimentology and Paleontology*, 7, pp. 210.

Pysklywec, R.N. and Mitrowica, J.X. (1999). The role of subduction-induced subsidence in the evolution of the Karoo Basin. *Journal of Geology*, 107, pp. 155-164.

Range, P. (1912). Geologie des deutschen Namalandes. *Beiträge zur geologischen Erforschung der Deutschen Schutzgebiet*, 2, pp. 1-104.

Reeves, C. V. (1978). Reconnaissance Aeromagnetic survey of Botswana 1975 - 1977. Final Interpretation Report. Geological Survey Department, Botswana, 84.

Reineck, H.E. and Singh, I.B. (1973). Depositional sedimentary environments. Springer-Verlag, New York, 439 pp.

Reynolds, A.D. (1999). Dimensions of paralic sandstone bodies. *American Association of Petroleum Geologists Bulletin*, 83, pp. 211–229.

Rimmer, S.M. (2004). Geochemical paleoredox indicators in Devonian- Mississippian black shales, central Appalachian Basin (U.S.A.). *Chemical Geology*, 206, pp. 373－391.

Roberts, D.L. (1986). Depositional framework and controls on peat accumulation in the Vryheid Formation of northern Natal (Utrecht and Newcastle areas). Unpublished PhD Thesis, Natal University, Durban, pp. 233.

Roser, B. P. and Korsch, R. J. (1986). Determination of tectonic setting of sandstone-mudstone suites using SiO2 content and K2O/Na2O ratio. *Journal of Geology*, 94, pp. 635-650.

Rubidge, R.N. (1858). Notes on the geology of some parts of South Africa. *Quarterly Journal of the Geological Society of London* ,12, pp. 237–238.

Rubidge, B.S., Hancox, P.J. and Catuneanu, O. (2000). Sequence analysis of the Ecca-Beaufort contact in the southern Karoo of South Africa. *South African Journal of Science*, 103, pp. 81-96.

Rust, I.C. (1975). Tectonic and sedimentary framework of Gondwana basins in southern Africa. In: Gondwana Geology (Ed. K.S.W. Campbell). Australian National University Press, Canberra, pp. 537–564.

Ryan, P.J. (1967).Stratigraphic and palaeocurrent analysis of the Ecca Series and lowermost Beaufort Beds in the Karoo Basin of South Africa. Unpublished PhD Thesis, University of the Witwatersrand, Johannesburg, pp. 210.

SACS (1980). South African Commitee for Stratigraphy: Stratigraphy of South Africa. Part 1 (Comp. Kent, L.E.) Lithostratigraphy of the Republic of South Africa, South West Africa/Namibia, and the Republics of Bophuthatswana, Transkei and Venda. *Handbook of the Geological Survey of South Africa*, 8, pp. 690.

Santos, P.R.d., Rocha-Camos, A.C. and Canuto, J.R. (1996). Patterns of late Palaeozoic deglaciation in the Paraná Basin, Brazil. *Palaeogeography, Palaeoclimatology, Palaeoecology*, 125, pp. 165-184.

Schalk, K.E.L. and Germs, G.J.B. (1980). The geology of the Mariental area. Explanation of Sheet 2416 Scale 1:250000. Geological Survey of South West Africa/Namibia, 7.

Scheffler, K., Hoernes, S. and Schwark, L. (2003). Global changes during Carboniferous–Permian glaciation of Gondwana: Linking polar and equatorial climate evolution by geochemical proxies. *Geology*, 31, pp. 605–608.

Scheffler, K., Buehmann D. and Schwark L. (2006). Analysis of late Palaeozoic glacial to postglacial sedimentary successions in South Africa by geochemical proxies – Response to climate evolution and sedimentary environment. *Palaeogeography, Palaeoclimatology, Palaeoecology*, 240, pp. 184–203.

Schreuder, C.P. and Genis, G. (1975). Die Geologie van die Karasburgse Karookom. *Annals of the Geological Survey of South Africa*, 10, pp. 7-22.

Segwabe, T. (2008). The geological framework and depositional environments of the coal-bearing Karoo strata in the Central Kalahari Karoo Basin, Botswana. Unpublished MSc Thesis, Rhodes University, Grahamstown, South Africa.

Seiberits, L.B. (1987). Die sedimentology van die Formasie Carnarvon in die omgewing van Carnarvon. Unpublished MSc Thesis, University of Port Elizabeth, pp. 92.

Seilacher, A. (1953a). Studien zur Palichnotogie.-N. Jb. *Geology*, *Mineralogy*, *Palaont*ology, 96, pp. 421-452.

Seilacher, A. (1977). Pattern analysis of Paleodictyon and related trace fossils. In: Trace Fossils 2 (Eds. T.P Crimes and J.C. Harper). *Geological Journal*, 9, pp. 289-334.

Seilacher, A. (2007). Trace Fossil Analysis. Springer-Verlag, Berlin.

Sinha, S., Islam, R., Ghosh, S.K., Rohtash Kumar and Sangode, S.J. (2007). Geochemistry of Neogene Siwalik mudstones along Punjab re-entrant, India: Implications for source area weathering, provenance and tectonic setting. *Current Science*, 92 (8), pp. 1103-1113.

Smith, R. A. (1984). The lithostratigraphy of the Karoo Supergroup in Botswana. Geological Survey Department, Botswana, 26, pp. 239.

Smith, R.M.H., Eriksson, P.G. and Botha, W.J. (1993). A review of the stratigraphy and sedimentary environments of the Karoo-aged basins of Southern Africa. *Journal of African Earth Sciences*, 16, pp. 143-169.

Somayajulu, B.L.K., Yadav, D.N. and Sarin, M.M. (1994). Recent sedimentary records from the Arabian Sea. *Proceedings of the Indian Academy of Sciences*, 103(2), pp. 315-327.

Stevens, K. (2004). Re-evaluating the origin of isolated sandstones encased in marine mudstone: the Cretaceous Prairie Canyon Member of the Mancos Shale at Hatch Mesa, eastcentral Utah. Unpublished MSc Thesis, Colorado School of Mines, 124 pp.

Stollhofen, H. (1999). Karoo Synrift-Sedimentation und ihre tektonische Kontrolle am entstehenden Kontinentalrand Namibias. *Zeitschrift der deutschen geologischen Gesellschaft*, 149, pp. 519-632.

Stollhofen, H., Werner, M., Stanistreet, I.G. and Armstrong, R.A. (2008). Single-zircon U-Pb dating of Carboniferous- Permian tuffs, Namibia, and the intercontinental deglaciation cycle framework. In: Resolving the Late Paleozoic Ice Age in Space and Time (Eds. C.R. Fielding, T.D. Frank and J. Isbell). *Geological Society of America Special Paper*, 441, pp. 83-96.

Stow, D. A. V. and Bowen, A. J. (1978). Origin of lamination in deep sea, fine-grained sediments. *Nature*, 274, pp. 324-328.

Stratten, T. (1977). Conflicting directions of Dwyka ice flow in the Western Cape Province and southern South West Africa. *Transactions of the Geological Society of South Africa*, 80, pp. 79-86.

Suttner, L. J., Basu, A. and Mack, G. H. (1981). Climate and the origin of quartz arenites. *Journal of Sedimentary Petrology*, 51, pp. 1235–1246.

Tanner, W.F. (1967). Ripple mark indices and their uses. *Sedimentology*, 9, pp. 89-104.

Tavener-Smith, R., Mason, T.R., Christie, A.D.M., Roberts, D.L., Smith, A.M. and Van der Spuy, A. (1988). Sedimentary models for coal formation in the Vryheid Formation, Northern Natal. *Bulletin of the Geological Survey of South Africa*, 94, pp. 1–46.

Taylor, S. R. and McLennan, S. M. (1985). The continental crust: its composition and evolution. Blackwell Scientific Publications, Oxford, UK.

Taylor, S. R. and McLennan, S. M. (1991). Sedimentary rocks and crustal evolution: tectonic setting and secular trends. *The Journal of Geology*, pp. 1-21.

Taylor, D.R. and Lovell, R.W.W. (1995). High-frequency sequence stratigraphy and paleogeography of the Kenilworth Member, Blackhawk Formation, Book Cliffs, Utah, USA. In: Sequence Stratigraphy of Foreland Basin Deposits: Outcrop and Subsurface Examples from the Cretaceous of North America (Eds. J.C. Van Wagoner and G.T. Bertram), *American Association of Petroleum Geologists Memoir*, 64, pp. 257–275.

Terblanche, J.C. (1979). Die geologie van ‘n gebied oos van Carnarvon. Unpublished MSc Thesis, University of the Orange Free Statae, Bloemfontein, pp. 161.

Tiwari, R.P., Rajkonwar, C., Lalchawimawii, Malsawma, P.L.J., Ralte, V.Z. and Patel, S.J. (2011). Trace fossils from Bhuban Formation, Surma Group (Lower to Middle Miocene) of Mizoram India and their palaeoenvironmental significance. *Journal of Earth System Sci*ence, 120 (6), pp. 1127–1143.

Tortosa, A., Palomares, M. and Arribas, J. (1991). Quartz grain types in Holocene deposits from the Spanish Central System: some problems in provenance analysis. In: Developments in Sedimentary Provenance Studies (Eds. A.C. Morton, S.P. Todd and P.D.W. Haughton). *Geological Society of London Special Publication*, 57, pp. 47–54.

Traykovski, P., Wiberg, P.L. and Geyer, W.R. (2005). Observations and modelling of wave-supported sediment gravity flows on the Po prodelta and comparison to prior observations from the Eel shelf. *Continental Shelf Research*, 27, pp. 375-399.

Tribovillard, N., Algeo, T.J., Lyons, T. and Riboulleau, A. (2006). Trace metals as paleoredox and paleoproductivity proxies: An update. *Chemical Geology*, 232, pp. 12–32.

Tucker, M. E. (2011). Sedimentary rocks in the field: a practical guide. John Wiley and Sons, 32.

Turner, B. R. (1999). Tectonostratigraphical development of the Upper Karooforeland basin: Orogenic unloading versus thermally-induced Gondwana rifting. *Journal of African Earth Sciences*, 28(1), pp. 215-238.

Vakarelov, B.K., Ainsworth, R.B. and MacEachern, J.A. (2012). Recognition of wave-dominated, tide-influenced shoreline systems in the rock record: Variations from a microtidal shoreline model. *Sedimentary Geology*, 279, pp. 23–41.

Van de Kamp, P.C. and Leake, B.E. (1995). Petrology and geochemistry of siliciclastic rocks of mixed feldspathic and ophiolitic provenance in the Northern Apennines, Italy. *Chemical Geology*, 122, pp. 1-20.

Van der Werff, W. and Johnson, S.D. (2003). Deep-sea fan pinch-out geometries and their relationship to fan architecture, Tanqua Karoo Basin (South Africa). *International Journal of Earth Sciences*, 92, pp. 728-742.

Van Loon, A.J. (2009). Soft-sediment deformation structures in siliciclastic sediments: an overview. *Geologos*, 15 (1), pp. 3–55.

Van Wagoner, J.C., Mitchum, R.M., Campion, K.M. and Rahmanian, V.D. (1990). Siliciclastic Sequence Stratigraphy in Well Logs, Cores, and Outcrops. *American Association of Petroleum Geologists Methods in Exploration*, 7, pp. 55.

Van Rooy, J.L. (1991). The durability characteristics and testing of Drakensberg basalts. Unpublished PhD Thesis, University of Pretoria, pp. 182.

Veevers, J.J., Clare, A. and Wopfner, H. (1994a). Neocratonic magmatic sedimentary basins of post-Variscan Europe and post-Kanimblan eastern Australia generated by right-lateral transtension of Permo-Carboniferous Pangea. *Basin Research*, 6, pp. 141–157.

Veevers, J.J., Powell, C.McA., Collinson, J.W. and Lopez-Gamundi, O.R. (1994b). Synthesis. In: Permian-Triassic Pangean Basins and Foldbelts along the Panthalassan Margin of Gondwanaland (Eds. J.J. Veevers and C.McA. Powell). *Geological Society of America*, 184, pp. 331–353.

Veevers, J.J., Cole, D.I. and Cowan, E.J. (1994c). Southern Africa: Karoo basin and Cape Fold Belt. In: Permian- Triassic Pangean Basins and Foldbelts along the Panthalassan Margin of Gondwanaland (Eds. J.J. Veevers and C.McA. Powell). *Geological Society of America*, 184, pp. 223–279.

Versfeld, W. (1914). The geological structure of portions of German South-West Africa. *South Africa Journal of Science*,10, pp. 187-238.

Visser, J.N.J. (1982). Implications of a diachronous contact between the Dwyka Formation and Ecca Group in the Karoo Basin. *South Africa Journal of Science*, 78, pp. 249-251.

Visser, J.N.J. (1983a). An analysis of the Permo-Carboniferous glaciation in the marine Kalahari Basin, Southern Africa. *Palaeogeography, Palaeoclimatology, Palaeoecology*, 44, pp. 295-315.

Visser, J.N.J. (1983b). Glacial-marine sedimentation in the Late Paleozoic Karoo Basin, southern Africa. In: Glacial-marine sedimentation (Ed. B.F. Molnia). Plenum Press, New York, pp. 667-701.

Visser, J.N.J. (1987). The palaeogeography of part of southwestern Gondwana during the Permo-Carboniferous glaciation. *Palaeogeography, Palaeoclimatology, Palaeoecology*, 61, pp. 205–219.

Visser, J.N.J. (1990). The age of the late Palaeozoic glacigene deposits in southern Africa. *South African Journal of Geology*, 93, pp. 366–375.

Visser, J.N.J. (1991a). Geography and climatology of the Late Carboniferous to Jurassic Karoo Basin in south-western Gondwana. *Annals of the South African Museum*, 99, pp. 415–431.

Visser, J.N.J. (1991b). The paleoclimatic setting of the Late Paleozoic marine ice sheet in the Karoo Basin of Southern Africa. In: Glacial Marine Sedimentation: Paleoclimatic Significance (Eds. J.B. Anderson and G.M. Ashley). *Geological Society of America Special Paper*, 261, pp. 181–189.

Visser, J.N.J. (1992a). Basin tectonics in southwestern Gondwana during the Carboniferous and Permian. In: Inversion Tectonics of the Cape Fold Belt, Karoo and Cretaceous Basins of Southern Africa (Eds. M.J. de Wit and I.G.D. Ransome). Balkema, Rotterdam, pp. 109–115.

Visser, J.N.J. (1992b). Deposition of the early to Late Permian Whitehill Formation during a sea-level highstand in a juvenile foreland basin. *South African Journal of Geology*, 95, pp. 181–193.

Visser, J.N.J. (1993). Sea-level changes in a back-arc-foreland transition: the late Carboniferous-Permian Karoo Basin of South Africa. *Sedimentary Geology*, 83, pp. 115-131.

Visser, J.N.J. (1997). Deglaciation sequences in the Permo-Carboniferous Karoo and Kalahari basins of southern Africa: a tool in the analysis of cyclic glaciomarine basin fills. *Sedimentology*, 44, pp. 507–521.

Visser, J.N.J. and Kingsley, C.S. (1982). Upper Carboniferous glacial valley sedimentation in the Karoo Basin, Orange Free State. *Transactions of the Geological Society of South Africa*, 85, pp. 71-79.

Visser, J.N.J. and Praekelt, H.E. (1996). Subduction, mega-shear systems and Late Palaeozoic basin development in the African segment of Gondwana. *Geologische Rundschau*, 85, pp. 632-646.

Visser, J.N.J. and Praekelt, H.E. (1998). Late Palaeozoic crustal block rotations within the Gondwana sector of Pangea. *Tectonophysics*, 287, pp. 201-212.

Wagner, P.A. (1915). The Dwyka Series in South-West Africa. *Transactions of the Geological Society of South Africa*, 18, pp. 102-117.

Walker, R.G., Plint, A.G., (1992). Wave and storm-dominated shallow marine systems. In: Facies Models: Response to Sea-Level Change (Eds. R.G. Walker and N.P. James). *Geological Association of Canada*, pp. 219–238.

Walker, R. G., Duke, W. L. and Leckie, D. A. (1983). Hummocky stratification: Significance of its variable bedding sequences: Discussion and reply Discussion. *Geological Society of America Bulletin*, 94(10), pp. 1245-1249.

Wanas, H.A. and Abdel-Maguid, N.M. (2006). Petrography and geochemistry of the Cambro-Ordovician Wajid Sandstone, southwest Saudi Arabia: Implications for provenance and tectonic setting. *Journal of Asian Earth Science*, 27 (4), pp. 416-429.

Wang, Y., Lin, J. P., Zhao, Y. L. and Orr, P. J. (2009). Palaeoecology of the trace fossil Gordia and its interaction with nonmineralizing taxa from the early Middle Cambrian Kaili Biota, Guizhou Province, South China. *Palaeogeography Palaeoclimatology, Palaeoecology*, 277, pp. 141–148.

Weimer, R.J. (1970). Rates of deltaic sedimentation and intrabasin deformation, Upper Cretaceous of Rocky Mountain region. In: Deltaic Sedimentation Modern and Ancient (Ed. J.P. Morgan). *Society for Sedimentary Geology Special Publication*, 15, pp. 270—292.

Werner, M. (2006). The stratigraphy, sedimentology, and age of the Late Palaeozoic Mesosaurus Inland Sea, SW-Gondwana. Unpublished PhD Thesis, University of Würzburg.

Werner, M., Stanistreet, I.G. and Stollhofen, H. (2002). Tracing the Whitehill Fm. (Karoo Supergroup) into Namibia: a combined lithostratigraphic, biostratigraphic, tephrostratigraphic, and sequence-stratigraphic approach. *Abstracts of the 16th International Sedimentology Congress*, pp. 399-400.

Wickens, H. de V. (1994). Basin floor fan building turbidites of the southwestern Karoo Basin, Permian Ecca Group, South Africa. Unpublished PhD Thesis, University of Port Elizabeth, pp. 223.

Wickens, H. de V. (1996). Die stratigrafie en sedimentologie van die Groep Ecca wes van Sutherland. *Bulletin of the Geolological Survey of South Africa*, 107, pp. 49.

Wignall. P. B. (1994). Black Shales. Oxford University Press, New York.

Wignall, P. B. and Myers, K. J. (1988). Interpreting benthic oxygen levels in mudrocks: a new approach. *Geology*, 16(5), pp. 452-455.

Wignall, P.B. and Twitchett, R.J. (1996). Oceanic anoxia and the end Permian mass extinction. *Science*, 272, pp. 1155－1158.

Wild, R.J. (2005). Sedimentological and sequence stratigraphic evolution of a Permian Lower Slope to Shelf Succession, Tanqua Depocentre, SW Karoo Basin, South Africa. Unpublished PhD Thesis, University of Liverpool, 350 pp.

Wilson, E.O. (1971). The Insect Societies. Belknap Press, Cambridge. pp. 548.

Woodland, A.W. (1938). Petrologicla studies in Harlech Grit series of Merionethshire II. *Geological Magazine*, 74, pp. 440-454.

Wopfner, H. (1993). Structural development of Tanzanian Karoo basins and the break-up of Gondwana. *Proceedings of the Eighth Gondwana Symposium,* pp. 531–539.

Wopfner, H. (1994). The Malagasy Rift, a chasm in the Tethyan margin of Gondwana. *Journal of Southeast Asian Earth Science*, 9, pp. 451–461.

Wopfner, H. (2002). Tectonic and climatic events controlling deposition in Tanzanian Karoo basins. *Journal of African Earth Sciences*, 34, pp. 167–177.

Wright, M. E. and Walker, R. G. (1981). Cardium Formation (Upper Cretaceous) at Seebee, Alberta-storm transported sandstone and conglomerate in shallow marine depositional environments below fair weather wave base. *Canadian Journal of Earth Science*, 8, pp. 794-809.

Wunderlich, F. (1970). Genesis and environment of the'Nellenkoepfchenschichten' (lower Emsian, Rheinian Devon) at locus typicus in comparison with modern coastal environment of the German Bay. *Journal of Sedimentary Research*, 40, pp. 102-130.

Yokokawa, M. (1995). Combined-flow ripples: genetic experiments and applications for geologic records: Kyushu University. *Memoirs of the Faculty of Science, Series D, Earth and Planetary Sciences,* 29, pp. 1–38.

Chapter 7: Appendices

Appendix A

	98
	76
	101
	100
	59
	143
	105
	100
	93
	90
	102
	100
	98
	97
	43
	165
	120
	100
	98
	67
	98
	96
	79
	85
	80
	90
	90
	100
MEAN	**95**

Table 7.1. Corrected palaeocurrents obtained from asymmetric ripples.

	34	214
	119	299
	86	266
	71	251
	128	308
	125	305
	49	229
	80	260
	119	299
	59	239
	34	214
	109	289
	123	303

	119	299
	149	329
	60	240
	103	283
	53	233
	99	279
	139	319
	109	289
	119	299
	99	279
	114	294
	179	359
	114	294
	114	294
	114	294
	69	249
	124	304
	93	273
	89	269
	124	304
	124	304
	109	289
	99	279
	69	249
	129	309
	119	299
	139	319
	119	299
	129	309
	79	259
	99	279
	89	269
	109	289
	109	289
	114	294
	96	276
	98	278
	55	235
	131	311
	105	285
	109	289
	115	295
	110	290
	119	299
	59	239
	129	309
	129	309
	104	284

	84	264
	79	259
	114	294
	84	264
	89	269
	99	279
	139	319
	79	259
	89	269
	79	259
	69	249
	99	279
	29	209
	100	280
	112	292
	98	278
	67	247
	79	259
	89	269
	97	277
	90	270
	100	280
	101	281
	100	280
	102	282
	103	283
	110	290
	111	291
	98	278
	99	279
	100	280
	103	283
	102	282
	105	285
	109	289
	130	310
	98	278
	141	321
	121	301
	113	293
	104	284
	105	285
	104	284
	101	281
	110	290
MEAN	**101**	**281**

Table 7.2. Corrected palaeocurrents obtained from symmetric ripples.

Appendix B

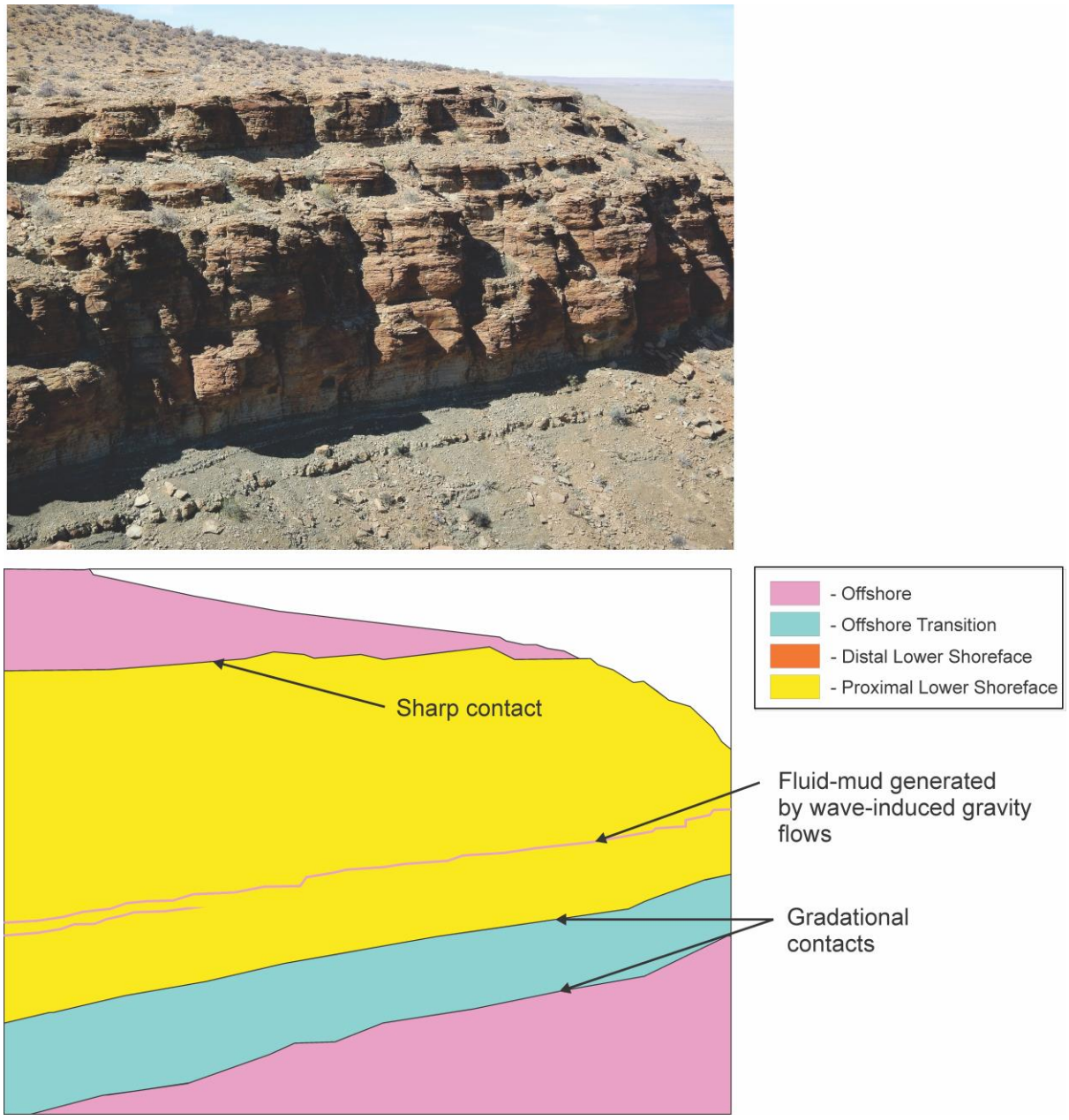


Figure 7.1. Lowermost pLSF desposit in the study area.

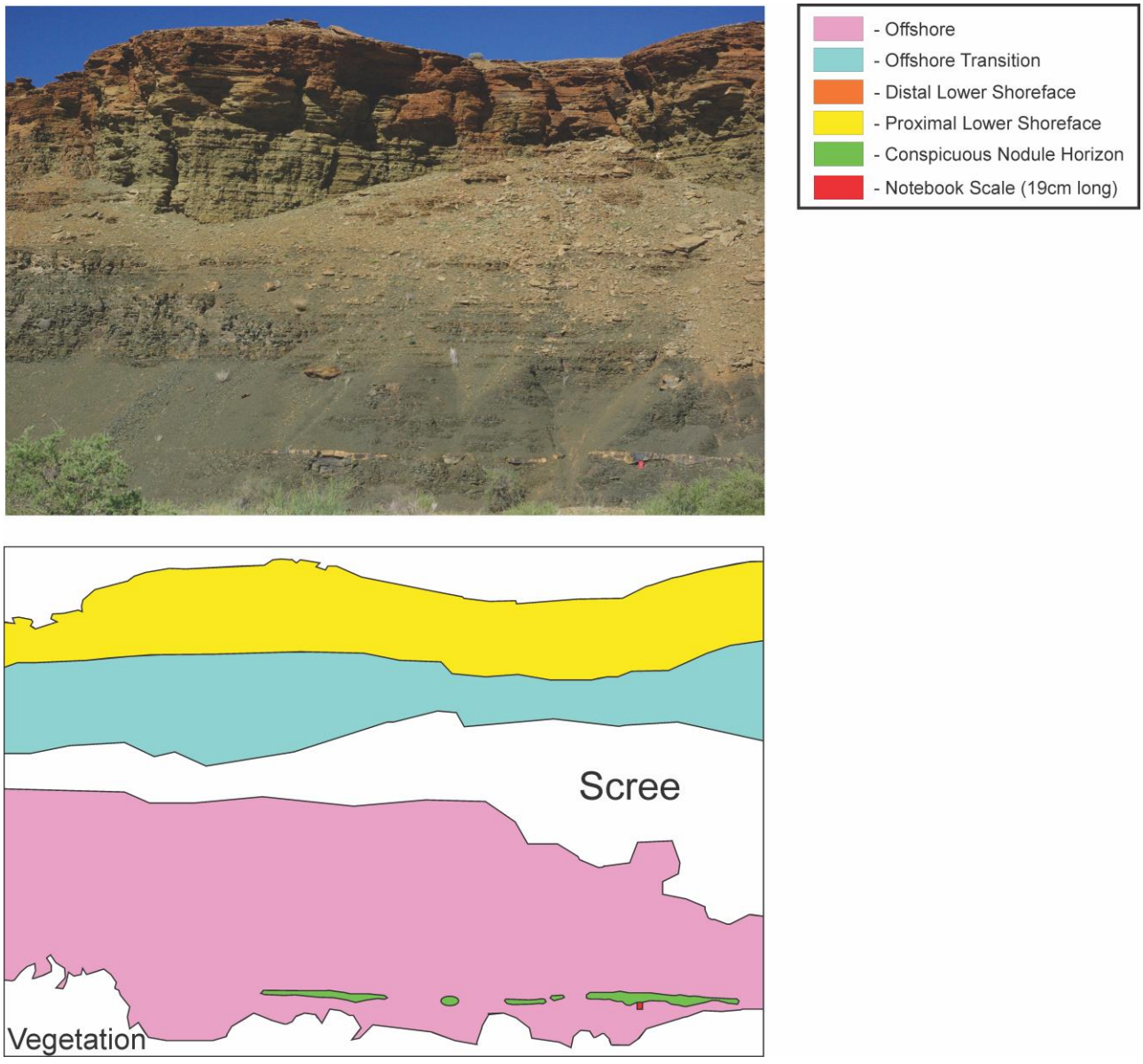


Figure 7.2. Second lowest pLSF deposit in the study area.

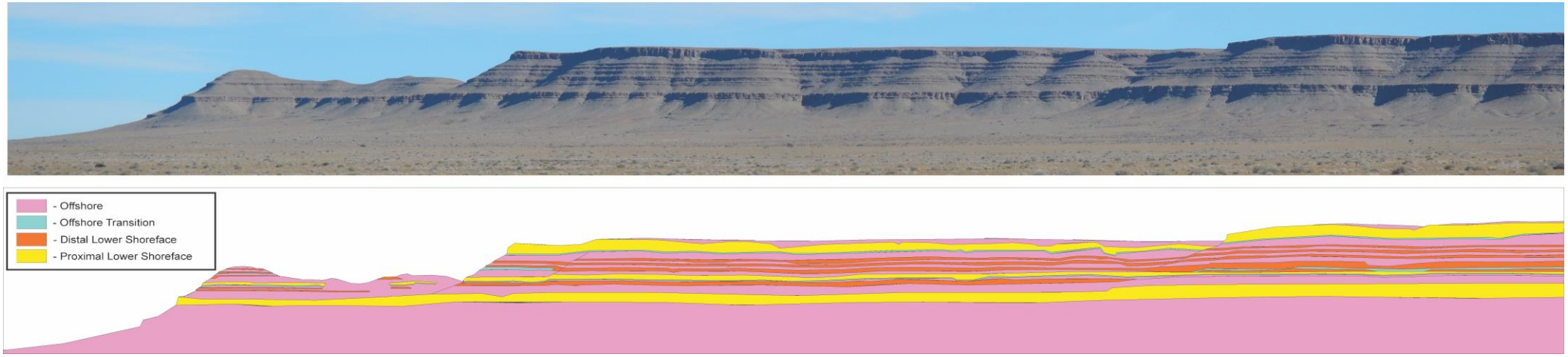


Figure 7.3. Interpreted photomosaic of the Amibberg Massif.

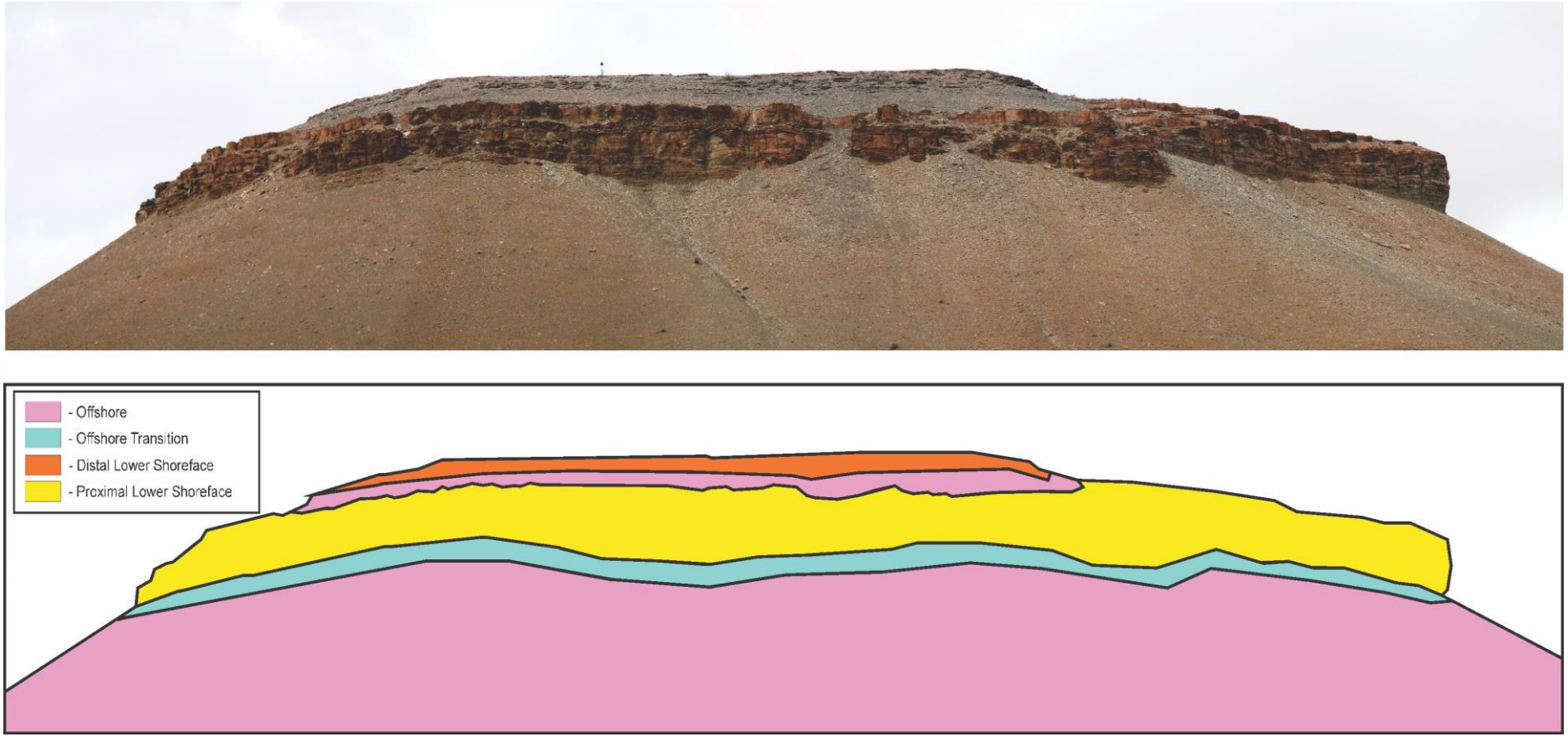


Figure 7.4. Interpreted photomosaic of the uppermost pLSF deposit in the study area.

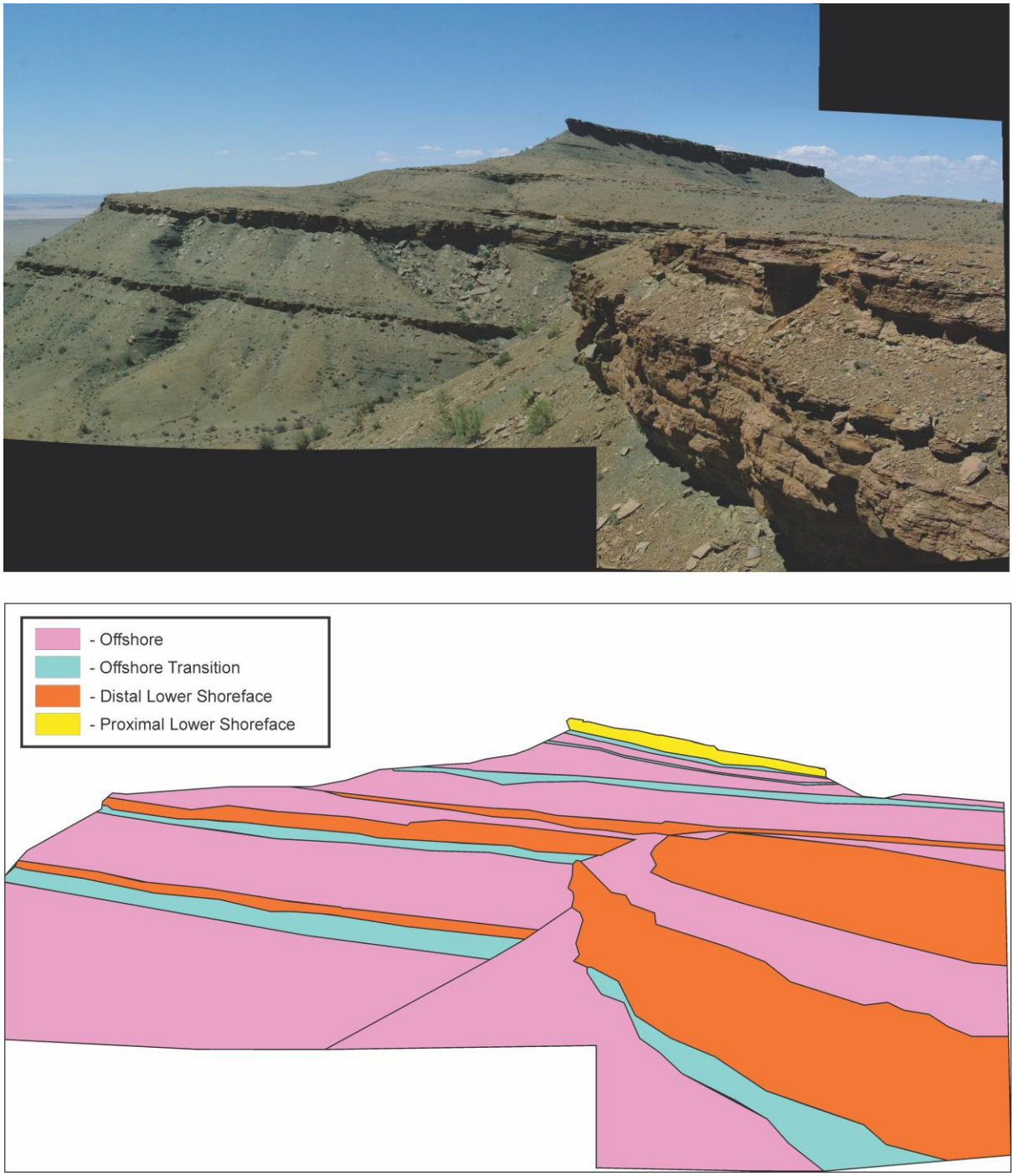


Figure 7.5. Interpreted photomosaic of the Tafelberg locality.

Appendix C

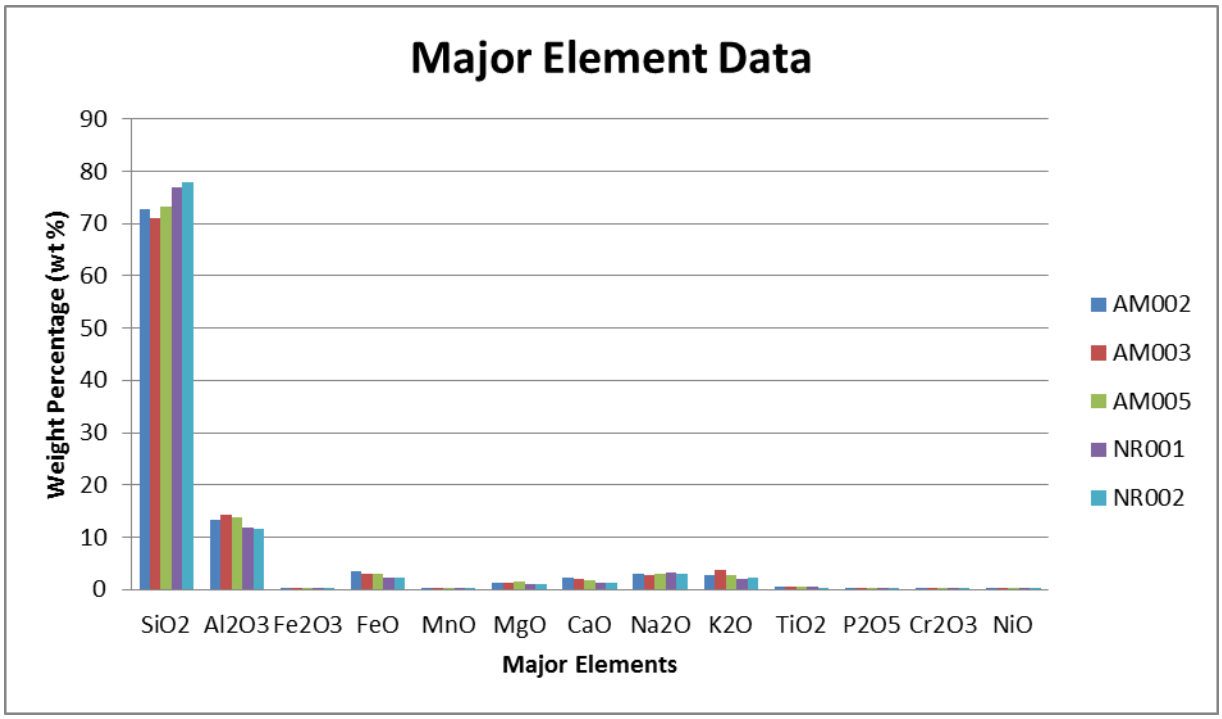


Figure 7.6. Bar graph showing weight percentage of various major elements from mudstones.

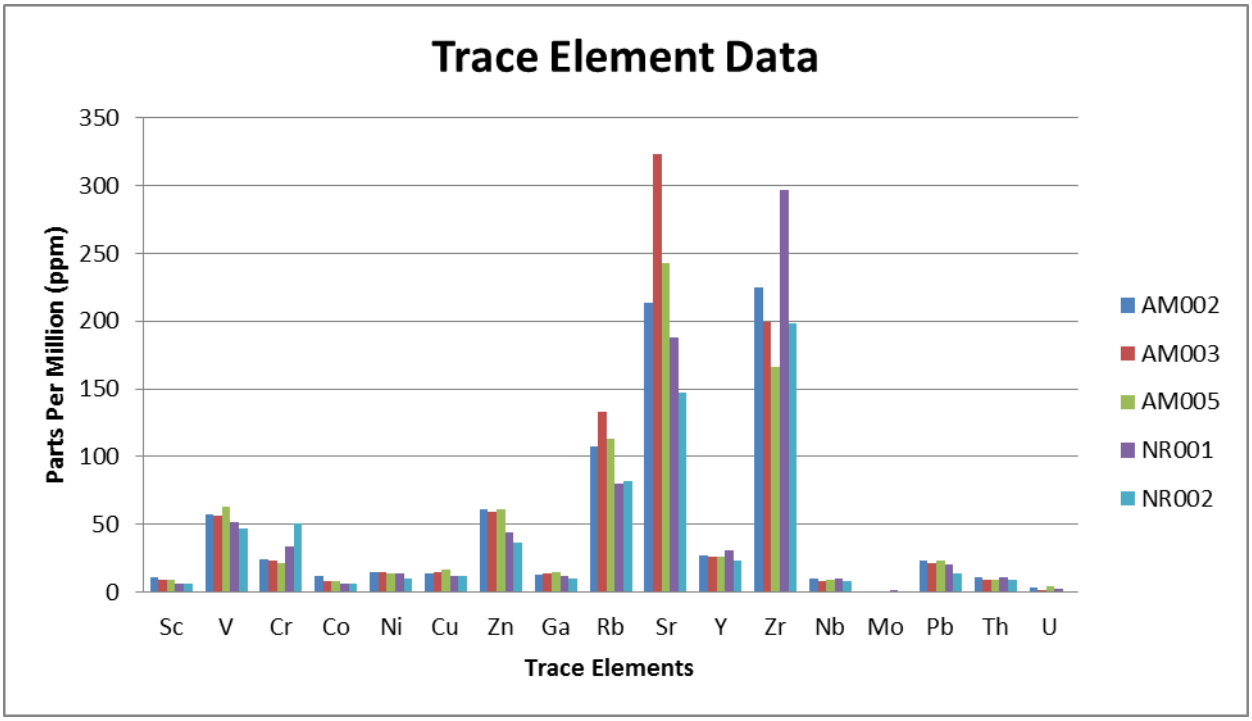


Figure 7.7. Bar graph of various trace elements (in ppm) from mudstones.

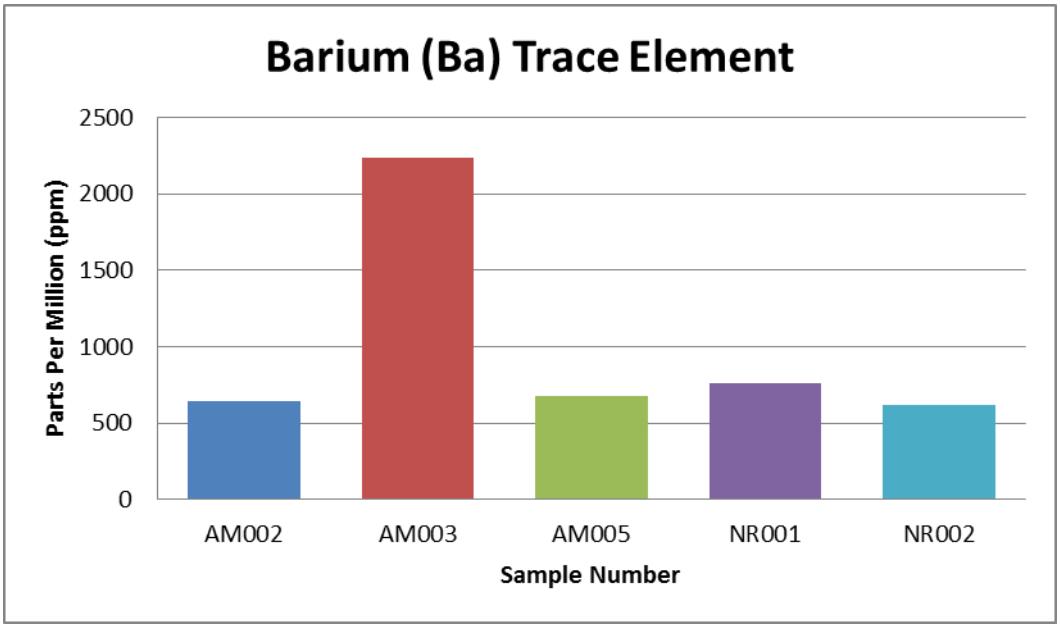


Figure 7.8. Bar graph showing Barium (in ppm) for various mudstone samples.

Sample Number	SiO2	Al2O3	Fe2O3	FeO	MnO	MgO	CaO	Na2O	K2O	TiO2	P2O5	Cr2O3	NiO	TOTAL	LOI
AM002	72.75	13.41	0.42	3.41	0.06	1.4	2.16	3.09	2.73	0.5544	0.18	0.0078	0.0035	100.18	3.2
AM003	71.12	14.32	0.37	3.02	0.06	1.38	2.13	2.86	3.84	0.4612	0.15	0.0041	0.0005	99.72	3.29
AM005	73.18	13.7	0.38	3.12	0.06	1.43	1.88	3.08	2.83	0.4903	0.17	0.0029	0.0017	100.32	3.04
NR001	77.01	11.96	0.29	2.36	0.05	0.99	1.24	3.34	2.12	0.5115	0.17	0.0052	0.0009	100.06	2.18
NR002	77.88	11.57	0.28	2.23	0.03	0.95	1.35	3.09	2.18	0.4268	0.11	0.0096	-0.0003	100.11	2.37

Table 7.3. Major element geochemistry for mudstones of the upper Aussenkjer Formation and the Amibberg Formation.

Sample Number	Sc	V	Cr	Co	Ni	Cu	Zn	Ga	Rb	Sr	Y	Zr	Nb	Mo	Ba	Pb	Th	U
AM002	11.21	57.62	24.41	11.93	14.79	13.47	61.42	13.35	107.63	213.21	26.85	224.93	9.73	0.3	644.91	23.35	10.88	3.1
AM003	9.36	56.27	23.22	8.21	14.67	15.07	59.5	14.23	133.18	322.73	26	199.52	8.02	0.61	2238.6	21.93	9.08	1.66
AM005	8.77	63.3	21.91	8.07	13.52	17.06	60.97	14.39	112.75	242.93	26.24	166.52	8.99	0.31	678.56	23.33	9.26	4.05
NR001	6.42	51.28	33.52	6.6	13.6	12.18	43.99	11.63	79.97	188.32	30.49	296.51	10.01	1.6	765.67	20.71	11.48	2.91
NR002	6.23	46.56	50.4	6.48	10.21	12.01	36.51	10	81.95	147.68	23.47	198.02	7.83	0.56	621.26	13.9	9.16	0.81

Table 7.4. Trace element geochemistry for mudstones of the upper Aussenkjer Formation and the Amibberg Formation.

		Normalized		Normalized		Normalized		Percent of Whole	Pettijohn (1975)
	Quartz	Quartz	Feldspar	Feldspar	Lithics	Lithics	Clay Matrix	Clay Matrix	
148SSA	197	96	8	4	0	0	104	30	Quartz wacke
148SSB	173	92	15	8	0	0	88	25	Feldspathic wacke
148SSC	181	94	12	6	0	0	96	27	Feldspathic wacke
148SSD	201	96	8	4	0	0	84	24	Quartz wacke
148SSE	164	91	16	9	0	0	94	27	Feldspathic wacke
148SSF	191	90	21	10	0	0	100	29	Feldspathic wacke
148SSG	227	95	12	5	0	0	80	23	Quartz wacke
148CCB	211	93	16	7	0	0	95	27	Feldspathic wacke
148SIS	148	96	6	4	0	0	138	39	Quartz wacke
158PLATSSTOP1	212	95	10	5	0	0	97	28	Quartz wacke
228DNEUS2SS1	188	85	34	15	0	0	92	26	Feldspathic wacke
228DNEUS2SS2	176	91	18	9	0	0	108	31	Feldspathic wacke
SAMPLE178	105	100	0	0	0	0	178	51	Quartz wacke
178JAGDSS1	220	93	17	7	0	0	74	21	Feldspathic wacke
178JAGDSS2	207	96	9	4	0	0	98	28	Quartz wacke
178JAGDSS3	189	96	7	4	0	0	112	32	Quartz wacke
178JAGDSS4	174	94	12	6	0	0	99	28	Feldspathic wacke
178JADGSS5	194	96	9	4	0	0	102	29	Quartz wacke
178JAGDSS6	196	92	16	8	0	0	85	24	Feldspathic wacke
178JAGDSS7	206	93	16	7	0	0	94	27	Feldspathic wacke
178JAGDSS8	189	94	13	6	0	0	102	29	Feldspathic wacke
178JAGDSS9	168	97	5	3	0	0	112	32	Quartz wacke
178JAGDSS10	176	95	10	5	0	0	130	37	Quartz wacke
178JAGDSS11	137	96	5	4	0	0	161	46	Quartz wacke
178JAGDSS12	187	97	5	3	0	0	126	36	Quartz wacke
208TAFELSS1	186	96	8	4	0	0	79	23	Quartz wacke
208TAFELSS2	195	94	12	6	0	0	103	29	Feldspathic wacke
208TAFELSS3	188	98	4	2	0	0	135	39	Quartz wacke
208TAFELSS4	210	96	9	4	0	0	93	27	Quartz wacke
208TAFELSS5	171	97	5	3	0	0	105	30	Quartz wacke
218NOROSS1	171	94	11	6	0	0	56	16	Feldspathic wacke
218NOROSS2	207	96	9	4	0	0	96	27	Quartz wacke
218NOROSS3	202	94	13	6	0	0	104	30	Feldspathic wacke
218NOROSS4	175	95	9	5	0	0	128	37	Quartz wacke
218NOROSS5	203	96	9	4	0	0	107	31	Quartz wacke
218NOROSS6	237	96	11	4	0	0	53	15	Quartz wacke
218NOROSS7	236	95	12	5	0	0	72	21	Quartz wacke
218NOROSS8	181	97	6	3	0	0	113	32	Quartz wacke
218NOROSS9	212	96	9	4	0	0	98	28	Quartz wacke
218NOROEX1	207	90	22	10	0	0	82	23	Feldspathic wacke

Table 7.5. Normalised point count data used for classification of sandstones

	Quartz	Clay (Cement)	Clay (Rounded)	Clay (Angu	Clay (Clast)	Orthoclase	Plagioclase	Mica	Heavy Minerals	Oxide Minerals	Pore Space	Calcite Cement	Hematite	Burrow Fill	Total
Sample Number and Percentage															
228DNEUS2SS2	176	108	12	20	0	11	7	6	4	3	0	0	3	0	350
Percentage	50.29	30.86	3.43	5.71	0.00	3.14	2.00	1.71	1.14	0.86	0.00	0.00	0.86	0	100
148SSE	164	94	12	13	0	12	4	12	6	10	4	0	19	0	350
Percentage	46.86	26.86	3.43	3.71	0.00	3.43	1.14	3.43	1.71	2.86	1.14	0.00	5.43	0	100
148SSB	173	88	16	14	0	10	5	10	6	5	0	0	23	0	350
Percentage	49.43	25.14	4.57	4.00	0.00	2.86	1.43	2.86	1.71	1.43	0.00	0.00	6.57	0	100
DIKCNEUSLIMESTONE	55	0	0	0	0	0	0	0	0	8	0	285	2	0	350
Percentage	15.71	0.00	0.00	0.00	0.00	0.00	0.00	0.00	0.00	2.29	0.00	81.43	0.57	0	100
SAMPLE178	105	178	4	0	19	0	0	3	0	16	0	0	25	0	350
Percentage	30.00	50.86	1.14	0.00	5.43	0.00	0.00	0.86	0.00	4.57	0.00	0.00	7.14	0	100
148SSC	181	96	12	12	1	9	3	8	4	5	0	2	17	0	350
Percentage	51.71	27.43	3.43	3.43	0.29	2.57	0.86	2.29	1.14	1.43	0.00	0.57	4.86	0	100
148SSD	201	84	5	14	0	6	2	8	2	3	0	2	23	0	350
Percentage	57.43	24.00	1.43	4.00	0.00	1.71	0.57	2.29	0.57	0.86	0.00	0.57	6.57	0	100
178JAGDSS4	174	99	13	5	1	11	1	4	4	7	7	0	24	0	350
Percentage	49.71	28.29	3.71	1.43	0.29	3.14	0.29	1.14	1.14	2.00	2.00	0.00	6.86	0	100
218NOROSS3	202	104	6	5	0	12	1	14	2	3	0	0	1	0	350
Percentage	57.71	29.71	1.71	1.43	0.00	3.43	0.29	4.00	0.57	0.86	0.00	0.00	0.29	0	100
218NOROSS4	175	128	6	7	6	7	2	5	3	7	0	0	4	0	350
Percentage	50.00	36.57	1.71	2.00	1.71	2.00	0.57	1.43	0.86	2.00	0.00	0.00	1.14	0	100
218NOROSS1	171	56	8	6	74	11	0	12	5	4	0	0	3	0	350
Percentage	48.86	16.00	2.29	1.71	21.14	3.14	0.00	3.43	1.43	1.14	0.00	0.00	0.86	0	100
178JAGDSS11	137	161	18	11	0	4	1	2	4	7	1	0	4	0	350
Percentage	39.14	46.00	5.14	3.14	0.00	1.14	0.29	0.57	1.14	2.00	0.29	0.00	1.14	0	100
178JAGDSS8	189	102	11	6	1	9	4	7	4	2	1	3	11	0	350
Percentage	54.00	29.14	3.14	1.71	0.29	2.57	1.14	2.00	1.14	0.57	0.29	0.86	3.14	0	100
148SIS	148	138	8	3	26	3	3	6	4	7	2	0	2	0	350
Percentage	42.29	39.43	2.29	0.86	7.43	0.86	0.86	1.71	1.14	2.00	0.57	0.00	0.57	0	100
218NOROSS2	207	96	4	3	0	6	3	7	9	4	0	0	11	0	350
Percentage	59.14	27.43	1.14	0.86	0.00	1.71	0.86	2.00	2.57	1.14	0.00	0.00	3.14	0	100
208TAFELSS4	210	93	5	4	0	7	2	11	4	3	0	2	9	0	350
Percentage	60.00	26.57	1.43	1.14	0.00	2.00	0.57	3.14	1.14	0.86	0.00	0.57	2.57	0	100
178JAGDSS1	220	74	12	7	2	13	4	9	5	0	0	0	4	0	350
Percentage	62.86	21.14	3.43	2.00	0.57	3.71	1.14	2.57	1.43	0.00	0.00	0.00	1.14	0	100
148CCB	211	95	5	6	0	12	4	7	5	5	0	0	0	0	350
Percentage	60.29	27.14	1.43	1.71	0.00	3.43	1.14	2.00	1.43	1.43	0.00	0.00	0.00	0	100
148SSF	191	100	3	6	0	18	3	11	3	1	2	0	12	0	350
Percentage	54.57	28.57	0.86	1.71	0.00	5.14	0.86	3.14	0.86	0.29	0.57	0.00	3.43	0	100
228DNEUS2SS1	188	92	10	4	0	26	8	8	7	1	0	0	6	0	350
Percentage	53.71	26.29	2.86	1.14	0.00	7.43	2.29	2.29	2.00	0.29	0.00	0.00	1.71	0	100
208TAFELSS2	195	103	8	4	0	9	3	12	4	1	0	0	11	0	350
Percentage	55.71	29.43	2.29	1.14	0.00	2.57	0.86	3.43	1.14	0.29	0.00	0.00	3.14	0	100
148SSA	197	104	8	6	0	5	3	5	5	5	8	0	4	0	350
Percentage	56.29	29.71	2.29	1.71	0.00	1.43	0.86	1.43	1.43	1.43	2.29	0.00	1.14	0	100
218NOROEX1	207	82	9	12	0	18	4	6	6	2	0	0	4	0	350
Percentage	59.14	23.43	2.57	3.43	0.00	5.14	1.14	1.71	1.71	0.57	0.00	0.00	1.14	0	100
178JAGDSS6	196	85	0	7	23	12	4	5	4	5	0	1	8	0	350
Percentage	56.00	24.29	0.00	2.00	6.57	3.43	1.14	1.43	1.14	1.43	0.00	0.29	2.29	0	100
178JADGSS5	194	102	6	10	10	7	2	7	5	3	0	0	4	0	350
Percentage	55.43	29.14	1.71	2.86	2.86	2.00	0.57	2.00	1.43	0.86	0.00	0.00	1.14	0	100
148SSG	227	80	2	3	3	7	5	5	3	1	0	0	14	0	350
Percentage	64.86	22.86	0.57	0.86	0.86	2.00	1.43	1.43	0.86	0.29	0.00	0.00	4.00	0	100
158PLATSSTOP1	212	97	5	10	0	6	4	5	4	3	0	0	4	0	350
Percentage	60.57	27.71	1.43	2.86	0.00	1.71	1.14	1.43	1.14	0.86	0.00	0.00	1.14	0	100
218NOROSS6	237	53	4	19	0	8	3	8	1	5	0	0	12	0	350
Percentage	67.71	15.14	1.14	5.43	0.00	2.29	0.86	2.29	0.29	1.43	0.00	0.00	3.43	0	100
218NOROSS7	236	72	8	2	0	7	5	7	2	4	1	0	6	0	350
Percentage	67.43	20.57	2.29	0.57	0.00	2.00	1.43	2.00	0.57	1.14	0.29	0.00	1.71	0	100
218NOROSS5	203	107	2	3	2	6	3	9	5	2	2	0	6	0	350
Percentage	58.00	30.57	0.57	0.86	0.57	1.71	0.86	2.57	1.43	0.57	0.57	0.00	1.71	0	100
178JAGDSS10	176	130	4	4	2	6	4	4	4	8	0	0	8	0	350
Percentage	50.29	37.14	1.14	1.14	0.57	1.71	1.14	1.14	1.14	2.29	0.00	0.00	2.29	0	100
178JAGDSS3	189	112	6	6	6	4	3	3	3	2	2	0	14	0	350
Percentage	54.00	32.00	1.71	1.71	1.71	1.14	0.86	0.86	0.86	0.57	0.57	0.00	4.00	0	100
208TAFELSS5	171	105	4	5	37	3	2	8	2	4	0	0	9	0	350
Percentage	48.86	30.00	1.14	1.43	10.57	0.86	0.57	2.29	0.57	1.14	0.00	0.00	2.57	0	100
178JAGDSS9	168	112	2	4	35	3	2	10	3	5	0	0	6	0	350
Percentage	48.00	32.00	0.57	1.14	10.00	0.86	0.57	2.86	0.86	1.43	0.00	0.00	1.71	0	100
218NOROSS9	212	98	6	10	0	6	3	6	3	5	0	0	1	0	350
Percentage	60.57	28.00	1.71	2.86	0.00	1.71	0.86	1.71	0.86	1.43	0.00	0.00	0.29	0	100
208TAFELSS1	186	79	7	8	44	6	2	5	1	1	0	0	11	0	350
Percentage	53.14	22.57	2.00	2.29	12.57	1.71	0.57	1.43	0.29	0.29	0.00	0.00	3.14	0	100
208TAFELSS3	188	135	1	1	8	3	1	4	2	2	2	0	3	0	350
Percentage	53.71	38.57	0.29	0.29	2.29	0.86	0.29	1.14	0.57	0.57	0.57	0.00	0.86	0	100
178JAGDSS12	187	126	2	3	0	3	2	2	3	11	0	0	11	0	350
Percentage	53.43	36.00	0.57	0.86	0.00	0.86	0.57	0.57	0.86	3.14	0.00	0.00	3.14	0	100
178JAGDSS2	207	98	5	4	1	6	3	5	3	4	8	0	6	0	350
Percentage	59.14	28.00	1.43	1.14	0.29	1.71	0.86	1.43	0.86	1.14	2.29	0.00	1.71	0	100
218NOROSS8	181	113	4	13	0	5	1	4	0	11	0	0	18	0	350
Percentage	51.71	32.29	1.14	3.71	0.00	1.43	0.29	1.14	0.00	3.14	0.00	0.00	5.14	0	100
178JAGDSS7	206	94	3	8	0	14	2	5	3	1	1	0	13	4	350
Percentage	58.86	26.86	0.86	2.29	0.00	4.00	0.57	1.43	0.86	0.29	0.29	0.00	3.71	1.14	100

Table 7.6. All point count data and percentages per sample.

	Quartz	Clay (Cement)	Clay (Rounded)	Clay (Angu	Clay (Clast)	Orthoclase	Plagioclase	Mica	Heavy Minerals	Oxide Minerals	Pore Space	Calcite Cement	Hematite	Large Balls	Around Balls	Lithic Fragment	Fibrous Mineral	Hematite Ball	Total
DIKCNEUSLIMESTONE	55	0	0	0	0	0	0	0	0	8	0	285	2	0	0	0	0	0	350
Percentage	15.71	0.00	0.00	0.00	0.00	0.00	0.00	0.00	0.00	2.29	0.00	81.43	0.57	0.00	0.00	0.00	0.00	0.00	100
14811MLM/STN	55	0	0	0	0	0	0	1	0	0	0	279	11	0	0	0	0	4	350
Percentage	15.71	0.00	0.00	0.00	0.00	0.00	0.00	0.29	0.00	0.00	0.00	79.71	3.14	0.00	0.00	0.00	0.00	1.14	100
14811MLMSTN	54	0	0	1	0	0	1	1	0	8	0	270	13	0	0	0	0	2	350
Percentage	15.43	0.00	0.00	0.29	0.00	0.00	0.29	0.29	0.00	2.29	0.00	77.14	3.71	0.00	0.00	0.00	0.00	0.57	100
178LMBALL2	133	140	0	0	0	0	0	0	0	1	1	23	1	36	15	0	0	0	350
Percentage	38.00	40.00	0.00	0.00	0.00	0.00	0.00	0.00	0.00	0.29	0.29	6.57	0.29	10.29	4.29	0	0	0	100
178LMBALL1	41	0	0	0	0	0	0	0	0	0	0	8	17	275	0	1	8	0	350
Percentage	11.71	0.00	0.00	0.00	0.00	0.00	0.00	0.00	0.00	0.00	0.00	2.29	4.86	78.57	0.00	0.29	2.29	0.00	100

Table 7.7. All point count data and percentages for carbonate nodules.